Commensal-Specific Immune Responses At The Intestinal Mucosa

By
Djenet Bousbaine

B.Sc. Life Sciences and Technology
Swiss Federal Institute of Technology (EPFL), Lausanne, Switzerland (2010)
M.Sc. Life Sciences and Technology
Swiss Federal Institute of Technology (EPFL), Lausanne, Switzerland (2012)

Submitted to the Microbiology Graduate Program in partial fulfillment of the requirements for the degree of

Doctor of Philosophy
at the
MASSACHUSETTS INSTITUTE OF TECHNOLOGY

February 2020

Signature of Author……
Djenet Bousbaine
Microbiology Graduate Program
January 15, 2020

Certified by……...
Hidde Ploegh
Senior investigator
Boston Children's Hospital
Thesis supervisor

Accepted by……
Jacquin C. Niles
Associate Professor of Biological Engineering
Chair of Microbiology Program

Commensal-Specific Adaptive Immune Response At The Intestinal Mucosa

by
Djenet Bousbaine

Submitted to the Microbiology Graduate Program
on January 15, 2020, in partial fulfillment of the
requirements for the degree of
Doctor of Philosophy

Abstract

The intestinal mucosa harbors a dense community of microbes that breaks down polysaccharides indigestible by the host, synthesizes essential vitamins, stimulates maturation of the immune system, and outcompetes the growth of pathogenic species. In return, the host provides commensals with a habitat rich in energy derived from ingested food. The intestinal immune system faces the daunting task of maintaining homeostasis despite the enormous load and diversity of antigens present at this site. Failure to maintain this balance has dramatic consequences and can cause food allergies, inflammatory bowel disease or invasive infections. Peripherally-induced $Foxp3^+$-regulatory T cells (pTregs) maintain immune homeostasis at the intestinal mucosa by regulating effector T cell responses against dietary antigens and microbes. Similarly to pTregs, a subset of small intestine intraepithelial lymphocytes $CD4^+CD8\alpha\alpha^+$ ($CD4_{IELs}$) exhibit regulatory properties and promote tolerance against dietary antigens. In this thesis, I describe a new commensal-specific $CD4^+$ T cell model obtained by somatic cell nuclear transfer using, as a donor, a single pTreg from the mesenteric lymph node. In chapter 1, I provide an overview of the interplay between the microbiota and the mucosal immune system. In chapter 2, we describe our newly developed model and use it to assess how the identity of the T cell receptor (TCR) affect the fate of a T cell. In chapter 3, I describe the antigen and epitope recognized by this transnuclear (TN) TCR and show that TN cells can protect against intestinal inflammation in a colitis model. In chapter 4, I describe how TN cells can also differentiate into T follicular helper and promote systemic

responses. In chapter 5, we developed a strategy to target antigens to outer membrane vesicles (OMVs) of *Bacteroides* and thereby assess the antigen-specific responses to OMVs. In chapter 6, I provide concluding remarks and discuss future prospective for our findings. In the appendix, I describe a new mouse model to site-specifically label and track the B cell receptor of primary B cells.

Thesis Supervisor: Hidde Ploegh

Title: Senior investigator

Acknowledgments

My time in graduate school has been some of the most fulfilling years in my life. MIT is a unique place to learn and contribute to science alongside friendly and talented people. I cannot begin to express my gratitude to all the amazing people who have supported and encouraged me during these past few years and the ones who have helped me get to where I am today.

To my advisor, Hidde Ploegh, thank you for your insatiable curiosity and contagious enthusiasm. I will forever be grateful to you for taking me in your lab and the opportunities you have provided me that I would not have had elsewhere. Thank you for creating such a unique environment, filled with exceptionally talented people, where I could explore my own ideas and for always providing everything I needed. You taught me how to navigate complex problems, scientific and personal, and come up with out-of-the-box solutions. I'm very thankful to the incredible amount of freedom I had in your lab while knowing that your door was always open when I needed guidance or someone to be excited with me about new data. Thank you for always being supportive and providing sincere feedback.

I am indebted to my partner in crime in the lab, Angelina Bilate, for your generous and perpetual support long after you left the lab. For your mentorship, your "we can do it" attitude and pushing me to achieve the highest standards every day, every experiment. For your scientific excellence and essentially serving as a second unofficial advisor to me. For your friendship and making the lab such a wonderfully fun place to be. Your support in the last few years is invaluable to me and I can surely say my journey throughout graduate school would have been very different without you.

To my thesis committee, Mike Laub and Darrell Irvine, I am very thankful for your support and thoughtful advice along the years. To my expert, Jim Moon for taking the time to meet with me, offer your guidance and providing critical reagents.

I also would like to thank my former advisers, John McKinney and Jorge Galán for establishing the basis of my training and helping to pave my path to MIT. Thank you for your continuing support well after I left your labs.

To the wonderful students I had the pleasure to train and learn from. Priscillia Perrin, Preksha Bhagchandani, Paris Pallis and Laura Fisch thank you for your hard work, positive attitude and your contribution to this thesis.

Many of my best ideas and solutions came from conversations with nearby scientists who were generous enough to provide long email responses or brainstorm over a coffee. Thank you especially to Gabriel Victora, Luka Mesin, Dave Vanlnsberghe and Mark Mimee.

To the members of the Ploegh lab past and present. For the people who welcomed me in the lab and made me feel at home- Jasdave Chahal for your positive energy, Ana Avalos for getting me up and running and my buddies Ali Rashidfarrokhi, Andi Kratzert and Kaspar Bresser for all the fun. Florian Schmidt, Nick McCaul, Matthias Truttmann and Jingjing Ling for always helping and teaching others. Ross Cheloha and Ella Li for always being available for my questions. Mohammad Rashidian for distracting me with politics when I needed to be cheered up. To the constant influx of European master students for bringing fun and positivity to the lab.

To my terrific collaborators, Mark Mimee, Mathilde Poyet, Scott Olesen, Dave Vanlnsberghe for your contributions to this thesis, our many discussions and your friendship.

To my microbiology class for being absolutely awesome and fun! Ben, Dave, Mary and Isaak, you were always a community I could rely on for basically anything. To my close friends from MIT and across the river, Rasmus Herlo for your upbeat attitude, Liron David for being the sunshine you are, Mark Sieber for your positive attitude and David Angeles for cheering me up when I needed it. To my roommates Vania Crisstiany and Kerline Moncy for creating a home away from home. To the members of the MIT gamelan Galak Tika for keeping me sane. Andreas Liapis for feeding me, Emeric Viani, Leslie Tilley, Evan Ziporyn, Ryan Mbira, Ilya Sukhotin and Mark Stewart for your friendship.

Thank you to the people who keep the lab up and running, Robert Miller and Simona Stella, you provide the necessary foundations for the Ploegh lab research. Thank you for feeding me chocolate and your wisdom in times of trouble.

To my family for sending me back to Boston with enough chocolate and spices to last until the next visit. Thank you for being supportive of my career even though it is difficult to be so far apart. Last but not least thank you to Conor for taking care of me over the past 6 years and making sure I was never hangry. For making my life full of puns and cat videos and the fun adventures we took along the years. Finally, thank you for troubleshooting all my cloning, reading and editing this document and reminding me that not everyone is an immunologist.

List of figures

List of tables

List of abbreviations

A_{2A}	Adenosine receptor 2A
Ag	Antigen
AHR	Aryl hydrocarbon receptor
AHR	Aryl hydrocarbon receptor
ALDH	Aldehyde dehydrogenase
APC	Antigen-presenting cell
APRIL	A proliferation inducing ligand
BAFF	B-cell activating factor
BCR	B cell receptor
cAMP	Cyclic Adenosine Monophosphate
$CD4_{IELs}$	CD4 intraepithelial cells
CDR3	Complementarity determining region 3
CFSE	Carboxyfluorescein succinimidyl ester
cLP	Colonic lamina propria
CR	Charles River
CTLA-4	Cytotoxic T-lymphocyte-associated gene 4
DC	Dendritic cell
DP	Double-positive
DT	Diphtheria toxin
EAE	Experimental autoimmune encephalomyelitis
EDTA	Ethylenediaminetetraacetic acid
EF	Excluded flora
ESC	Embryonic stem cell
FACS	Fluorescence activated cell sorting
Flt3L	FMS-like tyrosine kinase 3 ligand
GALT	Gut-associated lymphoid tissue
GF	Germ-free
GFP	Green fluorescent protein
Gzm	Granzyme
HDAC	Histone deacetylase
IBD	Inflammatory bowel disease
ICOS	Inducible T-cell costimulator
IDO	Indolamine 2,3-dioxygenase
IE	Intraepithelial
IEC	Intestinal epithelial cell
IEL	Intraepithelial lymphocyte
IFN	Interferon
Ig	Immunoglobulin
IgA	Immunoglobulin A
IL	Interleukin
ILCs	Innate lymphoid cells
ILF	Isolated lymphoid follicles
iLN	Inguinal lymph node

iNK	Invariant natural killer
IPEX	immune dysregulation, polyendocrinopathy, enteropathy, X-linked
Jax	Jackson
KO	Knock-out
LAG-3	Lymphocyte-activation gene 3
LCN2	Lipocalin-2
LiLP	Large intestine lamina propria
LN	lymph node
LP	Lamina propria
MAIT	Mucosal associated invariant T
MHC	Major histocompatibility complex
MsLN	Mesenteric LN
NF-κB	Nuclear factor-kappaB
NK	Natural killer
nTreg	natural regulatory T cells
OMV	Outer membrane vesicle
OTU	Operational taxonomic unit
OVA	Ovalbumin
PBS	Phosphate buffered saline
PP	Peyer's Patches
PSA	capsular polysaccharide A
pTreg	Peripheral regulatory T cell
qPCR	Quantitative PCR
RA	Retinoic acid
RNA-seq	RNA sequencing
RORγT	retinoid-related orphan receptor gamma T
rRNA	Ribosomal ribonucleic acid
SCFAs	Short-chain fatty acids
SCNT	Somatic cell nuclear transfer
SFB	Segmented filamentous bacteria
SFB	Segmented filamentous bacteria
SiLP	Small intestine lamina propria
SP	Single-positive
SPF	Specific pathogen free
SPF	Specific pathogen free
Tac	Taconic
Tconvs	Conventional $CD4^+$ T cell
TCR	T cell receptor
Tfh	T follicular helper
TGFβ	Tumor growth factor beta
Th	CD4+ T helper
TL	Thymus-leukemia antigen
TN	Transnuclear
Tr1	Type 1 regulatory cells
Treg	Regulatory T cell
WT	Wild-type

ZPS	Zwitterionic capsular polysaccharides
β -hex	β-N-acetylhexosaminidase

Chapter 1 - Adaptive immune responses at the intestinal mucosa

1.1 Introduction

The human body is home to a wide range of microbes, belonging to all three domains of life (*1*). Some of these microbes are beneficial to their host. They are often referred to as *commensals*, while other microbes can cause disease and are called *pathogens*. Commensals play an important role in human metabolism, provide essential nutrients and protect against invading pathogens (*2*). They colonize our skin and mucosal surfaces with high efficiency and comprise at least as many cells as the human body (*3*) . Perhaps even more impressive is the diversity of the species present (estimated to be between 500-1000 species), and their massive gene content (100 times greater than the human genome) (*4*). Changes in microbiome composition have been associated with pathology, ranging from inflammatory bowel disease, cardiometabolic disorders, cancer and neuropsychiatric disorders (*5-12*). The highest concentration of microbes is present in the intestinal mucosa. This location harbors trillions of microbes and represents one of the densest and most diverse ecosystems known (*2, 13*). The close proximity of commensals, the continuous exposure to dietary antigens and pathogens represents a unique challenge to the immune system. To achieve homeostasis, the immune system has developed a highly sophisticated network of cells that promotes tolerance towards beneficial antigens while protecting the body against invading pathogens. As a result, gut-associated tissues contain the highest number of immune cells in our body which display a fascinating complexity of immune phenotypes. Dysregulation of this network can cause disease: tolerance to pathogens may lead to infection, while an overactive immune response directed towards commensals or food antigens can lead to inflammatory bowel disease and food allergies, respectively (*14, 15*). In this chapter, I discuss the role of the microbiome in the development, maintenance and function of the immune system. I provide a deeper look at the gastrointestinal tract and mechanism of immune tolerance to commensal antigens.

1.2 The Immune system

The different layers of the immune system

Our bodies have evolved a set of defense strategies that protect us from external attacks by pathogenic invaders. These strategies are mediated by components that comprise anatomic and physiologic barriers, inflammatory mediators and cells, all collaborate to maintain health. The first line of defense of the immune system are physical barriers such as the skin and epithelia. The importance of this barrier is highlighted by the increased risk of infection after burns or wounds. Mucus is another type of physical barrier, the significance of which is exemplified by the pathologies of cystic fibrosis patients who cannot efficiently secrete mucus. These mechanical lines of defense are complemented by chemical protective layers such as the low pH present in the stomach or the secretion of antimicrobial peptides in the gut. Finally, these two barriers are supported by the presence of microbes that prevent the invasion of our body by pathogens (*16*).

The cellular compartment (i.e the ensemble of cells) of the immune system is composed of a network of specialized subsets of cells, all of which derive from pluripotent hematopoietic stem cells. These different subsets belong to either the innate immune system, which provides immediate responses, or the adaptive immune system, which supports long-term specific responses to a particular pathogen. The main cell types of the immune system are summarized in Fig. 1.1. For the purpose of this thesis I will focus mainly on the adaptive immune response. I direct the readers to an excellent review by Iwasaki and Medzhitov on the innate immune system and its cross talk with adaptive immunity (*17*).

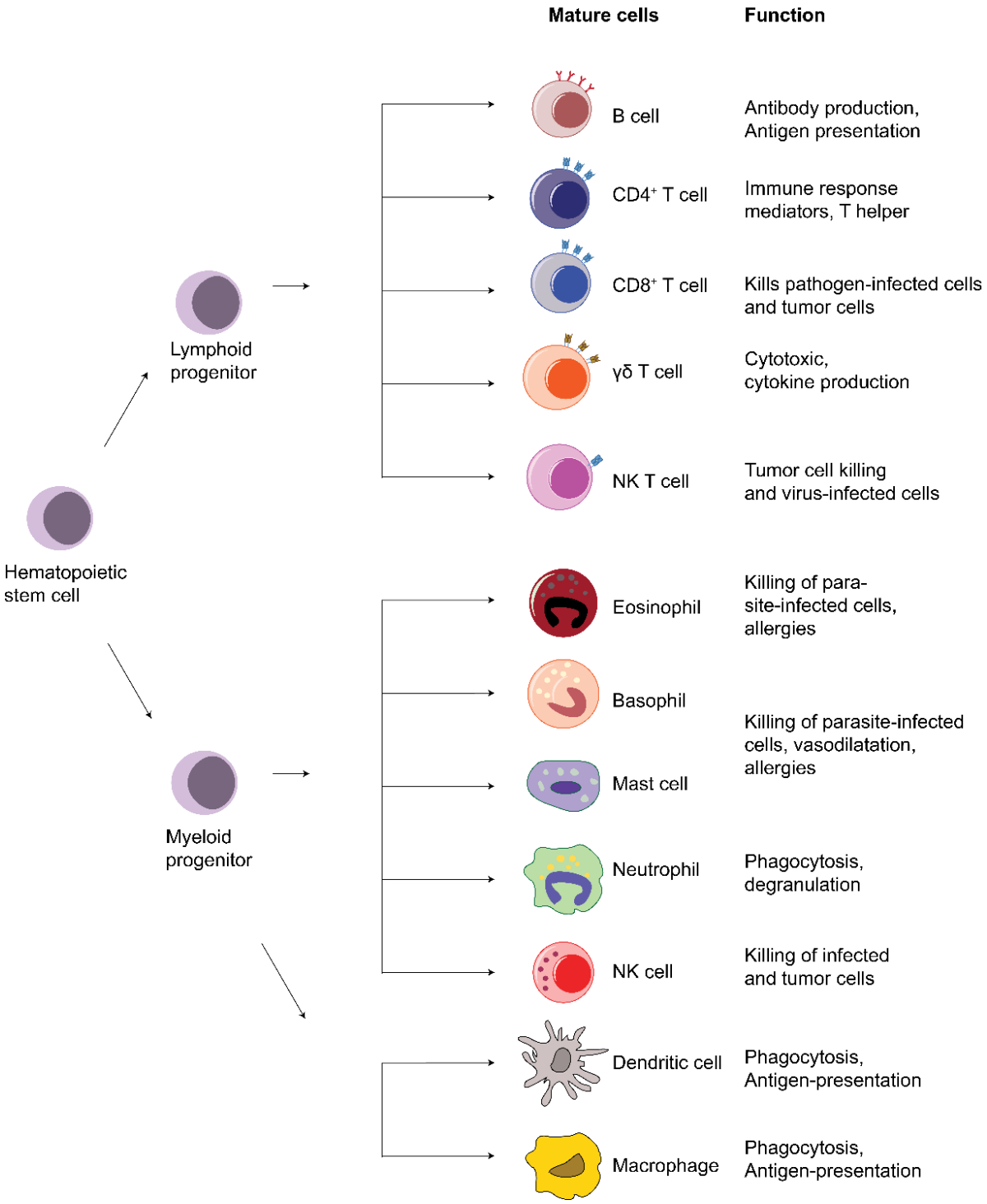

Figure 1.1 Cell types of the immune system.

The immune system is composed of many different cell types and subtypes. Bone marrow hematopoietic stem cell can differentiate into lymphoid and myeloid progenitor cells. Lymphoid stem cells yield T and B-lymphocytes and natural killer (NK) T cells. Myeloid stem cells give rise to granulocytes (neutrophils, eosinophils, mast cells and basophils), NK cells and phagocytic cells (dendritic cells and macrophages).

Adaptive immune responses

The *adaptive immune system,* can recognize virtually any molecule or antigen (an antigen is defined as any substance that can evoke an immune response). The molecules involved in this process are the antigen receptors: the B cell receptor (BCR) expressed exclusively on B cells and the T cell receptor (TCR) on T cells. Both BCRs and TCRs possess a variable region, important for interaction with antigen, and a constant region. The diversity of the variable regions available to the TCR and BCR is specified in the genome: variable regions are assembled by somatic gene rearrangement of diverse genetic elements, a process known as V(D)J recombination (*18*). All antigen receptors of the adaptive immune system use two subunits, each equipped with a variable region, one of which is constructed from V, D and J elements, while its partner uses V and J elements. The variable region is assembled from randomly chosen V (variable), D (diversity) and a J (joining) segments. This rearrangement is mediated by complex enzymatic machinery that includes the Rag1 and 2 recombinase (*18*). The importance of these receptors is evident from the phenotype of RagKO animals ($Rag1^{-/-}$ or $Rag2^{-/-}$), which do not possess either mature B or T cells and are thus severely immunocompromised (*19*). In fact, conditional ablation of the BCR leads to B cell death (*20*). Therefore, these receptors are essential for both the development and survival of B and T cells.

An important difference between these receptors is the type of antigens they recognize. BCRs can recognize nearly any type of intact antigen such as protein, carbohydrate, DNA or even small molecules, to name a few. In contrast, the TCR only recognizes antigens displayed on the surface of other cells, bound to major histocompatibility complex (MHC) molecules. These complexes of proteins bind to pre-processed peptides and present them to T cells (*21, 22*). Another important difference is the absence of secreted form of the TCR, in contrast to B cells, which secrete antibodies, the secreted version of the BCR. Secretion of antibodies is important to neutralize extracellular pathogens and is an essential function of B cells.

T cells can be subdivided into two main classes, $CD4^+$ or $CD8^+$ T cells, based on the co-receptors they express. These co-receptors are important not only as markers but also to

stabilize the interaction between the TCR and the MHC molecules with which they interact. Indeed, the CD4 co-receptor recognizes MHC class II molecules (MHCII), while CD8 interacts with MHC class I molecules (MHCI). These two classes of T cells have very different effector functions. $CD8^+$ T cells are cytotoxic and kill cells that display their cognate antigens on MHCI, while $CD4^+$ T cells orchestrate the immune response by cell-cell contacts and through release of cytokines. $CD4^+$ T cells can activate other cells, for example to induce them to secrete antibodies. Importantly, MHCI and MHCII have different distributions among cells, which reflects the function of the T cells that interact with them. $CD8^+$ T cells recognize predominantly intracellular pathogens present in the cytosol such as viruses. Because any cell can be infected by viruses, all nucleated cells express MHCI. In contrast, only a subset of cells expresses MHCII. These cells are called antigen-presenting cells and include B cells, dendritic cells and macrophages. Antigens destined for presentation by MHCII molecules are picked up from extracellular space, proteolytically processed and presented to $CD4^+$ T cells. When a $CD4^+$ T cell interacts with a B cell that presents the cognate antigen, it activates the B cell to differentiate and secrete antibodies. Similarly, $CD4^+$ T cells can activate infected macrophages to destroy intracellular pathogens when the appropriate antigens are presented to $CD4^+$ T cells.

Upon activation by antigen-presenting cells, $CD4^+$ T cells can differentiate into a variety of effector subsets including Th1, Th2, Th17, T follicular helper (Tfh) and peripheral T regulatory (pTreg) (Fig. 1.2). Decision to differentiate into each of these lineages is governed primarily by the cytokines present in the microenvironment and the affinity of the TCR for its antigen (*23*). In addition, the presence of certain microbes and pathogens can influence the fate decision of $CD4^+$ T cells in both antigen-dependent and independent manners. Each of these subsets produces a defined set of cytokines and chemokines largely driven by transcription factors which act as “master regulators”. Long considered irreversible, these fates appear to be more plastic than initially thought, especially in the intestine (*24*). For example, a majority of colonic Tregs express both Foxp3 and RORγT, the characteristic master regulators of Tregs and Th17, respectively (*25*). During homeostasis, these cells selectively restrict pro-inflammatory Th17 but under inflammation, they lose Foxp3 expression and promote intestinal inflammation (*26*). This

example illustrates how plasticity of CD4⁺ T cells in the intestine can influence tissue homeostasis.

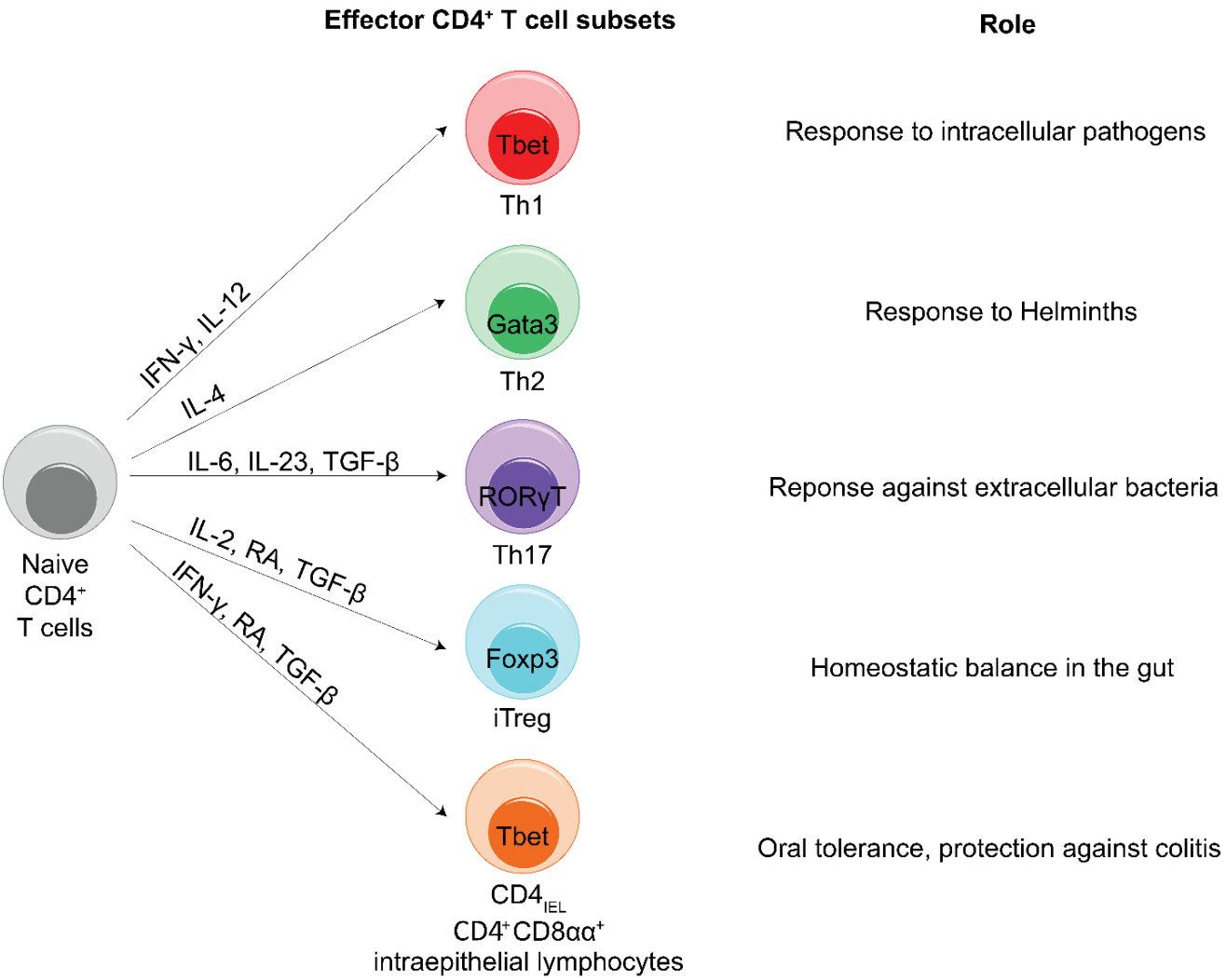

Figure 1.2 CD4⁺ T helper cell subsets.

CD4⁺ T cells can differentiate into a diverse set of effector T cell lineages with distinct functions. Activation of naïve CD4⁺ T cells by antigen-presenting cells in the presence of the appropriate cytokine environment leads to commitment into one of these fates (or others not represented here). Each subset expressed a defined set of cytokines and surface markers, mostly controlled by transcription factors which act as master regulators such as Foxp3 for Tregs.

Central tolerance

An essential feature of the adaptive immune system is its ability to recognize almost any antigen. This comes in handy when dealing with rapidly evolving pathogens, but it poses a risk- our immune cells can recognize and destroy our own tissues. In fact, it is estimated that close to 75% of human immature B cells show some measure of self-reactivity (*27*). Therefore, the immune system must have mechanisms in place to ignore and tolerate "self" antigens, while actively responding to pathogenic or "non-self" antigens.

Central tolerance prevents the development of auto-reactive T or B cells. After rearrangement of their TCR genes, T cells go through a selection process to test the functionality of their properly assembled TCR. This process takes place in the thymus. Newly generated T cells are tested for their ability to interact with self-peptide, loaded onto MHC molecules. T cells that express a TCR unable to properly interact will not survive, while T cells that interact too strongly with MHC products complexed with self-peptides will be deleted. These positive and negative selection steps ensure that only functional T cells contribute to the pool of mature T cells. Because negative selection is imperfect, additional mechanisms are in place in the periphery to ensure that self-reactive T cells become non-responsive or anergic. Similar to T cells, B cells can be deleted during development or rendered anergic in the periphery when they recognize self-antigens (*16*).

BCR and TCR repertoires

The ensemble of antigen receptors found in a tissue is referred to as the repertoire. These repertoires are affected by the antigens present in a given tissue. When lymphocytes are activated by their cognate antigens, they proliferate and their representation within the repertoire increases. Studies of repertoires are usually done by sequencing the TCR or BCR either at the population level, or after single-cell sorting. The use of animal models in which one of the two receptor chains is "fixed" reduces diversity and facilitates repertoire analysis (*28-33*). Analysis of the TCR repertoire of T cells in the colonic lamina propria showed that the majority of colonic Tregs were induced locally in response to microbiota-derived antigens (*34*). Analysis of the TCR repertoire can also inform on the

development of a particular T cell subset. Colonic Th17 and RORγt^{+}Foxp3^{+} Tregs were found to share a subset of TCRs, suggesting that RORγt^{+}Foxp3^{+} Tregs could be the precursors of some Th17 cells. This hypothesis was subsequently validated using a commensal-specific transgenic line (see below) (*35, 36*). A major question remains the extent to which receptor repertoires are linked to the function of the cells that express particular antigen receptors.

1.3 Microbiome

The microbiome is the ensemble of microbes living in and on our bodies. This dense community of microbes helps digest our food, provides essential nutrients, regulates and supports maturation and continued education of our immune system and protects us against invading pathogens (*2, 37-39*). Over the past decade, the number of studies on the microbiome has exploded. We now appreciate its contribution to human health. Imbalance in the composition of these microbial communities, called dysbiosis, is associated with a range of chronic diseases, including atherosclerosis, metabolic disorders, asthma, and autism spectrum disorder (*40-49*). Early work established that transfer of the microbes associated with these phenotypes can transfer disease from a sick donor to a healthy recipient in cases such as obesity, and conversely, that a microbiota from a healthy donor, when transferred into a sick recipient, can ameliorate disease. This raises the possibility of using microbes as therapies (*50*). As often is the case in a new field of research, many of these early findings report associations. Much effort is currently concentrated on moving from correlation to causation and identification of the molecular mechanisms responsible for the phenotypes observed (*8, 51*). The lack of suitable tools complicates the study of the molecular mechanisms at play in these complex communities. Contrary to common belief, the majority of gut microbes can be cultured, although many require specialized growth conditions not easily accessible to most laboratories (*2, 52-56*). As of today, most of these microbes are genetically intractable, making mechanistic studies a challenge (*2*).

The microbiome is established at birth, evolves considerably over the first 3 years of life and then remains mostly constant throughout adulthood (*37, 57-59*). Each individual

harbors a unique set of microbes, often similar between family members (*60*). Within an individual, different anatomical sites carry distinct populations of microbes. Variations in microbial composition are affected by both genetics and the environment in ways still poorly understood (*2*). Within the intestine, the type and abundance of microbes varies along the gastrointestinal tract. For instance, aerobic bacteria colonize the upper GI tract while anaerobes are found mostly in the large intestine. The load of bacteria also varies along the intestine, ranging from 10^3-10^4 bacteria/ml in the upper part of the GI tract, 10^8 bacteria/ml in the ileum and up to 10^{11} in the colon (*61, 62*). The emergence of high-throughput sequencing of the 16s ribosomal RNA (rRNA) gene has enabled identification of the bacterial composition in the intestine, irrespective of our ability to culture them *in vitro*. All bacterial species and archea carry a 16s rRNA gene, which can be specifically amplified and sequenced to identify the relative abundance of operational taxonomic units (OTUs) in a given sample (*63*). Gram-positive *Firmicutes* such as *Clostridia* and gram-negative *Bacteroidetes* (primarily *Bacteroides*, *Parabacteroides*, *Alistipes*, and *Prevotella*) are the two most abundant phyla found in the mammalian gut (*64*). The remaining bacteria make up less than ten percent and include mainly *Actinobacteria*, *Verrucomicrobia*, *Proteobacteria* and *Fusobacteria* (*2, 64*).

While most microbes reside in the lumen of the intestine, others establish their niche in the crypts, the mucus, attached to the epithelium or even beyond the epithelium (*65*) (Fig. 1.3). These distinct localizations reflect the different microbial lifestyles and allow unique interactions with the immune system. A notable example is segmented filamentous bacteria (SFB) which intimately attaches to epithelial cells in the small intestine and promotes the specific induction of pro-inflammatory Th17 cells (*66*).

The mucus is a thick layer of glycoproteins produced by goblet cells that serves as a physical barrier to the microbiome. Microbes found in the mucus are highly specialized to survive in this environment (*2*). Only a limited number of bacteria have an adequate repertoire of genes that encode catabolic glyosidic enzymes capable of digesting mucus-derived glycoproteins. They include members of the genus *Akkermansia* such as *A. muciniphila*, the genus *Bacteroides* like *B. thetaiotaomicron* and *Bifidobacterium*, such as *B. bifidum*. Some of these species establish a stable relationship with mucus while others,

like *B. thetaiotaomicron*, digest host mucus when preferred food sources become scarce (*67, 68*).

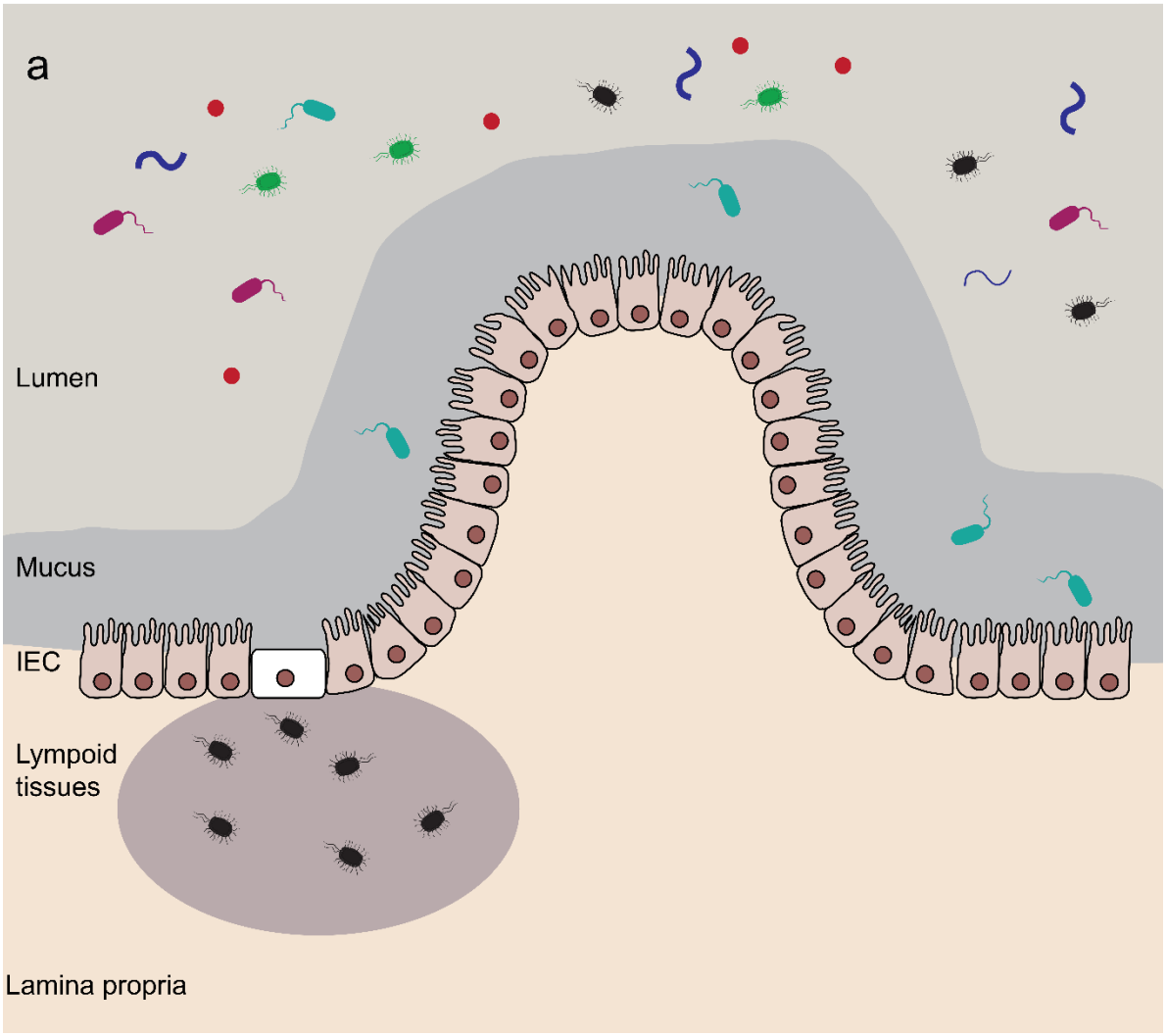

Figure 1.3 Localization of commensals at the intestinal mucosa

Commensal bacteria in the intestine can be found in the lumen, the mucus or within gut-associated lymphoid tissues.

Intestinal microbes are largely confined to the luminal side of the gut, but a few bacterial species can breach through the epithelial barrier and stably colonize gut-associated lymphoid tissues (*69, 70*). Inside Peyer's patches (PPs) in mice, monkeys and humans, these bacteria can promote the secretion of commensal-specific IgA (*69*). The most dominant species found in PPs belong to the *Alcaligenes* genus, with less abundant

members derived from *Ochrobactrum* spp., *Serratia* spp. and *Burkholderia* spp. The anatomical containment of these species is mediated by Innate lymphoid cells (ILCs) and is disrupted in patients with HIV, cancer or cystic fibrosis, causing peripheral dissemination of these bacteria (*70*). More studies are required to better understand how these species establish a stable niche within gut-associated lymphoid tissues.

1.4 Mucosal immune system

Most of what is known about our immune system derives from studies that examine the responses to pathogens. However, the majority of interactions between microbes and the immune system occurs at barrier sites and are mostly symbiotic in nature. The particularities and properties of this type of immunity remain mostly obscure. As described above, a dense population of microbes lives closely and even within lymphoid organs in our intestine. This population of microbes constantly interacts, communicates with and educates our immune system (*71-73*). In turn, the immune system maintains homeostasis and prevents dissemination of these microbes via a sophisticated network of cells and structures at mucosal surfaces. The intestinal mucosal immune system contains the largest number of immune cells in our body, most of which express complex effector phenotypes not observed anywhere else in the body.

Organization of the gut mucosal system

The barrier that physically separates the luminal microbes of the gut from our body is made of a single layer of epithelial cells connected by tight junctions. The epithelium itself is home to a set of specialized cells that support the barrier function of intestinal epithelial cells (IECs). These include the mucus-secreting goblet cells, anti-microbial peptide-producing cells named Paneth cells and a complex set of lymphocytes, the intraepithelial lymphocytes (IELs). Below the epithelium, another set of specialized structures is found. The Peyer's patches (PPs) of the small intestine and the numerous isolated lymphoid follicles are both present on the submucosal layer of the intestinal wall and are important for the induction of IgA. Beneath the epithelium, separated by a loose layer of connective tissue, is the lamina propria, which contains a high number of activated lymphocytes. All

of these sites are connected to afferent lymphatics, which drain cells and antigens to the mesenteric lymph nodes (*16*).

The microbes present in the lumen of the gut are also separated from our body by a mucus layer, which is approximately 400µM thick in humans and 150µM in mice and prevent most microbes from entering in direct contact with the epithelium (*74, 75*). In the colon, the mucus forms two distinct layers, the innermost of which is mostly sterile (*74*). The mucus itself contains lysozyme and other antimicrobial peptides (AMPs) (*76*). Antimicrobial peptides are short 10-50 amino acid peptides with an overall positive charge and broad specificity against most pathogenic but also commensal bacteria (*77*). Paneth cells, present in the crypts of the small intestine, are a major source of such AMPs (*77*).

Antigen uptake and presentation in GALT

Also present in the epithelium are microfold or “M” cells, which are continually picking up antigens from the lumen of the intestine and transferring them to gut-associated lymphoid tissue (GALT). This route of entry is highjacked by pathogens such as *Salmonella enterica* (*78*). On the basal side of M cells, antigens are released into the extracellular space by transcytosis and are then in turn picked up by antigen-presenting cells (APCs). Antigen-loaded APCs can then move to the Peyer’s patches (PPs) for antigen presentation to T cells or the APCs migrate to the mesenteric lymph nodes where they activate cognate T cells (*16*). Yet another mode of entry for antigens is via CX3CR1-positive macrophages, which possess long dendrites that extend between epithelial cells, project into the gut lumen and sample luminal antigens (*79*). Remarkably, these dendrites can engulf whole bacteria before delivering them to the lamina propria.

Intraepithelial lymphocytes (IELs).

The other class of cells present in the epithelium are called intraepithelial lymphocytes (IELs). This compartment contains the largest number of T cells in our body as well as a diverse range of other immune cells such as eosinophils and Innate Lymphoid Cells (ILCs) (*80, 81*). IELs represent the front line of defense against invading pathogens due to their immediate proximity to antigens present in the gut lumen. As a result, IELs express

activation markers such as CD69 but also inhibitory types of receptors. They are therefore often referred to as “activated yet resting” (*82*). IELs are further characterized by the expression of gut-homing markers such as CD103, cytotoxic markers such as granzyme B and anti-inflammatory molecules such as LAG-3 (*83, 84*). Another typical characteristic of IELs is the expression of the CD8αα homodimer, which can recognize both classical major histocompatibility complex I (MHC-I) and non-conventional MHC-I molecules such as the thymus leukemia (TL)-antigen on epithelial cells (*85, 86*). Interaction between CD8αα and TL-antigen attenuates TCR activation and may contribute to keeping IELs in a non-responsive state (*87*). In fact, mice deficient in TL-antigen are more susceptible to intestinal inflammation in a spontaneous model of colitis (*87*). A summary of the IELs found in the small intestine is described in Table 1.1.

Cell type	Subtype	Phenotype	Antigen	Function
Natural IEL	TCRγδ	$CD4^-CD8^-$	Self and non-self	Antimicrobial and anti-inflammatory responses, immune regulation, homeostasis of the gut epithelium, tolerance to intestinal antigens.
		$CD8\alpha\alpha^+$		
	TCRαβ	$CD4^-CD8^-$		
		$CD8\alpha\alpha^+$		
Induced IEL	TCRαβ	$CD8\alpha\beta^+$	Non-self	Oral tolerance, Immune regulatory function, protective antimicrobial responses
		$CD8\alpha\alpha^+CD8\alpha\beta^+$		
		$CD4^+$		
		$CD4^+CD8\alpha\alpha^+$		
TCR^- IEL	None	ILC1-like		Intestinal inflammatory responses, batcerial clearance, Involved in refractory celiac disease lymphomas
		iCD8α		
		iCD3		

Table 1-1 Characteristics of the different populations of intraepithelial lymphocytes found in the small intestine.

IgA production in the gut

The production of commensal-specific IgA antibodies is yet another strategy used by the immune system to maintain homeostasis at the gut mucosa. IgA is the dominant antibody isotype present at mucosal surfaces. IgA dimers can be transcytosed to the intestinal lumen where they can coat commensals, toxins and pathogens and thus restrict access to mucosal surfaces (*88*). Class-switching to and secretion of IgA can either require T cell help in the presence of cognate antigen, or be T-independent in the presence of TGF-β, BAFF and APRIL.

T-cell deficient mice have starkly reduced amounts of free IgA, suggesting that most IgA production is T-dependent (*89*). Sequence analyses showed that most of the IgA produced sustained somatic hypermutation consistent with T cell involvement (*88, 90*). Sorting of IgA-coated bacteria in T-deficient mice (*91*) has yielded conflicting results concerning the relative contribution of T cells in IgA responses in the gut. Therefore, further studies are required to reach a consensus. Beyond providing a physical barrier to antigens in the lumen, IgA can modulate the expression of genes by commensals. For example, coating of *B. thetaiotaomicron* with IgA prevents the expression of genes that elicit inflammatory responses in the host (*92*).

1.5 Development of the immune system in the gut and commensals

Studies in germ-free and mice harboring a defined minimal flora (gnotobiotic) mice have shown that interactions between the microbiome and the immune system are important for the development and normal physiology of the immune system (*1*). Germ-free or antibiotic-treated mice have impaired immune responses to pathogens (*66, 93-95*). This is not surprising, since germ-free mice possess abnormal anatomical immune structures and immune cell numbers in the gut: they lack mucosal-associated invariant T cells (MAIT) cells (*96*), display poorly formed Peyer's patches, have small mesenteric lymph nodes (*1*), show impaired development of isolated lymphoid follicles and present with altered composition of $CD4^+$ T cells, including a lower frequency of Tregs (*97, 98*) and IgA-producing B cells (*96, 99*). Antibiotic-treated mice likewise show altered gut structures, such as a reduced number of Peyer's patches, smaller lymph nodes as well

as an altered myeloid and lymphoid compartment (*100*). Both single isolates and consortia can repair some of these abnormalities (*97, 98*). The importance of the microbiome is also observed at weaning in Standard Pathogen-Free (SPF) mice. The transition from a milk-based diet to solid food is associated with a drastic shift in microbial composition and a marked increase in pTregs specific for commensal antigens in the colon (*34, 97, 98, 101, 102*).

1.6 Homeostasis at the gut mucosa is mainly maintained by T cells

Although homeostasis at the gut mucosa is maintained by many arms of the immune system, T cell responses appear to be central to this regulation. Lack of T cells is associated with spontaneous development of colitis in SPF but not in germ-free mice (*103, 104*). Similarly, MHCII-deficient mice develop colitis, suggesting that $CD4^+$ T cells play an important role in the prevention of spontaneous colitis (*103*). In humans, a decrease in the number of $CD4^+$ T cells in HIV patients is often associated with intestinal inflammation, even in the absence of pathogens (*105, 106*). Conversely, inappropriate T cell responses are also associated with disease. $TCR\alpha^{-/-}$ mice develop spontaneous colitis, mediated by pathogenic IL-4 -producing $CD4^+TCR\beta\beta^+$ cells (*107*). Overall, these experiments suggest that T cell responses at the gut mucosa must be tightly regulated to avoid the development of colitis.

Regulatory T cells (Tregs)

Tolerance to commensal and dietary antigens is mediated by $Foxp3^+$ peripheral T regulatory cells (pTregs). In contrast to natural Tregs (nTregs), which develop in the thymus and recognize self-antigens, pTregs develop from naïve $CD4^+$ T cells and are specific for antigens found within tissues. Foxp3 is a transcription factor essential for Treg development, maintenance and function and its expression serves as the canonical marker of Tregs (*108, 109*). Tregs are present in every organ of the body, but it is in the intestine that they are the most abundant, accounting for up to 30% of $CD4^+$ T cells in the colonic lamina propria (*97-99, 110, 111*). Development of intestinal Tregs is heavily dependent on the microbiota. Treg numbers are decreased in both germ-free and

antibiotic-treated mice. Their functional maturation is also affected by the presence of the microbiota. The few Tregs that remain in the absence of commensals exhibit a severe reduction in the expression of ICOS, CTLA-4 and IL-10, all key markers for the function of Tregs (*97, 98, 110-112*).

The essential suppressive role of Tregs was originally demonstrated by depletion of $CD4^+CD25^+$ Treg cells, which led to the development of multi-organ autoimmunity, including intestinal inflammation (*113*). These findings received support from results in the colitis model developed by Powrie and colleagues. Transfer of naïve $CD4^+CD45RB^{high}$ lymphocytes into a syngeneic lymphopenic host causes a progressive and chronic wasting disease similar to Inflammatory bowel disease (IBD) (*114, 115*). Co-transfer of pathogenic cells ($CD4^+CD45RB^{high}$ cells) and $CD4^+CD25^+$ Tregs efficiently prevented and even reversed the development of colitis in this model (*116, 117*). Conclusions from these experiments were further complemented by the study of genetic deficiencies. Null mutations in *Foxp3* in both mice and humans are associated with diarrhea, colitis and a multitude of other severe autoimmune phenotypes (*118-121*). More recently, administration of antibodies directed against cytotoxic T lymphocyte antigen-4 (CTLA-4) to cancer patients, which targets a central suppressive marker on Tregs, caused development of colitis as a side effect (*122*). The regulatory function of Tregs is therefore essential throughout the body and in particular in the intestine.

$\underline{CD4_{IELS}}$

While Tregs are key players in the establishment and maintenance of intestinal tolerance, they are not solely responsible for this regulation. Deficiencies in IL-10R in humans is associated with the development of colitis, with an earlier onset and higher penetrance than patients with *Foxp3* deficiencies (*123*). In humans, intestinal inflammation is not associated with a decreased frequency of $Foxp3^+$ Tregs (*124, 125*). This supports the notion that other cell types could play a role complementary to that of Tregs, for example via the (immunosuppressive) IL-10 pathway.

$CD4^+CD8\alpha\alpha^+$ intraepithelial lymphocytes ($CD4_{IELS}$) are a subset of lymphocytes that reside in the epithelium of the small intestine (*126*). Their frequency is decreased in germ-

free mice, and in IBD and celiac disease patients (*127-129*). Similarly to Tregs, $CD4_{IELS}$ display regulatory functions and promote tolerance to dietary antigens (*128*). The function of $CD4_{IELS}$ appears to be complementary to that of Tregs. Depletion of $CD4_{IELs}$ in mice that lack Tregs causes disease (*128*). Forced differentiation of $CD4^+$ cells into $CD4_{IELs}$ prevents intestinal inflammation. Blocking the development of $CD4_{IELs}$ can accelerate intestinal damage in a model of colitis (*130*). Therefore, $CD4_{IELs}$ is a distinct subset of T cells that works in concert with Tregs to maintain intestinal homeostasis.

The development of $CD4_{IELs}$ is initiated when a naïve $CD4^+$ T cell encounters its cognate tissue-derived antigen in the draining lymph nodes. Migration to the intestine requires acquisition of gut-homing markers such as CD103, possibly mediated by migratory DC in the mesenteric lymph nodes, which produce TGFβ and retinoic acid (RA) (*131-137*). The activated cells then travel to the lamina propria of the small intestine and finally the epithelium (*130, 137-140*). The final step in the acquisition of the IEL phenotype likely occurs once the cells have reached the epithelium (*128*). There, the transcription factors T-bet and Runx-3 are induced, while the master regulator of the T-helper lineage, Thpok is lost (*130, 139, 141*). *In vitro*, naïve $CD4^+$ T cells can be converted to $CD4^+CD8\alpha\alpha^+$ IELs in the presence of RA, TGFβ, IFNγ and their cognate antigen (*141*). The exact mechanism responsible for this remarkable imprinting *in vivo* remains to be defined.

IFNγ is another factor that is essential for the development of $CD4_{IELs}$, as IFNγR-deficient mice show a sharp decrease in the frequency of $CD4_{IELs}$ (*141*). *In vitro*, the T-bet inducing cytokine IL-27 promotes the differentiation of $CD4_{IELs}$, similarly to IFNγ. While IL-27 is not required *in vivo* for development of $CD4_{IELs}$, localized production of IL-27 by the engineered commensal *L. lactis* promotes the production of IL-10 by $CD4_{IELs}$ (*141, 142*). $CD4_{IELs}$ can also develop from pTregs through loss of Foxp3 expression after having settled in the epithelium (*128, 143*).

The nature of the antigens recognized by $CD4_{IELs}$ is currently unknown. Germ-free mice show few $CD4_{IELs}$, while their frequency increases with age in SPF mice. Microbial antigens and/or other microbial components may therefore be important for their development (*139, 144-148*). In contrast to peripheral T cells, IELs, including $CD4_{IELs}$,

appear to have a restricted TCR repertoire (*149-157*). This suggests that a limited number of antigens may be sufficient to shape this compartment. Regardless of antigen specificity, secretion of indole derivates by *L. reuteri* promotes $CD4_{IELs}$ development in a TCR-independent manner, via the aryl-hydrocarbon receptor (AHR) (*151*). However, this process only occurs in the presence of a normal microbiota, suggesting that these small molecules are not sufficient for the development of $CD4_{IELs}$.

Tr1 cells

T regulatory type 1 (Tr1) cells are a T cell subset also important for maintenance of homeostasis in the gut. While their suppressive capability is established both *in vitro* and *in vivo*, their phenotype is still poorly characterized. Like Tregs, these cells require activation by their cognate antigen to exert their function (*158*). Defects in the frequency or function of Tr1 cells was shown in different models of autoimmune and inflammatory diseases (*159*). Tr1 cells can be generated *in vitro* under conditions of chronic activation in the presence of Interleukin-10 (IL-10) (*160*). *In vivo*, these cells produce high levels of IL-10 and appear short-lived. I address the reader to an excellent review for further information (*161*).

1.7 Mechanism of suppression by Tregs and $CD4_{IELs}$

Tregs

Despite the importance of Tregs in imposition of peripheral tolerance, the molecular mechanism(s) of suppression involved remain incompletely understood and somewhat controversial (*162*). Tregs can suppress the function of multiple cell types, including B cells, NKT cells, NK cells, $CD4^+$ and $CD8^+$ T cells, monocytes and dendritic cells. Several mechanisms have been described including cell-to-cell- (i.e in the absence of APC), contact-dependent- or independent-suppression, as well as through the intermediate of APCs. Instead of relying on a single, universal strategy to suppress cells, Tregs seem to leverage a variety of mechanisms, alone or in combination, depending on the context (Fig. 1.4). Regardless of the mechanism used, Tregs need to be activated by their

cognate antigen to become suppressive (*163-167*). Once activated, Tregs can suppress T cells independently of their antigen leading to “bystander-suppression” (*168, 169*).

Cytolysis

One strategy used by Tregs to suppress immune responses is via cell killing of effector T cells using granzyme-B (Gzm-B) or granzyme A (Gzm-A) (*170, 171*), important, for example, to maintain transplant tolerance (*172*).

Metabolic disruption

Tregs can also create an environment that disfavors T cell proliferation. Cyclic AMP (cAMP) is a potent repressor of T cell proliferation. Tregs produce high levels of intracellular cAMP, which can be delivered to the cytoplasm of target cells via gap junctions (*173*). Additionally, Tregs can repress T cell functions by generating high levels of extracellular adenosine. CD39/CD73 present on the surface of Tregs can convert extracellular ATP into adenosine. Adenosine in turn binds to adenosine receptor 2A (A_{2a}) on effector T cells, leading to repression of their function (*174-176*). Tumors maintain high levels of adenosine in their microenvironment (*177, 178*). Mice deficient for A_{2A} show enhanced elimination of tumors compared to WT mice (*178*). Tregs maintain surface expression of CD25, the α subunit of the $\alpha\beta\gamma$ high-affinity IL-2 receptor. Surrounding Tregs are deprived of IL-2, a cytokine essential for T cell survival. This scavenging of IL-2 leads to apoptosis of the target cell (*179*).

Inhibitory cytokines

Tregs also express cytokines, either membrane-bound or secreted, that can suppress other immune cells. TGF-β can be produced in large amounts by Tregs and in so doing suppress T cell proliferation *in vitro* (*180*). Mice deficient in TGF-β develop T cell-mediated autoimmunity (*181, 182*). IL-10 is another cytokine produced by Tregs, important for their suppressive activity. Indeed, IL-10-deficient Tregs fail to maintain homeostasis in a T cell transfer-induced colitis models (*183*). IL-35 is a cytokine central to Treg cell function,

including the control of T cell proliferation (*184*). This cytokine is preferentially expressed by Tregs, upregulated on cells with suppressive activity and required for maximal suppression by Tregs (*185, 186*). Deficiencies in either of the IL-35 chains reduces Treg function *in vitro* and in IBD models *in vivo* (*187*).

Suppression by targeting APCs

An alternative strategy used by Tregs to exert suppression is by their action on antigen presenting cells (APCs). Intravital microscopy showed that Tregs form long-lasting interactions with DCs upon entry into lymph nodes. This in turn impairs the ability of effector T cells to be activated by DCs (*188*). Tregs could thus affect T cell responses by acting directly on APCs.

Expression of key checkpoint molecules such as CTLA-4 on Tregs could account for this property. Treg-specific deficiencies in expression of CTLA-4 leads to spontaneous fatal autoimmune diseases, underlining the importance of CTLA-4 for Treg function (*189*). Interaction between CTLA-4 and DCs stimulates them to produce indoleamine 2,3-dioxygenase (IDO), an enzyme that catabolizes tryptophan. Starvation of T cells in the absence of tryptophan prevents T cell proliferation and may eventually lead to T cell apoptosis (*190*). The presence of the tryptophan metabolite kynurenine also favors expansion of Tregs, presumably by activation of AHR (*191*). CTLA-4 similarly promotes downregulation of costimulatory molecules CD80 and CD86 on DCs, negatively affecting their ability to activate T cells (*192*).

LAG-3 is a checkpoint molecule involved in Treg function. LAG-3 is expressed on the surface of Tregs and binds to MHCII with high affinity, affecting the maturation and ability of DCs to activate T cells (*193*). LAG-3 deficiency or blockade reduces Treg functions, while ectopic expression of LAG-3 confers regulatory properties to $CD4^+$ T cells (*194*). Other checkpoint molecules present on Tregs, such as induced costimulatory molecule (ICOS), have been investigated for their suppressive function. Their role is less apparent than the examples cited (*195, 196*).

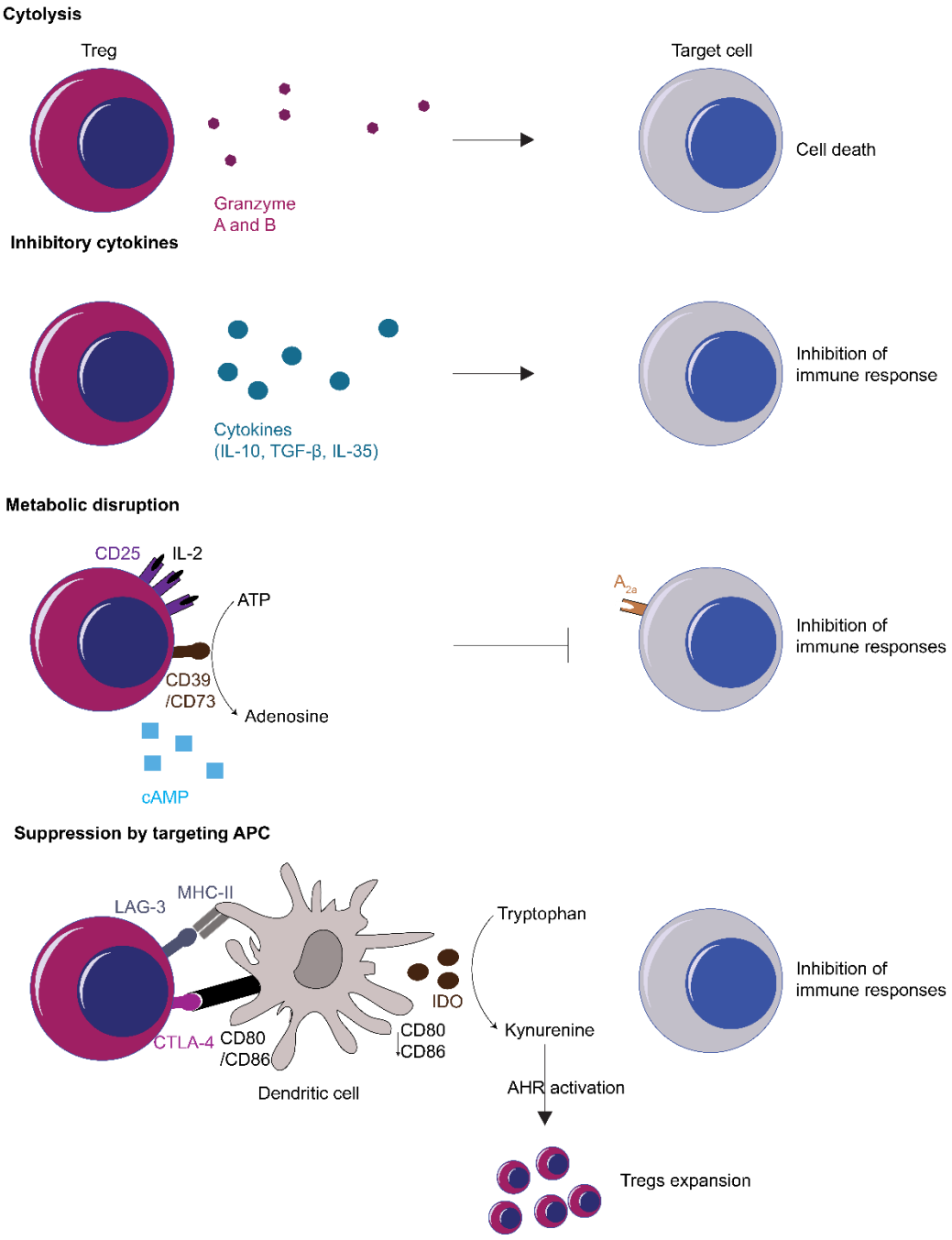

Figure 1.4 Mechanisms of suppression by regulatory T cells.

Tregs can suppress T conventional cells using a range of strategies. Tregs can induce cell death in effector cell via secretion of granzymes. Alternatively, Tregs can secrete immunosuppressive cytokines (IL-10, TGF-β and IL-35), starve effector T cells by scavenging IL-2, produce high levels of adenosine and cAMP, which suppress effector T cells. Finally, Tregs can act indirectly on effector cells by promoting downregulation of co-stimulatory molecules on dendritic cells (DCs). Tregs also promote production of indoleamine 2,3-dioxygenase (IDO) by DCs, which catabolizes tryptophan into AHR ligands, which in turn promote Tregs expansion.

CD4$_{IELs}$

The mechanisms used by Tregs to prevent inflammation have been extensively studied, but the strategies used by CD4$_{IELs}$ are less clear. This is hardly surprising, given that the role of CD4$_{IELs}$ in intestinal homeostasis has been appreciated only recently. CD4$_{IELs}$ display a regulatory cytokine signature, including the expression of IL-10, TGF-β and IFN-γ (*138, 142*). RNAseq analysis showed that CD4$_{IELs}$ also express high levels of Gzm-A and Gzm-B (*143*). Upon reaching the epithelium, precursors of CD4$_{IELs}$ increase production of IL-10 (*138*). IL-10 is not required for development of CD4$_{IELs}$ but seems essential for their anti-inflammatory role in the intestine (*138*). Remarkably, IL-10 produced by CD4$_{IELs}$ and other cells in the small intestine can protect against inflammation in the colon (*138, 197, 198*).

1.8 TCR-independent modulation of T cell responses by commensals

The action of the immune system at mucosal surfaces is achieved through coordination of a complex set of cells and signaling networks. T cells can adopt different effector fates. The differentiation into each of these fates depends on environment, context and type of antigen(s) recognized (*23*). Specific microbes and pathogens likewise can skew the differentiation of immune cells towards specific fates (*23, 66, 97, 199*). However, the signals, molecules and pathways used by microbes in these processes are still poorly understood. In the following I will summarize current knowledge about TCR-dependent and independent mechanisms.

Clostridium species promote the development of both mucosal and systemic Tregs via induction of TGF-β by epithelial cells (*97, 112, 200*). Similarly, mice colonized with the Altered Schaedler Flora (ASF) show *de novo* generation and activation of pTregs, which in turn prevent immune deviation towards more inflammatory responses (*98*). It is unclear whether these responses are antigen-specific or not. Colonization with the probiotic *Bifidobacterium breve* promotes the development of IL-10 producing Tr1 cells and improves intestinal pathology in a colitis model while *B. longum* and *B.bifidum* promote Tregs development (*201-203*). Monocolonization of germ-free mice with *Bacteroides*

species boosts the frequencies of both tolerogenic pDC and pTregs (*204*). Tolerogenic pDcs and intestinal epithelial cells produce the enzyme Indoleamine 2,3-dioxygenase-1 (IDO) which promotes the development of pTregs in response to the gut microbiota (*97, 205, 206*). In turn, Tregs promote IDO expression in DCs via CTLA-4-B7-1 and -2 interaction thus essentially acting as a tolerogenic positive feedback loop (*190, 207*).

Microbes can shape the immune system by secretion of metabolites. Natural products produced by the microbiota are abundant and their concentrations can be equivalent or even higher than a typical drug dose (10uM-1mM) (*208*). Short chain fatty acids (SCFAs) produced by commensal microbes are some of the most abundant compounds secreted by microbes (*209*). SCFAs are released by anaerobic commensals when they ferment dietary carbohydrates that their host cannot digest. Typical SCFAs produced are acetate, propionate, and butyrate. Acetate and propionate are usually produced by *Bacteroidetes*, whereas *Firmicutes* generate most of the butyrate (*210, 211*). Besides their use as an energy source for the host, these molecules can be sensed by host receptors and modulate the immune system. A number of receptors specific for SCFAs have been described, including PPARγ, GPR109a, GPR41 and GPR43 (*72, 212-216*). PPARγ is a receptor essential for the protective effect of Tregs against T-cell induced colitis (*217*). Activation of PPARγ by a synthetic ligand is also protective against intestinal inflammation, in the dextran sulphate induced-colitis model (*218*). SCFA can also bind to the butyrate receptor GPR109a on macrophages and DCs to promote expression of IL-10 and aldehyde dehydrogenase (ALDH), which catabolizes vitamin A into retinoic acid (RA) (*72*). Secretion of RA by APC upregulates gut homing markers such as CD103 by pTregs (*134, 219*). GPR109a-deficient mice are prone to develop colonic inflammation and colon cancer (*213*). SCFA can also act directly on Foxp3 expression in T cells by repression of histone deacetylase (HDAC), thereby inducing Tregs differentiation and accumulation (*220, 221*).

Secretion of polysaccharide A (PSA) by *B. fragilis* via outer membrane vesicles (OMVs) expands Tregs and enhances their function in a TLR2-dependent manner (*222-224*). PSA is part of a larger family of molecules known as capsular zwitterionic polysaccharides (ZPSs), which can activate $CD4^+$ T cells in complex ways (*225-227*). Screening for

predicted ZPS operons in bacterial genomes identified a long list of commensals, some already associated with anti-inflammatory responses (*228*). Crude lysates from *P. distasonis*, and in particular membrane fractions, reduced intestinal inflammation in dextran sulphate sodium (DSS) colitis model and increased the frequency of Tregs in the mesenteric lymph nodes (*229*). *P. distasonis* is also recognized by a colonic Treg TCR, suggesting that its anti-inflammatory capacity might be both TCR-dependent and independent (*34*). Similarly, the most abundant member of the ASF (see above), *P. goldsteinii* (also referred to as ASF519), is predicted to produce ZPS, suggesting that the increased frequency of Tregs observed in ASF-colonized mice could be due to ZPS molecules from *P. goldsteinii* (*98, 228*). Neff and colleagues also identified *C. ramosum* and *C. symbiosum* as two potent producers of ZPS, both of which belong to the consortium of *Clostriums* shown to induce Tregs (*112*) (*228*).

In addition to the mechanisms described above, A number of isolated or consortiums of commensals can influence T cell fate in the gut. I direct the readers to excellent reviews for more information (*221, 230, 231*).

1.9 Antigen-specific T cell responses to commensals

Although the intestinal microbiota contains a vast diversity of species, only a handful of microbes have been shown to modulate the immune system. What is probably even more remarkable is the specificity with which these microbes modulate the immune system. Littman and colleagues pioneered this work by showing that Segmented Filamentous Bacteria (SFB) induced quasi-clonal Th17 cells in an antigen-specific manner (*232*). *Helicobacter spp.* induce antigen-specific colonic RORγt^{+} Tregs, further extending this concept (*26, 35*). *K. pneumoniae* from the oral cavity induces antigen-specific Th1 response in the colon after antibiotics treatment (*233*). Strains of *Staphylococcus epidermidis* induce specific and long-lasting CD8^{+} T cell response in the skin restricted by non-classical Class I MHC products (*234*) . The mucus-degrading bacterium *A. muciniphila* promotes the differentiation of Tfh and commensal-specific IgG1 (*235*). Therefore, specific commensal bacteria can reprogram a population of immune cells and thereby induce long-lasting and specific modulation of the immune response.

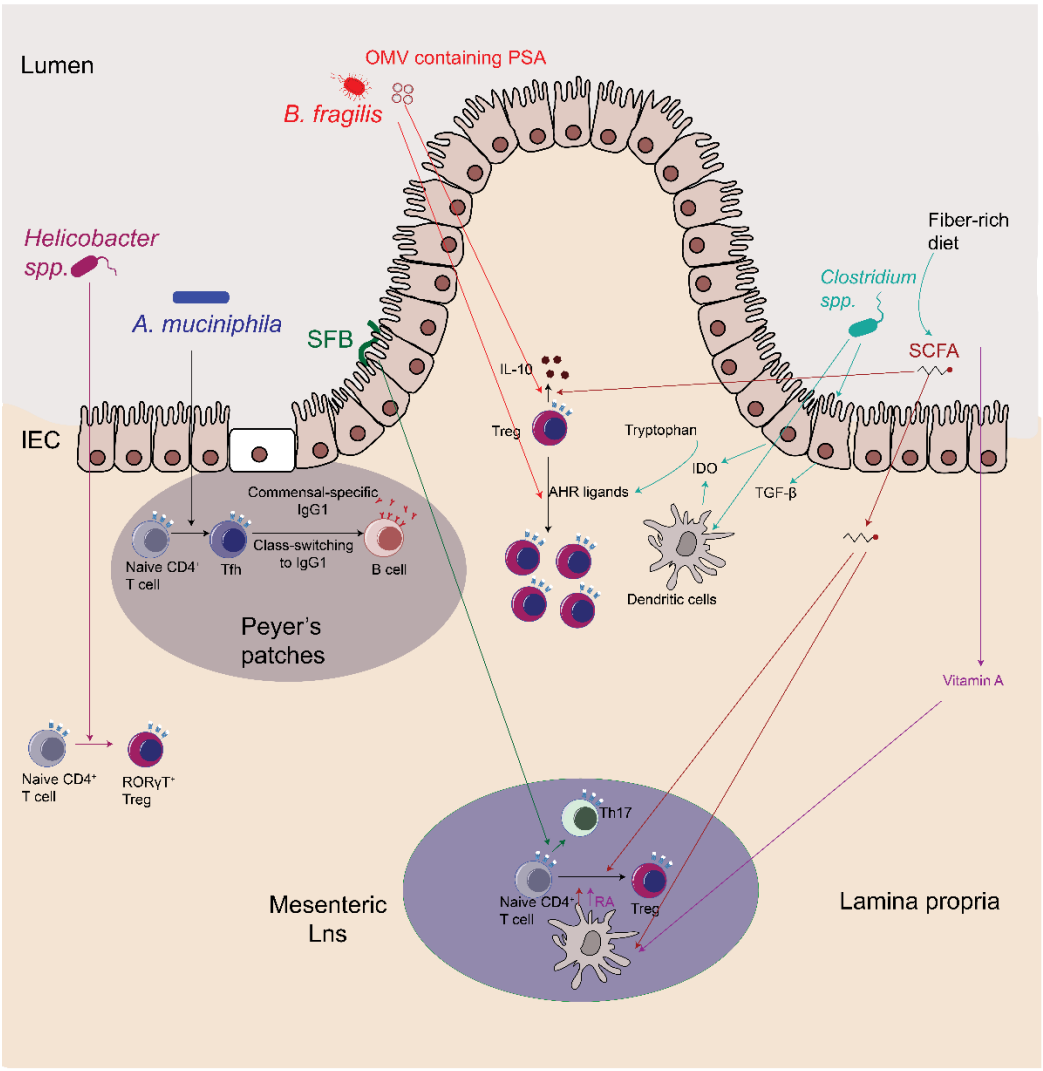

Figure 1.5 Antigen-specific and non-specific CD4⁺ T cell responses to commensals in the intestine.

(Left to right) *Helicobacter spp.* promote antigen-specific development of RORγT⁺ Tregs in the colonic lamina propria. The mucus-digesting commensal *A. muciniphila* promotes the secretion of commensal-specific IgG1 secretion via development of T follicular helper (Tfh) in the Peyer's patches. SFB induces the development of quasi-clonal Th17 cells in the small intestine, while outer-membrane vesicle containing polysaccharide A (PSA) from *B. fragilis* stimulates Treg expansion and IL-10 secretion. *Clostridium spp.* support the generation of peripheral Tregs (pTregs) via creation of a niche which favors their development by stimulating intestinal epithelial cells (IEC) and dendritic cells (DCs) to secrete TGF-β and indoleamine-2,3-dioxygenase (IDO), which degrades tryptophan into aryl hydrocarbon (AHR) ligands. These ligands in turn promote Treg expansion. The degradation of dietary fibers in short-chain fatty acids (SCFA) by *Clostridiums spp.* and others also enhances Tregs functions via stimulation of IL-10 secretion and Tregs expansion. SCFA can also act on DCs by binding to the G-protein-coupled receptor (GPR)109a and induce the expression of aldehyde dehydrogenase (ALDH), which catabolizes vitamin A into retinoic acid (RA). In addition, SCFA can repress histone deacetylase (HDACi) and thereby suppress the expression of pro-inflammatory cytokines. RA acquired from dietary vitamin A enhances Treg selection via induction of their master regulator, Foxp3 or via repression of effector cytokines by effector T cells.

1.10 tools to study immune-microbiota interactions

The previous section of this chapter highlighted how certain members of the microbiota exert strong effects on the immune system. The complexity of the microbiome and our current limited knowledge, elicits the question of how we can control, define and standardize microbiome studies in order to build more robust and representative models. Additional factors such as diet have profound effects on composition of the microbiota (*55, 236, 237*). In turn, diet affects metabolism of both host and the intestinal microbes, which are intimately interconnected (*238, 239*). The properties of many animal models are influenced by the microbiome. For instance, Experimental autoimmune encephalomyelitis (EAE) and arthritis disease models are affected by presence of SFB (*240, 241*). *Helicobacter spp.* drive colitis in immunocompromised animals (*242-246*). Beyond these examples, the microbiota impacts animal models of autoimmunity, cardiovascular disease, behavior, obesity, metabolic syndrome and tumorigenesis (*40, 247-252*).

Germ-free and gnotobiotic animals

A key tool in the study of host-microbiome interaction is the development of germ-free (GF) animals. Unlike normal rodents, GF animals are devoid of microbes (*253, 254*). GF mice are obtained by aseptically harvesting pups from the womb of their mothers by cesarean section. The pups are transferred to a sterile isolator where they are kept GF, or to be colonized with a single microbe or a defined set of microbes, such as the altered Schaedler flora (ASF) (*255, 256*). Gnotobiotic mice are therefore born GF and then colonized.

Because each condition requires a dedicated isolator (+/- microbiota for example), studies that seek to control multiple variables quickly become impracticable. Possible contamination is a problem. Isolators must be monitored regularly using a combination of different techniques (*100*). Only a limited number of strains are commercially available. Each new mouse strain to be studied will need to be rederived under GF conditions in the investigator's facility, thus reducing the number of genotypes that are practicable for study

(*100*). The use of gnotobiotic mice comes with yet other caveats. GF mice have underdeveloped immune system (see above) and colonization of adult GF mice with microbes may lack proper microbial exposure at essential stages of development. Reconstitution of GF mice with human or rat flora does not accurately recapitulate SPF mice. Indeed, gnotobiotic mice maintain an immature immune system. The microbiota thus imposes host-specific features on the immune system is (*257*).

Antibiotic treatment of mice

The use of GF animals is not always a practicable option. An alternative possibility is to use broad-spectrum antibiotics to deplete commensals and then recolonize them with a defined flora or with a single bacterial species. Antibiotic treatment is cheaper, does not require special equipment and can be used with any genotype (*100*). Antibiotics are usually provided ad libitum in the drinking water or by gavage. Nonetheless, antibiotic treatment can leave residual (antibiotic-resistant) bacteria, affect host cells or create an environment favorable for the outgrowth of fungal species (*258*). The unpleasant taste associated with certain antibiotics (i.e. metronidazole) when present in the drinking water may alter the daily consumption of water by the mice and lead to dehydration (*259*). Finally, antibiotic-treated mice have produced confounding findings due the variability in initial bacterial composition, the antibiotic cocktails used and duration of treatment (*100*). These different parameters must be weighed when deciding on the right procedure for a given experiment.

Commensal-specific CD4$^+$ T cell models

Unraveling the complexity of the interactions between the microbiota and the immune system has been difficult due to the limited number of available experimental models (Table 1.2). The first commensal-specific CD4$^+$ T cell model was generated to recognize the flagellin protein CBir-1 from *Clostridium* subphylum cluster XIVa (*260*). Flagellin is an immunodominant antigen recognized by T cells derived from both IBD patients and mouse models of colitis (*261*). This model has been useful for our understanding of the role of IgA in controlling mucosal homeostasis. In the CBir model, commensal-specific

Tregs promote class-switching and secretion of antigen-specific IgA (*260*). At steady state, CBir T cells do not usually proliferate in the intestine of mice colonized with *Clostridia*, even when the antigen is gavaged (*260*). In the absence of IgA, CBir-specific T cells proliferate both mucosally and systemically (*260*). Disruption of the mucosa by infection with *T. gondii* also allows proliferation and long-term survival of Th1 and Th17 CBir T cells in the intestine (*262*). The CBir model improved our understanding of commensal-specific responses in colitis development. Adoptive transfer of CBir-specific T cell into immunodeficient hosts colonized with *Clostridia* induces severe colitis (*261, 263*). Both innate and TCR-specific responses are required for colitis to develop (*263*). Th17 Cbir cells appear more potent at inducing colitis than Th1 cells (*264*). This model revealed the role of $MHCII^+$ ILC3s in controlling the frequency of activated commensal–specific T cells (*265*). Overall, the Cbir model was instrumental in our understanding of T cell recognition of microbial antigens at steady state and their role in the induction of intestinal inflammation.

Analysis of the antigen specificity of Th17 cells showed that most Th17 cells recognize antigens derived from SFB, a potent inducer of Th17 cells in mice (*232, 266*). Development of the transgenic line 7B8Tg, which expresses a TCR cloned from a SFB-specific Th17 cell, allowed the study of the development and behavior of commensal-specific Th17 cells (*232*). Transferred naïve 7B8Tg $CD4^+$ T cells develop into Th17 in the SiLP of mice colonized with SFB but are also present in the spleen. The presence of recirculating SFB-specific Th17 cells in the spleen could explain why SFB exacerbates autoimmune diseases (*240, 241*). The development of 7B8Tg T cells into Th17 cells can be modified. Expression of the 7B8Tg epitope on *L. monocytogenes*, a bacterial pathogen that induces a Th1 response, led to differentiation of 7B8Tg cells into Th1 rather than Th17 T cells. Therefore, the fate of commensal-specific $CD4^+$ T cells is thus dictated by the antigen recognized and by the context in which this antigen is presented.

Studies of the TCR specificity of colonic Tregs supported the notion that at least some colonic Tregs recognize commensals (*34*). Generation of transgenic lines from two of these TCRs, CT2 and CT6, improved our understanding of the behavior of commensal-specific T cells in homeostasis and inflammation (*34, 102*). Unlike the CBir model, which

requires an intestinal insult to allow T cell activation, the CT2 and CT6 TCRs recognize naturally occurring antigens in the colon (*102, 260*). At steady state, the majority of transferred CT2- and CT6-expressing T cells differentiate into RORγT^{+}Foxp3^{+} Tregs in the colonic lamina propria (cLP) (*36*). During inflammation, a large fraction of Th17 CT2 and CT6 T cells are found in the intestine (*35*). Thus, it is conceivable that in the course of inflammation, CT2 and CT6 Th17 cells could arise from RORγT^{+}Foxp3^{+} Tregs (*36*). Both of these TCRs recognize *Helicobacter* species, a common group of pathobionts found across SPF colonies around the globe (*35, 267*). Adoptive transfer of peripheral T cells transduced with CT2 or CT6 TCR into lymphopenic hosts leads to the development of colitis (*34*). These two models have highlighted the sometimes ambivalent role of commensal-specific T cells. At steady state, pathobiont-specific T cells contribute to homeostasis, while during inflammation they can worsen tissue damage and disease.

Echoing the results found by Hsieh and colleagues, the lab of Dan Littman developed two other *Helicobacter*-specific transgenic lines that recognize *H. hepaticus* (HH5-1tg and HH7-2tg) (*26*). Like CT2 and CT6, HH5-1tg and HH7-2tg cells develop into RORγT^{+}Foxp3^{+} Tregs in the cLP of healthy mice and convert into Th17 cells under inflammatory conditions in IL-10 knock-out (KO) mice. Building on these findings, they showed that commensal-specific pTregs were better at suppressing intestinal inflammation than polyclonal Tregs. This observation is important and provides a possible explanation why tissue homeostasis requires both commensal-specific pTregs and thymus-derived Tregs.

As a complement to the transgenic models described above, our lab developed a microbiota-specific T cell mouse model, cloned from a pTreg present in the mesenteric lymph node using somatic cell nuclear transfer (see below) (*143*). Transnuclear T cells (TN cells) harboring this TCR differentiate into both pTregs in the mesenteric lymph nodes and into CD4$_{\text{IELs}}$ in the small intestine in a microbiota-dependent fashion. Like nTregs, decreased intraclonal competition is required for pTreg but not CD4$_{\text{IELs}}$ development. Notwithstanding large numbers of TN CD4$_{\text{IELs}}$ and high levels of IFNγ did not lead to intestinal inflammation. A single T cell clone can thus give rise to two distinct non-inflammatory T cell fates: pTregs and CD4$_{\text{IELs}}$, at two distinct intestinal locations.

A recent study from the Barton lab explored the contribution of the microbiota to the induction of commensal-specific IgG1 (*235*). Class switching of B cells to IgG1 depends on T cell help and is therefore absent in TCRβ-deficient mice. Serum IgG1 from healthy WT mice binds to commensals, primarily of the *Akkermansia* and *Bacteroides* genera. Transgenic T cells specific for an *A. muciniphila* antigen (Amuc_RS03735, an outer membrane protein) differentiate mainly into T follicular helper (Tfh) in gnotobiotic mice (ASF + *A. muciniphila*) but can adopt other fates in SPF mice. These findings support the notion that commensal-specific T cell responses are context-dependent in both homeostasis and inflammatory situations.

Another key study in the field of commensal-specific T cell was published this year from the lab of Paul Allen (*268*). The study explored how the diet can affect T cell responses to commensals. They developed a TCR transgenic model specific for an antigen (SusE/F homolog) present in OMVs of *B. thetaiotaomicron*. Importantly, this particular TCR was chosen because the antigen it recognizes is differentially expressed under distinct growth conditions. This allowed to test what is the role of the diet in altering antigen-specific T cell responses. However, it is unclear whether this TCR-antigen pair is naturally-occurring since this TCR was isolated from the spleen of mice immunized with *B. thetaiotaomicron*. Transgenic T cells from this model can differentiate into both Tregs and other T effectors in the spleen and intestine of healthy mice. Depletion of these *B. thetaiotaomicron*-specific Treg population in adoptively-transferred $Rag^{-/-}$ mice leads to colitis. Once the tools become available (see chapter 5), it would be interesting to test whether this antigen is being recognized on OMVs or whole bacteria and how this affects T cell responses in this model.

Models	Commensal(s)	Antigen/Epitope	Differentiation	References
Cbir1	*Clostridium* subphylum cluster XIVa	Flagellin DMATEMVKYS-NANILSQAGQ	Naive under homeostasis, Th1, Th17 under inflammatory conditions	Cong 2009
7B8tg	SFB	SFBNYU_003340 FSGAVPNK	Th17	Yang 2014
1A2tg		SFBNYU_003340 QFSGAVPNK		
5A11tg		SFBNYU_004990 IRWFGSSVQ		
CT2	H. typhlonius	Unknown	RORγT+Foxp3+ Tregs, Th17 under inflamma-tory conditions	Lathrop 2011, Chai 2017
CT6	*H. apodemus*, *Clostridium spp.**	Unknown		
HH7-2tg	*H. hepaticus*	HH_1713, QESPRIAAAYTIKGA	RORγT+Foxp3+ Tregs, Th17 under inflamma-tory conditions	Xu 2018
HH5-1tg		HH_1713, GNAYISVLAHYGKNG		
TN	*Bacteroidetes*	β-N-acetylhexosamindase YKGSRVWLN	pTregs, $CD4_{IELs}$	Bilate 2016, Bousbaine unpub.
Amuc124	*A. muciniphila*	Amuc_RS03735	Tfh in PPs, Tfh, Treg, Th1, Th17 in SiLP	Ansaldo 2019
BθOM	*B. thetaiotaomicron*	BT4295, EEFNLPTTNGGHAT	Treg, RORγT+Foxp3+ Tregs and other T effector	Wegorzewska 2019
DP1	*B.vulgatus**, *B.acidifaciens**	Unknown	Unknown	Chai 2017, Lathrop 2011

Table 1-2 Commensal-specific $CD4^+$ T cell models

*Shown *in vitro* but not *in vivo*.

MHC Tetramers

In addition to antigen-specific T cell models (see above), the development of reagents that can visualize, quantify and help isolate antigen-specific T cells has revolutionized our understanding of T cell biology. In contrast to antigen-specific B cells, which can be tracked with a fluorescent protein or biotinylated protein/peptide antigen, identification of

antigen-specific T cells requires the use of peptide-loaded MHC reagents of the appropriate specificity. Because the affinity of an individual peptide MHC complex for the αβTCR is fairly low (micromolar range), the use of multivalent MHC molecules is required to detect antigen-specific T cells (*269*) through the gain in avidity afforded by these multivalent interactions. While production of MHCI tetramers is relatively easy, MHCII tetramers are far more challenging to produce (*270*). Technological advances in the production of MHCII tetramers, combined with enrichment strategies, have enabled the enumeration and isolation of antigen-specific $CD4^+$ T cells from healthy WT mice (*271*). Even though there are only few examples in the literature, without a doubt the study of commensal-specific T cells will benefit from this powerful technology (*26, 232, 235, 262, 272, 273*).

1.11 Transnuclear models to study specific immune cell types

Transgenic mouse models have revolutionized the study of T and B cells. In these models, a fixed, pre-rearranged TCR or BCR is expressed as a transgene. Lymphocytes isolated from transgenic mice serve as a source of mostly monoclonal lymphocytes of defined specificity. These models were used to lay the foundations for our understanding of development, selection, and allelic exclusion (see below) of T cells. They have similarly served to create models of autoimmune diseases (*274-286*). Likewise, the study of B cell development, anergy and BCR activation has greatly benefited from these models (*287-293*). More recently, somatic cell nuclear transfer (SCNT) was used in our lab and that of others as an attractive alternative to transgenesis to develop B cell, $CD4^+$ (including nTreg and pTregs) and $CD8^+$ T cell, invariant NK T cell (iNK T cell) as well as NK cells models (*143, 292, 294-304*).

Allelic exclusion is the process by which expression of a TCR or BCR prevents subsequent rearrangement and expression of a second antigen-receptor derived from the second receptor allele. This process ensures that a given B or T cell expresses one and only one antigen receptor. Because allelic exclusion is incomplete, transgenic mouse models are usually placed on a RagKO background to prevent secondary rearrangements and thus ensure that a single TCR or BCR is expressed.

SCNT is a technique in which the nucleus from a donor cell is transplanted into an enucleated oocyte. Upon chemical activation, these oocytes can differentiate into blastocysts. Their inner cell mass can serve as a source of embryonic stem cells (ESCs) for injection into blastocysts. ESCs are first expanded *in vitro* and then injected into multiple blastocysts. Pups born from these blastocysts will be chimeric for the V(D)J rearrangements of the donor lymphocyte and must be back-crossed to WT mice. Only chimeras that carry the donor nucleus V(D)J rearrangement in their germ cells will to transmit the sought-after allele. Direct implantation of the original blastocyst obtained by nuclear transfer, which avoids the chimera stage, is very inefficient and therefore generation of an ESC line from such blastocysts is preferred to preserve the product of a successful SCNT. This process is fast: it requires only about 6 weeks from injection of the nucleus to the birth of the chimeric mouse (*305*) and does not involve any manipulation of DNA, as would be required to make knock out or gene-targeted mice.

The first lymphocyte SCNT was performed by Hochedlinger and Jaenisch. They demonstrated that terminally differentiated lymphocytes can be reprogrammed into totipotent stem cells (*306*). Mice born through this procedure contained the characteristic V(D)J rearrangements from the donor cell in all somatic cells. Because $Rag2^{-/-}$ mice do not have any mature lymphocytes, injection of ESCs derived by SCNT from a lymphocyte complements this phenotype and all mature lymphocytes in the resulting chimaera are derived from the donor cell (*307*). Both T and B cells can be used as donor cells for this procedure (*306*). This technology was then used to not only demonstrate the reprogramming capacity of somatic cells but also for the generation of mice with antigen-receptors of known specificity.

We and others have used this technique extensively to develop antigen-specific models (Table 1.3). In chapters two and three, we describe how we used this strategy to develop the first commensal-specific transnuclear mouse model of known specificity (*143*).

Cell type	Nickname	Antigen	Donor cell	References
B cells	OB1	Ovalbumin	OVA-specific splenic IgG1 B cell	Dougan 2012
	FluB1	HA from Influenza	HA-specific Splenic IgG2b B cell	Dougan, Ashour 2013
$CD8^+$ T cells	T57-, G4- and R7-TN	T57, G4 and R7 from *Toxoplasma gondii*	CD8+ T cells specific for T57, G4, or R7	Kirak 2010
	TRP-$1i^{high}$ and TRP-1^{low}	Tumor TRP-1	TRP-1-specific CD8+ T cell	Dougan 2013
	ORF8 TN	Mouse γ-herpes virus ORF68	MHV-68-specific CD8+T cells	Sehrawat 2012
$CD4^+$ T cells	TN	β-N-acetylhexosamindase from *Bacteroidetes*	Naturally-occuring MsLN pTreg	Bilate 2016, Bousbaine unpub.
	T138	Unknown	Naturally-occuring splenic nTreg	Ku 2016
	Df (multiple)	*Dermatophagoides farinae*	*D. farinae*-specific $CD4^+$ T cells	Kaminuma 2017
	Der p1 (multiple)	*Dermatophagoides pteronyssinus*	*D. pteronyssinus*-specific $CD4^+$ T cells	Kaminuma 2017
	Der f	Ovalbumin	OVA-specific $CD4^+$ T cells	Kaminuma 2017
iNKT cells	Vα14, Vβ7A, Vβ7C and Vβ8.2	α-GalCer, α-Glc and OCH	Naturally-occuring iNKT cells	Clancy-Thompson 2017
NK cells		Unknown	Naturally-occuring liver NKT cells	Inoue 2005

Table 1-3 Antigen-specific transnuclear mouse models

References

1. D. Artis, Epithelial-cell recognition of commensal bacteria and maintenance of immune homeostasis in the gut. *Nat Rev Immunol* **8**, 411-420 (2008).
2. A. G. Wexler, A. L. Goodman, An insider's perspective: Bacteroides as a window into the microbiome. *Nat Microbiol* **2**, 17026 (2017).
3. R. Sender, S. Fuchs, R. Milo, Are We Really Vastly Outnumbered? Revisiting the Ratio of Bacterial to Host Cells in Humans. *Cell* **164**, 337-340 (2016).
4. J. A. Gilbert *et al.*, Current understanding of the human microbiome. *Nat Med* **24**, 392-400 (2018).
5. H. Jiang *et al.*, Altered fecal microbiota composition in patients with major depressive disorder. *Brain Behav Immun* **48**, 186-194 (2015).
6. P. Zheng *et al.*, Gut microbiome remodeling induces depressive-like behaviors through a pathway mediated by the host's metabolism. *Mol Psychiatry* **21**, 786-796 (2016).
7. G. Sharon *et al.*, Human Gut Microbiota from Autism Spectrum Disorder Promote Behavioral Symptoms in Mice. *Cell* **177**, 1600-1618 e1617 (2019).
8. S. V. Lynch, O. Pedersen, The Human Intestinal Microbiome in Health and Disease. *N Engl J Med* **375**, 2369-2379 (2016).
9. A. D. Kostic *et al.*, Fusobacterium nucleatum potentiates intestinal tumorigenesis and modulates the tumor-immune microenvironment. *Cell Host Microbe* **14**, 207-215 (2013).
10. D. N. Frank *et al.*, Molecular-phylogenetic characterization of microbial community imbalances in human inflammatory bowel diseases. *Proc Natl Acad Sci U S A* **104**, 13780-13785 (2007).
11. D. Gevers *et al.*, The treatment-naive microbiome in new-onset Crohn's disease. *Cell Host Microbe* **15**, 382-392 (2014).
12. N. K. Surana, D. L. Kasper, Moving beyond microbiome-wide associations to causal microbe identification. *Nature* **552**, 244-247 (2017).
13. S. R. Gill *et al.*, Metagenomic analysis of the human distal gut microbiome. *Science* **312**, 1355-1359 (2006).
14. Y. Belkaid, Regulatory T cells and infection: a dangerous necessity. *Nat Rev Immunol* **7**, 875-888 (2007).
15. R. M. Maizels, K. A. Smith, Regulatory T cells in infection. *Adv Immunol* **112**, 73-136 (2011).
16. C. Janeway. (Garland Science,, New York, 2005).
17. A. Iwasaki, R. Medzhitov, Control of adaptive immunity by the innate immune system. *Nat Immunol* **16**, 343-353 (2015).
18. F. W. Alt *et al.*, VDJ recombination. *Immunol Today* **13**, 306-314 (1992).
19. P. Mombaerts *et al.*, RAG-1-deficient mice have no mature B and T lymphocytes. *Cell* **68**, 869-877 (1992).
20. K. P. Lam, R. Kuhn, K. Rajewsky, In vivo ablation of surface immunoglobulin on mature B cells by inducible gene targeting results in rapid cell death. *Cell* **90**, 1073-1083 (1997).
21. M. T. Heemels, H. Ploegh, Generation, translocation, and presentation of MHC class I-restricted peptides. *Annu Rev Biochem* **64**, 463-491 (1995).
22. P. R. Wolf, H. L. Ploegh, How MHC class II molecules acquire peptide cargo: biosynthesis and trafficking through the endocytic pathway. *Annu Rev Cell Dev Biol* **11**, 267-306 (1995).
23. R. J. Boyton, D. M. Altmann, Is selection for TCR affinity a factor in cytokine polarization? *Trends Immunol* **23**, 526-529 (2002).
24. V. Brucklacher-Waldert, E. J. Carr, M. A. Linterman, M. Veldhoen, Cellular Plasticity of CD4+ T Cells in the Intestine. *Front Immunol* **5**, 488 (2014).

25. C. Ohnmacht *et al.*, MUCOSAL IMMUNOLOGY. The microbiota regulates type 2 immunity through RORgammat(+) T cells. *Science* **349**, 989-993 (2015).
26. M. Xu *et al.*, c-MAF-dependent regulatory T cells mediate immunological tolerance to a gut pathobiont. *Nature* **554**, 373-377 (2018).
27. H. Wardemann *et al.*, Predominant autoantibody production by early human B cell precursors. *Science* **301**, 1374-1377 (2003).
28. R. Pacholczyk, H. Ignatowicz, P. Kraj, L. Ignatowicz, Origin and T cell receptor diversity of Foxp3+CD4+CD25+ T cells. *Immunity* **25**, 249-259 (2006).
29. C. S. Hsieh *et al.*, Recognition of the peripheral self by naturally arising CD25+ CD4+ T cell receptors. *Immunity* **21**, 267-277 (2004).
30. J. Wong *et al.*, Adaptation of TCR repertoires to self-peptides in regulatory and nonregulatory CD4+ T cells. *J Immunol* **178**, 7032-7041 (2007).
31. J. M. Tas *et al.*, Visualizing antibody affinity maturation in germinal centers. *Science* **351**, 1048-1054 (2016).
32. N. Chaudhary, D. R. Wesemann, Analyzing Immunoglobulin Repertoires. *Front Immunol* **9**, 462 (2018).
33. D. R. Wesemann *et al.*, Microbial colonization influences early B-lineage development in the gut lamina propria. *Nature* **501**, 112-115 (2013).
34. S. K. Lathrop *et al.*, Peripheral education of the immune system by colonic commensal microbiota. *Nature* **478**, 250-254 (2011).
35. J. N. Chai *et al.*, Helicobacter species are potent drivers of colonic T cell responses in homeostasis and inflammation. *Sci Immunol* **2**, (2017).
36. B. D. Solomon, C. S. Hsieh, Antigen-Specific Development of Mucosal Foxp3+RORgammat+ T Cells from Regulatory T Cell Precursors. *J Immunol* **197**, 3512-3519 (2016).
37. T. Yatsunenko *et al.*, Human gut microbiome viewed across age and geography. *Nature* **486**, 222-227 (2012).
38. M. Fulde, M. W. Hornef, Maturation of the enteric mucosal innate immune system during the postnatal period. *Immunol Rev* **260**, 21-34 (2014).
39. N. Kamada, G. Y. Chen, N. Inohara, G. Nunez, Control of pathogens and pathobionts by the gut microbiota. *Nat Immunol* **14**, 685-690 (2013).
40. Z. Wang *et al.*, Gut flora metabolism of phosphatidylcholine promotes cardiovascular disease. *Nature* **472**, 57-63 (2011).
41. R. A. Koeth *et al.*, Intestinal microbiota metabolism of L-carnitine, a nutrient in red meat, promotes atherosclerosis. *Nat Med* **19**, 576-585 (2013).
42. W. H. Tang, S. L. Hazen, The contributory role of gut microbiota in cardiovascular disease. *J Clin Invest* **124**, 4204-4211 (2014).
43. P. J. Turnbaugh *et al.*, The effect of diet on the human gut microbiome: a metagenomic analysis in humanized gnotobiotic mice. *Sci Transl Med* **1**, 6ra14 (2009).
44. E. Le Chatelier *et al.*, Richness of human gut microbiome correlates with metabolic markers. *Nature* **500**, 541-546 (2013).
45. J. Qin *et al.*, A metagenome-wide association study of gut microbiota in type 2 diabetes. *Nature* **490**, 55-60 (2012).
46. F. Karlsson, V. Tremaroli, J. Nielsen, F. Backhed, Assessing the human gut microbiota in metabolic diseases. *Diabetes* **62**, 3341-3349 (2013).
47. K. E. Fujimura *et al.*, Neonatal gut microbiota associates with childhood multisensitized atopy and T cell differentiation. *Nat Med* **22**, 1187-1191 (2016).
48. M. C. Arrieta *et al.*, Early infancy microbial and metabolic alterations affect risk of childhood asthma. *Sci Transl Med* **7**, 307ra152 (2015).
49. E. Y. Hsiao *et al.*, Microbiota modulate behavioral and physiological abnormalities associated with neurodevelopmental disorders. *Cell* **155**, 1451-1463 (2013).

50. P. J. Turnbaugh *et al.*, An obesity-associated gut microbiome with increased capacity for energy harvest. *Nature* **444**, 1027-1031 (2006).
51. M. A. Fischbach, Microbiome: Focus on Causation and Mechanism. *Cell* **174**, 785-790 (2018).
52. H. P. Browne *et al.*, Culturing of 'unculturable' human microbiota reveals novel taxa and extensive sporulation. *Nature* **533**, 543-546 (2016).
53. E. A. Rettedal, H. Gumpert, M. O. Sommer, Cultivation-based multiplex phenotyping of human gut microbiota allows targeted recovery of previously uncultured bacteria. *Nat Commun* **5**, 4714 (2014).
54. M. O. Sommer, Advancing gut microbiome research using cultivation. *Curr Opin Microbiol* **27**, 127-132 (2015).
55. A. L. Goodman *et al.*, Extensive personal human gut microbiota culture collections characterized and manipulated in gnotobiotic mice. *Proc Natl Acad Sci U S A* **108**, 6252-6257 (2011).
56. J. C. Lagier *et al.*, Culture of previously uncultured members of the human gut microbiota by culturomics. *Nat Microbiol* **1**, 16203 (2016).
57. J. E. Koenig *et al.*, Succession of microbial consortia in the developing infant gut microbiome. *Proc Natl Acad Sci U S A* **108 Suppl 1**, 4578-4585 (2011).
58. C. Palmer, E. M. Bik, D. B. DiGiulio, D. A. Relman, P. O. Brown, Development of the human infant intestinal microbiota. *PLoS Biol* **5**, e177 (2007).
59. J. J. Faith *et al.*, The long-term stability of the human gut microbiota. *Science* **341**, 1237439 (2013).
60. P. J. Turnbaugh *et al.*, A core gut microbiome in obese and lean twins. *Nature* **457**, 480-484 (2009).
61. M. Wlodarska, A. D. Kostic, R. J. Xavier, An integrative view of microbiome-host interactions in inflammatory bowel diseases. *Cell Host Microbe* **17**, 577-591 (2015).
62. E. Bianconi *et al.*, An estimation of the number of cells in the human body. *Ann Hum Biol* **40**, 463-471 (2013).
63. J. Pollock, L. Glendinning, T. Wisedchanwet, M. Watson, The Madness of Microbiome: Attempting To Find Consensus "Best Practice" for 16S Microbiome Studies. *Appl Environ Microbiol* **84**, (2018).
64. C. Human Microbiome Project, Structure, function and diversity of the healthy human microbiome. *Nature* **486**, 207-214 (2012).
65. T. C. Fung, D. Artis, G. F. Sonnenberg, Anatomical localization of commensal bacteria in immune cell homeostasis and disease. *Immunol Rev* **260**, 35-49 (2014).
66. Ivanov, II *et al.*, Induction of intestinal Th17 cells by segmented filamentous bacteria. *Cell* **139**, 485-498 (2009).
67. M. K. Bjursell, E. C. Martens, J. I. Gordon, Functional genomic and metabolic studies of the adaptations of a prominent adult human gut symbiont, Bacteroides thetaiotaomicron, to the suckling period. *J Biol Chem* **281**, 36269-36279 (2006).
68. J. L. Sonnenburg *et al.*, Glycan foraging in vivo by an intestine-adapted bacterial symbiont. *Science* **307**, 1955-1959 (2005).
69. T. Obata *et al.*, Indigenous opportunistic bacteria inhabit mammalian gut-associated lymphoid tissues and share a mucosal antibody-mediated symbiosis. *Proc Natl Acad Sci U S A* **107**, 7419-7424 (2010).
70. G. F. Sonnenberg *et al.*, Innate lymphoid cells promote anatomical containment of lymphoid-resident commensal bacteria. *Science* **336**, 1321-1325 (2012).
71. Y. Belkaid, T. W. Hand, Role of the microbiota in immunity and inflammation. *Cell* **157**, 121-141 (2014).
72. K. Honda, D. R. Littman, The microbiota in adaptive immune homeostasis and disease. *Nature* **535**, 75-84 (2016).

73. E. G. Pamer, Resurrecting the intestinal microbiota to combat antibiotic-resistant pathogens. *Science* **352**, 535-538 (2016).
74. M. E. Johansson *et al.*, The inner of the two Muc2 mucin-dependent mucus layers in colon is devoid of bacteria. *Proc Natl Acad Sci U S A* **105**, 15064-15069 (2008).
75. M. E. Johansson *et al.*, Bacteria penetrate the normally impenetrable inner colon mucus layer in both murine colitis models and patients with ulcerative colitis. *Gut* **63**, 281-291 (2014).
76. U. Meyer-Hoffert *et al.*, Secreted enteric antimicrobial activity localises to the mucus surface layer. *Gut* **57**, 764-771 (2008).
77. L. J. Zhang, R. L. Gallo, Antimicrobial peptides. *Curr Biol* **26**, R14-19 (2016).
78. I. Martinez-Argudo, M. A. Jepson, Salmonella translocates across an in vitro M cell model independently of SPI-1 and SPI-2. *Microbiology* **154**, 3887-3894 (2008).
79. J. H. Niess *et al.*, CX3CR1-mediated dendritic cell access to the intestinal lumen and bacterial clearance. *Science* **307**, 254-258 (2005).
80. D. Darlington, A. W. Rogers, Epithelial lymphocytes in the small intestine of the mouse. *J Anat* **100**, 813-830 (1966).
81. A. M. C. Faria, B. S. Reis, D. Mucida, Tissue adaptation: Implications for gut immunity and tolerance. *J Exp Med* **214**, 1211-1226 (2017).
82. H. Cheroutre, F. Lambolez, D. Mucida, The light and dark sides of intestinal intraepithelial lymphocytes. *Nat Rev Immunol* **11**, 445-456 (2011).
83. T. L. Denning, Y. C. Wang, S. R. Patel, I. R. Williams, B. Pulendran, Lamina propria macrophages and dendritic cells differentially induce regulatory and interleukin 17-producing T cell responses. *Nat Immunol* **8**, 1086-1094 (2007).
84. L. A. Pobezinsky *et al.*, Clonal deletion and the fate of autoreactive thymocytes that survive negative selection. *Nat Immunol* **13**, 569-578 (2012).
85. H. Cheroutre, L. Madakamutil, Acquired and natural memory T cells join forces at the mucosal front line. *Nat Rev Immunol* **4**, 290-300 (2004).
86. M. Wu, L. van Kaer, S. Itohara, S. Tonegawa, Highly restricted expression of the thymus leukemia antigens on intestinal epithelial cells. *J Exp Med* **174**, 213-218 (1991).
87. D. Olivares-Villagomez *et al.*, Thymus leukemia antigen controls intraepithelial lymphocyte function and inflammatory bowel disease. *Proc Natl Acad Sci U S A* **105**, 17931-17936 (2008).
88. O. Pabst, New concepts in the generation and functions of IgA. *Nat Rev Immunol* **12**, 821-832 (2012).
89. M. Bemark, P. Boysen, N. Y. Lycke, Induction of gut IgA production through T cell-dependent and T cell-independent pathways. *Ann N Y Acad Sci* **1247**, 97-116 (2012).
90. C. Lindner *et al.*, Age, microbiota, and T cells shape diverse individual IgA repertoires in the intestine. *J Exp Med* **209**, 365-377 (2012).
91. J. J. Bunker *et al.*, Innate and Adaptive Humoral Responses Coat Distinct Commensal Bacteria with Immunoglobulin A. *Immunity* **43**, 541-553 (2015).
92. D. A. Peterson, N. P. McNulty, J. L. Guruge, J. I. Gordon, IgA response to symbiotic bacteria as a mediator of gut homeostasis. *Cell Host Microbe* **2**, 328-339 (2007).
93. J. J. Cebra, Influences of microbiota on intestinal immune system development. *Am J Clin Nutr* **69**, 1046S-1051S (1999).
94. J. A. Hall *et al.*, Commensal DNA limits regulatory T cell conversion and is a natural adjuvant of intestinal immune responses. *Immunity* **29**, 637-649 (2008).
95. S. K. Mazmanian, C. H. Liu, A. O. Tzianabos, D. L. Kasper, An immunomodulatory molecule of symbiotic bacteria directs maturation of the host immune system. *Cell* **122**, 107-118 (2005).
96. E. Treiner *et al.*, Selection of evolutionarily conserved mucosal-associated invariant T cells by MR1. *Nature* **422**, 164-169 (2003).

97. K. Atarashi *et al.*, Induction of colonic regulatory T cells by indigenous Clostridium species. *Science* **331**, 337-341 (2011).
98. M. B. Geuking *et al.*, Intestinal bacterial colonization induces mutualistic regulatory T cell responses. *Immunity* **34**, 794-806 (2011).
99. J. L. Round, S. K. Mazmanian, Inducible Foxp3+ regulatory T-cell development by a commensal bacterium of the intestinal microbiota. *Proc Natl Acad Sci U S A* **107**, 12204-12209 (2010).
100. E. A. Kennedy, K. Y. King, M. T. Baldridge, Mouse Microbiota Models: Comparing Germ-Free Mice and Antibiotics Treatment as Tools for Modifying Gut Bacteria. *Front Physiol* **9**, 1534 (2018).
101. I. G. Pantoja-Feliciano *et al.*, Biphasic assembly of the murine intestinal microbiota during early development. *ISME J* **7**, 1112-1115 (2013).
102. K. Nutsch *et al.*, Rapid and Efficient Generation of Regulatory T Cells to Commensal Antigens in the Periphery. *Cell Rep* **17**, 206-220 (2016).
103. P. Mombaerts *et al.*, Spontaneous development of inflammatory bowel disease in T cell receptor mutant mice. *Cell* **75**, 274-282 (1993).
104. A. K. Bhan, E. Mizoguchi, R. N. Smith, A. Mizoguchi, Spontaneous chronic colitis in TCR alpha-mutant mice; an experimental model of human ulcerative colitis. *Int Rev Immunol* **19**, 123-138 (2000).
105. J. M. Brenchley, D. C. Douek, HIV infection and the gastrointestinal immune system. *Mucosal Immunol* **1**, 23-30 (2008).
106. R. S. Veazey *et al.*, Gastrointestinal tract as a major site of CD4+ T cell depletion and viral replication in SIV infection. *Science* **280**, 427-431 (1998).
107. I. Takahashi, H. Kiyono, S. Hamada, CD4+ T-cell population mediates development of inflammatory bowel disease in T-cell receptor alpha chain-deficient mice. *Gastroenterology* **112**, 1876-1886 (1997).
108. A. M. Bilate, J. J. Lafaille, Induced CD4+Foxp3+ regulatory T cells in immune tolerance. *Annu Rev Immunol* **30**, 733-758 (2012).
109. S. Z. Josefowicz, L. F. Lu, A. Y. Rudensky, Regulatory T cells: mechanisms of differentiation and function. *Annu Rev Immunol* **30**, 531-564 (2012).
110. J. M. Weiss *et al.*, Neuropilin 1 is expressed on thymus-derived natural regulatory T cells, but not mucosa-generated induced Foxp3+ T reg cells. *J Exp Med* **209**, 1723-1742, S1721 (2012).
111. A. T. Stefka *et al.*, Commensal bacteria protect against food allergen sensitization. *Proc Natl Acad Sci U S A* **111**, 13145-13150 (2014).
112. K. Atarashi *et al.*, Treg induction by a rationally selected mixture of Clostridia strains from the human microbiota. *Nature* **500**, 232-236 (2013).
113. S. Sakaguchi, N. Sakaguchi, M. Asano, M. Itoh, M. Toda, Immunologic self-tolerance maintained by activated T cells expressing IL-2 receptor alpha-chains (CD25). Breakdown of a single mechanism of self-tolerance causes various autoimmune diseases. *J Immunol* **155**, 1151-1164 (1995).
114. F. Powrie, M. W. Leach, S. Mauze, L. B. Caddle, R. L. Coffman, Phenotypically distinct subsets of CD4+ T cells induce or protect from chronic intestinal inflammation in C. B-17 scid mice. *Int Immunol* **5**, 1461-1471 (1993).
115. F. Powrie, R. Correa-Oliveira, S. Mauze, R. L. Coffman, Regulatory interactions between CD45RBhigh and CD45RBlow CD4+ T cells are important for the balance between protective and pathogenic cell-mediated immunity. *J Exp Med* **179**, 589-600 (1994).
116. S. Read, V. Malmstrom, F. Powrie, Cytotoxic T lymphocyte-associated antigen 4 plays an essential role in the function of CD25(+)CD4(+) regulatory cells that control intestinal inflammation. *J Exp Med* **192**, 295-302 (2000).

117. C. Mottet, H. H. Uhlig, F. Powrie, Cutting edge: cure of colitis by CD4+CD25+ regulatory T cells. *J Immunol* **170**, 3939-3943 (2003).
118. C. L. Bennett *et al.*, The immune dysregulation, polyendocrinopathy, enteropathy, X-linked syndrome (IPEX) is caused by mutations of FOXP3. *Nat Genet* **27**, 20-21 (2001).
119. R. S. Wildin *et al.*, X-linked neonatal diabetes mellitus, enteropathy and endocrinopathy syndrome is the human equivalent of mouse scurfy. *Nat Genet* **27**, 18-20 (2001).
120. M. E. Brunkow *et al.*, Disruption of a new forkhead/winged-helix protein, scurfin, results in the fatal lymphoproliferative disorder of the scurfy mouse. *Nat Genet* **27**, 68-73 (2001).
121. I. Apostolou, H. von Boehmer, In vivo instruction of suppressor commitment in naive T cells. *J Exp Med* **199**, 1401-1408 (2004).
122. L. F. Langer, T. M. Clay, M. A. Morse, Update on anti-CTLA-4 antibodies in clinical trials. *Expert Opin Biol Ther* **7**, 1245-1256 (2007).
123. E. O. Glocker *et al.*, Inflammatory bowel disease and mutations affecting the interleukin-10 receptor. *N Engl J Med* **361**, 2033-2045 (2009).
124. T. Tanoue, K. Honda, Induction of Treg cells in the mouse colonic mucosa: a central mechanism to maintain host-microbiota homeostasis. *Semin Immunol* **24**, 50-57 (2012).
125. J. H. Buckner, Mechanisms of impaired regulation by CD4(+)CD25(+)FOXP3(+) regulatory T cells in human autoimmune diseases. *Nat Rev Immunol* **10**, 849-859 (2010).
126. D. P. Hoytema van Konijnenburg, D. Mucida, Intraepithelial lymphocytes. *Curr Biol* **27**, R737-R739 (2017).
127. J. Carton, B. Byrne, L. Madrigal-Estebas, D. P. O'Donoghue, C. O'Farrelly, CD4+CD8+ human small intestinal T cells are decreased in coeliac patients, with CD8 expression downregulated on intra-epithelial T cells in the active disease. *Eur J Gastroenterol Hepatol* **16**, 961-968 (2004).
128. T. Sujino *et al.*, Tissue adaptation of regulatory and intraepithelial CD4+ T cells controls gut inflammation. *Science* **352**, 1581-1586 (2016).
129. G. Sarrabayrouse *et al.*, CD4CD8alphaalpha lymphocytes, a novel human regulatory T cell subset induced by colonic bacteria and deficient in patients with inflammatory bowel disease. *PLoS Biol* **12**, e1001833 (2014).
130. B. S. Reis, A. Rogoz, F. A. Costa-Pinto, I. Taniuchi, D. Mucida, Mutual expression of the transcription factors Runx3 and ThPOK regulates intestinal CD4(+) T cell immunity. *Nat Immunol* **14**, 271-280 (2013).
131. M. Iwata *et al.*, Retinoic acid imprints gut-homing specificity on T cells. *Immunity* **21**, 527-538 (2004).
132. J. L. Coombes *et al.*, A functionally specialized population of mucosal CD103+ DCs induces Foxp3+ regulatory T cells via a TGF-beta and retinoic acid-dependent mechanism. *J Exp Med* **204**, 1757-1764 (2007).
133. D. Mucida *et al.*, Reciprocal TH17 and regulatory T cell differentiation mediated by retinoic acid. *Science* **317**, 256-260 (2007).
134. C. M. Sun *et al.*, Small intestine lamina propria dendritic cells promote de novo generation of Foxp3 T reg cells via retinoic acid. *J Exp Med* **204**, 1775-1785 (2007).
135. J. E. Konkel, W. Chen, Balancing acts: the role of TGF-beta in the mucosal immune system. *Trends Mol Med* **17**, 668-676 (2011).
136. D. Esterhazy *et al.*, Classical dendritic cells are required for dietary antigen-mediated induction of peripheral Treg cells and tolerance. *Nat Immunol* **17**, 545-555 (2016).
137. K. M. Luda *et al.*, IRF8 Transcription-Factor-Dependent Classical Dendritic Cells Are Essential for Intestinal T Cell Homeostasis. *Immunity* **44**, 860-874 (2016).
138. G. Das *et al.*, An important regulatory role for CD4+CD8 alpha alpha T cells in the intestinal epithelial layer in the prevention of inflammatory bowel disease. *Proc Natl Acad Sci U S A* **100**, 5324-5329 (2003).

139. D. Mucida *et al.*, Transcriptional reprogramming of mature CD4(+) helper T cells generates distinct MHC class II-restricted cytotoxic T lymphocytes. *Nat Immunol* **14**, 281-289 (2013).
140. D. Masopust, V. Vezys, E. J. Wherry, D. L. Barber, R. Ahmed, Cutting edge: gut microenvironment promotes differentiation of a unique memory CD8 T cell population. *J Immunol* **176**, 2079-2083 (2006).
141. B. S. Reis, D. P. Hoytema van Konijnenburg, S. I. Grivennikov, D. Mucida, Transcription factor T-bet regulates intraepithelial lymphocyte functional maturation. *Immunity* **41**, 244-256 (2014).
142. M. L. Hanson *et al.*, Oral delivery of IL-27 recombinant bacteria attenuates immune colitis in mice. *Gastroenterology* **146**, 210-221 e213 (2014).
143. A. M. Bilate *et al.*, Tissue-specific emergence of regulatory and intraepithelial T cells from a clonal T cell precursor. *Sci Immunol* **1**, eaaf7471 (2016).
144. T. Mota-Santos *et al.*, Divergency in the specificity of the induction and maintenance of neonatal suppression. *Eur J Immunol* **20**, 1717-1721 (1990).
145. Y. Umesaki, H. Setoyama, S. Matsumoto, Y. Okada, Expansion of alpha beta T-cell receptor-bearing intestinal intraepithelial lymphocytes after microbial colonization in germ-free mice and its independence from thymus. *Immunology* **79**, 32-37 (1993).
146. J. Fangmann, R. Schwinzer, K. Wonigeit, Unusual phenotype of intestinal intraepithelial lymphocytes in the rat: predominance of T cell receptor alpha/beta+/CD2- cells and high expression of the RT6 alloantigen. *Eur J Immunol* **21**, 753-760 (1991).
147. N. Torres-Nagel *et al.*, Differential thymus dependence of rat CD8 isoform expression. *Eur J Immunol* **22**, 2841-2848 (1992).
148. H. Takimoto *et al.*, Age-associated increase in number of CD4+CD8+ intestinal intraepithelial lymphocytes in rats. *Eur J Immunol* **22**, 159-164 (1992).
149. L. Helgeland, F. E. Johansen, J. O. Utgaard, J. T. Vaage, P. Brandtzaeg, Oligoclonality of rat intestinal intraepithelial T lymphocytes: overlapping TCR beta-chain repertoires in the CD4 single-positive and CD4/CD8 double-positive subsets. *J Immunol* **162**, 2683-2692 (1999).
150. L. Helgeland, J. T. Vaage, B. Rolstad, T. Midtvedt, P. Brandtzaeg, Microbial colonization influences composition and T-cell receptor V beta repertoire of intraepithelial lymphocytes in rat intestine. *Immunology* **89**, 494-501 (1996).
151. L. Cervantes-Barragan *et al.*, Lactobacillus reuteri induces gut intraepithelial CD4(+)CD8alphaalpha(+) T cells. *Science* **357**, 806-810 (2017).
152. L. Wojciech *et al.*, Non-canonicaly recruited TCRalphabetaCD8alphaalpha IELs recognize microbial antigens. *Sci Rep* **8**, 10848 (2018).
153. A. Regnault, A. Cumano, P. Vassalli, D. Guy-Grand, P. Kourilsky, Oligoclonal repertoire of the CD8 alpha alpha and the CD8 alpha beta TCR-alpha/beta murine intestinal intraepithelial T lymphocytes: evidence for the random emergence of T cells. *J Exp Med* **180**, 1345-1358 (1994).
154. A. Regnault *et al.*, The expansion and selection of T cell receptor alpha beta intestinal intraepithelial T cell clones. *Eur J Immunol* **26**, 914-921 (1996).
155. A. Regnault, P. Kourilsky, A. Cumano, The TCR-beta chain repertoire of gut-derived T lymphocytes. *Semin Immunol* **7**, 307-319 (1995).
156. B. D. McDonald, J. J. Bunker, I. E. Ishizuka, B. Jabri, A. Bendelac, Elevated T cell receptor signaling identifies a thymic precursor to the TCRalphabeta(+)CD4(-)CD8beta(-) intraepithelial lymphocyte lineage. *Immunity* **41**, 219-229 (2014).
157. C. G. Chapman *et al.*, Characterization of T-cell Receptor Repertoire in Inflamed Tissues of Patients with Crohn's Disease Through Deep Sequencing. *Inflamm Bowel Dis* **22**, 1275-1285 (2016).

158. M. K. Levings, M. G. Roncarolo, T-regulatory 1 cells: a novel subset of CD4 T cells with immunoregulatory properties. *J Allergy Clin Immunol* **106**, S109-112 (2000).
159. M. G. Roncarolo, S. Gregori, R. Bacchetta, M. Battaglia, Tr1 cells and the counter-regulation of immunity: natural mechanisms and therapeutic applications. *Curr Top Microbiol Immunol* **380**, 39-68 (2014).
160. H. Groux *et al.*, A CD4+ T-cell subset inhibits antigen-specific T-cell responses and prevents colitis. *Nature* **389**, 737-742 (1997).
161. A. M. White, D. C. Wraith, Tr1-Like T Cells - An Enigmatic Regulatory T Cell Lineage. *Front Immunol* **7**, 355 (2016).
162. A. Schmidt, N. Oberle, P. H. Krammer, Molecular mechanisms of treg-mediated T cell suppression. *Front Immunol* **3**, 51 (2012).
163. T. Takahashi *et al.*, Immunologic self-tolerance maintained by CD25+CD4+ naturally anergic and suppressive T cells: induction of autoimmune disease by breaking their anergic/suppressive state. *Int Immunol* **10**, 1969-1980 (1998).
164. A. M. Thornton, E. M. Shevach, CD4+CD25+ immunoregulatory T cells suppress polyclonal T cell activation in vitro by inhibiting interleukin 2 production. *J Exp Med* **188**, 287-296 (1998).
165. M. de la Rosa, S. Rutz, H. Dorninger, A. Scheffold, Interleukin-2 is essential for CD4+CD25+ regulatory T cell function. *Eur J Immunol* **34**, 2480-2488 (2004).
166. A. M. Thornton, E. E. Donovan, C. A. Piccirillo, E. M. Shevach, Cutting edge: IL-2 is critically required for the in vitro activation of CD4+CD25+ T cell suppressor function. *J Immunol* **172**, 6519-6523 (2004).
167. A. M. Thornton, C. A. Piccirillo, E. M. Shevach, Activation requirements for the induction of CD4+CD25+ T cell suppressor function. *Eur J Immunol* **34**, 366-376 (2004).
168. A. M. Thornton, E. M. Shevach, Suppressor effector function of CD4+CD25+ immunoregulatory T cells is antigen nonspecific. *J Immunol* **164**, 183-190 (2000).
169. M. Karim, G. Feng, K. J. Wood, A. R. Bushell, CD25+CD4+ regulatory T cells generated by exposure to a model protein antigen prevent allograft rejection: antigen-specific reactivation in vivo is critical for bystander regulation. *Blood* **105**, 4871-4877 (2005).
170. D. C. Gondek, L. F. Lu, S. A. Quezada, S. Sakaguchi, R. J. Noelle, Cutting edge: contact-mediated suppression by CD4+CD25+ regulatory cells involves a granzyme B-dependent, perforin-independent mechanism. *J Immunol* **174**, 1783-1786 (2005).
171. W. J. Grossman *et al.*, Human T regulatory cells can use the perforin pathway to cause autologous target cell death. *Immunity* **21**, 589-601 (2004).
172. D. C. Gondek *et al.*, Transplantation survival is maintained by granzyme B+ regulatory cells and adaptive regulatory T cells. *J Immunol* **181**, 4752-4760 (2008).
173. T. Bopp *et al.*, Cyclic adenosine monophosphate is a key component of regulatory T cell-mediated suppression. *J Exp Med* **204**, 1303-1310 (2007).
174. V. L. Wehbi, K. Tasken, Molecular Mechanisms for cAMP-Mediated Immunoregulation in T cells - Role of Anchored Protein Kinase A Signaling Units. *Front Immunol* **7**, 222 (2016).
175. C. M. Rueda, C. M. Jackson, C. A. Chougnet, Regulatory T-Cell-Mediated Suppression of Conventional T-Cells and Dendritic Cells by Different cAMP Intracellular Pathways. *Front Immunol* **7**, 216 (2016).
176. M. Klein, T. Bopp, Cyclic AMP Represents a Crucial Component of Treg Cell-Mediated Immune Regulation. *Front Immunol* **7**, 315 (2016).
177. J. Blay, T. D. White, D. W. Hoskin, The extracellular fluid of solid carcinomas contains immunosuppressive concentrations of adenosine. *Cancer Res* **57**, 2602-2605 (1997).
178. A. Ohta *et al.*, A2A adenosine receptor protects tumors from antitumor T cells. *Proc Natl Acad Sci U S A* **103**, 13132-13137 (2006).

179. P. Pandiyan, L. Zheng, S. Ishihara, J. Reed, M. J. Lenardo, CD4+CD25+Foxp3+ regulatory T cells induce cytokine deprivation-mediated apoptosis of effector CD4+ T cells. *Nat Immunol* **8**, 1353-1362 (2007).
180. K. Nakamura *et al.*, TGF-beta 1 plays an important role in the mechanism of CD4+CD25+ regulatory T cell activity in both humans and mice. *J Immunol* **172**, 834-842 (2004).
181. C. E. Tadokoro *et al.*, Regulatory T cells inhibit stable contacts between CD4+ T cells and dendritic cells in vivo. *J Exp Med* **203**, 505-511 (2006).
182. M. O. Li, S. Sanjabi, R. A. Flavell, Transforming growth factor-beta controls development, homeostasis, and tolerance of T cells by regulatory T cell-dependent and -independent mechanisms. *Immunity* **25**, 455-471 (2006).
183. C. Asseman, S. Mauze, M. W. Leach, R. L. Coffman, F. Powrie, An essential role for interleukin 10 in the function of regulatory T cells that inhibit intestinal inflammation. *J Exp Med* **190**, 995-1004 (1999).
184. L. W. Collison *et al.*, The inhibitory cytokine IL-35 contributes to regulatory T-cell function. *Nature* **450**, 566-569 (2007).
185. L. W. Collison *et al.*, IL-35-mediated induction of a potent regulatory T cell population. *Nat Immunol* **11**, 1093-1101 (2010).
186. M. Bettini, A. H. Castellaw, G. P. Lennon, A. R. Burton, D. A. Vignali, Prevention of autoimmune diabetes by ectopic pancreatic beta-cell expression of interleukin-35. *Diabetes* **61**, 1519-1526 (2012).
187. E. Bardel, F. Larousserie, P. Charlot-Rabiega, A. Coulomb-L'Hermine, O. Devergne, Human CD4+ CD25+ Foxp3+ regulatory T cells do not constitutively express IL-35. *J Immunol* **181**, 6898-6905 (2008).
188. Q. Tang *et al.*, Visualizing regulatory T cell control of autoimmune responses in nonobese diabetic mice. *Nat Immunol* **7**, 83-92 (2006).
189. K. Wing *et al.*, CTLA-4 control over Foxp3+ regulatory T cell function. *Science* **322**, 271-275 (2008).
190. F. Fallarino *et al.*, Modulation of tryptophan catabolism by regulatory T cells. *Nat Immunol* **4**, 1206-1212 (2003).
191. J. D. Mezrich *et al.*, An interaction between kynurenine and the aryl hydrocarbon receptor can generate regulatory T cells. *J Immunol* **185**, 3190-3198 (2010).
192. L. Cederbom, H. Hall, F. Ivars, CD4+CD25+ regulatory T cells down-regulate co-stimulatory molecules on antigen-presenting cells. *Eur J Immunol* **30**, 1538-1543 (2000).
193. B. Liang *et al.*, Regulatory T cells inhibit dendritic cells by lymphocyte activation gene-3 engagement of MHC class II. *J Immunol* **180**, 5916-5926 (2008).
194. C. T. Huang *et al.*, Role of LAG-3 in regulatory T cells. *Immunity* **21**, 503-513 (2004).
195. Q. Chen *et al.*, ICOS signal facilitates Foxp3 transcription to favor suppressive function of regulatory T cells. *Int J Med Sci* **15**, 666-673 (2018).
196. Y. P. de Jong *et al.*, Blocking inducible co-stimulator in the absence of CD28 impairs Th1 and CD25+ regulatory T cells in murine colitis. *Int Immunol* **16**, 205-213 (2004).
197. P. Poussier, T. Ning, D. Banerjee, M. Julius, A unique subset of self-specific intraintestinal T cells maintains gut integrity. *J Exp Med* **195**, 1491-1497 (2002).
198. H. De Winter *et al.*, Regulation of mucosal immune responses by recombinant interleukin 10 produced by intestinal epithelial cells in mice. *Gastroenterology* **122**, 1829-1841 (2002).
199. V. Gaboriau-Routhiau *et al.*, The key role of segmented filamentous bacteria in the coordinated maturation of gut helper T cell responses. *Immunity* **31**, 677-689 (2009).
200. W. Chen *et al.*, Conversion of peripheral CD4+CD25- naive T cells to CD4+CD25+ regulatory T cells by TGF-beta induction of transcription factor Foxp3. *J Exp Med* **198**, 1875-1886 (2003).

201. S. G. Jeon *et al.*, Probiotic Bifidobacterium breve induces IL-10-producing Tr1 cells in the colon. *PLoS Pathog* **8**, e1002714 (2012).
202. A. Lyons *et al.*, Bacterial strain-specific induction of Foxp3+ T regulatory cells is protective in murine allergy models. *Clin Exp Allergy* **40**, 811-819 (2010).
203. R. Verma *et al.*, Cell surface polysaccharides of Bifidobacterium bifidum induce the generation of Foxp3(+) regulatory T cells. *Sci Immunol* **3**, (2018).
204. N. Geva-Zatorsky *et al.*, Mining the Human Gut Microbiota for Immunomodulatory Organisms. *Cell* **168**, 928-943 e911 (2017).
205. G. Matteoli *et al.*, Gut CD103+ dendritic cells express indoleamine 2,3-dioxygenase which influences T regulatory/T effector cell balance and oral tolerance induction. *Gut* **59**, 595-604 (2010).
206. S. J. Rhee, W. A. Walker, B. J. Cherayil, Developmentally regulated intestinal expression of IFN-gamma and its target genes and the age-specific response to enteric Salmonella infection. *J Immunol* **175**, 1127-1136 (2005).
207. E. B. Finger, J. A. Bluestone, When ligand becomes receptor--tolerance via B7 signaling on DCs. *Nat Immunol* **3**, 1056-1057 (2002).
208. D. Dodd *et al.*, A gut bacterial pathway metabolizes aromatic amino acids into nine circulating metabolites. *Nature* **551**, 648-652 (2017).
209. M. Levy, C. A. Thaiss, E. Elinav, Metabolites: messengers between the microbiota and the immune system. *Genes Dev* **30**, 1589-1597 (2016).
210. T. Hoverstad, T. Midtvedt, Short-chain fatty acids in germfree mice and rats. *J Nutr* **116**, 1772-1776 (1986).
211. S. Macfarlane, G. T. Macfarlane, Regulation of short-chain fatty acid production. *Proc Nutr Soc* **62**, 67-72 (2003).
212. S. Alex *et al.*, Short-chain fatty acids stimulate angiopoietin-like 4 synthesis in human colon adenocarcinoma cells by activating peroxisome proliferator-activated receptor gamma. *Mol Cell Biol* **33**, 1303-1316 (2013).
213. N. Singh *et al.*, Activation of Gpr109a, receptor for niacin and the commensal metabolite butyrate, suppresses colonic inflammation and carcinogenesis. *Immunity* **40**, 128-139 (2014).
214. K. M. Maslowski *et al.*, Regulation of inflammatory responses by gut microbiota and chemoattractant receptor GPR43. *Nature* **461**, 1282-1286 (2009).
215. J. L. Pluznick, Gut microbiota in renal physiology: focus on short-chain fatty acids and their receptors. *Kidney Int* **90**, 1191-1198 (2016).
216. A. J. Brown *et al.*, The Orphan G protein-coupled receptors GPR41 and GPR43 are activated by propionate and other short chain carboxylic acids. *J Biol Chem* **278**, 11312-11319 (2003).
217. R. Hontecillas, J. Bassaganya-Riera, Peroxisome proliferator-activated receptor gamma is required for regulatory CD4+ T cell-mediated protection against colitis. *J Immunol* **178**, 2940-2949 (2007).
218. C. G. Su *et al.*, A novel therapy for colitis utilizing PPAR-gamma ligands to inhibit the epithelial inflammatory response. *J Clin Invest* **104**, 383-389 (1999).
219. S. G. Kang, H. W. Lim, O. M. Andrisani, H. E. Broxmeyer, C. H. Kim, Vitamin A metabolites induce gut-homing FoxP3+ regulatory T cells. *J Immunol* **179**, 3724-3733 (2007).
220. Y. Furusawa *et al.*, Commensal microbe-derived butyrate induces the differentiation of colonic regulatory T cells. *Nature* **504**, 446-450 (2013).
221. T. Tanoue, K. Atarashi, K. Honda, Development and maintenance of intestinal regulatory T cells. *Nat Rev Immunol* **16**, 295-309 (2016).

222. S. K. Mazmanian, Capsular polysaccharides of symbiotic bacteria modulate immune responses during experimental colitis. *J Pediatr Gastroenterol Nutr* **46 Suppl 1**, E11-12 (2008).
223. J. L. Round *et al.*, The Toll-like receptor 2 pathway establishes colonization by a commensal of the human microbiota. *Science* **332**, 974-977 (2011).
224. Y. Shen *et al.*, Outer membrane vesicles of a human commensal mediate immune regulation and disease protection. *Cell Host Microbe* **12**, 509-520 (2012).
225. N. K. Surana, D. L. Kasper, The yin yang of bacterial polysaccharides: lessons learned from B. fragilis PSA. *Immunol Rev* **245**, 13-26 (2012).
226. F. Y. Avci, D. L. Kasper, How bacterial carbohydrates influence the adaptive immune system. *Annu Rev Immunol* **28**, 107-130 (2010).
227. A. O. Tzianabos, A. B. Onderdonk, B. Rosner, R. L. Cisneros, D. L. Kasper, Structural features of polysaccharides that induce intra-abdominal abscesses. *Science* **262**, 416-419 (1993).
228. C. P. Neff *et al.*, Diverse Intestinal Bacteria Contain Putative Zwitterionic Capsular Polysaccharides with Anti-inflammatory Properties. *Cell Host Microbe* **20**, 535-547 (2016).
229. M. Kverka *et al.*, Oral administration of Parabacteroides distasonis antigens attenuates experimental murine colitis through modulation of immunity and microbiota composition. *Clin Exp Immunol* **163**, 250-259 (2011).
230. Ivanov, II, K. Honda, Intestinal commensal microbes as immune modulators. *Cell Host Microbe* **12**, 496-508 (2012).
231. E. V. Russler-Germain, S. Rengarajan, C. S. Hsieh, Antigen-specific regulatory T-cell responses to intestinal microbiota. *Mucosal Immunol* **10**, 1375-1386 (2017).
232. Y. Yang *et al.*, Focused specificity of intestinal TH17 cells towards commensal bacterial antigens. *Nature* **510**, 152-156 (2014).
233. K. Atarashi *et al.*, Ectopic colonization of oral bacteria in the intestine drives TH1 cell induction and inflammation. *Science* **358**, 359-365 (2017).
234. S. Naik *et al.*, Commensal-dendritic-cell interaction specifies a unique protective skin immune signature. *Nature* **520**, 104-108 (2015).
235. E. Ansaldo *et al.*, Akkermansia muciniphila induces intestinal adaptive immune responses during homeostasis. *Science* **364**, 1179-1184 (2019).
236. A. Cotillard *et al.*, Dietary intervention impact on gut microbial gene richness. *Nature* **500**, 585-588 (2013).
237. P. J. Turnbaugh, F. Backhed, L. Fulton, J. I. Gordon, Diet-induced obesity is linked to marked but reversible alterations in the mouse distal gut microbiome. *Cell Host Microbe* **3**, 213-223 (2008).
238. E. Holmes, J. V. Li, T. Athanasiou, H. Ashrafian, J. K. Nicholson, Understanding the role of gut microbiome-host metabolic signal disruption in health and disease. *Trends Microbiol* **19**, 349-359 (2011).
239. J. R. Swann *et al.*, Systemic gut microbial modulation of bile acid metabolism in host tissue compartments. *Proc Natl Acad Sci U S A* **108 Suppl 1**, 4523-4530 (2011).
240. H. J. Wu *et al.*, Gut-residing segmented filamentous bacteria drive autoimmune arthritis via T helper 17 cells. *Immunity* **32**, 815-827 (2010).
241. Y. K. Lee, J. S. Menezes, Y. Umesaki, S. K. Mazmanian, Proinflammatory T-cell responses to gut microbiota promote experimental autoimmune encephalomyelitis. *Proc Natl Acad Sci U S A* **108 Suppl 1**, 4615-4622 (2011).
242. M. C. Kullberg *et al.*, IL-23 plays a key role in Helicobacter hepaticus-induced T cell-dependent colitis. *J Exp Med* **203**, 2485-2494 (2006).
243. M. C. Kullberg *et al.*, Bacteria-triggered CD4(+) T regulatory cells suppress Helicobacter hepaticus-induced colitis. *J Exp Med* **196**, 505-515 (2002).

244. K. J. Maloy *et al.*, CD4+CD25+ T(R) cells suppress innate immune pathology through cytokine-dependent mechanisms. *J Exp Med* **197**, 111-119 (2003).
245. S. Buonocore *et al.*, Innate lymphoid cells drive interleukin-23-dependent innate intestinal pathology. *Nature* **464**, 1371-1375 (2010).
246. N. Powell *et al.*, The transcription factor T-bet regulates intestinal inflammation mediated by interleukin-7 receptor+ innate lymphoid cells. *Immunity* **37**, 674-684 (2012).
247. E. Elinav *et al.*, NLRP6 inflammasome regulates colonic microbial ecology and risk for colitis. *Cell* **145**, 745-757 (2011).
248. J. Henao-Mejia *et al.*, Inflammasome-mediated dysbiosis regulates progression of NAFLD and obesity. *Nature* **482**, 179-185 (2012).
249. F. Backhed *et al.*, The gut microbiota as an environmental factor that regulates fat storage. *Proc Natl Acad Sci U S A* **101**, 15718-15723 (2004).
250. J. G. Markle *et al.*, Sex differences in the gut microbiome drive hormone-dependent regulation of autoimmunity. *Science* **339**, 1084-1088 (2013).
251. J. F. Cryan, T. G. Dinan, Mind-altering microorganisms: the impact of the gut microbiota on brain and behaviour. *Nat Rev Neurosci* **13**, 701-712 (2012).
252. C. L. Sears, W. S. Garrett, Microbes, microbiota, and colon cancer. *Cell Host Microbe* **15**, 317-328 (2014).
253. P. Yi, L. Li, The germfree murine animal: an important animal model for research on the relationship between gut microbiota and the host. *Vet Microbiol* **157**, 1-7 (2012).
254. M. Al-Asmakh, F. Zadjali, Use of Germ-Free Animal Models in Microbiota-Related Research. *J Microbiol Biotechnol* **25**, 1583-1588 (2015).
255. R. W. Schaedler, R. Dubos, R. Costello, The Development of the Bacterial Flora in the Gastrointestinal Tract of Mice. *J Exp Med* **122**, 59-66 (1965).
256. R. P. Orcutt, F. J. Gianni, R. J. Judge, Development of an 'Altered Schaedler flora' for NCI gnotobiotic rodents. *Microecol. Ther. 17, 59*, (1987).
257. H. Chung *et al.*, Gut immune maturation depends on colonization with a host-specific microbiota. *Cell* **149**, 1578-1593 (2012).
258. Y. G. Kim *et al.*, Gut dysbiosis promotes M2 macrophage polarization and allergic airway inflammation via fungi-induced PGE(2). *Cell Host Microbe* **15**, 95-102 (2014).
259. J. O. Marx, D. Vudathala, L. Murphy, S. Rankin, F. C. Hankenson, Antibiotic administration in the drinking water of mice. *J Am Assoc Lab Anim Sci* **53**, 301-306 (2014).
260. Y. Cong, T. Feng, K. Fujihashi, T. R. Schoeb, C. O. Elson, A dominant, coordinated T regulatory cell-IgA response to the intestinal microbiota. *Proc Natl Acad Sci U S A* **106**, 19256-19261 (2009).
261. M. J. Lodes *et al.*, Bacterial flagellin is a dominant antigen in Crohn disease. *J Clin Invest* **113**, 1296-1306 (2004).
262. T. W. Hand *et al.*, Acute gastrointestinal infection induces long-lived microbiota-specific T cell responses. *Science* **337**, 1553-1556 (2012).
263. T. Feng, L. Wang, T. R. Schoeb, C. O. Elson, Y. Cong, Microbiota innate stimulation is a prerequisite for T cell spontaneous proliferation and induction of experimental colitis. *J Exp Med* **207**, 1321-1332 (2010).
264. T. Feng *et al.*, Th17 cells induce colitis and promote Th1 cell responses through IL-17 induction of innate IL-12 and IL-23 production. *J Immunol* **186**, 6313-6318 (2011).
265. M. R. Hepworth *et al.*, Innate lymphoid cells regulate CD4+ T-cell responses to intestinal commensal bacteria. *Nature* **498**, 113-117 (2013).
266. Y. Goto *et al.*, Segmented filamentous bacteria antigens presented by intestinal dendritic cells drive mucosal Th17 cell differentiation. *Immunity* **40**, 594-607 (2014).

267. N. S. Taylor, S. Xu, P. Nambiar, F. E. Dewhirst, J. G. Fox, Enterohepatic Helicobacter species are prevalent in mice from commercial and academic institutions in Asia, Europe, and North America. *J Clin Microbiol* **45**, 2166-2172 (2007).
268. M. M. Wegorzewska *et al.*, Diet modulates colonic T cell responses by regulating the expression of a Bacteroides thetaiotaomicron antigen. *Sci Immunol* **4**, (2019).
269. F. Crawford, H. Kozono, J. White, P. Marrack, J. Kappler, Detection of antigen-specific T cells with multivalent soluble class II MHC covalent peptide complexes. *Immunity* **8**, 675-682 (1998).
270. S. Sims, C. Willberg, P. Klenerman, MHC-peptide tetramers for the analysis of antigen-specific T cells. *Expert Rev Vaccines* **9**, 765-774 (2010).
271. J. J. Moon *et al.*, Naive CD4(+) T cell frequency varies for different epitopes and predicts repertoire diversity and response magnitude. *Immunity* **27**, 203-213 (2007).
272. P. Chiaranunt, J. T. Tometich, J. Ji, T. W. Hand, T Cell Proliferation and Colitis Are Initiated by Defined Intestinal Microbes. *J Immunol* **201**, 243-250 (2018).
273. J. L. Linehan *et al.*, Non-classical Immunity Controls Microbiota Impact on Skin Immunity and Tissue Repair. *Cell* **172**, 784-796 e718 (2018).
274. P. Kisielow, H. Bluthmann, U. D. Staerz, M. Steinmetz, H. von Boehmer, Tolerance in T-cell-receptor transgenic mice involves deletion of nonmature CD4+8+ thymocytes. *Nature* **333**, 742-746 (1988).
275. P. Kisielow, H. S. Teh, H. Bluthmann, H. von Boehmer, Positive selection of antigen-specific T cells in thymus by restricting MHC molecules. *Nature* **335**, 730-733 (1988).
276. H. S. Teh *et al.*, Thymic major histocompatibility complex antigens and the alpha beta T-cell receptor determine the CD4/CD8 phenotype of T cells. *Nature* **335**, 229-233 (1988).
277. W. C. Sha *et al.*, Selective expression of an antigen receptor on CD8-bearing T lymphocytes in transgenic mice. *Nature* **335**, 271-274 (1988).
278. W. C. Sha *et al.*, Positive and negative selection of an antigen receptor on T cells in transgenic mice. *Nature* **336**, 73-76 (1988).
279. J. Kaye *et al.*, Selective development of CD4+ T cells in transgenic mice expressing a class II MHC-restricted antigen receptor. *Nature* **341**, 746-749 (1989).
280. L. J. Berg *et al.*, Antigen/MHC-specific T cells are preferentially exported from the thymus in the presence of their MHC ligand. *Cell* **58**, 1035-1046 (1989).
281. L. J. Berg, B. Fazekas de St Groth, A. M. Pullen, M. M. Davis, Phenotypic differences between alpha beta versus beta T-cell receptor transgenic mice undergoing negative selection. *Nature* **340**, 559-562 (1989).
282. K. M. Murphy, A. B. Heimberger, D. Y. Loh, Induction by antigen of intrathymic apoptosis of CD4+CD8+TCRlo thymocytes in vivo. *Science* **250**, 1720-1723 (1990).
283. J. J. Lafaille, T-cell receptor transgenic mice in the study of autoimmune diseases. *J Autoimmun* **22**, 95-106 (2004).
284. J. Goverman *et al.*, Transgenic mice that express a myelin basic protein-specific T cell receptor develop spontaneous autoimmunity. *Cell* **72**, 551-560 (1993).
285. J. D. Katz, B. Wang, K. Haskins, C. Benoist, D. Mathis, Following a diabetogenic T cell from genesis through pathogenesis. *Cell* **74**, 1089-1100 (1993).
286. L. Mori, H. Loetscher, K. Kakimoto, H. Bluethmann, M. Steinmetz, Expression of a transgenic T cell receptor beta chain enhances collagen-induced arthritis. *J Exp Med* **176**, 381-388 (1992).
287. C. C. Goodnow, R. Brink, E. Adams, Breakdown of self-tolerance in anergic B lymphocytes. *Nature* **352**, 532-536 (1991).
288. C. C. Goodnow *et al.*, Altered immunoglobulin expression and functional silencing of self-reactive B lymphocytes in transgenic mice. *Nature* **334**, 676-682 (1988).
289. C. C. Goodnow, J. Crosbie, H. Jorgensen, R. A. Brink, A. Basten, Induction of self-tolerance in mature peripheral B lymphocytes. *Nature* **342**, 385-391 (1989).

290. C. C. Goodnow *et al.*, Clonal silencing of self-reactive B lymphocytes in a transgenic mouse model. *Cold Spring Harb Symp Quant Biol* **54 Pt 2**, 907-920 (1989).
291. M. J. Shlomchik, A. H. Aucoin, D. S. Pisetsky, M. G. Weigert, Structure and function of anti-DNA autoantibodies derived from a single autoimmune mouse. *Proc Natl Acad Sci U S A* **84**, 9150-9154 (1987).
292. S. K. Dougan *et al.*, IgG1+ ovalbumin-specific B-cell transnuclear mice show class switch recombination in rare allelically included B cells. *Proc Natl Acad Sci U S A* **109**, 13739-13744 (2012).
293. A. M. Avalos *et al.*, Monovalent engagement of the BCR activates ovalbumin-specific transnuclear B cells. *J Exp Med* **211**, 365-379 (2014).
294. E. Clancy-Thompson *et al.*, Transnuclear mice reveal Peyer's patch iNKT cells that regulate B-cell class switching to IgG1. *EMBO J* **38**, e101260 (2019).
295. S. K. Dougan *et al.*, Antigen-specific B-cell receptor sensitizes B cells to infection by influenza virus. *Nature* **503**, 406-409 (2013).
296. O. Kirak *et al.*, Transnuclear mice with predefined T cell receptor specificities against Toxoplasma gondii obtained via SCNT. *Science* **328**, 243-248 (2010).
297. S. K. Dougan *et al.*, Transnuclear TRP1-specific CD8 T cells with high or low affinity TCRs show equivalent antitumor activity. *Cancer Immunol Res* **1**, 99-111 (2013).
298. K. Hochedlinger, R. Jaenisch, Monoclonal mice generated by nuclear transfer from mature B and T donor cells. *Nature* **415**, 1035-1038 (2002).
299. O. Kirak *et al.*, Transnuclear mice with pre-defined T cell receptor specificities against Toxoplasma gondii obtained via SCNT. *J Vis Exp*, (2010).
300. M. Ku *et al.*, Nuclear transfer nTreg model reveals fate-determining TCR-beta and novel peripheral nTreg precursors. *Proc Natl Acad Sci U S A* **113**, E2316-2325 (2016).
301. O. Kaminuma *et al.*, Hyper-reactive cloned mice generated by direct nuclear transfer of antigen-specific CD4(+) T cells. *EMBO Rep* **18**, 885-893 (2017).
302. S. Sehrawat *et al.*, CD8(+) T cells from mice transnuclear for a TCR that recognizes a single H-2K(b)-restricted MHV68 epitope derived from gB-ORF8 help control infection. *Cell Rep* **1**, 461-471 (2012).
303. K. Inoue *et al.*, Generation of cloned mice by direct nuclear transfer from natural killer T cells. *Curr Biol* **15**, 1114-1118 (2005).
304. S. Kamimura *et al.*, Mouse cloning using a drop of peripheral blood. *Biol Reprod* **89**, 24 (2013).
305. A. M. Avalos, F. Meyer-Wentrup, H. L. Ploegh, B-cell receptor signaling in lymphoid malignancies and autoimmunity. *Adv Immunol* **123**, 1-49 (2014).
306. R. Jeanisch, K. Eggan, D. Humpherys, W. Rideout, K. Hochedlinger, Nuclear cloning, stem cells, and genomic reprogramming. *Cloning Stem Cells* **4**, 389-396 (2002).
307. J. Chen, R. Lansford, V. Stewart, F. Young, F. W. Alt, RAG-2-deficient blastocyst complementation: an assay of gene function in lymphocyte development. *Proc Natl Acad Sci U S A* **90**, 4528-4532 (1993).

Chapter 2 - Tissue-specific emergence of regulatory and intraepithelial T cells from a clonal T cell precursor

Authors:

Angelina M. Bilate, Djenet Bousbaine, Luka Mesin, Marianna Agudelo, Justin Leube, Andreas Kratzert, Stephanie K. Dougan, Gabriel D. Victora and Hidde L. Ploegh

The following chapter is adapted from an article published in Science Immunology (eaaf7471 (2016)).

Abstract

Peripheral Foxp3$^+$ regulatory T cells (pTregs) maintain immune homeostasis by controlling potentially harmful effector T cell responses toward dietary and microbial antigens. Although the identity of the T cell receptor (TCR) can impose commitment and functional specialization of T cells, less is known about how TCR identity governs pTreg development from conventional CD4$^+$ T cells. To investigate the extent to which TCR identity dictates pTreg fate, we used somatic cell nuclear transfer to generate a transnuclear (TN) mouse carrying a monoclonal TCR from a pTreg (pTreg TN mice). We found that the pTreg TCR did not inevitably predispose T cells to become pTreg but instead allowed for differentiation of noninflammatory CD4$^+$CD8αα$^+$ intraepithelial lymphocytes (CD4$_{IELs}$) in the small intestine. Only when we limited the number of T cell precursors that carried the TN pTreg TCR did we observe substantial pTreg development in the mesenteric lymph nodes and small intestine lamina propria of mixed bone marrow chimeras. Small clonal sizes and therefore decreased intraclonal competition were required for pTreg development. Despite bearing the same TCR, small intestine CD4$_{IEL}$ developed independently of precursor frequency. Both pTreg and CD4$_{IEL}$ development strictly depended on the resident microbiota. A single clonal CD4$^+$ T cell precursor can thus give rise to two functionally distinct and anatomically segregated T cell subsets in a microbiota-dependent manner. Therefore, plasticity of the CD4 T cell compartment depends not only on the microbiota but also on specialized environmental cues provided by different tissues.

Introduction

Foreign antigens derived from the diet and the microbiota pose a daily challenge to the gastrointestinal tract. Regulatory T cells (Tregs), abundant in the gut mucosa, prevent inflammatory bowel disease and food allergies through inhibition of harmful responses by effector T cells (*1, 2*). $CD4^+$ T cells exhibit plasticity and can differentiate into distinct subsets with diverse functional properties (*3, 4*). The intestinal lamina propria (LP), a location constantly exposed to commensal antigens, harbors many T cell subsets [e.g., T helper cell 1 (TH1), TH17, and peripheral Foxp3+regulatory T cell (pTreg)] living in relative harmony. How these T cell fates are determined *in vivo* is the subject of intense study, as is the role of T cell receptor (TCR) specificity in this process. The TCR repertoire of colonic Tregs shows little, if any, overlap with the repertoire of naïve or effector $CD4^+$ T cells present at the same location or with Tregs isolated from organs other than the intestine (*5*). Likewise, the repertoire of intestinal TH17 differs substantially from that of other intestinal T cells (*6*). Whereas colonic commensals such as *Clostridium spp.* favor pTreg development (*5, 7*), segmented filamentous bacteria (SFB) induce differentiation of conventional $CD4^+$ T cells (Tconvs) into quasi-clonal TH17 in the small intestine (*6, 8*). Thus, the repertoire and fate of $CD4^+$ T cells in the intestinal LP are determined by the microbiota. Fate decisions appear to be made at the clonal level so that different TCR specificities determine different developmental outcomes. The mechanism whereby TCR specificity drives T cell fate and function is unclear and may depend on the relative abundance of the antigens recognized, environmental cues, or a combination of both. Development and expansion of thymus-derived or natural Tregs (nTregs) are limited by intraclonal competition (*9, 10*). This process is driven by affinity for self-ligands: the higher the affinity for the antigen, the larger the nTreg “niche” size (*11*). When antigen presentation occurs under sub-immunogenic or non-inflammatory conditions, Tconvs may differentiate into pTregs (*1*). If and how the identity of the TCR dictates cell fate among Tconvs remains unsettled, as does the role of TCR specificity in determining the pTreg phenotype. To address these questions, we generated a monoclonal mouse line cloned from a pTreg nucleus and thus bearing the pre-rearranged TCR of a pTreg. We found that this TCR facilitates conversion of $CD4^+$ T cells into $CD4^+CD8\alpha\alpha^+$ intraepithelial

lymphocytes ($CD4_{IELs}$) while, at the same time, allowing development of pTreg in the mesenteric lymph nodes (mLNs) and small intestine LP (siLP), all in a microbiota-dependent manner. Thus, a single TCR specificity can give origin to two distinct T cell phenotypes in two distinct anatomical locations.

Results

We used somatic cell nuclear transfer (SCNT) to generate a transnuclear (TN) mouse line that carries a TCR cloned from the nucleus of a pTreg lymphocyte, isolated from the intestine-draining mLNs of a healthy, unmanipulated Foxp3-GFP (green fluorescent protein) reporter mouse (Fig 2.1A). To simplify the identification of the TCRα in the SCNT-derived mouse, we sorted $CD4^+CD8\alpha^-Foxp3^-GFP^+$ pTregs that expressed Vα2, Vα8.3, or Vα11 (Fig. 2.1B) by fluorescence-activated cell sorting (FACS) and used them as donors of nuclei for SCNT. Donor mLN pTregs were further identified as neuropilin-$1^{-/low}$, as previously reported (*12*). The resulting pTreg TN mouse line carries pre-rearranged endogenous TCRα and TCRβ loci that assemble into a functional receptor, as shown for other TN mouse lines (*13, 14*). Resulting chimeras from SCNT were bred to C57BL/6 wild-type (WT) mice to obtain germline transmission (Fig. 2.1C). TN mice were crossed to Rag1-deficient mice to preclude secondary TCR rearrangements (Fig. 2.1A). We used these TN mice (Fig. 2.1A) to investigate the role of the TCR in determining the fate of conventional $CD4^+$ T cells.

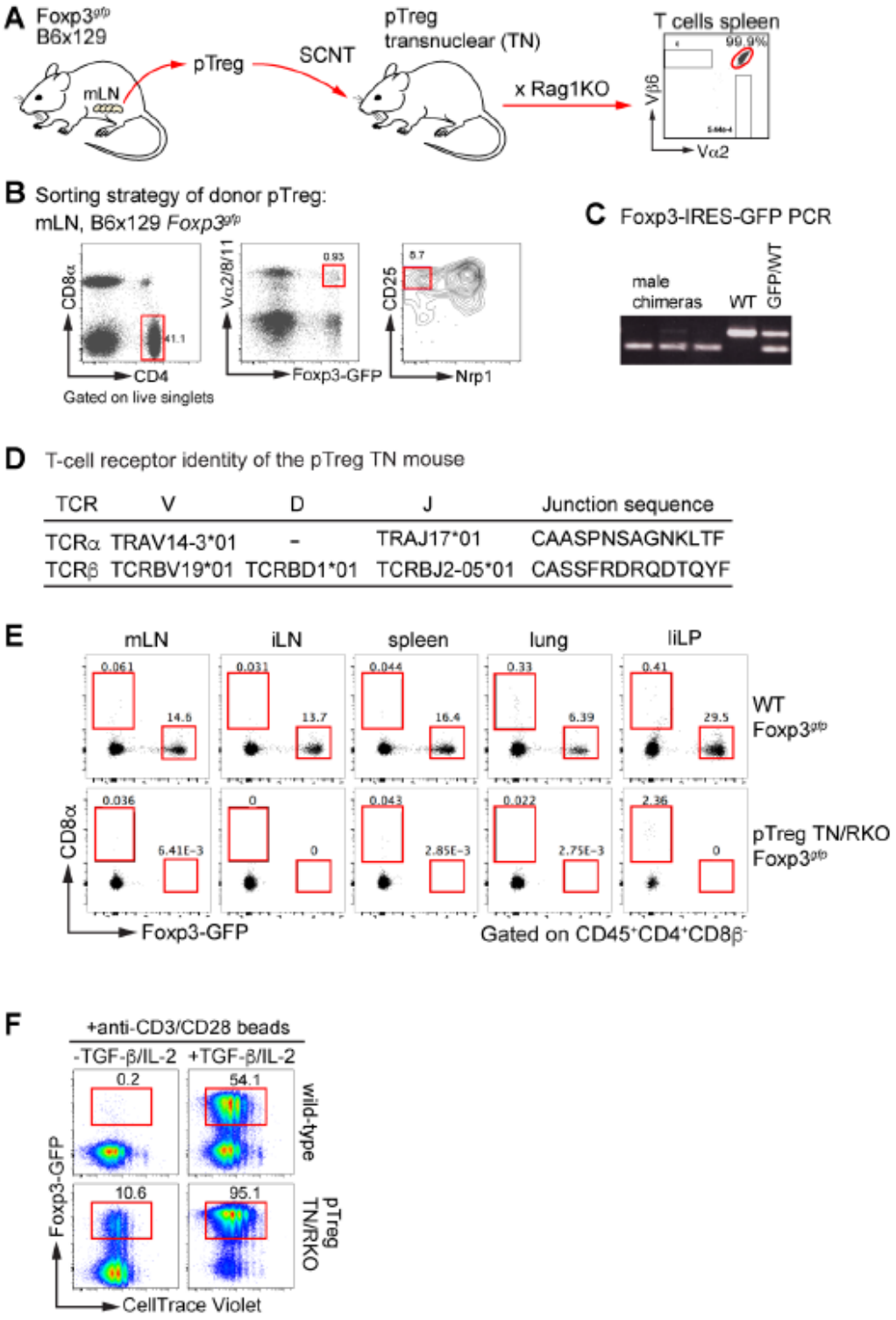

Figure 2.1 Generation of the pTreg TN mouse.

(**A**) Generation of the pTreg TN/RKO mouse line by somatic cell nuclear transfer (SCNT) that carries a monoclonal TCR (Vα2 Vβ6) isolated from pTreg cells sorted from mLN. (**B**) Sorting strategy used to generate the TN line. pTreg cells from mLN of Foxp3-GFP reporter mice were sorted on a FACS Aria instrument and used as donors of nuclei for SCNT. (**C**) Resulting chimeras were determined by agouti coat color and confirmed by PCR for IRES-GFP (left panel). Male chimeras were bred to Rag1-deficient (Rag1KO) females, and resulting offspring with agouti pups indicated germline transmission. (**D**) RNA from total splenocytes of pTreg TN/RAGKO mice was isolated and transcribed into cDNA. TRAV14 (Vα2) and TRBV19 (Vβ6) were then amplified by PCR using primers on the CDR1 and constant regions of TCRα and TCRβ. PCR product was sequenced and analyzed on the international ImMunoGeneTics information system® (http://www.imgt.org/v quest) and CDR3 sequences of TCRα and TCRβ were identified. (**E**) Frequency of Foxp3+ Treg cells at the indicated organs from pTreg TN/RKO and WT mice. Flow cytometry analysis representative of at least 5 pTreg TN/RKO mice. (**F**) *In vitro* proliferation and Treg cell conversion of CD4+ T cells isolated from TN/RAGKO mice or WT mice. (A) FACS-sorted naïve CD4+ Foxp3-GFP- T cells were cultured in the presence of anti-CD3/CD28 beads (Miltenyi) and in the presence or absence of TGF-β (20ng/ml) and IL-2 (100U/ml) to induce Treg differentiation. Proliferation was measured by CellTrace violet dilution, and Treg conversion by GFP expression.

Nearly all T cells in the peripheral lymphoid organs of these TN mice were $CD4^+CD8\alpha^-$ and carried a monoclonal Vα2 Vβ6 TCR pair with unique CDR3 sequences (referred to hereafter as pTregTN/RKO mice; Fig. 2.1 A, D, and Fig. 2.2A). pTregTN/RKO mice are viable and fertile and show no signs of overt autoimmune or wasting disease (follow-up >8 months after birth). Despite having been cloned from a $Foxp3^+$ pTreg, no $Foxp3^+$ cells could be detected in these mice in any of the organs analyzed (Fig. 2.2A and Fig. 2.1E). To rule out an intrinsic inability of the TN cells to become $Foxp3^+$ Treg, we purified naïve $CD4^+$ T cells from spleens of pTregTN/RKO mice and induced Treg differentiation *in vitro*. Activation with anti-CD3 and anti-CD28 in the presence or absence of transforming growth factor–β (TGF-β) and interleukin-2 (IL-2) elicited proliferation of naïve TN $CD4^+$ T cells to the same extent as WT polyclonal cells. Conversion into $Foxp3^+$ Treg was readily observed in the presence of TGF-β and IL-2 (Fig. 2.1F), establishing the potential of these TN cells to become Treg.

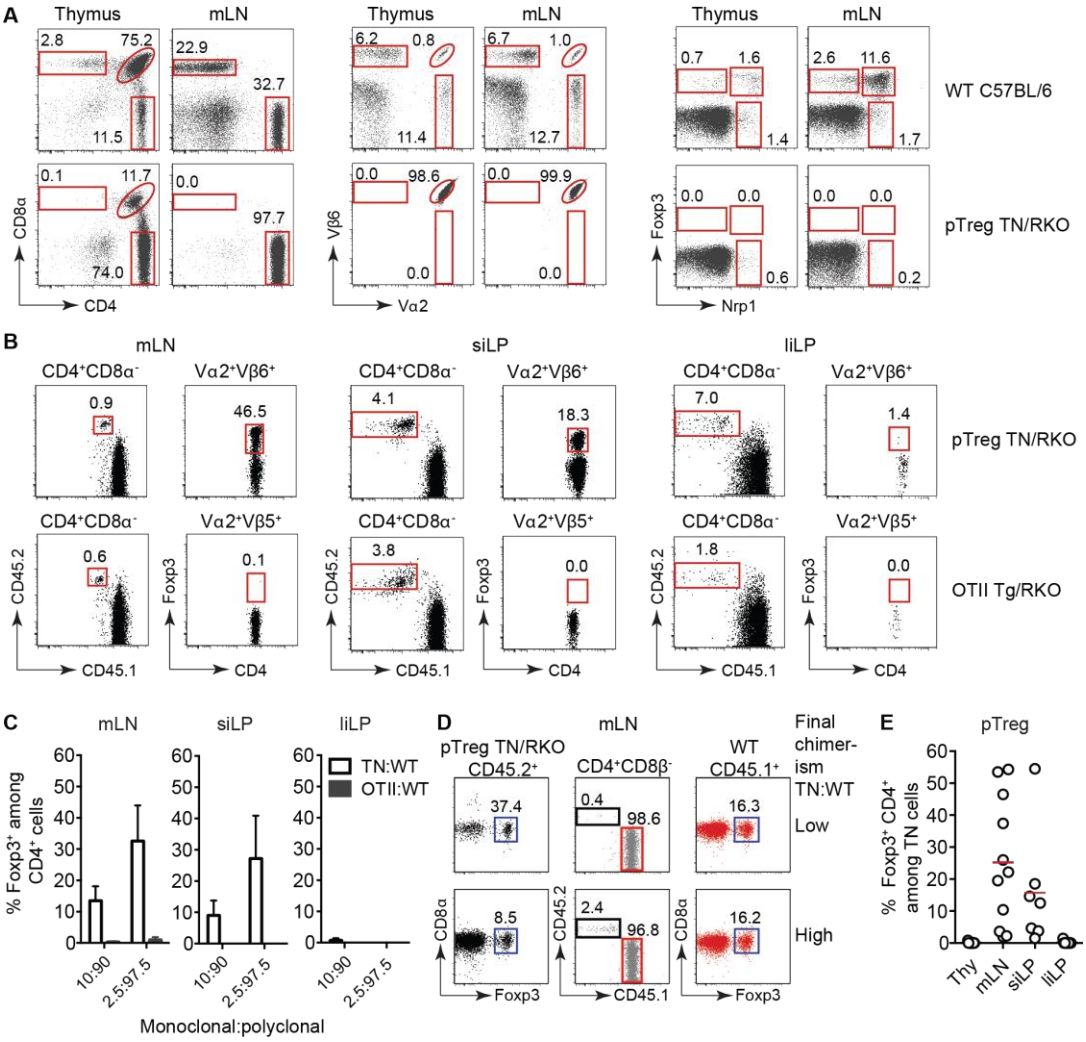

Figure 2.2 Low clonal frequency of pTreg precursors allows development of Tregs.

(**A**) Flow cytometry analysis of the indicated organs from WT and pTreg TN/RKO. Dot plots on the left show $CD3^+$ cells. Middle and right dot plots show $CD3^+CD4^+CD8\alpha^-$ cells. (**B**) Mixed bone marrow chimeras. Sublethally irradiated TCRabKO mice were reconstituted with a total of 5×10^6 T cell–depleted bone marrow cells from congenically marked WT (CD45.1) along with pTreg TN/RKO or OTII Tg/RKO (CD45.2) mice at different TN/WT ratios (2.5:97.5 or 10:90). Cells from the indicated locations were harvested 12 weeks after reconstitution and analyzed by flow cytometry. For each indicated location, dot plots on the left show the proportion of $CD4^+CD8\alpha^-$ T cells among the monoclonal (CD45.2) and polyclonal (CD45.1) compartments of two chimeric mice, and right plots show the frequency of Treg in the monoclonal compartment (top plots, reconstituted with pTreg TN/RKO bone marrow; bottom plots, with OTII Tg/RKO). Dot plots are representative of four to six mice per group and show mice reconstituted with 2.5:97.5 ratio. (**C**) Quantification of the frequency of Foxp3+ Tregs among $CD4^+CD8\alpha^-V\alpha2^+V\beta6^+$ (TN) or $V\beta5^+$ (OTII) cells in the indicated locations of the mixed bone marrow chimeric mice. Graph shows the mean and SD of all mice analyzed in one experiment. (**D**) Mixed bone marrow chimeras as in (B). Dot plots show two chimeric mice with different degrees of chimerism of TN/WT in the mLN. (**E**) Graph shows the frequency of Foxp3+ Tregs among TN lymphocytes recovered from the indicated locations from all mice analyzed in three independent experiments (different TN/WT ratios). Each symbol represents a mouse, and horizontal bars represent the means.

The development of thymus-derived nTreg can occur only when the number of precursors bearing the same TCR rearrangement is small (9,10). To determine whether this is the case for pTreg development from our TN TCR, we reconstituted sublethally irradiated TCRαβKO recipients with bone marrow preparations containing a mixture of cells from polyclonal (WT) and monoclonal pTregTN/RAGKO donors [or ovalbumin (OVA)–specific OTII RAGKO donors as a control] in different proportions and analyzed T cell development at 12 weeks after reconstitution (see Materials and Methods and Fig. 2.2,B -D). No Treg development was observed in any organ when the monoclonal precursors were OTII RAGKO, regardless of the degree of chimerism (Fig. 2.2 B,C), consistent with the idea that generation of pTreg requires exposure to antigen (*12, 15*). In contrast, Treg development from TN precursors was readily observed but only when the TN/WT ratio (2.5/97.5) was low. Polyclonal precursors gave rise to Treg regardless of the degree of chimerism (Fig. 2.2B-E). Although low precursor frequency facilitated some Treg development in inguinal LNs (iLNs) and spleen, Treg frequencies at these sites were much lower than those in mLN (Fig. 2.3A-C). No TN Tregs were found in the thymus, regardless of the extent of chimerism (Fig. 2.2E and Fig. 2.3A,B), indicating that this particular TCR does not support nTreg development, a further argument in favor of the notion that the quality of the TCR contributes to setting T cell fate.

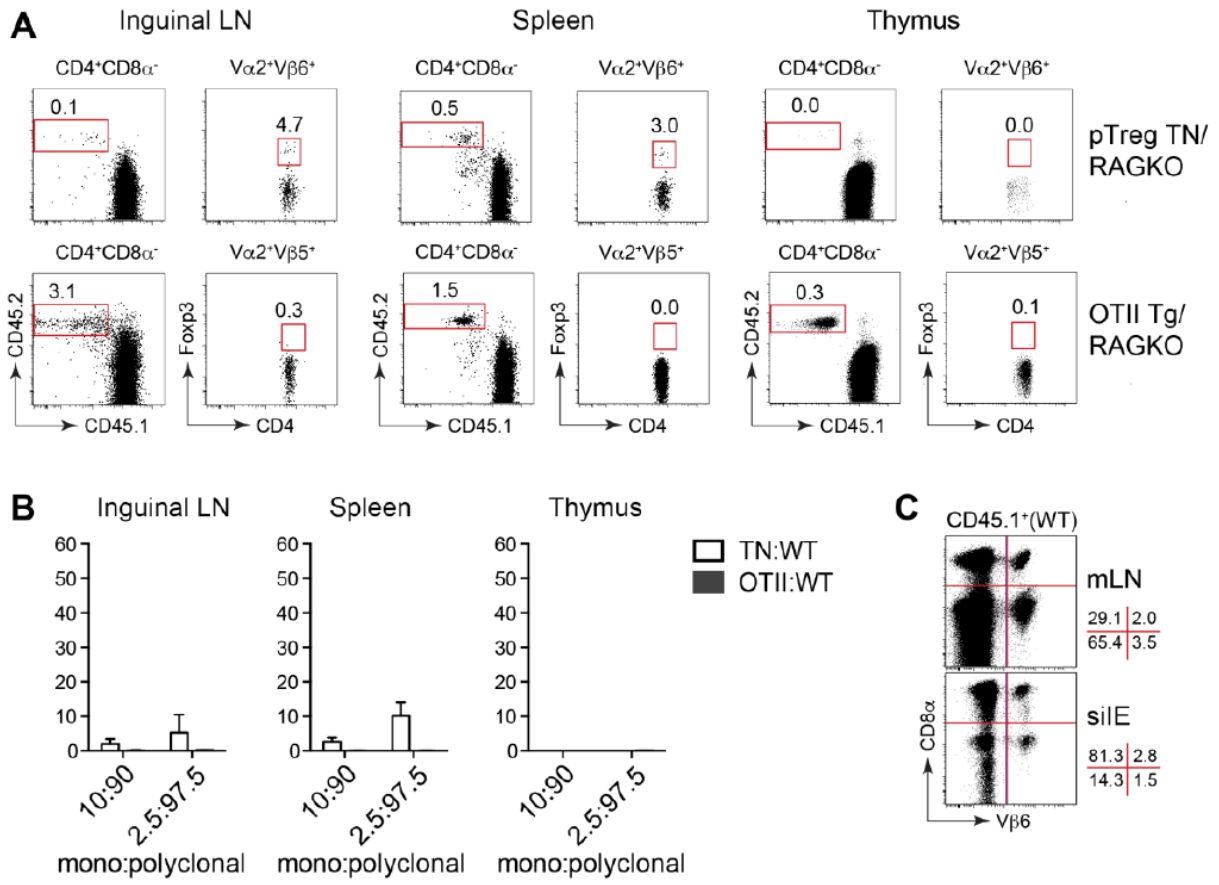

Figure 2.3 pTreg TN precursors do not facilitate development of Tregs in the thymus.

(**A**) Mixed bone marrow chimeras. Sublethally irradiated TCRαβKO mice were reconstituted with a total of $5X10^6$ T-cell depleted bone marrow cells from congenically-marked WT (CD45.1) along with pTreg TN/RKO or OTII Tg/RKO (CD45.2) mice at different TN/WT ratios (2.5:97.5 or 10:90). Cells from the indicated locations were harvested 12 weeks post-reconstitution and analyzed by flow cytometry. For each indicated location, dot-plots on the left show the proportion of $CD4^+CD8\alpha^-$ T cells among the monoclonal (CD45.2) and polyclonal (CD45.1) compartments of two chimeric mice and right plots show the frequency of Treg cells in the monoclonal compartment (top plots, reconstituted with pTreg TN/RKO BM and bottom plots with OTII Tg/RKO). Dot-plots are representative of 4-6 mice/group. (**B**) Quantification of the frequency of Foxp3+ Treg cells among $CD4^+CD8\alpha^-V\alpha2^+V\beta6^+$ (TN) or $V\beta5^+$ (OTII) cells in the indicated organs of the mixed bone marrow chimeric mice. Graph shows data from a single experiment. (**C**) Dot-plots show the positive and negative staining for CD8α gated on the WT cells ($CD45.1^+CD45.2^-$ cells, support figure for Fig 2.2D) of the indicated compartments. Numbers on the side indicate the frequency of each quadrant.

We next analyzed whether TN pTreg could also accumulate at the intestinal mucosa, given that their TCR was originally derived from a pTreg in the intestine-draining mLN. Again, the development of pTreg was dependent on low precursor frequencies and was seen only in the siLP, whereas very few pTregs were found in the large intestine LP (liLP)(Fig. 2.2 B,C).We conclude that, for this particular TCR, low clonal frequencies are a prerequisite for generation of pTreg in peripheral lymphoid organs and in the siLP. Given a previous report of niche-dependent pTreg generation in the colon (5), it is likely that precursor frequency effects are a common property of pTreg development in the gut. The absence of pTreg in the monoclonal pTregTN/RKO mice (Fig. 2.1 and Fig. 2.2) prompted us to investigate whether $CD4^+$ TN cells could adopt a phenotype other than that of a Treg *in vivo*. In lymphoid organs (mLN, iLN, and spleen), the vast majority of the TN cells retained a naïve $CD44^{low}$ phenotype (Fig. 2.4A). Because the mLN drains the intestine, we analyzed LP and intraepithelial (IE) compartments for the presence and phenotype of the TN cells. The few TN cells present in the liLP had a naïve phenotype, whereas $CD4^+$ TN T cells were abundant in the siLP and IE and expressed high levels of CD44 (Fig. 2.4A). Although no $Foxp3^+$ Tregs were present in the siLP and IE compartments (Fig. 2.4 B, C), unexpectedly, >50% of TN $CD4^+$ T cells at these sites co-expressed CD8α (but not CD8β), and almost all of these produced interferon-γ (IFN-γ) (Fig. 2.4 B-D). Only mice older than 10 weeks of age displayed these traits (Fig. 2.4 C,D and 2.5 A,B). In younger mice, $CD4^+$ T cells remained CD4 single-positive (SP) with a naïve phenotype and did not produce IFN-γ (Fig. 2.4 A,D). The trigger for differentiation and IFN-γ production is therefore likely to be a foreign antigen that accumulates over time, rather than a self-antigen present since birth. We did not detect production of IL-17A by TN cells isolated from siLP or IE (Fig. 2.4 D), yet these cells had no intrinsic defect in making IL-17 when stimulated *in vitro* under TH17-polarizing conditions (Fig. 2.5C). Therefore, in the small intestine, the TN TCR naturally favors the efficient conversion of $CD4^+$ T cells into IFN-γ–producing $CD4_{IELs}$ rather than into $Foxp3^+$ pTregs.

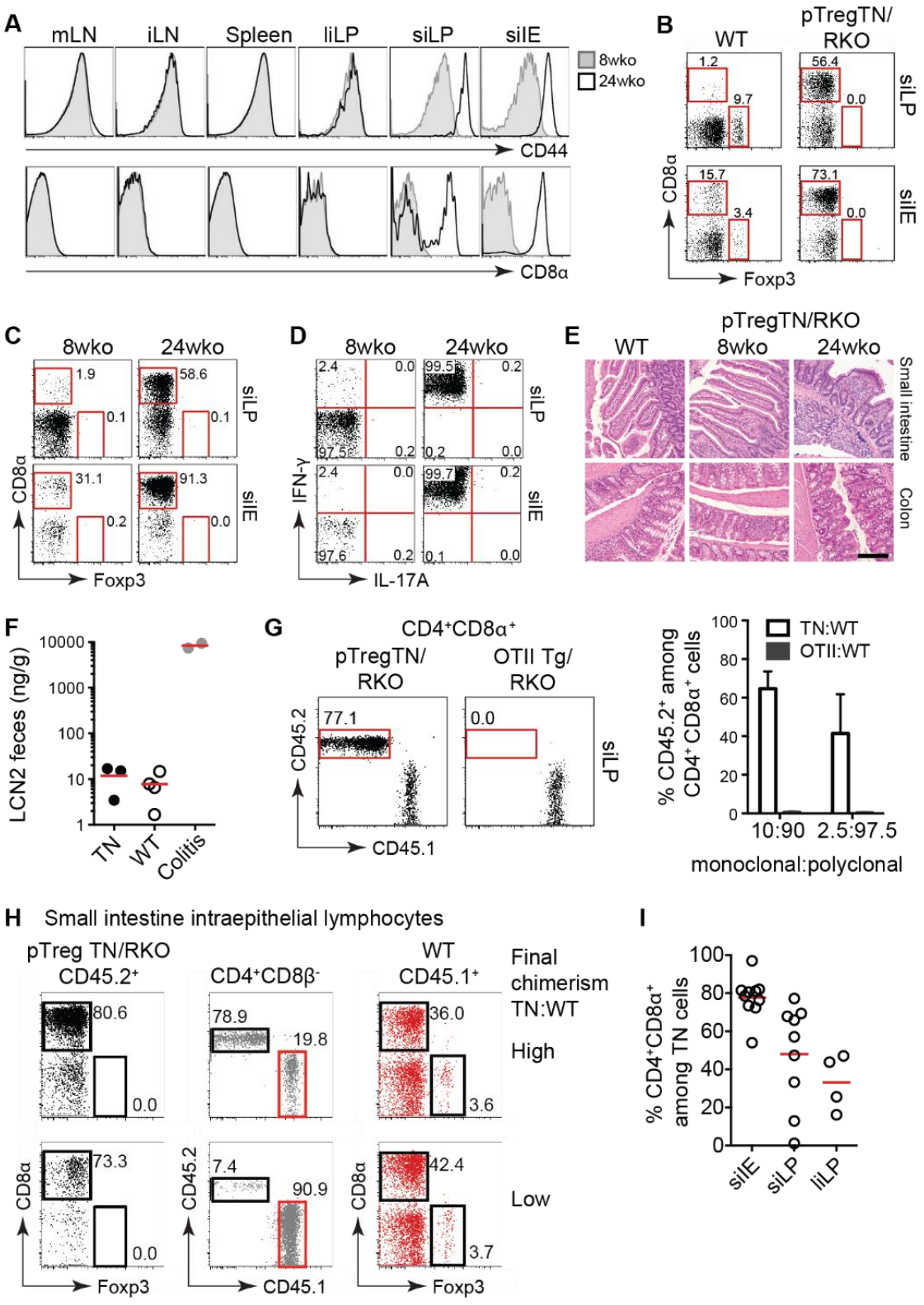

Figure 2.4 pTreg TCR allows for the development of CD4IEL.

(**A**) Flow cytometry analysis of CD44 and CD8a expression on CD45+CD4+CD8b−Va2+Vb6+ TN cells in the indicated lymphoid organs and intestinal compartments of 8-week-old (8 wko) and 24-week-old (24 wko) pTreg TN/RKO mice. (**B**) Dot plots show the frequencies of CD8a+ and Foxp3+ T cells among $CD45^+CD4^+CD8\beta^-V\alpha2^+V\beta6^+$ cells in the siLP and siIE compartment in C57BL/6 WT and pTreg TN/RKO mice. (**C and D**) Dot plots gated as in (B) showing the comparison between young (8-week-old) and old (24-week-old) pTreg TN/RKO mice. (**E**) Photomicrographs of the small intestine and colon H&E staining of WT C57BL/6 (24-week-old) and pTreg TN/RKO (8- and 24-week-old) mice. Original magnification, ×200; scale bar, 200 mm. (A to E) Representative of at least five mice per age group. (**F**) Fecal LCN2 levels measured by ELISA. Feces were collected from pTreg TN/RKO mice 4 to 6 months old and age-matched C57BL/6 WT mice. Colitis denotes positive controls for ELISA (feces from colitic mice). (**G**) Mixed bone marrow chimeras. Sublethally irradiated TCRabKO mice were reconstituted with a total of 5×10^6 T cell–depleted bone marrow cells from congenically marked WT mice (CD45.1) along with pTreg TN/RKO or OTII Tg/RKO (CD45.2) mice at the proportions indicated on the graph. Dot plots show the frequency of CD4+CD8a+ TN cells in the LP of two chimeric mice reconstituted with the indicated bone marrow cells. Graph shows the mean and SD of all mice analyzed in one experiment. (**H**) Mixed bone marrow chimeras as in (G). Dot plots show two chimeric mice with different degrees of chimerism of TN/WT among the siIEL. (**I**) Graph shows the frequency of CD4+CD8a+ in the IE and LP in all mice analyzed in three independent experiments (different TN/WT ratios). Each symbol represents a mouse, and the horizontal bars represent the means.

Production of IFN-γ is consistent with the cytotoxic phenotype reported for IEL (*16*). Despite massive expansion of these IFN-γ producers in the small intestine, pTregTN/RKO mice showed no signs of overt inflammatory or wasting disease. Tissue architecture was preserved with no signs of epithelial disruption (Fig. 2.3E). Levels of fecal lipocalin-2 (LCN2), a sensitive marker of intestinal inflammation (*17*), were low and similar to those in WT mice (Fig. 2.3F), confirming the absence of intestinal inflammation in our pTregTN/RKO mice. Using the mixed bone marrow chimera approach (Fig. 2.2), we analyzed the niche dependency of the conversion of TN precursors into $CD4_{IELs}$. In sharp contrast to pTreg development (Fig. 2.2), large numbers of $CD4^+CD8\beta^-CD8\alpha^+$ T cells emerged not only in the IE but also in the siLP (and less so in the liLP), irrespective of the extent of chimerism (Fig. 2.3 G-I). As expected, no $CD4^+CD8\beta^-CD8\alpha^+$ T cells emerged from the OTII bone marrow (Fig. 2.3G). In the majority of mice analyzed, TN $CD4_{IEL}$ outcompeted their polyclonal counterparts ($CD45.1^+$), as evidenced by the increased proportion of TN $CD45.2^+$ cells among the $CD4^+CD8\beta^-CD8\alpha^+$ population (Fig. 2.3 G,H). Thus, in the microenvironment of the small intestine, $CD4^+$ TN T cells engage a T cell program that preferentially leads to the expression of CD8αα. A single clonal $CD4^+$ T cell precursor originating from a naïve unmanipulated mouse can therefore spontaneously develop along two distinct cell fates (pTreg versus $CD4_{IEL}$), with different niche

requirements.TN cells cloned from an mLN pTreg yield not only pTreg but also $CD4_{IEL}$ in the small intestine, in the absence of any exogenous stimulation or immunization (Fig. 2.2 B-E, and 2.3 A-D,H and I). The TN TCR might therefore recognize an antigen constitutively present at these sites.

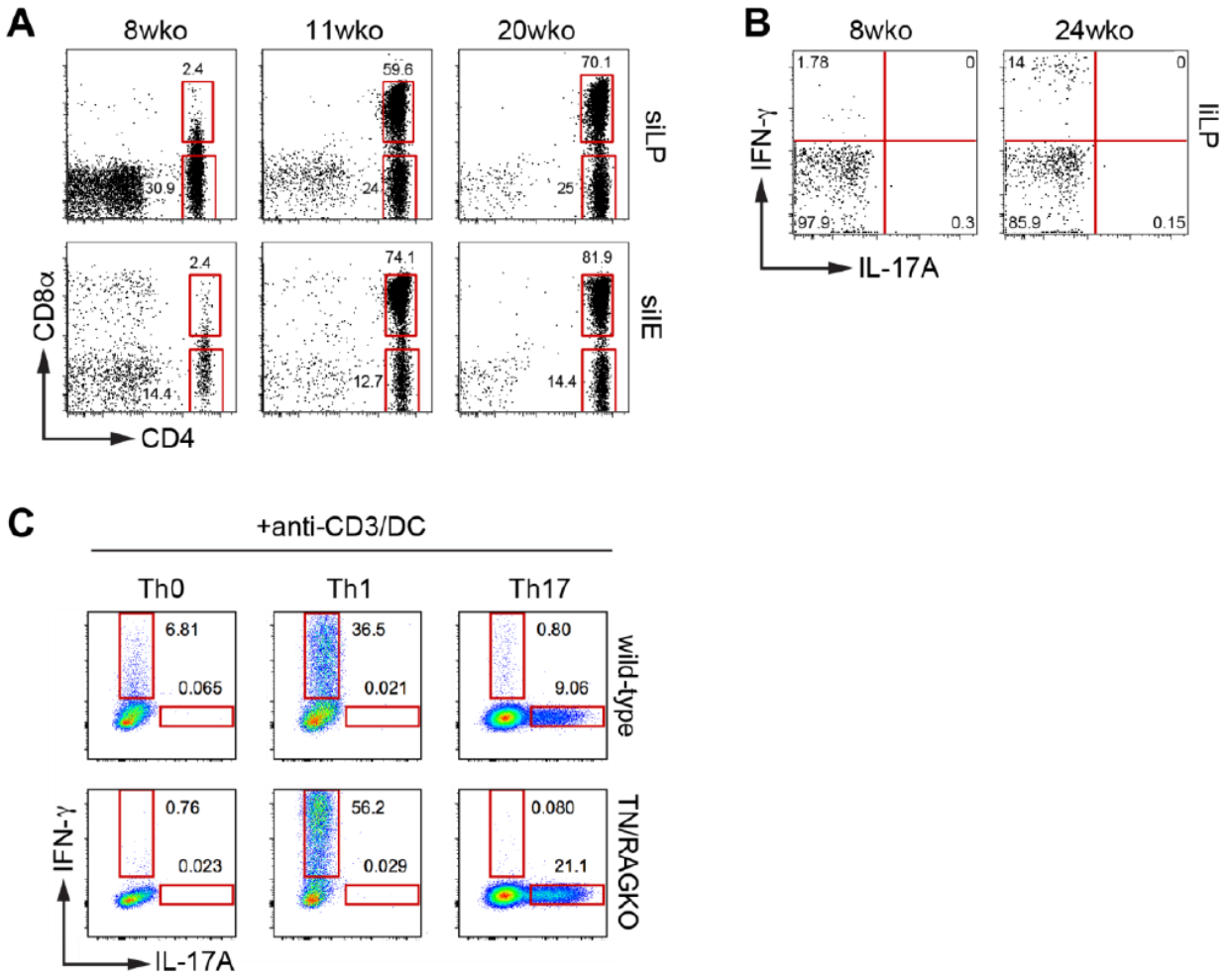

Figure 2.5 Age-dependent accumulation of $CD4^+CD8\alpha^+$ T cells in the small intestine of pTreg TN/RKO mice.

(**A**) Dot-plots show the frequency of $CD4^+CD8\alpha^+$ cells among $CD45^+CD8\alpha^-V\alpha2^+V\beta6^+$ cells in the small intestine lamina propria (siLP) and intraepithelial compartment (siIE) in young (8 weeks old) and old (24 weeks old) pTreg TN/RKO mice. (**B**) Dot-plots show the frequency of cytokine-producing cells among $CD45^+CD4^+CD8\alpha^-V\alpha2^+V\beta6^+$ cells from the large intestine lamina propria (liLP) in young (8 weeks old) and old (24 weeks old) pTreg TN/RKO mice. Dot-plots representative of 4-5 mice/ age (A, B). (**C**) Naïve $CD4^+$ T cells ($1X10^5$) were cultured in the presence of 5µg/ml of anti-CD3 (ebioscience) and WT DC ($1X10^5$) in the presence or absence of polarizing conditions (Th1, 10ng/ml IL-12 and 10µg/ml anti-IL-4; Th17, 0.5ng/ml TGF-β, 20ng/ml IL-6, 10ng/ml IL-23 and 10µg/ml anti-IFN-γ) for 4 days. Cultures were treated with PMA and ionomycin for the last 4h of culture and addition of monesin for the final 2h prior to intracellular staining for IFN-γ and IL-17A using cytofix/cytoperm (BD Biosciences).

We tested the ability of TN cells to undergo homeostatic expansion in lymphopenic hosts (*18*), which requires TCR engagement. We adoptively transferred naïve $CD4^+$ T cells isolated from spleens and mLNs of pTregTN/RKO or WT mice into TCRαβKO recipients and analyzed the recovery of TN cells from different anatomical sites 6 to 8 weeks after transfer. We found TN cells to be abundant in the siLP and IE but less so in the liLP (Fig. 2.6 A, B). Moreover, transferred cells converted into pTreg in mLN and siLP, but pTregs were almost entirely absent from the IE, where $CD4_{IEL}$ was the dominant population (Fig. 2.6 A,B). Because of the pre-rearranged TCR in TN mice, TCRα is expressed prematurely during thymic selection, resulting in an increased frequency of SP cells at the expense of double-positive (DP) precursors, as seen also in TCR transgenic mice. Conversion into $CD4_{IEL}$ from TN precursors might have been a result of aberrant thymic selection. To exclude the unlikely possibility that "spontaneous" conversion of mature $CD4^+CD8\alpha^-$ T cells (isolated from spleen and mLN) into $CD4_{IEL}$ is an inevitable outcome in TN mice that carry a monoclonal CD4 compartment, we transferred $CD4^+$ T cells from an unrelated TN line, cloned from pancreatic tumor-infiltrating $CD4^+$ T cells, into TCRαβKO hosts and analyzed their fate 6 weeks after transfer. As expected, these control TN T cells (also purified as $CD4^+CD8\alpha^-$) migrated poorly to the intestine compared with pTreg TN cells and did not convert into $CD4_{IELs}$ (Fig.2.6C).

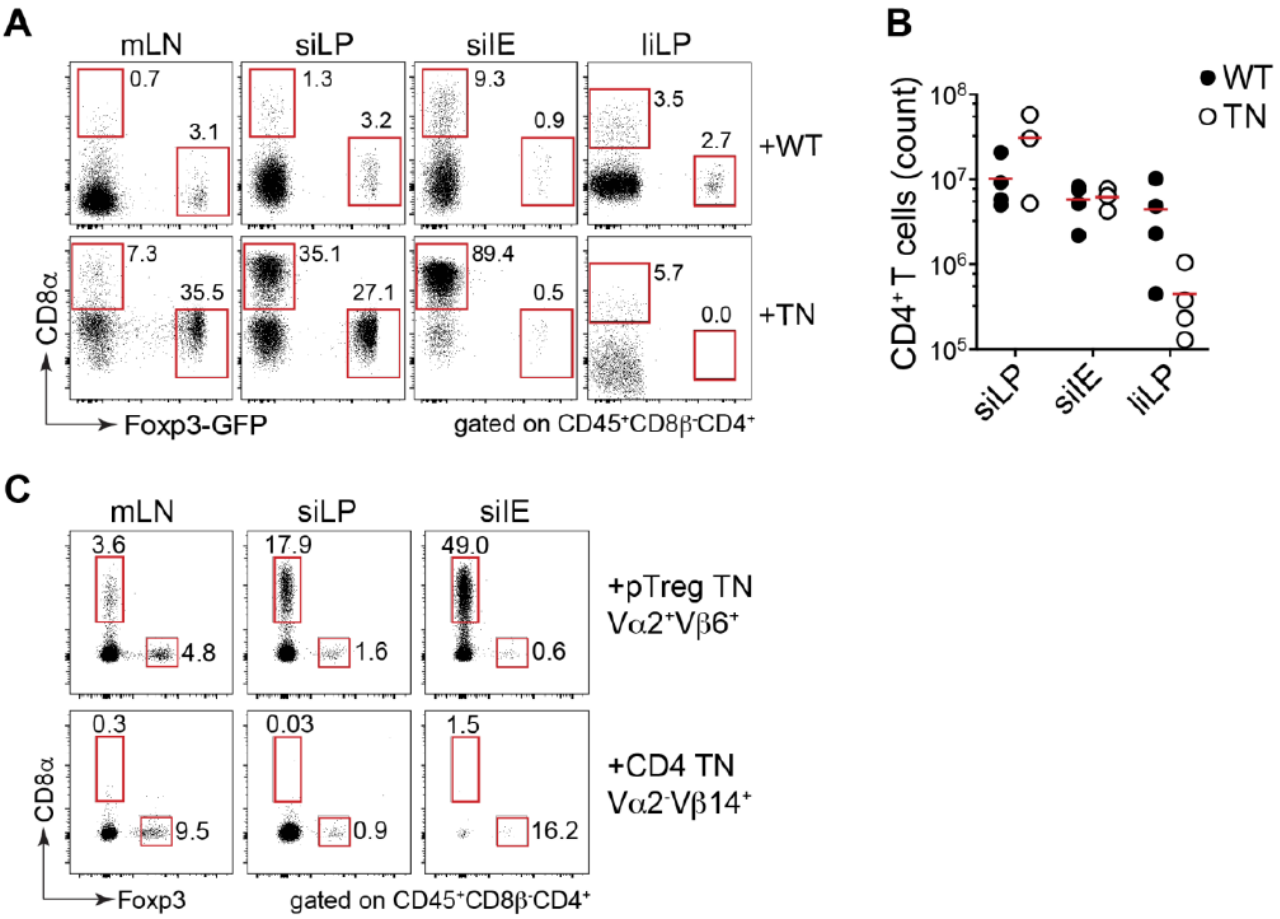

Figure 2.6 Naïve CD4⁺ TN T cells from pTreg TN/RKO expand and differentiate into pTregs and $CD4_{IELs}$ in immunodeficient hosts.

(**A**) $CD4^+CD8\alpha^-$Foxp3-GFP^- cells were FACS-sorted from spleen and mLN of pTreg TNRKO/Foxp3GFP or WT Foxp3 GFP mice and $5X10^5$ cells were transferred into TCRαβKO mice. Cells from the indicated locations were harvested 6-8 weeks post-transfer and analyzed for conversion into pTreg cells or $CD4_{IEL}$ by flow cytometry. (A) Dot-plots are representative of 3-4 mice/group. (**B**) Cell counts for the indicated organs. (**C**) $CD4^+CD8\alpha^-$ T cells were purified from spleens and mLN of pTreg TN/RKO or PancCD4/RKO TN mice (see Material and Methods) and $5X10^5$ cells were transferred into TCRαβKO mice. Cells from the indicated locations were harvested 6 weeks post-transfer and analyzed for conversion into pTreg cells or $CD4_{IEL}$ by flow cytometry.

When transferred into immunocompetent WT hosts, pTregTN $CD4^+$cells proliferated in the mLN but not in the iLN, as measured by carboxyfluorescein diacetate succinimidyl ester (CFSE) dilution 5 days after adoptive transfer (Fig. 2.7 A,B). We also observed expansion and differentiation into $CD4_{IEL}$ in the intestinal mucosa as well as into pTreg in the mLN (Fig. 2.7 C,D) 6 to 8 weeks after cell transfer.

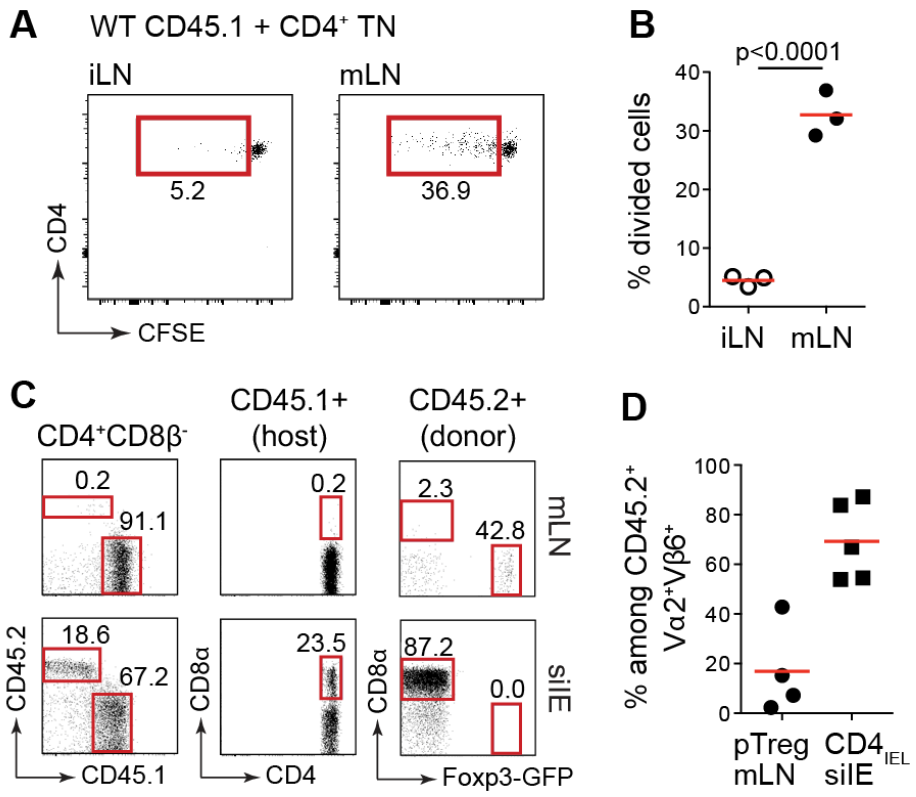

Figure 2.7 Expansion and differentiation of pTreg TN T cells in WT polyclonal hosts.

(**A**) Naïve CD4+ T cells from pTreg TN/RKO were labeled with CFSE, and 5 × 10^6 cells were transferred into WT CD45.1 mice. Five days later, the indicated LNs were harvested, and CFSE dilution was measured by flow cytometry. Dot plots are representative of three mice and show $CD45.1^-CD45.2^+V\alpha2^+V\beta6^+$ cells. (**B**) Graph shows all mice analyzed. (**C**) Naïve CD4+ T cells from pTreg TN/RKO/Foxp3GFP were bead purified, and 5 × 10^6 cells were transferred into congenically marked WT hosts (CD45.1). Conversion of transferred cells was analyzed 8 weeks after cell transfer at the indicated locations. Dot plots are representative of four to five mice. (**D**) Graph shows the mean and SD of all the mice analyzed. P values were calculated with Student's t test. P values of <0.05 were considered statistically significant.

Antigen presentation in the mLN and small intestine, but not in the iLN, supports proliferation and differentiation of TN cells into pTreg and $CD4_{IEL}$, and this is not a result of aberrant expansion driven by the lymphopenic environment in T cell–deficient hosts. TN $CD4^+$ T cells failed to expand when adoptively transferred into major histocompatibility complex class II (MHCII)–deficient (MHCIIKO) recipients (Fig. 2.8 A,B) and are thus MHCII-restricted. Likewise, pTregTN/RKO mice crossed to MHCIIKO mice develop few, if any, $CD4^+$ or $CD8^+$ T cells (Fig. 2.8C).

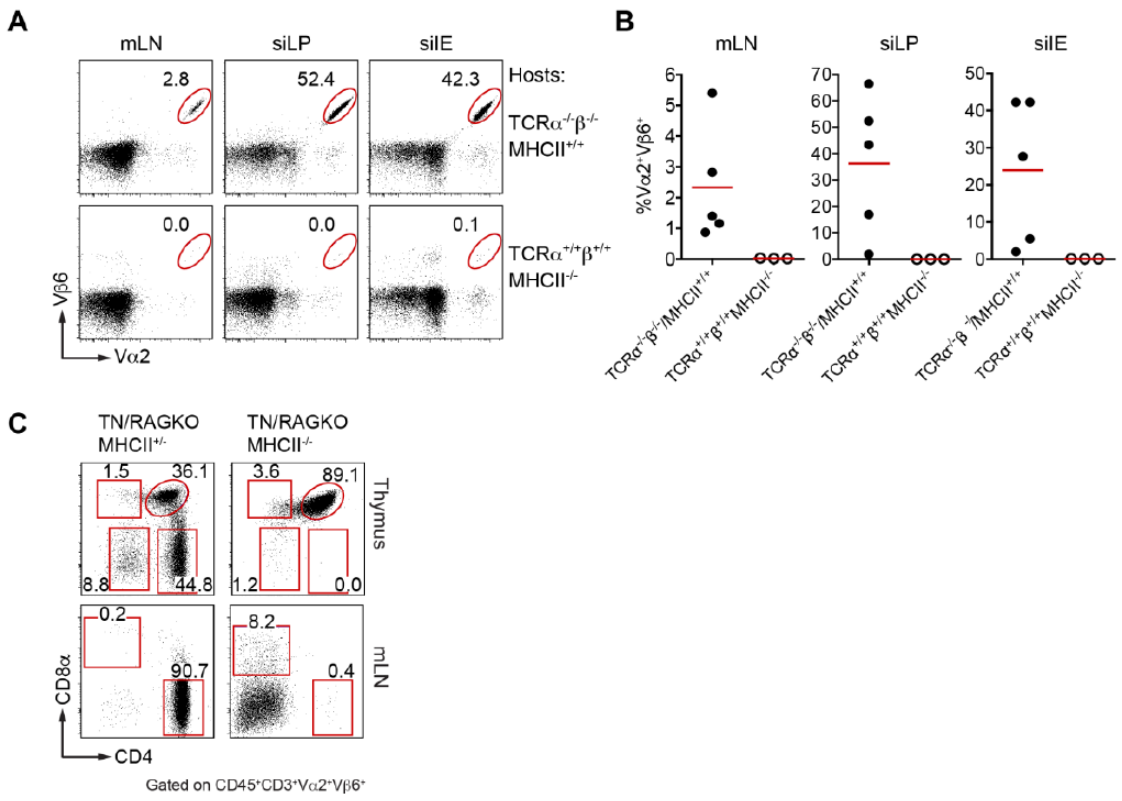

Figure 2.8 CD4⁺ T cells from pTreg TN/RKO mice are MHCII-restricted.

(**A**) Naïve CD4⁺ T cells (5X10⁵) isolated from pTreg TN/RKO mice were adoptively-transferred into the indicated hosts. Recovery of transferred cells was measured 8-10 weeks after transfer at the indicated organs by flow cytometry. (**B**) Graph shows the frequency of TN cells (identified by Vα2 Vβ6 expression) in the indicated locations of the indicated recipient mice. Each symbol represents a mouse. (**C**) pTreg TN/RAGKO mice were crossed to Class II MHC-deficient mice (MHCII$^{-/-}$) and development of CD4⁺ T cells were analyzed in the indicated locations compared to Class II MHC-sufficient mice (MHCII$^{+/-}$). Dot-plots are representative of 3 mice/genotype.

The late development of $CD4_{IEL}$ observed in the pTreg/RKO mice, together with the absence of any overt disease, suggested that the antigen recognized by the TN TCR was neither a dietary nor a self-antigen. We therefore investigated whether expansion and conversion of TN cells in TCRαβKO hosts depended on the resident microbiota. We treated TCRαβKO recipients of TN cells with a cocktail of antibiotics to deplete the microbiota (*19*). Efficiency of treatment was confirmed by the absence of bacterial colony growth under aerobic and anaerobic conditions and by a reduction of at least one log in 16S ribosomal DNA amplification from fecal samples when compared with untreated mice (see Materials and Methods) (Fig. 2.9 A,B).

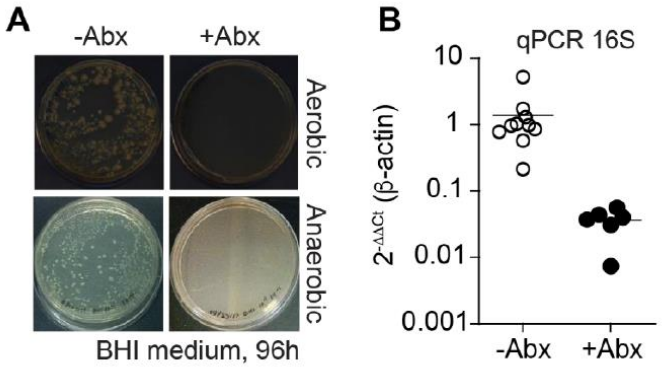

Figure 2.9 Antibiotic treatment depleted the microbiota.

(A) Stool test for mice shown in Figure 2.10. Fecal pellets from mice treated or not with antibiotics (Abx) were homogenized in PBS, plated on brain heart infusion (BHI) agar plates and incubated at 37ºC under aerobic and anaerobic conditions (anaerobic chamber: 90% nitrogen, 5% CO2, 5%) for 96h. Graph on the right shows the relative expression of 16S for fecal DNA of mice treated or not with antibiotics. Each symbol represents a mouse; horizontal bar stands for the mean.

We adoptively transferred naïve $CD4^+$ T cells isolated from pTregTN/RKO mice into antibiotic-treated or untreated recipients (Fig. 2.10A). TN cells expanded and converted into pTreg and $CD4_{IEL}$ in untreated mice, but TN T cells failed to do so in antibiotic-treated recipients. The few cells that did migrate to the small intestine remained $Foxp3^-$ and $CD8\alpha^-$ (Fig. 2.10B). Conversion into pTreg and $CD4_{IEL}$ thus depends on the microbiota, suggesting that this TN TCR recognizes a bacterial antigen. To confirm this, we adoptively transferred CFSE-labeled $CD4^+$ TN cells into TCRαβKO recipients previously treated or not with antibiotics for 7 to 14 days (Fig. 2.10C). As expected, transferred TN cells proliferated extensively in the mLN of untreated mice but not in antibiotic-treated mice. Proliferation of TN cells in antibiotic-treated mice was rescued by immunization with sonicated bacterial extracts obtained from fecal pellets or cecum lavage of Taconic mice with excluded flora (EF) (see Materials and Methods) (Fig. 2.10D). Extensive TN T cell proliferation was also triggered in iLN by subcutaneous immunization of both TCRαβKO and WT recipients, whereas no proliferation was observed in iLN of non-immunized mice (Fig. 2.10 E-H). Last, TN T cell proliferation was also inducible *in vitro* by coculture with dendritic cells (DCs) in the presence of sonicated fecal extracts from Taconic EF but not from germ-free (GF) mice (Fig. 2.10 I,J).

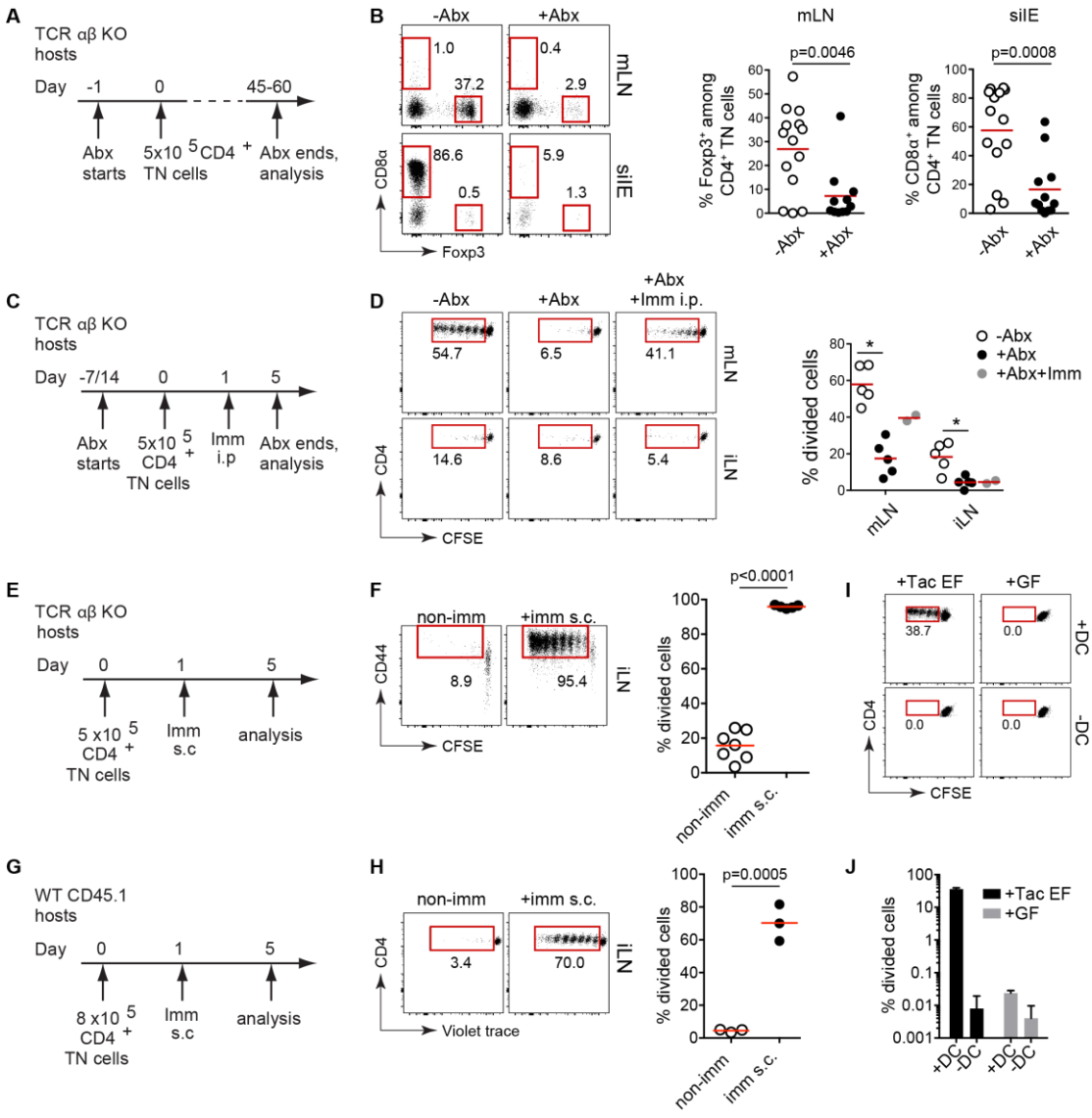

Figure 2.10 pTreg and $CD4_{IEL}$ development and expansion are dependent on the microbiota.

(**A**) Experimental design. TCRabKO mice were treated or not with antibiotics (Abx) for 6 to 8 weeks and adoptively transferred with 5 × 10^5 naïve CD4+ T cells isolated from pTreg TN/RKO mice. (**B**) Dot plots show the frequency of pTreg in mLN and CD4IEL TN cells (gated on $CD45^+CD8\beta^-CD4^+V\alpha2^+V\beta6^+$) 6 to 8 weeks after adoptive transfer. Graphs show all mice analyzed in four independent experiments. P values were determined with unpaired Student's t test. (**C**) Experimental design. TCRabKO mice were treated or not with antibiotics for 7 to 14 days and adoptively transferred with 5 × 10^5 CFSE-labeled naïve $CD4^+$ T cells. One day later, mice were immunized intraperitoneally (imm i.p.) with 50 mg of bacterial antigen extract adsorbed in alum. Bacterial extract was obtained from feces and cecum of Taconic mice (EF health status). (**D**) Dot plots show CFSE dilution in $CD4^+V\alpha2^+V\beta6^+$ T cells in the LNs of the indicated mice. Graph shows all mice that were analyzed in two independent experiments. *P = 0.0015, iLN, treated with antibiotics versus untreated; *P = 0.0008, mLN, treated with antibiotics versus untreated. (B and D) Each symbol represents a mouse, and the horizontal bars represent the means. (**E**) Experimental design. (**F**) Frequency of activated ($CD44^{high}$) and divided ($CFSE^{low}$) TN cells in the iLN of TCRabKO mice transferred with 5 × 10^5 CFSE-labeled naïve $CD4^+$ T cells and immunized subcutaneously (imm s.c.) or not with 50 mg of bacterial antigen extract adsorbed in alum as in (C). Graph shows the frequency of divided cells in all mice analyzed in two experiments. (**G**) Experimental design. WT CD45.1 mice were adoptively transferred with CellTrace Violet–labeled naïve CD4+ T cells isolated from pTreg TN/RKO mice (CD45.2) and subcutaneously immunized or not with 50 mg of bacterial antigen extract adsorbed in alum as in (C) 1 day later. Four days after the immunization, iLNs were harvested and analyzed. (**H**) Dot plots show CellTrace Violet dilution in $CD45.1^-CD45.2^+CD4^+V\alpha2^+V\beta6^+$ T cells in the iLN of the indicated mice. Graph shows all mice analyzed in one experiment. (**I**) *In vitro* culture of CFSE-labeled $CD4^+$ T cells isolated from pTreg TN/RKO mice in the presence or absence of DCs purified from B16-Flt3L–injected mice and in the presence of fecal bacterial antigen extract (50 µg/ml) from Taconic EF or GF mice. Proliferation was measured 3.5 days after coculture by CFSE dilution. (**J**) Graph shows the mean and SD of one experiment (representative of two independent experiments). P values were calculated with Student's t test. P values of <0.05 were considered statistically significant.

Bacterial antigen extracts derived from feces of mice housed in different animal facilities induced different degrees of proliferation in TN cells, but never to the same extent as the Taconic EF (Fig. 2.11 A-C), possibly reflecting differential abundance of the targeted commensal in mice with different microbiota. No proliferation was observed in the absence of DCs or when DCs were deficient in MHCII (Fig. 2.10 I,J, and 2.11A). Proliferation induced by Taconic EF bacterial extracts was abolished by treatment with trypsin and by heat inactivation (Fig. 2.11D).

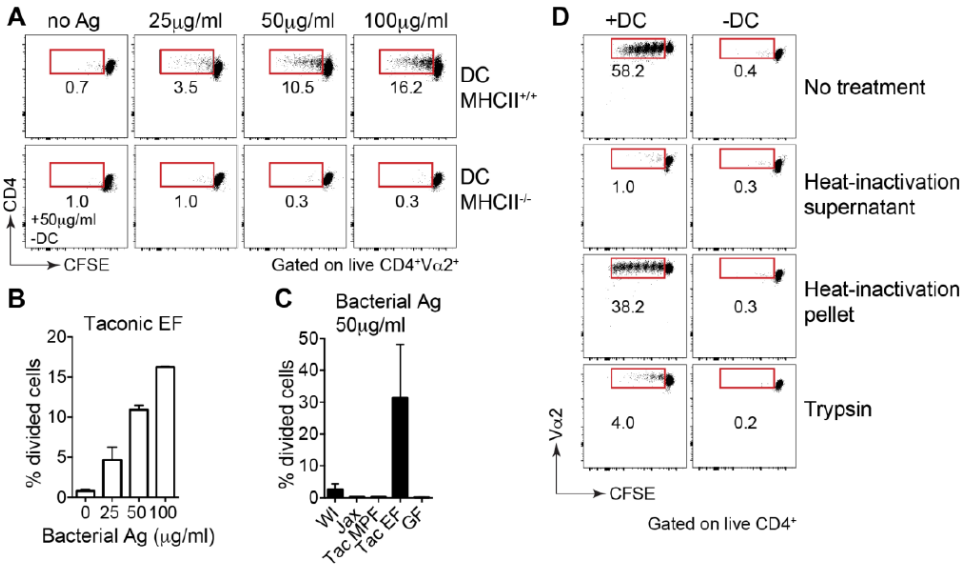

Figure 2.11 Intestinal bacterial antigens induce proliferation of CD4⁺ T cells from pTreg TN/RKO mice.

(**A**) *In vitro* proliferation assay. CD4⁺ T cells were isolated from pTreg TN/RKO, labeled with CFSE and co-cultured with dendritic cells (DC) purified from spleens of B16-Flt3L-injected WT (MHCII$^{+/+}$) or MHCII-deficient mice (MHCII$^{-/-}$) in the presence of the indicated concentrations of bacterial extract obtained from feces and cecum of Taconic mice. Proliferation was measured by CFSE dilution 3.5 days after culture. (**B**) Graph shows the data of one experiment. (**C**) *In vitro* proliferation assay as in A. Co-culture of TN T cells and DC with bacterial antigen extract (50 µg/ml) obtained from feces of mice housed in the indicated animal facilities. Graph shows the average + SD of 3 independent experiments. Fecal pellets were collected on the day the mice were delivered from the vendors Jackson (Jax) or Taconic (Tac) or from mice housed in our facility (WI). Tac MPF, mice from Taconic with murine pathogen free health status; Tac EF, mice from Taconic with excluded flora health status. (**D**) *In vitro* proliferation assay as in A. CD4+ T cells were co-cultured with and without DC with bacterial antigen extract (50µg/ml) obtained from cecal bacteria of Taconic EF mice. Antigen extracts were subjected or not to heat-inactivation or trypsin treatment. Proliferation was measured by CFSE dilution 3.5 days after culture.

The relevant microbial antigen is therefore likely to be a protein that requires internalization, processing into peptides, and presentation at the cell surface via MHCII products. When RAGKO mice purchased from Taconic Biosciences or Jackson Laboratory (and kept in microisolators) were adoptively transferred with naïve CD4⁺ T cells isolated from pTreg/RKO mice, TN T cells expanded and converted into $CD4_{IEL}$ in Taconic recipients but not in Jackson Laboratory recipients. Expansion and conversion were readily observed in Jackson Laboratory mice cohoused with Taconic mice (Fig. 2.12A). We conclude that the antigen recognized by the pTregTN TCR is a protein derived from the intestinal microbiota prevalent in Taconic mice.

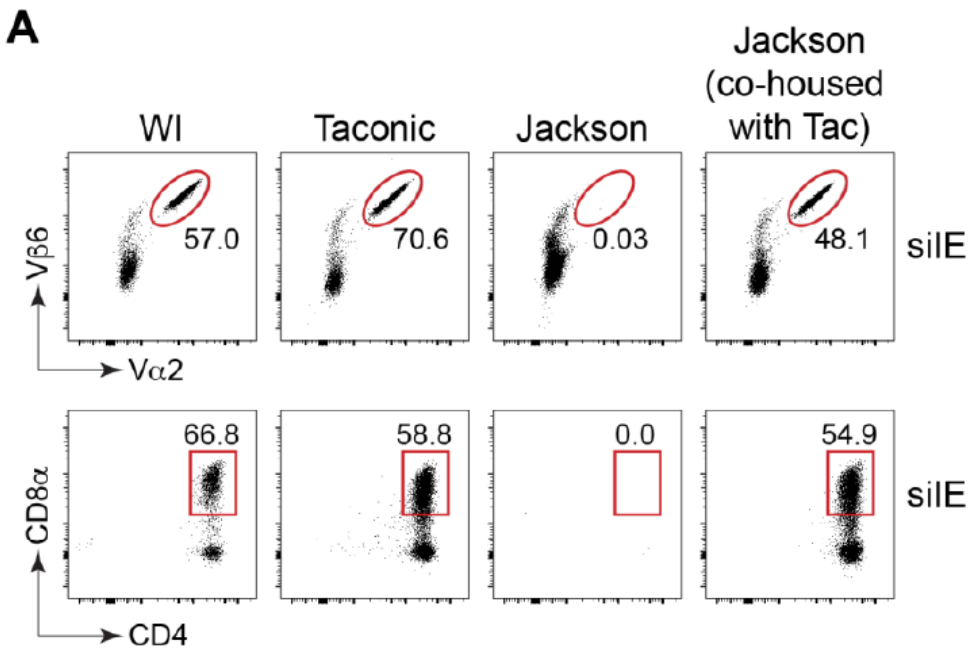

Figure 2.12 CD4⁺ T cells from pTreg TN/RKO expand and convert into $CD4_{IEL}$ in lymphopenic hosts obtained from Taconic but not from Jackson Laboratory.

CD4⁺ T cells from pTreg TN/RKO were bead-purified and transfer into RAG1KO mice purchased from Taconic or Jackson. After 6-8 weeks, cells were harvested from the siIE compartment and analyzed by flow cytometry. Upper dot-plots are gated on $CD45^+CD8\alpha^-$ cells, and lower dot-plots are further gated on $V\alpha2^+V\beta6^+$ cells. Recipient mice were kept in microisolators and individual ventilation for the duration of the experiment. Taconic and Jackson mice were co-housed for 2 weeks prior to adoptive transfer of TN T cells, and mice were co-housed during the entire duration of the experiment. Dot-plots representative of 3 mice/group.

We used RNA sequencing (RNA-seq) to characterize the pTreg and $CD4_{IEL}$ that had differentiated from the same clonal TN pre-cursor and recovered from the intestinal mucosa. We adoptively transferred $CD4^+CD8\alpha^-Foxp3^-GFP^-$ isolated from pTregTN/RKO/Foxp3-GFP mice into TCRαβKO hosts. After 6 weeks, we sorted $CD4^+CD8a^+Foxp3^+$ pTregs and "unconverted" $CD4^+CD8\alpha^-Foxp3^-GFP^-$ cells from the siLP and IE compartments for whole-transcriptome analysis by RNA-seq (Fig. 2.13A).

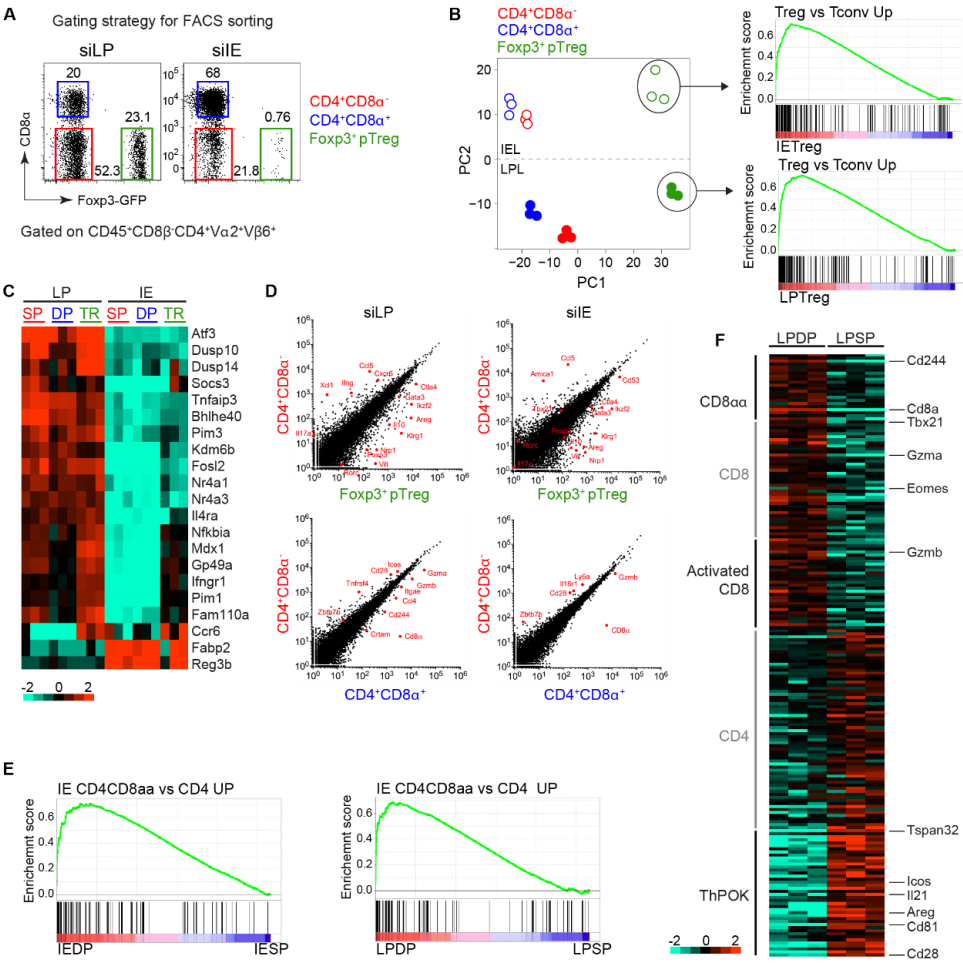

Figure 2.13 Gene expression analysis of pTreg and $CD4_{IEL}$ TN cells.

TCRabKO mice were transferred with 5 × 10^5 naïve $CD4^+CD8\alpha^-Foxp3^-GFP^-$ T cells purified from the spleen of pTreg TN/RKO/Foxp3gfp mice. Small intestine lymphocytes were harvested 6 weeks after transfer, and the indicated donor T cell subsets were sorted for RNAseq library preparation and sequencing. (**A**) Gating strategy for FACS sorting of the indicated populations. (**B**) Principal components analysis of the top 300 differentially expressed genes by plotting contribution of each T cell population to the first two principal components (PC1 and PC2) (left). Gene set enrichment analysis (GSEA) of $Foxp3^+$ pTregs versus "rest" within each intestinal compartment defined by the PC2 shows significant enrichment ($P < 0.001$) of transcriptional signatures associated with $Foxp3^+$ Tregs (right). (**C**) Heat map of fold change expression in log scale of major genes contributing to the PC2 shown in triplicate for each T cell population from the LP versus IE compartment. (**D**) Diversity of gene expression plotted as correlation of transcript expression levels (log-scale, normalized counts) between each sorted T cell population. Differentially expressed genes described to be characteristic of different T cell subsets are shown in red. (**E**) GSEA showing a highly significant enrichment ($P < 0.001$) of genes previously found to be up-regulated in $CD4^+CD8\alpha\alpha^+$ IEL for both IE (left; enrichment score, 0.71) and LP ($CD4^+CD8\alpha^+$ versus $CD4^+$ lymphocytes; right; enrichment score, 0.69). (**F**) Heat map of normalized gene expression across three biological replicates of LP $CD4^+CD8\alpha^+$ and $CD4^+$ lymphocytes. Differentially expressed transcripts (log2 fold change) of selected genes known to be up-regulated in the indicated T cell subsets are shown.

Comparison of gene expression profiles from our sorted populations with signatures of pTreg and $CD4^+CD8\alpha^+$cells in the published record (Fig. 2.13 B-F) (*12, 16, 20, 21*), confirmed the similarity between differentiated TN cells and polyclonal pTreg and $CD4_{IEL}$. As expected, $CD4^+CD8\alpha^+$ cells down-modulated expression of the transcription factor ThPOK in comparison to $CD4^+CD8\alpha^-Foxp3^-GFP^-$ cells and up-regulated the surface marker CD103 (Fig. 2.14 A-E), corroborating results obtained for WT IELs (*16, 22*). In our system, converted pTregs did not up-regulate retinoid-related orphan receptor γt (RORγt) expression (Fig. 2.14F), the transcription factor of TH17 and expressed by a fraction of intestinal pTregs (*21, 23, 24*).

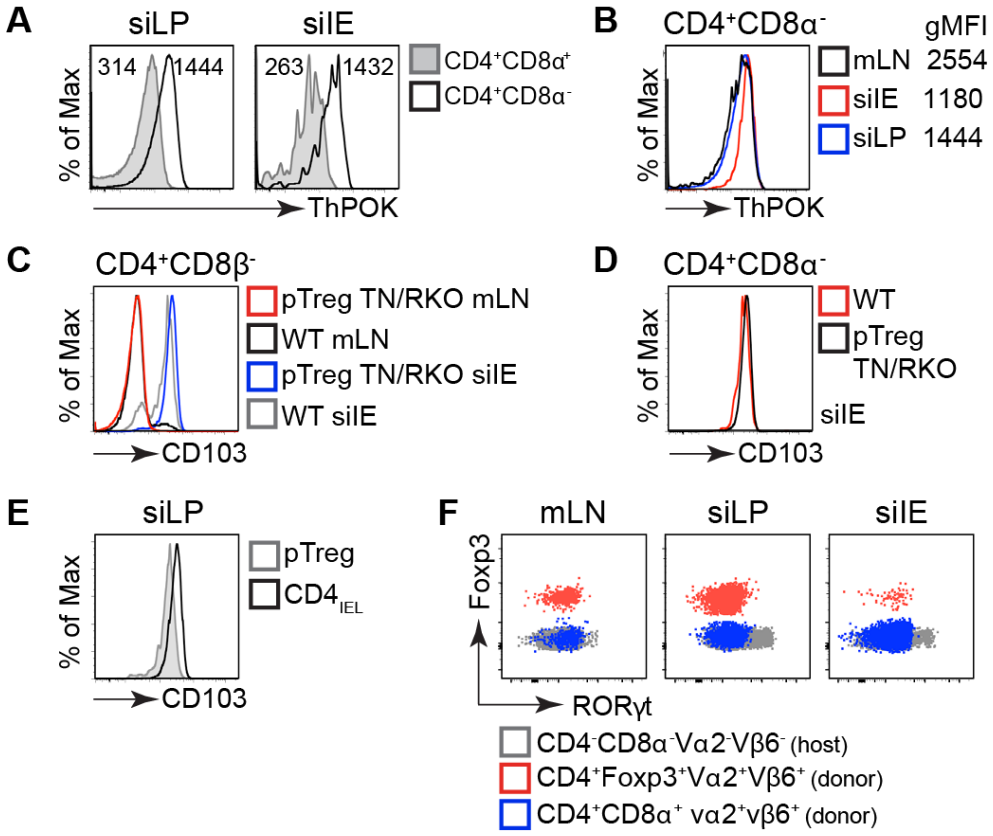

Figure 2.14 Low levels of ThPOK and high levels of CD103 in TN $CD4_{IEL}$.

ThPOK, CD103, and RORγt expression in the indicated populations were measured by flow cytometry. TCRαβKO mice were adoptively transferred as described in Fig. 2.10, and small intestine or mLN lymphocytes were analyzed by flow cytometry 6 to 8 weeks after transfer. Unless otherwise stated, cells were gated on $CD45^+CD8\beta^-$ singlets. Histograms in (**A**) to (**E**) are representative of five mice. Numbers indicate the geometric median fluorescence intensity (gMFI). Histograms in (C) and (**D**) also show levels of CD103 in polyclonal T cells from WT mice for comparison. Dot plots in (**F**) are representative of three mice.

We conclude that adoptive transfer of TN T cells leads to differentiation and expansion of bona fide pTreg and $CD4_{IEL}$ T cells from the same clonal precursors. The preferential conversion into pTreg or IFN-γ–producing $CD4_{IEL}$ *in vivo* and the absence of TH17 conversion were not due to a lack of SFB colonization of our recipient mice, as a quantitative polymerase chain reaction (qPCR) assay specific for SFB readily detected them in the TCRαβKO mice housed in our facility, but less so or not at all in EF mice purchased from Taconic (Fig. 2.15A).

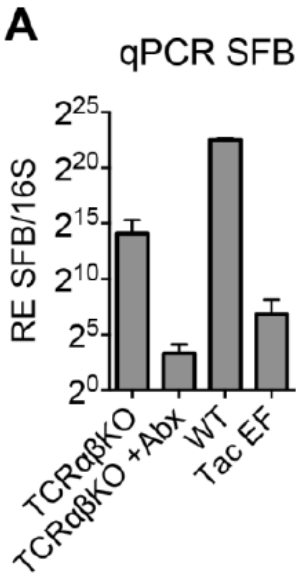

Figure 2.15 Mice from the WIBR animal facility are colonized by SFB.

Total fecal DNA was extracted from fecal pellets. qPCR was performed using SFB-specific primers and 16S generic primers and in fig. S6. RE, relative expression of SFB amplification compared to 16S amplification. TCRαβKO mice were treated or not with antibiotics and adoptively transferred with $CD4^+$ T cells isolated from pTreg TN/RKO mice. Fecal pellets were collected 6-8 weeks post-transfer. WT, wild-type kept in the same facility but not transferred with TN T cells nor treated with antibiotics. Tac EF, WT mice with health status excluded flora (EF) purchased from Taconic and kept in microisolators and individual ventilation in the WIBR animal facility. Each bar denotes the average and SD of 2-4 mice/group.

The ability of TN T cells to differentiate into both the pTreg and the $CD4_{IEL}$ phenotypes raised the possibility that $CD4_{IEL}$ development may require transient expression of

Foxp3$^+$. We therefore crossed the pTregTN/RKO mice to RAGKO/scurfy (Foxp3-deficient) mice and used the resulting offspring as donors of CD4$^+$ T cells that were adoptively transferred into TCRαβKO hosts. Although TN cell expansion was unaffected in these hosts (Fig. 2.16 A-C), CD4$^+$ T cells no longer converted into pTreg. However, differentiation of $CD4_{IEL}$ occurred to the same extent as in Foxp3-sufficient mice (Fig. 2.16D). Development of $CD4_{IEL}$ is thus Foxp3-independent. The massive expansion of IFN-γ–producing TN T cells in the siLP and IE compartment of pTregTN/RKO mice or in TCRαβKO mice transferred with TN T cells causes neither wasting disease nor disruption of epithelial integrity (Figs. 2.4 D,E, and 2.16 E,G).This is in contrast to the colitis model induced by Treg-depleted polyclonal T cells transferred into immunodeficient hosts (*25*). Thus, it was possible that the pTreg generated in TCRαβKO mice transferred with TN T cells might have prevented excessive inflammation or disease caused by the $CD4_{IEL}$. Despite increased production of IFN-γ in the IE compartment, mice that received Foxp3-deficient TN cells showed no signs of disease 8 to 12 weeks after transfer (Fig. 2.16 E-H). Histopathological analysis of the intestine showed extensive lymphocyte infiltration of the LP in both groups to the same extent but no signs of epithelial disruption (Fig. 2.16G). Mice that received either Foxp3-deficient or Foxp3-sufficient TN CD4$^+$ T cells also had overall similar levels of LCN2 in the feces (Fig. 2.16H). Therefore, despite their activated status and robust production of IFN-γ, $CD4_{IELs}$ derived from the pTregTN/RKO mice are not overtly pathogenic, even in the absence of Foxp3$^+$ Treg, presumably related to the absence of recognition of a self-antigen in the gut and to their potential regulatory properties.

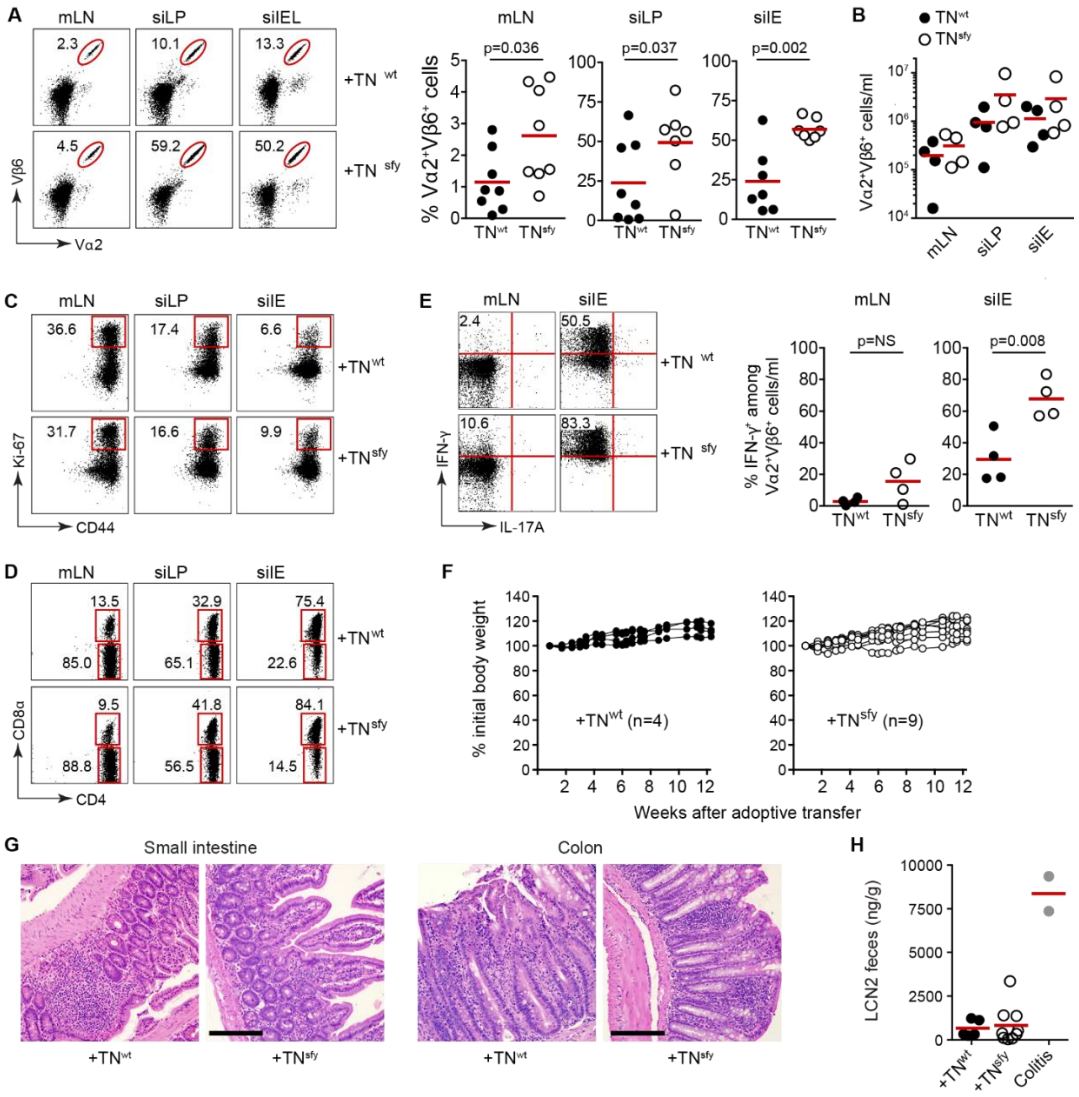

Figure 2.16 Foxp3 deficiency does not confer pathogenicity to $CD4_{IEL}$.

TCRabKO mice were adoptively transferred with 5 × 10^5 naïve $CD4^+$ T cells isolated from the spleen and mLN of pTreg TN/RKO (TNwt) or pTreg TN/RKO/scurfy (TNsfy) mice. Recovery of transferred cells was analyzed after 8 to 12 weeks at the indicated locations. (**A**) Dot plots show the frequency of TN cells recovered in the intestine and in the mLN among $CD45^+CD8\beta^-CD4^+$ cells. Graphs show the quantification of three independent experiments. Each symbol represents a mouse, and the horizontal bars represent the means. (**B**) Cell counts from mice shown in (A). (**C**) Frequency of Ki-67 cells among transferred TN cells identified as $CD45^+CD8\beta^-CD4+V\alpha2^+V\beta6^+$. (**D**) Frequency of $CD8\alpha^+$ cells among transferred TN cells. (**E**) Frequency of IFN-γ^- and IL-17A–producing cells among transferred TN cells identified as $CD45^+CD8\beta^-CD4^+V\alpha2^+V\beta6^+$. Graphs show data from two independent experiments. (**F**) Animals transferred with TNwt or TNsfy cells were cohoused (four to five mice per cage), and weight was recorded periodically up to 12 weeks after transfer. (**G**) Photomicrographs of H&E staining of the indicated organs of TCRαβKO mice transferred with TNwt or TNsfy. Original magnification, ×200; scale bars, 200 mm. (**H**) Fecal levels of LCN2 were measured by ELISA. Colitis denotes positive controls for ELISA (feces from colitic mice). P values were calculated with Student's t test. NS, nonsignificant. P values of <0.05 were considered statistically significant.

Discussion

We show that T cell precursors of TN mice cloned from and bearing the TCR rearrangements of a mLN peripheral Treg can adopt two distinct fates (pTreg and $CD4_{IEL}$) upon encounter with microbial antigen in the intestinal environment. We believe that our experiments have identified a compelling example of a naturally occurring pTreg TCR that promotes spontaneous $CD4_{IEL}$ conversion in response to a component of the microbiota. The unimpaired differentiation of $CD4_{IEL}$ from Foxp3-deficient TN precursors suggests that the pathways that lead to $CD4_{IEL}$ differentiation in this case are independent of pTreg conversion. However, pTreg can acquire the $CD4_{IEL}$ phenotype in a microbiota-dependent manner (*26*), indicating that there is more than one pathway for $CD4_{IEL}$ development. Although the TN pTreg and $CD4_{IEL}$ presumably recognize the same bacterial species, these populations accumulate in distinct anatomical locations—mLN and intestinal epithelium, respectively. Whether this dichotomy is due to the independent priming of pTreg and $CD4_{IEL}$ in situ at each of these locations or is due to migration to distinct sites after priming in the mLN is unclear. One possibility is that priming in the mLN may give rise simultaneously both to pTreg and to undifferentiated but activated T cells that will further acquire the $CD4_{IEL}$ phenotype upon a second encounter with the bacterial antigen in the intestine. Alternatively, antigen presentation by different antigen-presenting cell (APC) subsets in distinct microenvironments may promote independent differentiation of the two cell types. Previous work using a TCR transgenic model showed that the extracellular commensal SFB drive the intestinal T cells to adopt the TH17 program, whereas infection with the intracellular pathogen Listeria monocytogenes expressing the SFB epitope directs the same SFB-specific cells toward TH1 (*6*). Thus, in this model, monomorphic differentiation of T cells is directed by the changes in the environment in which T cell priming occurs. The constantly stimulated epithelial environment could be both inhospitable for pTreg and favorable for $CD4_{IEL}$ differentiation, whereas the mLN favors pTreg differentiation and allows the accumulation of pTregs at that site. Whether and how the relative abundance of ligands (*5, 6*), TCR-independent factors such as microbial metabolites (*27, 28*), and cell-intrinsic mechanisms, as well as the different types of APCs (*29-31*), cooperate to define T cell fate in the gut environment remain to

be determined. Although pTreg development is dependent on low precursor frequencies, $CD4_{IELs}$ carrying the identical TCR are not limited in anyway by clonal size. Intrinsic properties of the T cell subset concerned can thus directly affect their expansion. Development of nTreg requires small niche sizes (*9, 10*), possibly due to intraclonal competition for a limited amount of ligands. Development of *Clostridium*-specific pTreg also appears to be dependent on small clonal sizes (*5*). In contrast, when clonal sizes are larger, $CD4^+$ T cells no longer convert into Tregs and remain as effector or naïve T cells. Therefore, the small niche requirement may be a common property of Treg populations. Although relative abundance for ligands is suspected to play a major role in Treg development, the precise mechanisms at play remain to be unveiled. Dietary antigens may stimulate the bulk of pTregs present in the small intestine (*24*), whereas induction of colon pTregs depends almost exclusively on the microbiota (*5, 7*). However, constant stimulation by the microbiota in the small intestine can also allow for the generation of microbiota-specific pTregs at this site. On the basis of experiments using GF and antigen-free mice, it is estimated that a sizable proportion of pTreg in the siLP is induced by the microbiota and expresses RORγt (*21, 23, 24*). We report a different lineage of pTregs that does not up-regulate RORγt expression but does recognize bacterial antigens present in the intestinal microbiota. The T cell precursors that give rise to these pTregs do not allow for differentiation of TH17 *in vivo*, despite SFB colonization and the ability to produce IL-17 under polarizing conditions *in vitro*. Instead, these precursors showed a strong tendency to develop into $CD4_{IELs}$. It remains to be determined whether other $CD4^+$ T cell precursors that can simultaneously differentiate into pTreg and $CD4_{IEL}$, or pTreg that can also differentiate into $CD4_{IEL}$ (*26*), express RORγt and/or could interconvert into TH17-like cells. Premature expression of TCRα in transgenic mice may contribute to the development of unconventional IELs (*32, 33*). However, unlike the TN cells in our mice, these cells predominantly consist of unconventional IELs that expressed only CD8αα. Moreover, we show microbiota-dependent $CD4_{IEL}$ differentiation from mature $CD4^+$ T cells isolated from secondary lymphoid organs (spleen and mLN), thus discounting a potential role for direct development of $CD4_{IEL}$ from DN (double-negative) or DP thymic precursors in our model. Accordingly, $CD4_{IELs}$ are absent in GF and antibiotic-treated WT mice (*16*). The microbiota must play a specific role in the generation/expansion of this T cell subset.

$CD4^+$ T cells isolated from an unrelated TN line cloned from a pancreatic tumor–infiltrating lymphocyte fail to convert to $CD4_{IELs}$, demonstrating that $CD4_{IEL}$ differentiation is directed by TCR specificity. Mice harboring microbiota-specific TN cells remain healthy despite massive accumulation of IFN-γ–expressing $CD4_{IEL}$ and irrespective of the presence of Tregs. This suggests that additional factors may suppress pathogenic inflammation in the intestine, for example, by inducing a regulatory response related to the $CD4_{IEL}$ phenotype. IFN-γ–producing IELs can display regulatory functions rather than proinflammatory activity (*34*). Using a model antigen (OTII and OVA) in which antigen-specific Treg development was impaired by the scurfy mutation, antibody-mediated depletion of $CD4_{IEL}$ led to intestinal inflammation and diarrhea (*26*), suggesting a regulatory role for $CD4_{IEL}$. Although the mechanisms by which $CD4_{IEL}$ and other IELs regulate the immune response at intestinal surfaces remain to be fully elucidated, our studies showcase the importance of location in determining T cell fate and functions.

Materials and methods

Study design

The present study was designed to investigate the extent to which TCR identity dictates pTreg fate in vivo. We conducted adoptive transfer experiments and *in vitro* proliferation assays and used FACS analyses and RNA-seq as described in the figure legends. As indicated in the figures and figure legends, the number of mice per experiments varied from 2 to 14 per experimental group. All experiments were repeated at least once. Mice were arbitrarily assigned to each experimental group, and both males and females were used for the experiments. All data obtained are presented, including outliers. For the *in vitro* proliferation assays, experiments were performed in duplicate and repeated two to three times.

Mice

TN mice for pTregTCR (pTregTN) were generated by SCNT in a mixed C57BL/6 and 129 background as described (fig. S1) (*14*). All mice were housed at the Whitehead Institute for Biomedical Re-search (WIBR) under specific pathogen–free conditions, and all

procedures were approved and performed according to the Institutional AnimalCare and Use Committee of the Massachusetts Institute of Technology (MIT). C57BL/6 CD45.1,Rag1−/−, MHCII−/−, Tcra−/−, Tcrb−/−, and scurfy mice were purchased from Taconic Biosciences and Jackson Laboratory and maintained at our facility. Tcra−/− and Tcrb−/− were intercrossed to originate Tcra−/−b−/−(TCRabKO). Foxp3gfpmice were generated as described (*35*) and provided by V. Kuchroo and M. Oukka. Scurfy mice and pTregTN mice were crossed toRag1−/−. pTregTN/RAG1KO and scurfy/RAG1KO were interbred to generate pTregTN/RAG1KO/scurfy. pTregTN/RAG1KO mice were crossed to Foxp3gfp and MHCII−/−to generate pTregTN/RAG1KO/Foxp3gfpmice and pTregTN/RAG1KO/MHCII−/−. pTregTN mice were backcrossed at least for six generations into C57BL/6 RAG1KO background. Panc CD4 TN mouse was cloned from pancreatic tumor–infiltrating CD4+T cells and used as a control in fig. S4. They were generated by SCNT in a mixed C57BL/6 and 129 background as described (*14*) and back crossed at least for six generations into C57BL/6 RAG2KO background.

Antibodies, reagents, and FACS analysis

Fluorescent dye–conjugated antibodies were purchased from BD Biosciences (anti-Vb6, RR4-7; anti-CD69, H1.2F3; anti-CD3, 145-2C11; anti-Vb5, MR9-4; anti–IL-17, TC11-18H10; and anti-ThPOK,T43-94), eBioscience (anti-CD45.1, A20; anti-Foxp3, FJK-16s; anti–Ki-67, Sol A15; anti-CD4, RM4-5; Va2, B20.1; anti-CD19, eBio1D3;anti-CD11c, N418; anti–IFN-γ, XMG1.2; and anti-Va11, RR 8-1), or BioLegend (anti-CD45.2, 104; anti-CD8a, 53-6.7; anti-CD8b, YTS156.7.7; anti-CD44, IM7; anti–I-A/I-E, M5/114.15.2; and anti-Va8.3,KT50). Cell dyes CFSE and CellTrace Violet for proliferation assays were purchased from Sigma-Aldrich and Life Technologies, respectively. Cell viability dye 7-AAD (Via-Probe) was purchased from BD Biosciences. Flow cytometry data were acquired on an LSRFortessa (Becton Dickinson) instrument and analyzed with the FlowJo soft-ware package (Tri-Star). Staining with cell proliferation dyes was per-formed according to the manufacturer's instructions. Staining for surface markers was performed at 4°C for 25 to 30 min. Intracellular staining of Foxp3 and Ki-67 staining were performed with Foxp3/Transcription Factor Staining Buffer Set (eBioscience), and intra-cellular cytokine staining was performed with Cytofix/Cytoperm Kit (BD Biosciences), according

to the manufacturer's instructions. For the cytokine staining, cells were incubated with phorbol 12-myristate13-acetate (100 ng/ml; Sigma), ionomycin (200 ng/ml; Sigma), and 2mMmonensin (Sigma) for 4 hours at 37°C. Monensin was added for the last 2 hours of incubation.

Antibiotic treatment

Vancomycin (0.5 g/liter), ampicillin (1.0 g/liter), neomycin (1.0 g/liter) (Amresco), and metronidazole (1.0 g/liter) (Sigma) cocktail was given ad libitum in the drinking water for 7 to 14 days or for 6 to 8 weeks as indicated in the figure legends.

Quantification of fecal LCN2

LCN2 was measured in fecal homogenates as described (*17*) using the Mouse Lipocalin-2/NGAL DuoSet ELISA (enzyme-linked immunosorbent assay) kit according to the manufacturer's protocol (R&D Systems, Minneapolis, MN).

Isolation of mononuclear cells from intestine

Small and large intestines were harvested, and mononuclear cells were isolated from LP as previously described (*36*). IELs were recovered from the supernatants of 1 mM dithiothreitol and 30 mM EDTA washes.

16S and SFB qPCR of fecal DNA

DNA was extracted from fecal pellets using the Zymo Research Fecal DNA Isolation Kit, according to the manufacturers' protocol. qPCR was performed using SYBR Green Master Mix (Bio-Rad). Primer sequences used for 16Swere 5′-gtgStgcaYggYtgtcgtca-3′and 5′-acgtcRtccMcaccttcctc-3′ (*37*), and those used for SFB were SFB225F5′-aggaggagtctgcggcacattagc-3′ and SFB558R 5′-cgcatcctttacgcccagt-tattc-3′ (*38*).

Stool test for bacterial growth

Single fecal pellets were resuspended into 500ml of phosphate-buffered saline (PBS) and spun briefly to remove fibers. Supernatant was diluted 1:10 and 1:100 and then streaked

on brain-heart infusion plates and incubated under aerobic and anaerobic conditions. After 48 to 72 hours, plates were examined for colony growth.

Bacterial extracts for proliferation assays

Feces (2 to 10 pellets) from healthy WT or Rag1−/−mice housed at different animal facilities (WIBR, Jackson Laboratory, and Taconic Biosciences) were homogenized in PBS and shaken at 2000 rpm for 20 min at 4°C. Large debris was removed by centrifugation (700g, 1 min). Supernatants were centrifuged at 13,500g for 10 min at 4°C, and bacterial pellet was resuspended in 1 ml of PBS containing protease inhibitors (cOmplete Mini, Roche; 1 tablet per 10 ml of PBS following the manufacturer's instructions) and deoxyribonuclease I(Roche). Bacteria were lysed by three rounds of sonication (BransonSonifier 450) for 1 min, 60 pulses, followed by 5 min of cooling on ice between each round (output control,4; duty cycle, 50%). Cellular debris was removed by centrifugation at 14,000g for 30 min at 4°C. Protein concentration was measured by bicinchoninic acid assay (BCA)and used for *in vitro* and in vivo proliferation assays as indicated. In some experiments (Fig. 2.11), bacterial extracts were subjected to trypsin nor heat inactivation treatment before being used in *in vitro* proliferation assays. For trypsin treatment, bacterial extract (50mg/ml; prepared in the absence of protease inhibitor) was incubated with trypsin (2.5mg/ml) for 4 hours at 37°C. Trypsin was inactivated by adding protease inhibitor as described above. For heat inactivation, bacterial extracts were boiled for 20 min and then centrifuged at 14,000g for 10 min at 4°C. Supernatant was collected, and pellet was resuspended in PBS containing protease inhibitors and sonicated in a water bath sonicator for 10 min. Supernatants and resolubilized pellets were used for the *in vitro* proliferation assays at a maximum of 20ml per well.

***In vitro* proliferation assay**

DCs were purified with the Pan Dendritic Cell Isolation Kit (MiltenyiBiotec) from spleens of WT mice injected with 1×10^6 B16-FLT3Lcells. T cells were purified with the Naïve $CD4^+$ T Cell Isolation Kit (Miltenyi Biotec) from the spleens and mLNs of pTregTN/RKO mice and labeled with 2.5mM CFSE (Sigma). Purity was always greater than 98% for

both DCs and T cells. DCs (1×10^5) were incubated with sonicated bacterial extracts (25, 50, or 100mg/ml) for 2 hours before the addition of 1×10^5 TN CD4+T cells. Cell division was assessed by CFSE dilution and analyzed by flow cytometry after 3.5 days of coculture. *In vivo* proliferation assay TCRαβKO or WT mice were treated with a cocktail of antibiotics (ampicillin, 1 g/liter; metronidazole, 1 g/liter; neomycin, 1 g/liter; and vancomycin, 0.5 g/liter) for 1 to 2 weeks and adoptively transferred with 5×10^5 CFSE- or CellTrace Violet–labeled T cells. One day later, mice were immunized with 50µg of sonicated bacterial extract adsorbed in alum (Imject, Thermo Fisher Scientific). Bacterial extracts used for immunization were obtained from fecal pellets of WT mice (EF health status) purchased from Taconic. Cell division and activation markers were measured 5 days after adoptive transfer by flow cytometry.

Isolation of CD4$^+$ T cells

Naïve CD4$^+$ T cells were purified from the spleen and mLN using the Naïve CD4 Isolation Kit according to the manufacturer's instructions (Miltenyi, Germany). Purity was always greater than 98%. In some experiments as indicated in the figure legends, naïve CD4$^+$ T cells were FACS-sorted on a FACSAria instrument (BD Biosciences) by the Flow Cytometry Core Facility at the WIBR. Purity was always greater than 98%. Purified CD4$^+$ T cells were used in adoptive transfer (by intra-venous injection) experiments or *in vitro* proliferation assays as indicated in the figure legends.

Generation of mixed bone marrow chimeras

TCRabKO host mice were sublethally irradiated (6 Gy) 4 hours before bone marrow reconstitution. Bone marrow cells were har-vested from CD45.2 pTregTN/RKO or CD45.2 OTII Tg/RKO and CD45.1 WT mice and depleted of T cells using CD90.2 MACS beads (Miltenyi) according to the manufacturer's instructions. A total of 5×10^6 cells (composed of 2.5 to 10% of CD45.2 cells and 90 to 97.5% of CD45.1 cells) were intravenously injected into host mice. After 12 weeks of reconstitution, T cell development was analyzed in different organs of recipient mice by flow cytometry.

Histopathological analysis

Small and large intestines were fixed in 10% buffered formalin and subjected to hematoxylin and eosin (H&E) staining. Slides were scored blindly by a pathologist from the Division of Comparative Medicine of MIT.

RNA-seq library preparation and sequencing

Sorted cells were lysed in a guanidine thiocyanate buffer (Qiagen) supplemented with 1% β-mercaptoethanol. RNA isolated by solid-phase reversible immobilization bead cleanup was reversely transcribed into complementary DNA and pre-amplified as described (*39*). Nextera XT was used to prepare a pooled library of fragmented and uniquely indexed samples. Sequencing was performed on an Illumina HiSeq2000. For RNA-seq analysis, 40–base pair single-end reads were aligned to the mouse reference genome (mm10) using TopHat. Generead count was performed using HT seq-count with RefSeq mm10 annotation.

Statistical analysis

Mean and SD values were calculated with GraphPad Prism (GraphPadSoftware). Unpaired Student's t test was used to compare two variables, as indicated in each figure legend. P values of <0.05 were considered significant and are indicated in the figure or figure legends.

References

1. A. M. Bilate, J. J. Lafaille, Induced CD4+Foxp3+ regulatory T cells in immune tolerance. *Annu Rev Immunol* **30**, 733-758 (2012).
2. M. Shale, C. Schiering, F. Powrie, CD4(+) T-cell subsets in intestinal inflammation. *Immunol Rev* **252**, 164-182 (2013).
3. L. Zhou, M. M. Chong, D. R. Littman, Plasticity of CD4+ T cell lineage differentiation. *Immunity* **30**, 646-655 (2009).
4. V. Brucklacher-Waldert, E. J. Carr, M. A. Linterman, M. Veldhoen, Cellular Plasticity of CD4+ T Cells in the Intestine. *Front Immunol* **5**, 488 (2014).
5. S. K. Lathrop *et al.*, Peripheral education of the immune system by colonic commensal microbiota. *Nature* **478**, 250-254 (2011).
6. Y. Yang *et al.*, Focused specificity of intestinal TH17 cells towards commensal bacterial antigens. *Nature* **510**, 152-156 (2014).
7. K. Atarashi *et al.*, Treg induction by a rationally selected mixture of Clostridia strains from the human microbiota. *Nature* **500**, 232-236 (2013).
8. Ivanov, II *et al.*, Induction of intestinal Th17 cells by segmented filamentous bacteria. *Cell* **139**, 485-498 (2009).
9. J. L. Bautista *et al.*, Intraclonal competition limits the fate determination of regulatory T cells in the thymus. *Nat Immunol* **10**, 610-617 (2009).
10. M. W. Leung, S. Shen, J. J. Lafaille, TCR-dependent differentiation of thymic Foxp3+ cells is limited to small clonal sizes. *J Exp Med* **206**, 2121-2130 (2009).
11. H. M. Lee, J. L. Bautista, J. Scott-Browne, J. F. Mohan, C. S. Hsieh, A broad range of self-reactivity drives thymic regulatory T cell selection to limit responses to self. *Immunity* **37**, 475-486 (2012).
12. J. M. Weiss *et al.*, Neuropilin 1 is expressed on thymus-derived natural regulatory T cells, but not mucosa-generated induced Foxp3+ T reg cells. *J Exp Med* **209**, 1723-1742, S1721 (2012).
13. K. Hochedlinger, R. Jaenisch, Monoclonal mice generated by nuclear transfer from mature B and T donor cells. *Nature* **415**, 1035-1038 (2002).
14. O. Kirak *et al.*, Transnuclear mice with predefined T cell receptor specificities against Toxoplasma gondii obtained via SCNT. *Science* **328**, 243-248 (2010).
15. M. A. Curotto de Lafaille *et al.*, Adaptive Foxp3+ regulatory T cell-dependent and -independent control of allergic inflammation. *Immunity* **29**, 114-126 (2008).
16. D. Mucida *et al.*, Transcriptional reprogramming of mature CD4(+) helper T cells generates distinct MHC class II-restricted cytotoxic T lymphocytes. *Nat Immunol* **14**, 281-289 (2013).
17. B. Chassaing *et al.*, Fecal lipocalin 2, a sensitive and broadly dynamic non-invasive biomarker for intestinal inflammation. *PLoS One* **7**, e44328 (2012).
18. M. A. Curotto de Lafaille, A. C. Lino, N. Kutchukhidze, J. J. Lafaille, CD25- T cells generate CD25+Foxp3+ regulatory T cells by peripheral expansion. *J Immunol* **173**, 7259-7268 (2004).
19. S. Rakoff-Nahoum, J. Paglino, F. Eslami-Varzaneh, S. Edberg, R. Medzhitov, Recognition of commensal microflora by toll-like receptors is required for intestinal homeostasis. *Cell* **118**, 229-241 (2004).
20. D. Haribhai *et al.*, A requisite role for induced regulatory T cells in tolerance based on expanding antigen receptor diversity. *Immunity* **35**, 109-122 (2011).
21. E. Sefik *et al.*, MUCOSAL IMMUNOLOGY. Individual intestinal symbionts induce a distinct population of RORgamma(+) regulatory T cells. *Science* **349**, 993-997 (2015).

22. B. S. Reis, A. Rogoz, F. A. Costa-Pinto, I. Taniuchi, D. Mucida, Mutual expression of the transcription factors Runx3 and ThPOK regulates intestinal CD4(+) T cell immunity. *Nat Immunol* **14**, 271-280 (2013).
23. C. Ohnmacht *et al.*, MUCOSAL IMMUNOLOGY. The microbiota regulates type 2 immunity through RORgammat(+) T cells. *Science* **349**, 989-993 (2015).
24. K. S. Kim *et al.*, Dietary antigens limit mucosal immunity by inducing regulatory T cells in the small intestine. *Science* **351**, 858-863 (2016).
25. C. Mottet, H. H. Uhlig, F. Powrie, Cutting edge: cure of colitis by CD4+CD25+ regulatory T cells. *J Immunol* **170**, 3939-3943 (2003).
26. T. Sujino *et al.*, Tissue adaptation of regulatory and intraepithelial CD4+ T cells controls gut inflammation. *Science* **352**, 1581-1586 (2016).
27. P. M. Smith *et al.*, The microbial metabolites, short-chain fatty acids, regulate colonic Treg cell homeostasis. *Science* **341**, 569-573 (2013).
28. K. Atarashi *et al.*, Th17 Cell Induction by Adhesion of Microbes to Intestinal Epithelial Cells. *Cell* **163**, 367-380 (2015).
29. B. Johansson-Lindbom *et al.*, Functional specialization of gut CD103+ dendritic cells in the regulation of tissue-selective T cell homing. *J Exp Med* **202**, 1063-1073 (2005).
30. G. E. Diehl *et al.*, Microbiota restricts trafficking of bacteria to mesenteric lymph nodes by CX(3)CR1(hi) cells. *Nature* **494**, 116-120 (2013).
31. D. Esterhazy *et al.*, Classical dendritic cells are required for dietary antigen-mediated induction of peripheral Treg cells and tolerance. *Nat Immunol* **17**, 545-555 (2016).
32. T. A. Baldwin, M. M. Sandau, S. C. Jameson, K. A. Hogquist, The timing of TCR alpha expression critically influences T cell development and selection. *J Exp Med* **202**, 111-121 (2005).
33. B. D. McDonald, J. J. Bunker, I. E. Ishizuka, B. Jabri, A. Bendelac, Elevated T cell receptor signaling identifies a thymic precursor to the TCRalphabeta(+)CD4(-)CD8beta(-) intraepithelial lymphocyte lineage. *Immunity* **41**, 219-229 (2014).
34. H. Cheroutre, F. Lambolez, D. Mucida, The light and dark sides of intestinal intraepithelial lymphocytes. *Nat Rev Immunol* **11**, 445-456 (2011).
35. E. Bettelli *et al.*, Reciprocal developmental pathways for the generation of pathogenic effector TH17 and regulatory T cells. *Nature* **441**, 235-238 (2006).
36. Y. Valdez *et al.*, Nramp1 drives an accelerated inflammatory response during Salmonella-induced colitis in mice. *Cell Microbiol* **11**, 351-362 (2009).
37. H. Maeda *et al.*, Quantitative real-time PCR using TaqMan and SYBR Green for Actinobacillus actinomycetemcomitans, Porphyromonas gingivalis, Prevotella intermedia, tetQ gene and total bacteria. *FEMS Immunol Med Microbiol* **39**, 81-86 (2003).
38. Z. Ge, Y. Feng, S. E. Woods, J. G. Fox, Spatial and temporal colonization dynamics of segmented filamentous bacteria is influenced by gender, age and experimental infection with Helicobacter hepaticus in Swiss Webster mice. *Microbes Infect* **17**, 16-22 (2015).
39. J. J. Trombetta *et al.*, Preparation of Single-Cell RNA-Seq Libraries for Next Generation Sequencing. *Curr Protoc Mol Biol* **107**, 4 22 21-24 22 17 (2014).

Chapter 3 - Antigen-specific induction of CD4+CD8αα+ intraepithelial T lymphocytes by *Bacteroidetes* species

Authors:

Djenet Bousbaine, Preksha Bhagchandani*, Mariya London*, Mark Mimee, Scott Olesen, Mathilde Poyet, Ross W. Cheloha, John Sidney, Jingjing Ling, Aaron Gupta, Timothy K. Lu, Alessandro Sette, Eric J. Alm, Daniel Mucida, Angelina M. Bilate[#] and Hidde L. Ploegh[#]

This chapter is currently under revision.

Abstract

The microbiome contributes to the development and maturation of the immune system(*1-3*). In response to commensal bacteria, $CD4^+$ T cells can differentiate into distinct functional subtypes with regulatory or effector functions along the intestine. Peripherally-induced $Foxp3^+$-regulatory T cells (pTregs) maintain immune homeostasis at the intestinal mucosa by regulating effector T cell responses against dietary antigens and microbes(*4*). Similarly to pTregs, a subset of small intestine intraepithelial lymphocytes $CD4^+CD8\alpha\alpha^+$ ($CD4_{IELs}$) exhibit regulatory properties and promote tolerance against dietary antigens (*5*). Development of $CD4_{IELs}$ from conventional $CD4^+$ T cells or from Treg precursors depends on the microbiota(*5*)(*6*). However, the identity of the microbial antigens recognized by $CD4_{IELs}$ remains unknown. We identified species belonging to the *Bacteroidetes* phylum as commensal bacteria capable of generating $CD4_{IEL}$ from naïve $CD4^+$ T cells expressing the pTreg transnuclear (TN) monoclonal TCR(*6*) as well as from polyclonal WT T cells. We found that β-hexosaminidase, a widely conserved carbohydrate-metabolizing enzyme in the *Bacteroidetes* phylum, is recognized by TN T cells, which share their TCR specificity with $CD4^+$ T cells found in the intraepithelial compartment of polyclonal specific-pathogen-free (SPF) mice. In a mouse model of colitis, β-hexosaminidase-specific $CD4_{IELs}$ provided protection from ulceration of the colon and weight loss. Thus, a single T cell clone can recognize a variety of abundant commensal bacteria and elicit a regulatory immune response at the intestinal epithelial surface.

Main text

The microbiota contributes to functional specification of adaptive immunity, both through direct interactions and via soluble mediators released into the environment. In turn, adaptive and innate immunity shape the microbiota, for example through production of antibacterial peptides and antibodies. The protective functions of T cells induced by microbes range from antibacterial defense to cancer immunity(*7*) and assistance in wound healing(*8*), but diseases such as colitis can ensue when these interactions are perturbed. The microbiota shapes the plasticity and adaptation of $CD4^+$ T cells in the intestinal lamina propria. Colonic bacteria such as *Helicobacter hepaticus* promote differentiation of antigen-specific $CD4^+$ T cells into $Foxp3^+$ regulatory T cells (Tregs) in the colon, while Segmented Filamentous Bacteria (SFB) induce quasi-clonal pro-inflammatory TH17 cells in the ileum (*9-13*). These studies highlight the importance of a specialized and diverse intestinal immune response to commensals and pathobionts localized in different intestinal niches. Such interactions are not only species-specific, but depending on the anatomical sites where they occur, can influence T cell fates(*6*). Ablation of SFB eliminates the corresponding TH17 T cells(*14*), while Class Ib MHC-restricted $CD8^+$ T cells require the presence of *S. epidermidis* in the skin (*15*). Fate decisions must thus be made at the clonal level and different T-cell receptor (TCR) specificities ought to drive distinct developmental and functional outcomes.

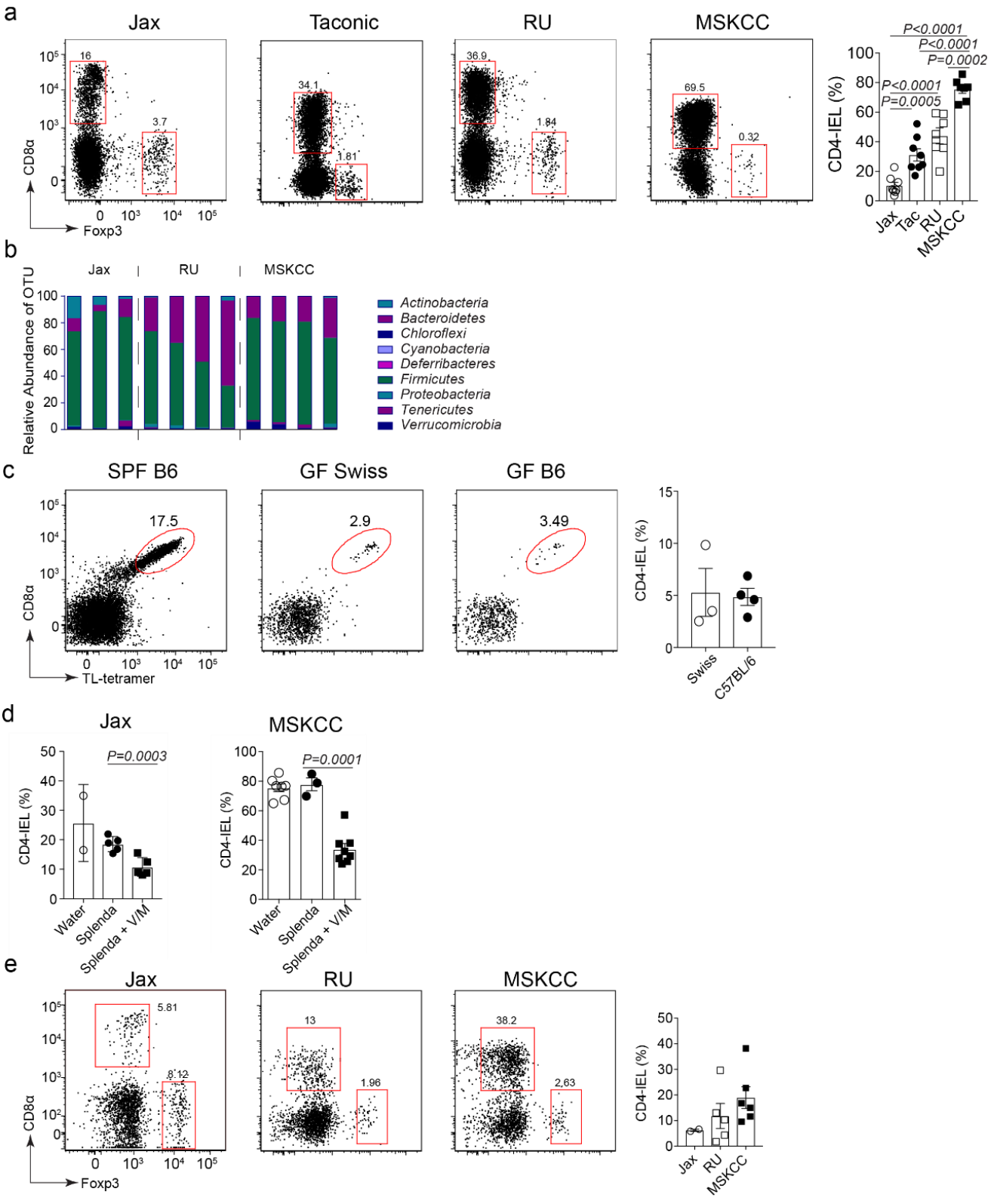

Figure 3.1 The microbiome influences the development and maintenance of $CD4_{IELs}$.

(**a**) Frequency of $CD4_{IELs}$ in mice housed in different facilities. $CD4_{IELs}$ from 8-16-week-old WT mice were harvested and their frequency determined by flow cytometry. (left) Dot plots show one representative mouse for the different experiments performed on different days (Jax n=8, Tac n=8, RU =7, MSKCC n=7). Graph on the right shows the quantitation of all mice analyzed. (**b**) The graph shows the relative abundance of the indicated phyla in WT mice housed in 3 different facilities (Jax=3, RU=4, MSKCC=4). Total DNA was extracted from fecal pellets upon arrival at the RU facility. The V4 region of 16s rRNA was amplified by nested PCRs and sequenced using Illumina technology. The graph shows all mice analyzed in two experiments. (**c**) Frequency of $CD4_{IELs}$ in germ-free (GF) mice, analyzed after export from their isolator. (Swiss Webster GF n=3, C57BL/6 GF n=4). (left) Dot plots of one representative mouse per group. (Right) Quantitation of all mice analyzed. (**d**) Frequency of $CD4_{IEls}$ in eleven-week-old Jax mice treated with vancomycin and metronidazole (V/M) for 8 weeks (left) and in five-week-old mice from MSKCC treated with V/M for 4 weeks (right). (V/M) = 0.5g/L vancomycin /1g/L metronidazole. This combination was chosen because it impacted $CD4_{IELs}$ without affecting the frequency of Tregs in the IE compartment. (Jax water n=2, Jax Splenda n=5, Jax Splenda + V/M n=5, MSKCC water n=7, MSKCC Splenda n=3, MSKCC Splenda + V/M n=). (**e**) Fecal matter transplant (FMT) from the indicated mice into GF mice. Four weeks after FMT, the frequency of $CD4_{IELs}$ was assessed by flow cytometry. Dot plots show one representative mouse/group. The graph on the right shows all mice analyzed. (Jax n=2, RU n=5, MSKCC n=6). (a,c,e) Dot plots shows cells pre-gated on $CD45^+CD8\beta^-CD4^+TCR\beta^+TCR\gamma\delta^-$. (Jax= Jackson, Tac= Taconic, RU=Rockefeller University, MSKCC= Memorial Sloan Kettering Cancer Center). P values were calculated using unpaired one-sided Student's t tests. P values <0.05 were considered statistically significant. The graphs show the mean and standard deviations. Each symbol represents a single mouse.

Two important subsets of $CD4^+$ lymphocytes regulate adaptive immunity at the intestinal mucosa: peripheral regulatory T cells (pTregs) and double-positive ($CD4^+CD8\alpha\alpha^+$) intraepithelial lymphocytes (IEL), hereafter referred to as $CD4_{IELs}$. Maintenance of immune homeostasis at the intestinal mucosa requires the action of pTregs(*16*)(*17*), which regulate the response of effector T cells against dietary antigens and commensals. Small intestine $CD4_{IELs}$ likewise promote tolerance to dietary antigens(*5, 18*). Depletion of $CD4_{IELs}$ causes disease in mice that lack functional Foxp3(*5*). $CD4_{IELs}$ and pTregs thus cooperate in the regulation of local intestinal inflammation. In specific-pathogen-free (SPF) mice, $CD4_{IELs}$ are present mostly in the epithelium of the small intestine. Their abundance varies with both age and diet and depends on the indigenous microbiota(*19-21*) (Fig. 3.1a,b). $CD4_{IELs}$ can develop either from conventional $CD4^+$ T cells or from $Foxp3^+$ Treg precursors in a microbiota-dependent manner(*5*),(*6*). Germ-free (GF) mice have few if any $CD4_{IELs}$, regardless of their genetic background(*5*),(*22*) (Fig. 3.1c). Mice treated with antibiotics(*5*),(*22*) show a similar decline in $CD4_{IELs}$ (Fig. 3.1d). Fecal transplants from mice housed in different SPF facilities restore the $CD4_{IEL}$ compartment in GF mice to different extents(*19*),(*20*) (Fig. 3.1e). Secretion of metabolites by certain

commensals can further promote accumulation of $CD4_{IELs}$(*19*). The microbiota therefore contributes not only to the development but also to the maintenance of $CD4_{IELs}$. However, the identity(ies) of the microbial antigens recognized by $CD4_{IEL}$ TCRs is unknown. Most IEL populations, including $CD4_{IELs}$, appear to have a somewhat restricted TCR repertoire(*19, 23-29*). A limited diversity of antigens might thus suffice to shape this compartment, raising the possibility that a common antigen is recognized by $CD4_{IELs}$ TCRs**.** We used the microbiota-specific transnuclear (TN) monoclonal model(*6*) to identify naturally-occurring TCR ligands of $CD4_{IELs}$. T cells from the TN mouse carry a monoclonal TCR cloned from a pTreg derived from the intestine-draining mesenteric lymph nodes (mLN)[13]. Upon transfer, naïve T cells isolated from TN mice populate not only the recipient's mLNs, where they can differentiate into pTregs, but also the epithelium of the small intestine, where they convert into $CD4_{IELs}$(*6*) (Fig. 3.2a,b). TN $CD4^+$ T cells require the presence of the microbiota to reside, persist and differentiate into $CD4_{IELs}$ at that location(*6*).

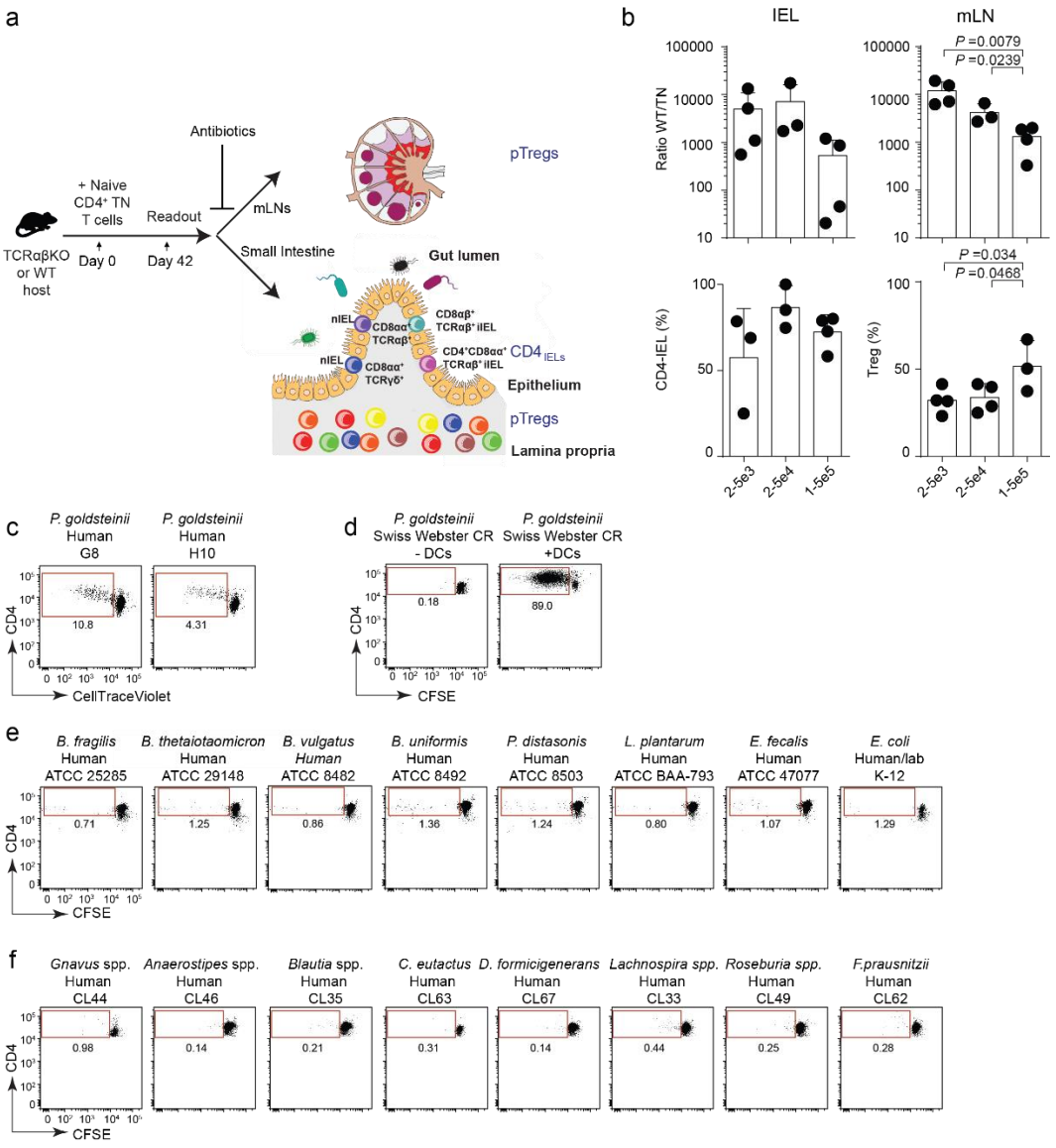

Figure 3.2 The pTreg TN TCR recognizes the predominant member of the Altered Schaedler Flora.

(**a**) Schematic of the TN model. (**b**) Congenically-marked WT hosts received different numbers of naïve $CD4^+$ TN T cells (2-5X10^3 n=4, 2-5X10^4 n=3, 1-5X10^5 n=4). After 4 weeks, the IEL and mesenteric lymph nodes (mLN) were harvested, stained and analyzed by flow cytometry. The graphs on top show the ratio of WT/TN cells in the IEL (left) and mLN (right), respectively. The bottom graphs show the frequency of $CD4_{IELs}$ among TN cells in the IEL (left) and Tregs in the mLN (right). All graphs show the mean and standard deviation (SD); each symbol represents a single mouse. TN cells were gated on $CD45.2^+CD45.1^-Aqua^-$ $CD4^+Vα2^+Vβ6^+$ $TCRβ^+TCRγδ^-$ in addition to $CD8β^-CD8α^+Foxp3^-$ for $CD4_{IELs}$ and $CD8β^-CD8α^-Foxp3^+$ for Tregs. WT cells were gated on $CD45.2^-CD45.1^+Aqua^-$. (**c**) Naïve $CD4^+$ TN T cells were labeled with CellTrace-Violet and co-cultured with dendritic cells (DCs) purified from B16-Flt3L-injected mice in the presence of bacterial extracts derived from the indicated bacteria isolated from healthy human volunteers. 3.5 days later, CFSE dilution was assessed by flow cytometry. Dot plots are representative of at least 3 experiments. Cells were gated on Via-$probe^-$ $CD4^+$ $Vα2^+$ $Vβ6^+$. (**d**) Same experimental setup as (c) but using CFSE instead of CellTrace-Violet and extracts derived from mouse *P. goldsteinii* in the presence or absence of DCs. (**e**) Same as (c) using human isolates bought from ATCC. (**f**) Same as (c).

We thus sought to identify the commensal member(s) recognized by the TN cells that allow them to migrate and convert into $CD4_{IELs}$ at the intestinal epithelium. The microbiota of mice sourced from Taconic was enriched for the antigen recognized by the TN TCR(*6*). To identify the species recognized by the TN TCR, we grew fecal bacteria derived from Taconic excluded flora (EF) mice under various culture conditions to select for a diverse array of culturable bacteria. We then co-cultured TN T cells with dendritic cells (DCs) in the presence of sonicated bacterial extracts obtained from different bacterial cultures. We observed strong proliferation of TN T cells in the presence of bacterial extracts isolated from Bacteroides bile esculin (BBE) agar plates or aerotolerant bacteria isolated from Schaedler blood agar plates (Fig. 3.3a,b). 16S rRNA sequencing showed enrichment for operational taxonomic units (OTUs) of the *Parabacteroides* genus in the cultures that yielded proliferation of TN cells (Fig. 3.3c). We tested several *Parabacteroides* strains isolated from mice and humans and observed extensive proliferation of TN T cells in the presence of *Parabacteroides goldsteinii* extracts, the predominant member of the Altered Schaedler Flora (ASF)(*30*) (3.2c and 3.3d). Proliferation of TN T cells in response to *P. goldsteinii* protein-rich extract was Class II MHC-restricted and dependent on antigen presentation by dendritic cells(*6*) (Fig. 3.2d). Neither the related *Parabacteroides distasonis* nor any other species tested induced proliferation of TN T cells *in vitro* (Fig. 3.2e,f and 3.3d). To determine whether *P. goldsteinii* extracts could also induce TN T cell proliferation *in vivo*, we transferred $CD4^+$ TN T cells into congenically-marked recipients that were then immunized subcutaneously with bacterial extracts in alum. Robust proliferation of TN T cells occurred in the draining lymph nodes (inguinal lymph nodes; iLNs) of mice that received *P. goldsteinii* extract but not *P. distasonis* extract or PBS (Fig. 3.3e,f), thus unequivocally identifying *P. goldsteinii* as a bacterium capable of engaging the pTreg TN TCR.

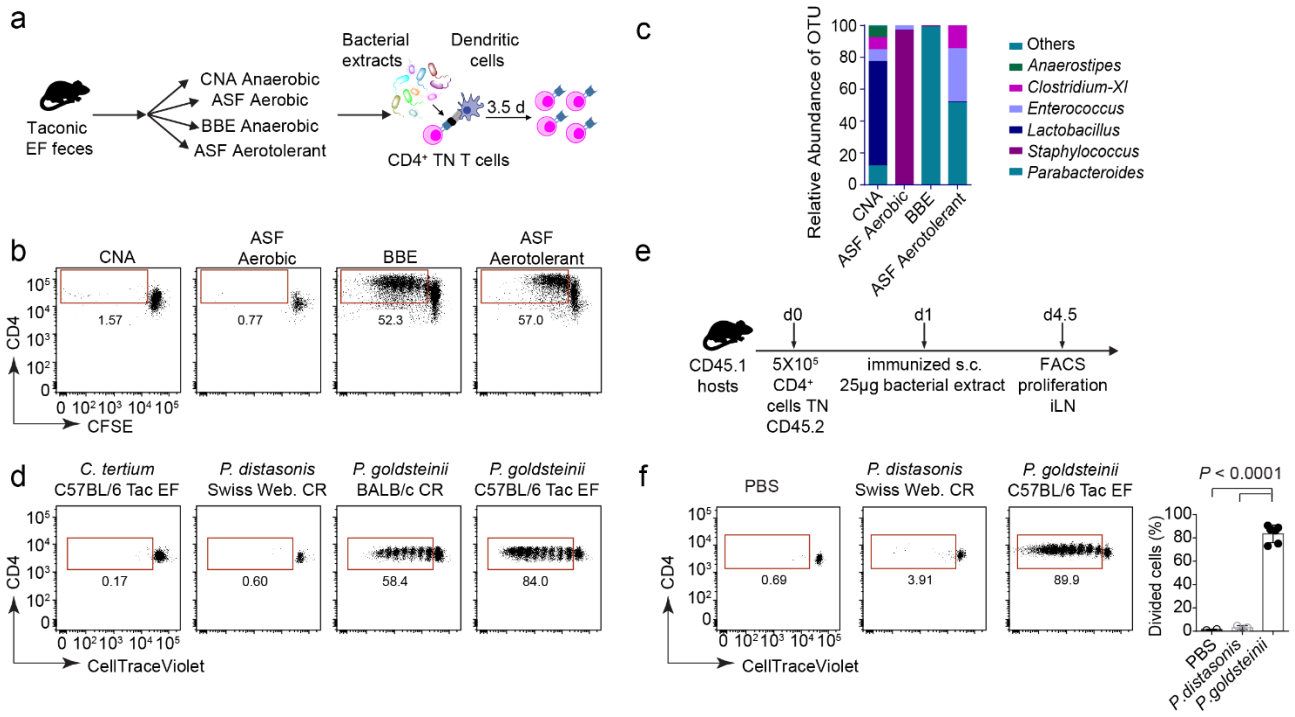

Figure 3.3 The pTreg TN TCR recognizes *P. goldsteinii*.

(**a**) Schematic of the *in vitro* proliferation assay. (**b**) Naïve CD4⁺ TN T cells were labeled with CFSE and co-cultured with dendritic cells (DCs) purified from B16-Flt3L-injected mice in the presence of bacterial extracts derived from Taconic EF fecal bacteria, isolated using the indicated growth conditions. After 3.5 days, CFSE dilution was assessed by flow cytometry. Dot plots are representative of at least 3 experiments. Cells were gated on Via-probe⁻ CD4⁺ Vα2⁺ Vβ6⁺. (**c**) DNA from the bacterial extracts depicted in (a) was isolated, the V4 region of 16s rRNA was amplified using nested PCRs and sequenced using Illumina technology. (**d**) *In vitro* proliferation as in (a): co-culture of CellTrace Violet-labeled naïve CD4⁺ TN T cells and DCs purified from B16-Flt3L–injected mice in the presence of the indicated bacterial extracts. Dot plots are representative of at least 3 experiments. (**e**) Schematic of the *In vivo* proliferation assay shown in (f). Congenically marked WT CD45.1⁺ mice received 7X10⁵ CellTrace-Violet-labeled naïve CD45.2⁺ CD4⁺ TN T cells and were immunized subcutaneously with 25µg of bacterial extracts adsorbed in alum 1 day later. 3.5 days after immunization, proliferation was assessed in the draining lymph node (inguinal lymph node, iLN) by flow cytometry. (**f**) Dot plot shows dilution of CellTrace-Violet in CD45.1⁻CD45.2⁺CD4⁺Vα2⁺Vβ6⁺ T cells in one representative mouse per condition. The graph shows all mice analyzed in two independent experiments (PBS n=2, *P. distasonis* n=3, *P. goldsteinii* n=6). The graph shows means +/- standard deviation and each symbol represents a single mouse. P values were calculated using unpaired one-sided Student's t tests. P values <0.05 were considered statistically significant. Tac=Taconic, CR=Charles River, Web.=Webster.

We next asked whether colonization with *P. goldsteinii* could induce proliferation of naïve $CD4^+$ TN T cells and their conversion into $CD4_{IELs}$ *in vivo*. We adoptively transferred TN T cells into RAG-deficient recipients pre-treated with antibiotics (*31*), which we then colonized with *P. goldsteinii* (Fig. 3.4a). Colonization was confirmed by *P. goldsteinii*-specific qPCR (3.5a). Mice treated only with antibiotics or colonized with unrelated bacteria (*Clostridium tertium*) isolated from the cecum of mice that served as the source of *P. goldsteinii*, failed to expand and convert TN cells (Fig. 3.4b-d). In contrast, in mice colonized with *P. goldsteinii,* TN cells proliferated extensively and converted into $CD4_{IELs}$ (Fig. 3.4b-d). We conclude that *P. goldsteinii* promotes the development of $CD4_{IELs}$ from TN T cells *in vivo*.

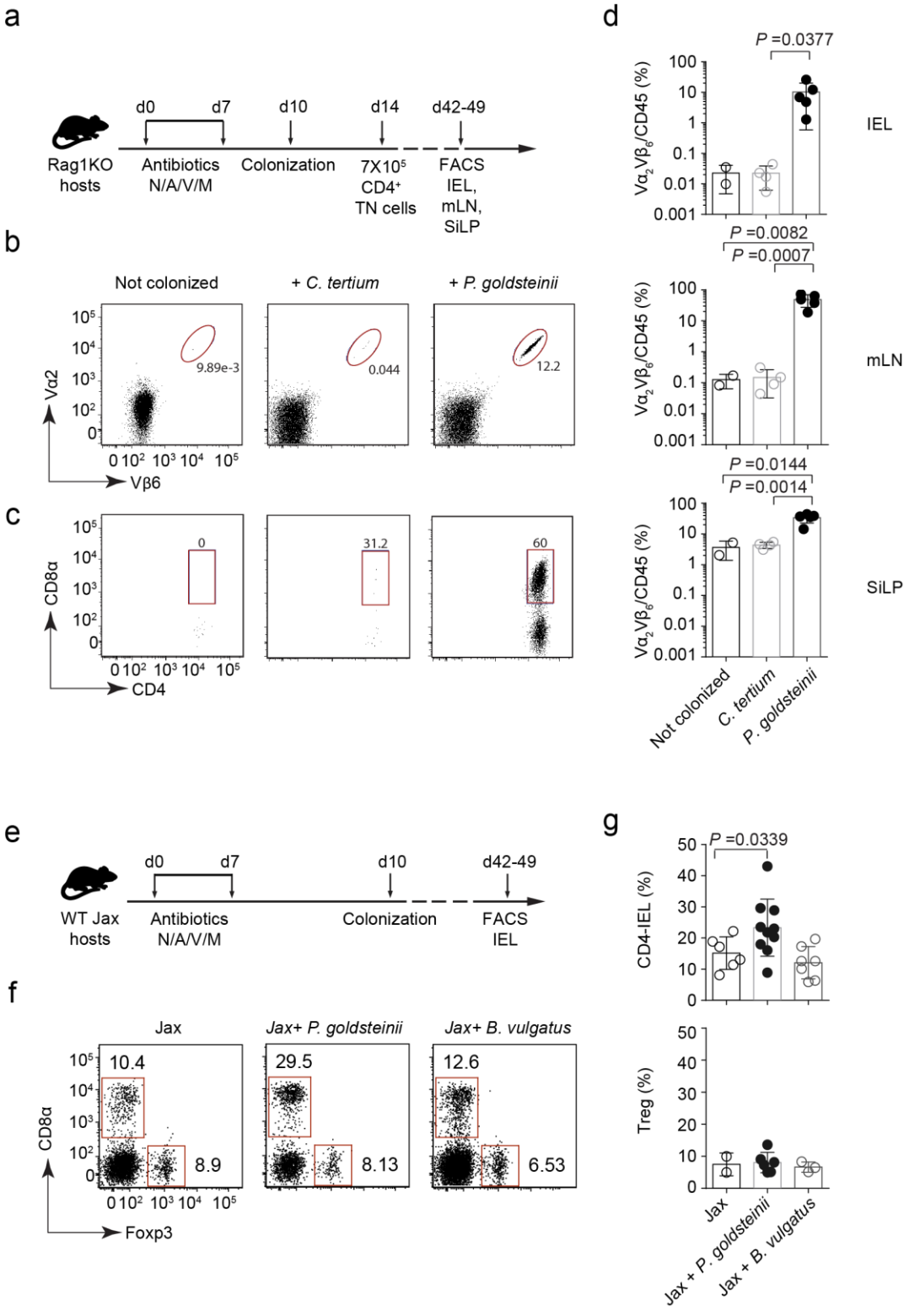

Figure 3.4 *P. goldsteinii* induces $CD4_{IELs}$ in both monoclonal and polyclonal SPF mice.

(**a**) Experimental design. Rag1KO hosts were treated with antibiotics (ABX) for 7 days. At day 10, recipient mice were colonized or not (n=2) with the indicated bacteria (*C. tertium* n=4, *P. goldsteinii* n=5). The following day, mice received 7X10^5 naïve CD45.2$^+$ CD4$^+$ TN T cells. On day 42-49, the small intestine intraepithelial compartment (IEL), small intestine lamina propria (SiLP) and the mesenteric lymph nodes (mLNs) were harvested. We analyzed their cellular composition by flow cytometry. (**b**) Dot plots show the frequency of TN cells (Vα2$^+$Vβ6$^+$) among CD45$^+$ cells of one representative mouse per group in the SiLP. (**c**) Dot plots shows the frequency of CD4$_{IELs}$ among TN cells in one representative mouse per group. Cells were gated on CD45$^+$ CD4$^+$ Vα2$^+$Vβ6$^+$. (**d**) Graphs show all mice analyzed in two independent experiments shown in (b,c). The graphs show the mean +/- standard deviation (SD) and each symbol represents a single mouse. P values were calculated using unpaired one-sided Student's t tests. P values <0.05 were considered statistically significant. (**e**) Experimental design. WT Jax mice were treated with ABX for 1 week. Three days later they were colonized with the indicated bacteria (Jax n=6, *P. golsteinii* n=10, *B. vulgatus* n=7). At day 42-49, IELs were analyzed by flow cytometry. (**f**) Dot plots show the frequency of WT cells in the IEL of one representative mouse per group. Cells were gated on live Aqua$^-$CD45$^+$TCRγδ$^-$ TCRβ$^+$CD8β$^{-/lo}$CD4$^+$. (**g**) Graphs show all mice analyzed in two independent experiments performed in two different animal facilities shown in (e). The frequency of both CD4$_{IELs}$ and Tregs was assessed in the small intestine intraepithelial compartment. The graphs show the means +/- SD and each symbol represents a single mouse. P values were calculated using unpaired one-sided Student's t tests. P values <0.05 were considered statistically significant.

P. goldsteinii is prevalent in many animal facilities(*32*), but less so in mice from Jackson Laboratories (Jax) (Fig. 3.5b,c) which also harbor fewer CD4$_{IELs}$ than mice from other facilities (Fig. 3.1a). Indeed, we could not detect any *P. goldsteinii* 16s read in the feces of Jax mice in contrast to mice housed at RU (Data not shown). To test whether the CD4$_{IEL}$ compartment of WT Jax mice could be boosted by *P. goldsteinii*, we colonized them with *P. goldsteinii* or with the related species *B. vulgatus,* or with the unrelated SFB (Fig. 3.4e-g and 3.5d,e). While CD4$_{IELs}$ were increased in mice colonized with *P. goldsteinii*, mice colonized with *B. vulgatus* or SFB showed similar frequencies of CD4$_{IELs}$ as non-colonized mice. Thus, *P. goldsteinii* promotes the accumulation of CD4$_{IELs}$ not only in the pTreg TN monoclonal model but also in WT polyclonal mice. However, in contrast to supplementation with *P. goldsteinii* in antibiotic-treated mice, colonization of fully germ-free (GF) mice with *P. goldsteinii* alone failed to expand CD4$_{IELs}$ (Fig. 3.5f). Thus, although recognition of *P. goldsteinii* antigens can promote CD4$_{IEL}$ differentiation from naïve precursors, other commensals are required for full differentiation into the CD4$_{IEL}$ phenotype in GF mice.

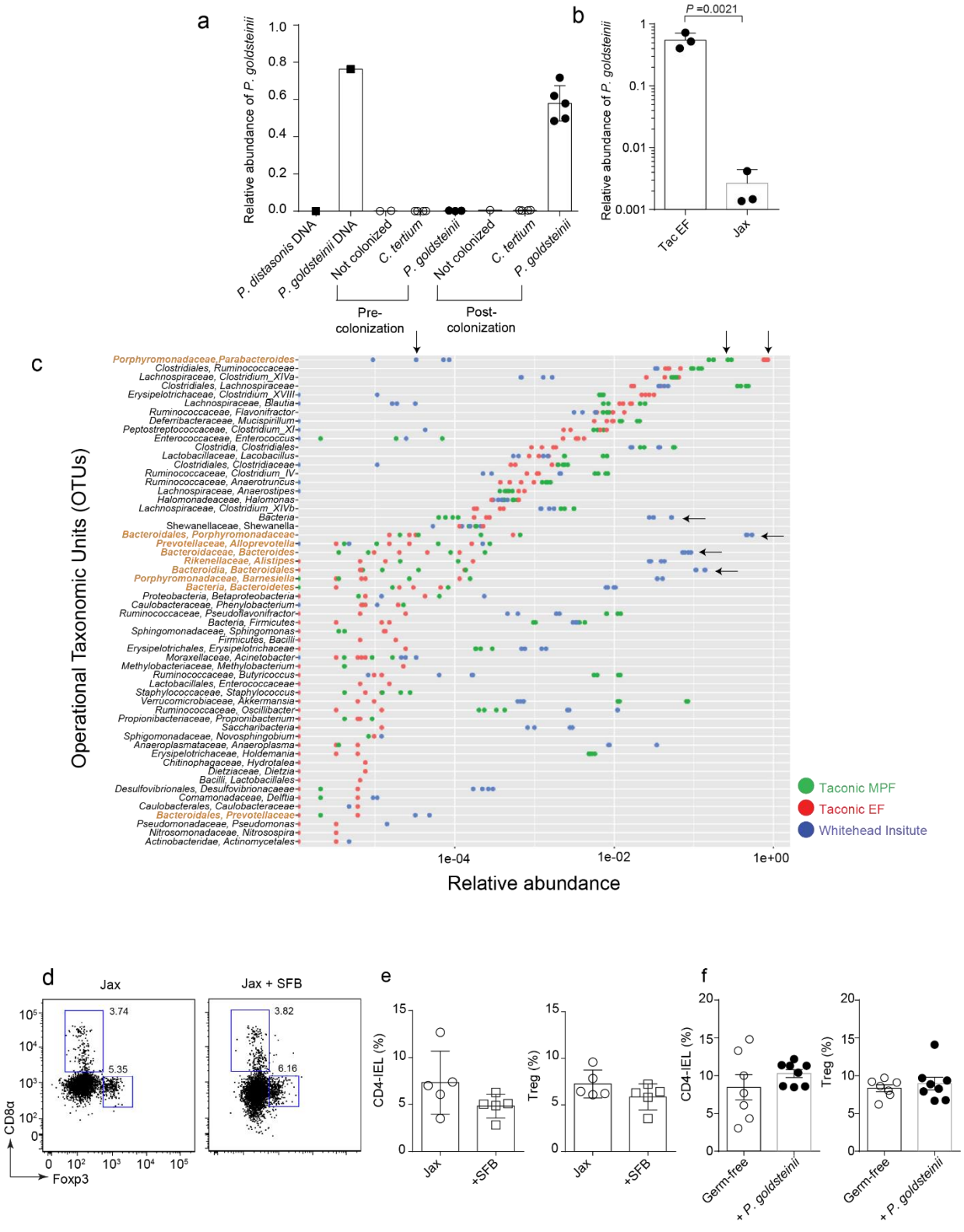

Figure 3.5 *P. goldsteinii* is abundant in SPF mice but does not rescue $CD4_{IEL}$ accumulation in germ-free mice.

(**a**) At the experimental end point (~4 weeks post-colonization), total fecal DNA was extracted from Rag1KO mice colonized or not with the indicated bacteria (see Fig. 2a-d). qPCR was performed using *P. goldsteinii*-specific and 16s generic primers. The graph shows the relative abundance of *P. goldsteinii* normalized to the total 16s (i.e Relative Abundance of *P. goldsteinii* = $2^{-(CT\ P.\ goldsteinii\ -CT\ 16s)}$) in all mice analyzed in two independent experiments. Each graph denotes the mean +/- SD and each symbol represents a single mouse. (**b**) Relative abundance of *P. goldsteinii* in the feces of Jackson (Jax) or EF mice as measured in (a) in all mice analyzed in one experiment (n=3/group). (**c**) The graph shows bacterial composition of fecal matter from mice housed in 3 different facilities. Total DNA was extracted from fecal pellets upon arrival at the WIBR facility (Taconic health status excluded flora (EF) and Taconic MPF) or in WT mice housed at WIBR facility. The V4 region of 16s rRNA was amplified by nested PCRs and sequenced using Illumina technology. Each symbol represents a single mouse in technical duplicate (n=2/facility). Arrows highlight the differences in bacterial composition between the flora analyzed. OTUs colored in orange are derived from *Bacteroidetes*. (**d**) Jax mice were colonized or not by gavage with SFB. After 4 weeks, IELs were harvested and stained for flow cytometry analysis. Dot plots show one representative mouse per group (n=5 for each group) of 1 experiment. (**e**) Graphs show all mice analyzed in (d). Graphs show the mean +/- standard deviation (SD) of all mice analyzed. (**f**) C57BL/6 germ-free (GF) mice (8-10 weeks-old), kept in isolator cages under GF conditions, were colonized or not (n=7) by gavage with *P. goldsteinii* (n=8) grown anaerobically in BHIS. After 3-5 weeks, IELs were harvested and stained for analysis by flow cytometry. Graphs show the mean +/- standard deviation (SD) of all mice analyzed in 3 independent experiments. P values were calculated using unpaired one-sided Student's t tests. P values <0.05 were considered statistically significant.

To identify the TCR ligands produced by *P. goldsteinii* that can induce TN and WT cells to become $CD4_{IELs}$, we undertook a biochemical approach. We fractionated *P. goldsteinii* lysate by ammonium sulfate precipitation, followed by anion and cation exchange chromatography (Fig. 3.6a-d). These separations yielded fractions that were highly stimulatory to TN cells as assessed by *in vitro* proliferation assays (Fig. 3.6b-d and 3.7a). Analysis of the most highly stimulatory fraction by LC-MS/MS identified 33 proteins with excellent tryptic peptide coverage (Fig. 3.7b).

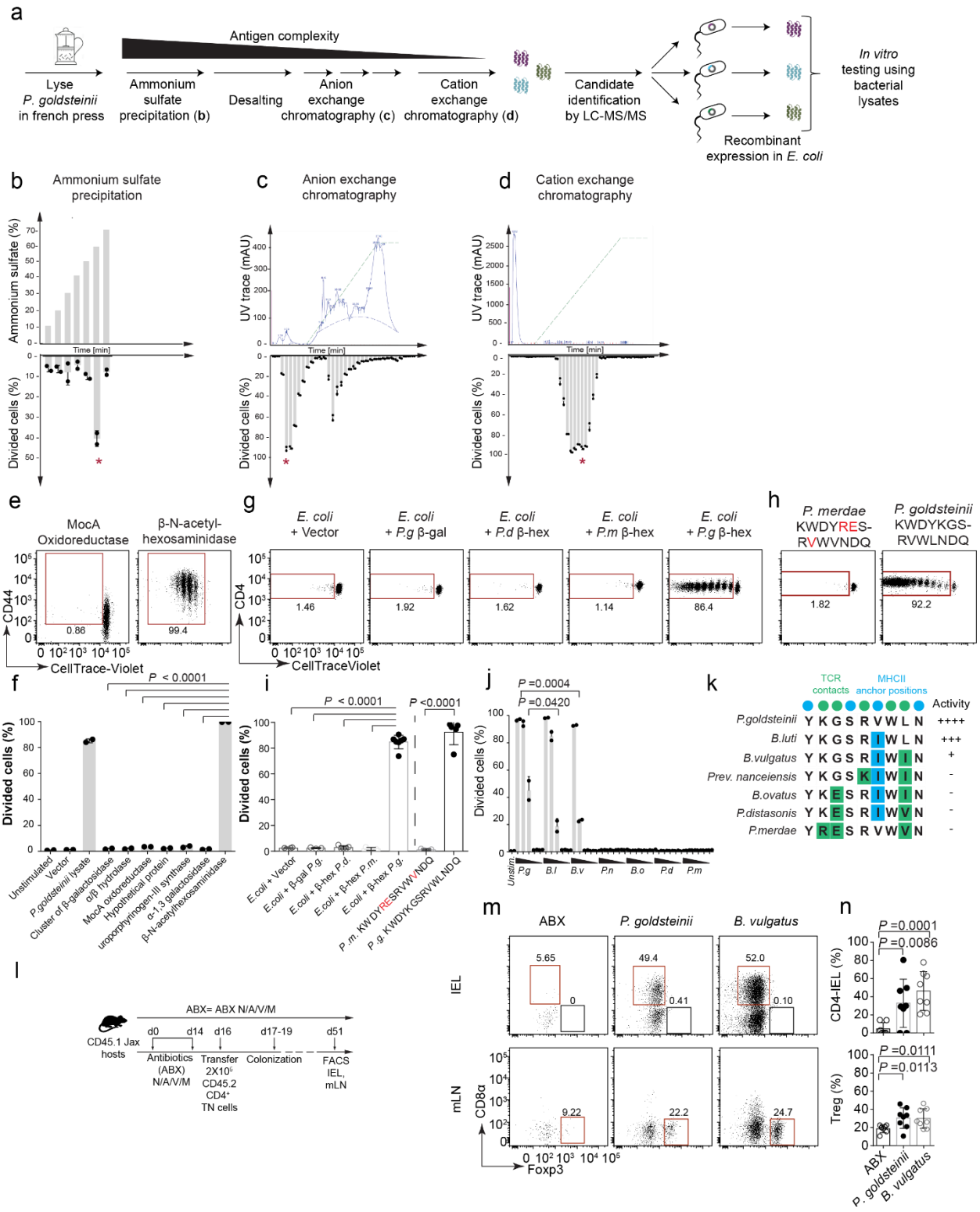

Figure 3.6 The TN TCR specifically recognizes epitopes from Bacteroidetes β-N-acetylhexosaminidase in complex with I-A^b.

(**a**) Experimental design. *P. goldsteinii* was grown anaerobically and lysed using a French press. Antigen recognized by the TN TCR was isolated by fractionating the lysate using a combination of ammonium sulfate precipitation (b), anion (c) and cation (d) exchange chromatography. Candidate polypeptides in the strongly stimulatory fractions were identified by mass spectrometry. The candidate polypeptides with the greatest sequence coverage and highest spectral counts were then recombinantly expressed in *E. coli* and tested individually *in vitro* for their ability to induce proliferation of TN cells (e,f). (**b**) *P. goldsteinii* lysate was fractionated using ammonium sulfate precipitation. Each fraction was desalted and tested for the presence of the antigen *in vitro*: naïve $CD4^+$ TN T cells were labeled with CellTrace-Violet and co-cultured with dendritic cells purified from B16-Flt3L–injected mice in the presence of the indicated fractions. 3.5 days later, CellTrace-Violet dilution was assessed by flow cytometry. The graph shows the mean and standard deviation (SD) of one representative of at least two independent experiments. Each symbol represents one technical replicate. Cells were gated on Via-$probe^-CD4^+V\alpha2^+V\beta6^+$. (**c**) *P. goldsteinii* lysate was fractionated using anion exchange chromatography. The presence of the antigen was tested *in vitro* similarly to (b). (**d**) *P. goldsteinii* lysate was fractionated using cation exchange chromatography. The presence of the antigen was tested *in vitro* similarly to (b). (**e**) Extracts derived from recombinant *E. coli* expressing the indicated candidate proteins were tested *in vitro* for the presence of the antigen, similarly to (b). Dot plots are representative of at least 3 independent experiments. Cells were gated on Via-$probe^-$ $CD4^+$ $V\alpha2^+$ $V\beta6^+$. (**f**) The graph shows the mean and SD of one representative experiment described in (e) of at least 3 independent experiments. Each symbol represents one technical replicate. (**g-h**) Congenically marked WT $CD45.1^+$ mice received $7X10^5$ CellTrace Violet-labeled naïve $CD4^+$ TN T cells ($CD45.2^+$), and were immunized sub-cutaneously with 25µg of bacterial extracts (g) or with 2 µg of peptide in alum (h) 1 day later. 3.5 days after immunization, proliferation was assessed in the draining lymph node (inguinal Lymph Node) by flow cytometry. The dot plots show dilution of CellTrace-Violet in $CD45.1^-CD45.2^+CD4^+V\alpha2^+V\beta6^+$ T cells in one representative mouse per condition. Mutations in the core epitope are indicated in red. (**i**) The graph shows all mice analyzed in two independent experiments. Experiments involving immunization with bacterial extracts and peptides were done independently. The graph shows the means +/- SDs and each symbol represents a single mouse (Vector n=4, β-gal n=3, *P.d* β-hex n=5, *P.m* β-hex n=3, *P.g* β-hex n=7, *P.m/P.g* peptide n=5 each). (**j**) Same as (b), using as the source of antigen peptide concentrations of 500nM-50pM in serial 10-fold dilutions. The graph shows the mean and SD of one experiment, representative of at least three independent experiments. Each symbol represents one technical replicate. Cells were gated on Via-$probe^-CD4^+V\alpha2^+V\beta6^+$. Any of the activating peptides (*P.g*, *B.l* or *B.v*) compared to any of the inactive peptides (*P.n*, *B.o*, *P.d* or *P.m*) yield P values <0.0001 using 500nM peptide as a reference. (**k**) Alignment of sequences homologous to the TN epitope. Green positions indicate predicted TCR contact sites and blue the $I\text{-}A^b$ anchor positions. "Activity" represents the ability of each peptide to activate the TN TCR *in vitro* (see j). (**l**) Congenically marked $CD45.1^+$ WT recipients were treated with antibiotics (ABX) for 2 weeks. At day 16, mice received $2X10^5$ naïve $CD45.2^+$ $CD4^+$ TN T cells. The following day, the mice were colonized (*P. goldsteinii* or *B. vulgatus* n=8 each) or not (n=7) with the indicated bacteria. Four weeks post-colonization, the small intestine intraepithelial compartment (IEL) and the mesenteric lymph nodes (mLN) were harvested and analyzed by flow cytometry. (**m**) Dot plots show the frequency of TN cells in the IEL (top) and mLN (bottom) of one representative mouse per group. TN cells were gated on live $Aqua^-CD4^+V\alpha2^+V\beta6^+CD45.2^+CD45.1^-CD8\beta^{-/lo}$. (**n**) Graphs show all mice analyzed in two independent experiments shown in (m). The frequency of $CD4_{IELs}$ was assessed in the IEL (top) and the frequency of Tregs in the mLN (bottom). The graphs show the mean+/- standard deviation (SD) and each symbol represents a single mouse. P values were calculated using unpaired one-sided Student's t tests. P values <0.05 were considered statistically significant. (*P.g= P. goldsteinii*, *B.l= B. luti*, *B.v= B. vulgatus, P.n= P. nanceiensis*, *B.o= B. ovatus*, *P.d= P. distasonis*, *P.m= P. merdae*, β-hex= β-N-acetylhexosamindase).

The top 15 candidates from this list were expressed recombinantly in *Escherichia coli*, and sonicates prepared from the resulting *E. coli* recombinants served as a source of candidate antigens in the antigen presentation assay (Fig. 3.6a,e,f). This strategy identified β-N-acetylhexosaminidase (β-hex) as the protein recognized by the TN TCR. The β-hex gene is part of a polysaccharide utilization locus (Fig. 3.7c), suggesting its involvement in the digestion of complex glycoproteins, either host or diet-derived (*33*).

a

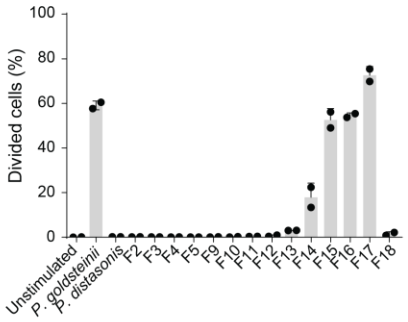

b

Identified proteins	Accession #	MW	Spectral counts
MULTISPECIES: glycosyl hydrolase family 109 [Parabacteroides]	WP_007658430.1	52 kDa	950
hypothetical protein [Parabacteroides goldsteinii]	WP_007652946.1	126 kDa	258
Cluster of beta-galactosidase [Parabacteroides goldsteinii] (WP_046145798.1)	WP_046145798.1	106 kDa	184
alpha/beta hydrolase [Parabacteroides goldsteinii]	WP_048316167.1	92 kDa	181
MULTISPECIES: 50S ribosomal protein L24 [Parabacteroides]	WP_009859538.1	12 kDa	170
beta-N-acetylhexosaminidase [Parabacteroides goldsteinii]	WP_009860534.1	78 kDa	159
gfo/Idh/MocA family oxidoreductase [Parabacteroides goldsteinii]	WP_007652944.1	47 kDa	86
MULTISPECIES: alkaline phosphatase [Parabacteroides]	WP_007657316.1	33 kDa	78
MULTISPECIES: sugar phosphate isomerase/epimerase [Parabacteroides]	WP_007653129.1	35 kDa	64
hypothetical protein [Parabacteroides goldsteinii]	WP_082207493.1	83 kDa	64
uroporphyrinogen-III synthase [Parabacteroides goldsteinii]	WP_009860404.1	29 kDa	47
sugar hydrolase [Parabacteroides goldsteinii]	WP_048316259.1	87 kDa	31
glycoside hydrolase [Parabacteroides goldsteinii]	WP_009860113.1	61 kDa	25
elongation factor Tu [Parabacteroides goldsteinii]	WP_007654184.1	44 kDa	21
beta-galactosidase [Parabacteroides goldsteinii]	WP_009860027.1	152 kDa	21
alpha-1,3-galactosidase [Parabacteroides goldsteinii]	WP_087880775.1	63 kDa	19
Cluster of alpha-1,3-galactosidase [Parabacteroides goldsteinii] (WP_087880775.1)	WP_087880775.1	63 kDa	19
hypothetical protein [Parabacteroides goldsteinii]	WP_009859671.1	67 kDa	15
alpha-N-acetylglucosaminidase [Parabacteroides goldsteinii]	WP_009860112.1	83 kDa	15
MULTISPECIES: preprotein translocase subunit SecA [Parabacteroides]	WP_007658948.1	128 kDa	13
MULTISPECIES: 30S ribosomal protein S2 [Parabacteroides]	WP_007655339.1	31 kDa	12
acetyl-CoA carboxylase biotin carboxyl carrier protein subunit [Parabacteroides goldsteinii]	WP_007657776.1	15 kDa	11
MULTISPECIES: 30S ribosomal protein S5 [Parabacteroides]	WP_009859532.1	18 kDa	10
MULTISPECIES: transcription termination factor Rho [Parabacteroides]	WP_010803566.1	75 kDa	10
MULTISPECIES: gfo/Idh/MocA family oxidoreductase [Parabacteroides]	WP_009859855.1	54 kDa	9
MULTISPECIES: flagellar motor protein MotA [Parabacteroides]	WP_007654887.1	26 kDa	6
phosphopyruvate hydratase [Parabacteroides goldsteinii]	WP_009859515.1	46 kDa	6
MULTISPECIES: 50S ribosomal protein L16 [Parabacteroides]	WP_005634742.1	16 kDa	5
MULTISPECIES: peptidylprolyl isomerase [Parabacteroides]	WP_009859573.1	61 kDa	4
glycoside hydrolase [Parabacteroides goldsteinii]	WP_007656168.1	83 kDa	4
hypothetical protein [Parabacteroides goldsteinii]	WP_009860769.1	95 kDa	4
MULTISPECIES: cell division protein [Parabacteroides]	WP_007652658.1	18 kDa	3
MULTISPECIES: 30S ribosomal protein S12 [Parabacteroides]	WP_009859549.1	15 kDa	2

c

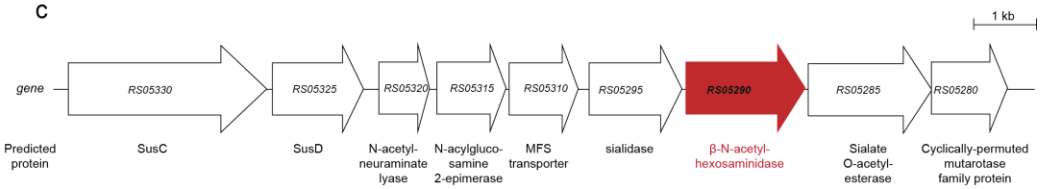

Figure 3.7 Mass spectrometry of *P. goldsteinii* antigen-enriched fraction.

(**a**) *P. goldsteinii* lysate was fractionated using a combination of ammonium sulfate precipitation, anion and cation exchange chromatography. The resulting fractions were tested in an *in vitro* proliferation assay: Naïve $CD4^+$ TN T cells were labeled with CellTrace-Violet and co-cultured with dendritic cells purified from B16-Flt3L–injected mice in the presence of the indicated fractions. 3.5 days later, CellTrace-Violet dilution was assessed by flow cytometry. The graph shows the mean and standard deviation of one experiment. Each symbol represents one technical replicate. Cells were gated on Via-probe$^-$ $CD4^+$ $V\alpha2^+$ $V\beta6^+$. (**b**) Fraction 17 from (a) was digested with trypsin in solution. The resulting peptides were analyzed by mass spectrometry. MS/MS-derived sequence data were used to search for matches against the *P. goldsteinii* proteome (refseq_P_goldsteinii_np1_20170705) and hits were validated using Scaffold. The table in (b) shows all hits identified on Scaffold using a 99% probability and a cutoff of at least 2 peptides/protein. (**c**) Representation of *P. goldsteinii* β-N-acetylhexosaminidase gene locus (*P. goldsteinii* CL02T12C30 supercont1.1, HMPREF1076).

Homologous sequences of this gene can be found across several bacterial phyla (Data not shown). TN T cells proliferated extensively in the draining lymph nodes of recipient mice immunized with a protein extract of *E. coli* expressing *P. goldsteinii* β-hex, but not when immunized with β-hex derived from closely related species (Fig 3.6g,i)*.*Truncation analysis defined a ~70 residue stretch that contained the cognate epitope of the pTreg TN TCR (Fig. 3.8a). Overlapping peptides of this region identified the epitope in a 14 amino acid stretch (Fig. 3.8b). Taking advantage of the knowledge of anchor residues for $I\text{-}A^b$ (*34*)**,** we identified the minimal epitope as YKGSRVWLN (Fig. 3.8c,d). We confirmed YKGSRVWLN as the cognate epitope of TN T cells by the *in vitro* and *in vivo* proliferative response of TN T cells to its synthetic version, both by sub-cutaneous and intranasal injections (Fig. 3.6h,i and 3.8c,e,f). Homologous synthetic β-hex peptides from *Parabacteroides merdae* failed to stimulate TN T cells. Lack of proliferation of TN T cells in response to the 14-mer N-acetylated *P. merdae* peptide was not due to an inability to bind class II MHC, as it was shown to bind $I\text{-}A^b$ with intermediate affinity, albeit at about a 3-fold lower level than the *P. goldsteinii* epitope (Fig. 3.8g).

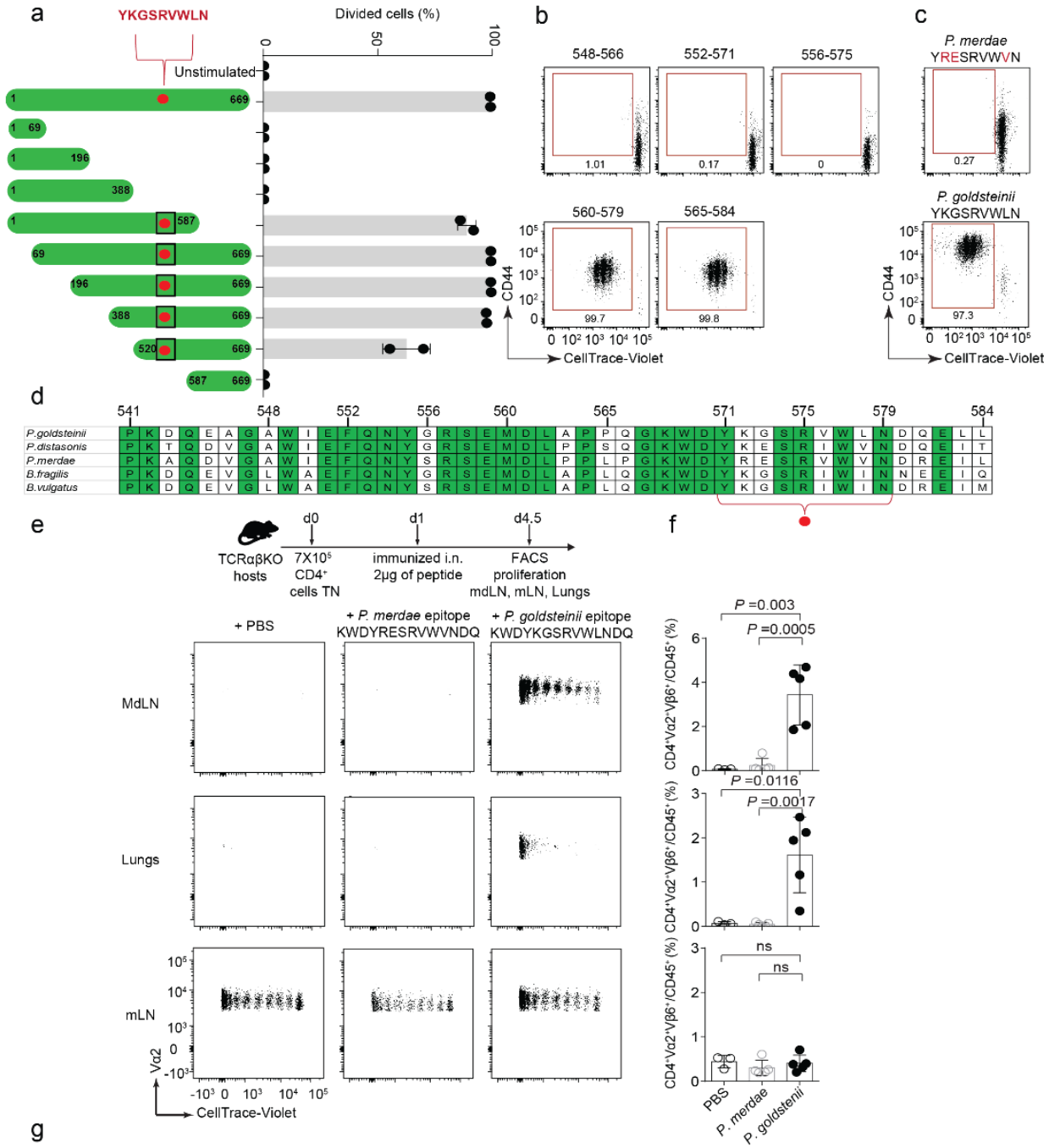

g

Antigen source	Sequence	Modification	IC_{50} ($H2\text{-}IA^b$)	+/-	SD	IC_{50} ($H2\text{-}IA^d$)	+/-	SD
P. goldsteinii	YKGSRVWLN		**519**		2.1	21327		1.6
B. luti	YKGSRIWLN		1884		1.3	32000		1.6
B. vulgatus	YKGSRIWIN		4796		3.4	2633		3.8
Prevotella nanceiensis	YKGSKIWIN		4920		1.7	8553		2.7
B. ovatus	YKESRIWIN		18277		1.4	**744**		2.4
P. distasonis	YKESRIWVN		21224		1.3	**109**		1.4
P. merdae	YRESRVWVN		9799		1.6	**402**		1.1
P. goldsteinii	KWDYKGSRVWLNDQ	N-acetylation	**492**		1.3	**420**		1.2
P. merdae	KWDYRESRVWVNDQ	N-acetylation	1508		1.2	**584**		3.2

Figure 3.8 Truncations identify the segment of β-hexosaminidase recognized by the TN TCR.

(**a**) Left: Truncations of β-N-acetylhexosaminidase (β-hex) were cloned and expressed in *E. coli*. The TN epitope is highlighted with a red dot. Right: Naïve $CD4^+$ TN T cells were labeled with CellTrace-Violet and co-cultured with dendritic cells purified from B16-Flt3L–injected mice in the presence of the lysate derived from recombinant *E. coli* expressing the indicated β-hex truncations. 3.5 days later, dilution of CellTrace-Violet was assessed by flow cytometry. The graph shows the mean and standard deviation (SD) of one representative experiment of at least three independent experiments. Each symbol represents one technical replicate. Cells were gated on Via-probe$^-$$CD4^+$$Vα2^+$$Vβ6^+$. (**b**) Same as (a) but using synthetic peptides derived from *P. goldsteinii* β-hex as a source of antigen. The dot plots depict one representative replicate of three independent experiments. (**c**) Same as (b) but using minimal peptide epitopes derived from the *P. goldsteinii* and *P. merdae* β-hex. (**d**) Alignment of residues 541-584 of β-hex from different species (indicated on the left). Conserved positions are indicated in green. The TN epitope is highlighted with a red dot. (**e**) TCRαβKO hosts received $7X10^5$ naïve $CD4^+$ TN T cells. The following day, the mice were immunized intranasally (i.n.) with 2μg of peptide. 3.5 days later, the mediastinal lymph nodes (mdLNs), lungs and mesenteric lymph nodes (mLNs) were harvested and analyzed by flow cytometry. Dot plots show one representative mouse for each group. Cells were gated on $CD45.2^+$$CD4^+$$Vα2^+$$Vβ6^+$. (**f**) Graphs show the frequency (mean +/- SD) of TN cells ($CD4^+$$Vα2^+$$Vβ6^+$) among $CD45^+$ cells in the indicated organs of all mice analyzed in one experiment. Each symbol represents one mouse. (**g**) The table shows the IC_{50} and the geometric standard deviation (SD) for the binding of the indicated peptides to $I\text{-}A^b$ and $I\text{-}A^d$. IC_{50} values were assessed in at least 3 independent experiments. Bold values represent good binders (IC_{50}<1000), while IC_{50} values between 1000-10,000 represent weaker binders. Peptide YRESRVWVN was flanked by sequences from the P*. goldsteinii* peptide (underlined in the table) to yield the longer *P. merdae* peptide KWDYRESRVWVNDQ. P values were calculated using unpaired one-sided Student's t tests. P values <0.05 were considered statistically significant.

While the microbiome of the Whitehead Institute colony (WI) contained sufficient antigen to induce strong proliferation of the TN cells *in vivo* (*6*), the relative abundance of the *P. goldsteinii* OTU was small compared to the microbiome of Taconic mice (Fig. 3.5c). However, the WI microbiota was highly enriched in closely related species belonging to the *Bacteroidetes* phylum, one of the most abundant taxa in many animal facilities (*35*). This prompted us to ask whether homologous sequences derived from related species could also activate the TN TCR which was originally cloned from a mouse housed at the WI facility. The corresponding β-hex peptides (non-N-acetylated forms) derived from *B. vulgatus* and *Bacteroides luti* could indeed induce proliferation of TN cells *in vitro*, but only at higher concentrations (Fig. 3.6j,k). Using a combination of BlastP and Jackhmmer analyses(*36*), we found possible immunostimulatory sequences in a wide range of organisms belonging to the *Bacteroidetes* phylum, from *Bacteroides* and *Parabacteroides* genuses to more distantly related species such as *Spirosoma panaciterrae* (Fig. 3/9). All such sequences mapped to the β-hex gene and over 99% of the species are found in the gastrointestinal tract. We also found several isolates containing a β-hex epitope among a library of 11,000 isolates derived from healthy human donors (*37*), suggesting that the β-

hex epitope recognized by TN T cells is also present in the human gut microbiota (Data not shown).

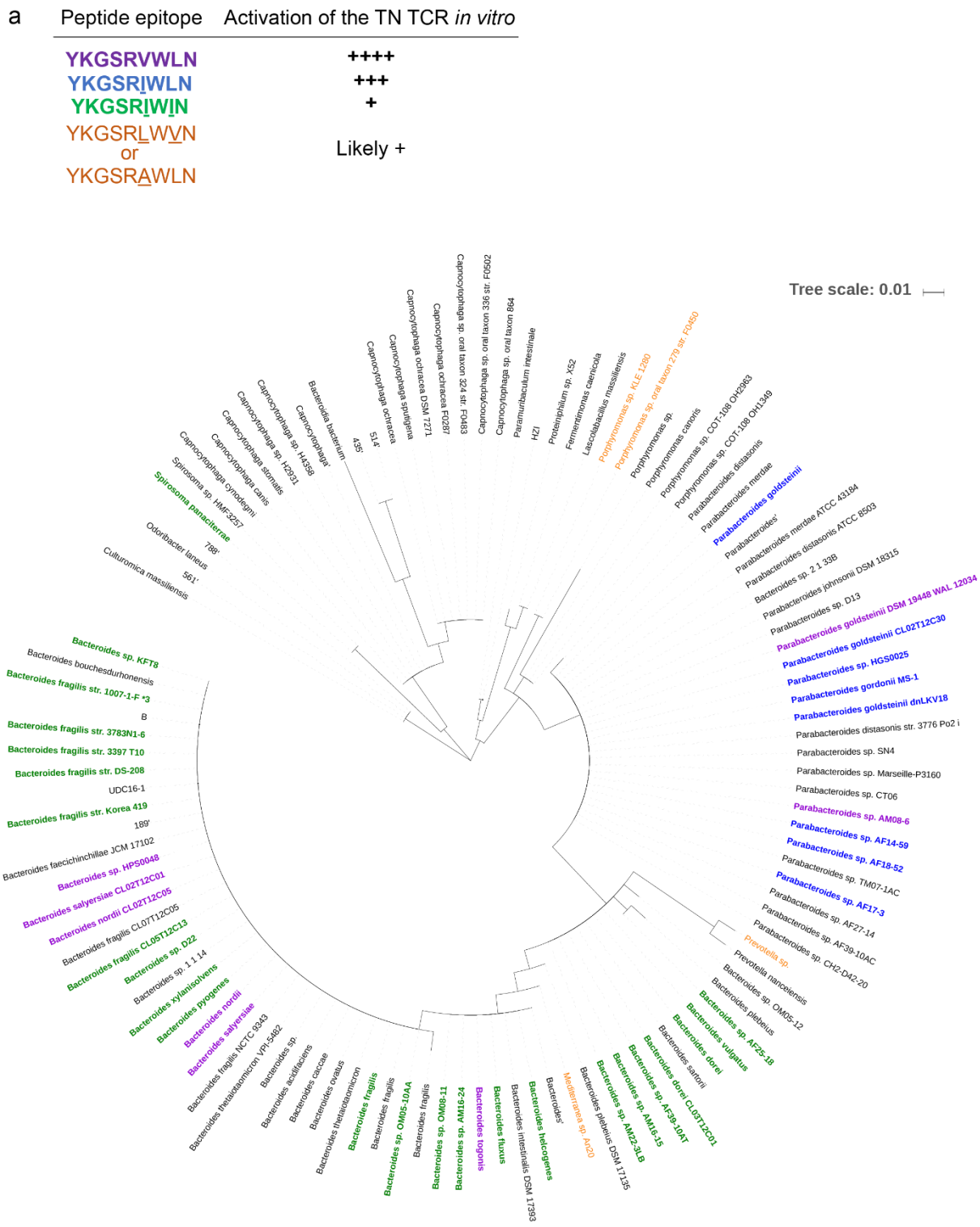

Figure 3.9 A broad range of Bacteroidetes species encode epitopes recognized by the TN TCR.

(**a**) Phylogenetic tree constructed using the marker gene RNA polymerase β (RpoB) of species encoding a sequence similar to the TN epitope (YKGSRVWLN). Identification of species with similar epitopes was achieved by retrieving and aligning β-hexosaminidase (β-hex) sequences using Jackhmmer. Bold colored species encode the cognate sequence of TN T cells, orange species contain a likely activating sequence, while species in black do not. The bar shows the evolutionary distance that separates the bacterial species indicated (number of base substitutions per site).

We then asked whether any of these bacteria could promote expansion and conversion of TN T cells into $CD4_{IELs}$ and pTregs *in vivo.* WT SPF hosts were pre-treated with antibiotics and then received congenically-marked TN $CD4^+$ T cells. Hosts were colonized with mouse isolates of *P. goldsteinii* or *B. vulgatus*. Colonization with either species promoted the expansion and development of $CD4_{IELs}$ in the intestine and pTregs in the mLNs (Fig. 3.6l-n). We obtained similar results with immunodeficient mice (TCRαβKO) as recipients (Fig. 3.10). The pTreg TN TCR therefore likely recognizes an even broader collection of bacterial species (encoding the β-hex epitope) belonging to the *Bacteroidetes* phylum, rather than a single bacterial species. Microbes other than *P. goldsteinii* or *B. vulgatus* that express similar or even the identical antigen may thus be capable of engaging $CD4^+$ T cells that would migrate to the intestine and convert into $CD4_{IELs}$**.**

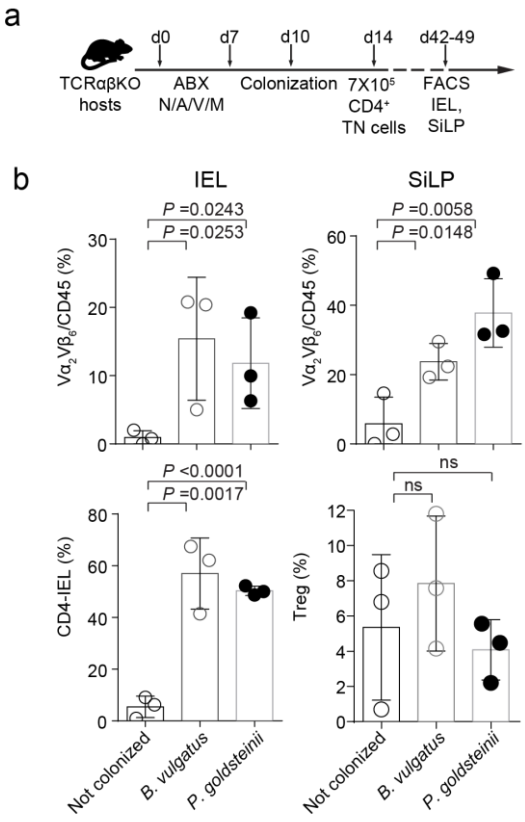

Figure 3.10 TN T cells differentiate into CD4IELs upon colonization of immunodeficient hosts.

(**a**) Experimental setup: TCRαβKO hosts were treated with antibiotics (ABX) for 7 days. On day 10, the host mice (n=3/group) were colonized or not with the indicated bacteria. On day 14, mice received $7X10^5$ naïve CD45.2$^+$ CD4$^+$ TN T cells. At day 42-49, the small intestine intraepithelial compartment (IEL) and the small intestine lamina propria (SiLP) were harvested and analyzed by flow cytometry. (**b**) Graphs shows all mice analyzed in one experiment. The frequency of $CD4_{IELs}$ was assessed in the IEL and Tregs in the SiLP. Cells were gated on CD45.2$^+$Aqua$^-$CD4$^+$ Vα2$^+$Vβ6$^+$TCRβ$^+$TCRγδ$^-$ in addition to CD8β$^-$CD8α$^+$Foxp3$^-$ for $CD4_{IELs}$ and CD8β$^-$CD8α$^-$Foxp3$^+$ for Tregs. The graphs show the means +/- SD. Each symbol represents a single mouse. P values were calculated using unpaired one-sided Student's t tests. P values <0.05 were considered statistically significant.

We then asked whether oral provision of antigen in microbiota-depleted mice would suffice to induce $CD4_{IELs}$ as suggested in another model (*5*). Prior to transfer of TN cells, we treated SPF recipient mice with broad-spectrum antibiotics to deplete the microbiota (*31*). One day after T cell transfer, β-hex peptide was administered orally via gavage. Oral administration of peptide induced robust proliferation of TN cells in all gut-draining mLNs. In contrast, mice that received neither antibiotics nor peptide, therefore relying solely on indigenous commensals as a source of antigen, showed stronger proliferation in the

jejunum/ileum mLN (Fig. 3.11a-c). We conclude that the β-hex antigen is naturally presented in the distal parts of the small intestine. When the antigen is provided as a dietary component, it reaches all gut-draining LNs. This data is in agreement with compartmentalization of intestinal T cell responses by the gut segment drained by specific mLNs, as shown using dietary and pathobiont-specific models (*38*). We also analyzed the fate of transferred TN cells four weeks later and found that the *P. goldsteinii* β-hex peptide induced $CD4_{IELs}$ in the small intestine in the absence of microbiota (Fig. 3.11d-g). Provision of this TCR ligand replaces the strict requirement of microbiota for $CD4_{IEL}$ development in antibiotic-treated mice.

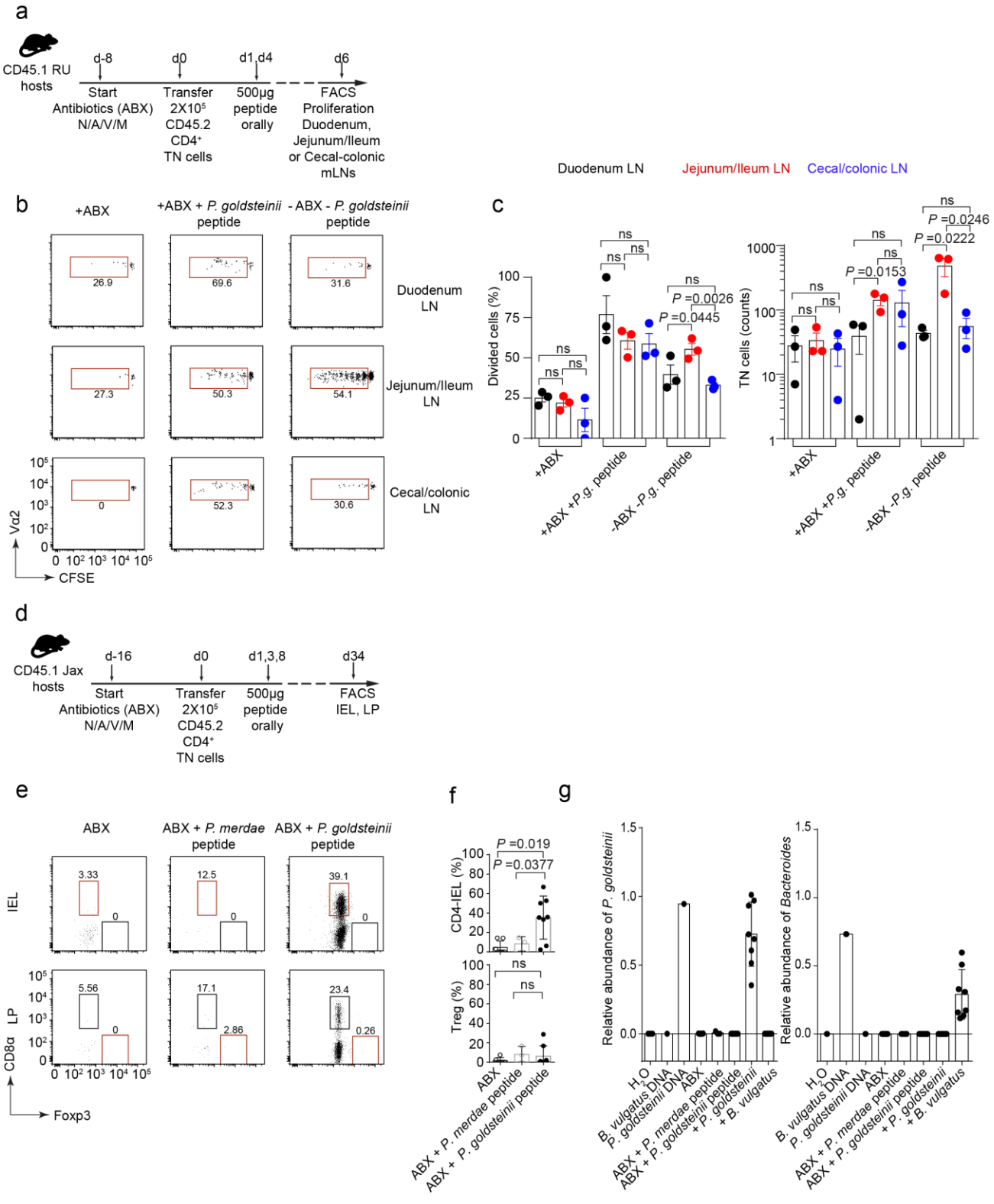

Figure 3.11 Oral delivery of cognate peptide is sufficient to induce proliferation and conversion of TN cells into $CD4_{IELs}$.

(**a**) Experimental setup: Congenically marked CD45.1 WT mice were treated with antibiotics (ABX) or not (n=5). Eight days later (d0), mice received $2X10^5$ $CD45.1^+CD45.2^+$ naïve CFSE-labeled $CD4^+$ TN cells. At d1 and d4 post-transfer, some mice were given 500µg of β-hex peptide (KWDYKGSRVWLNDQ, n=5) by gavage. Six days post-transfer, T cell proliferation was assessed in the different mesenteric lymph nodes (mLNs). (**b**) Dot plots show CFSE dilution in live $Aqua^-CD4^+V\alpha2^+V\beta6^+$ $CD45.1^+CD45.2^+$T cells in the indicated mLN of one representative mouse. (**c**). Graphs show all mice analyzed in one experiment. (**d**) Experimental setup: Congenically marked CD45.1 WT mice were treated with antibiotics (ABX). Sixteen days later, mice received $2X10^5$ $CD45.2^+$ naïve VioletTrace-labelled $CD4^+$ TN cells. One, four- and eight-days post-transfer, the mice received 500µg of β-hex peptide from *P. goldsteinii* (KWDYKGSRVWLNDQ, n=8), from *P. merdae* (KWDYRESRVWVNDQ, n=3) or no peptide (n=7) by gavage. Thirty-four days post-transfer, expansion and conversion of TN cells into $CD4_{IELs}$ (in the IEL) and Tregs (in the lamina propria, LP) was assessed by flow cytometry. (**e**) Dot plots show one representative mouse per group. Cells were gated on $CD45.2^+CD45.1^-Aqua^-CD4^+V\alpha2^+V\beta6^+CD8\beta^-$. (**f**) Graphs show all mice analyzed in two independent experiments shown in (e). (**g**) Colonization efficiency measured by qPCR. At the experimental end point (~4 weeks post-colonization), total fecal DNA was extracted from mice that received T cells, and colonized or not with the indicated bacteria (see e-f and Fig. 3l-n). qPCR was performed using *P. goldsteinii*-specific, *Bacteroides*-specific and 16s generic primers. The graphs show the relative abundance of *P. goldsteinii* and *Bacteroides* normalized to the total 16s (i.e Relative Abundance of *P. goldsteinii* = $2^{-(CT\ P.\ goldsteinii\ -CT\ 16s)}$) in all mice analyzed in two independent experiments. The experiments shown in Fig. 3l-n and Extended Data Fig. 8d-f were performed together and shown separately for clarity. The ABX group of mice represented in this figure is the same as the one shown in Fig. 3l-n. All mice were kept in microisolators with individual ventilation in the BCH facility. Each bar denotes the average+/- SD and each symbol represents a single mouse. The graphs show the means +/- SD and each symbol represents a single mouse. P values were calculated using unpaired one-sided Student's t tests. P values <0.05 were considered statistically significant.

Next, we sought to investigate whether this prevalent epitope that is able to induce $CD4_{IELs}$ from TN precursors is also recognized by $CD4_{IELs}$ of SPF mice. We designed a *P. goldsteinii* β-hex MHCII tetramer spanning the β-hex epitope, (Fig. 3.12a) and enumerated β-hex specific $CD4^+$ T cells by flow cytometry (Fig. 3.12b and 3.13a,b). SPF mice showed few β-hex-positive cells in the mLNs (Extended Data Fig. 9b) compared to the IELs (Fig. 3.13a,b). Considering the diversity of TCRs present in mLNs (*10*), this is not surprising. In the IE compartment, we observed an enrichment of *P. goldsteinii* β-hex specific $CD4^+$ cells but not of the related *P. merdae* or *P. distasonis.* $CD4^+$ T cells isolated from the IE compartment of GF mice did not bind to *P. goldsteinii* β-hex tetramer (Fig. 3.12c). The frequency of β-hex-specific cells, both in mLNs and IEL, varied in WT mice housed in different rooms (Fig. 3.12b and 3.13b), potentially due to differences in microbiome composition. Accordingly, $CD4_{IELs}$ specifically produce IFN-γ in response to *P. goldsteinii* β-hex peptide (Fig. 3.12d,e). The *P. goldsteinii* β-hex epitope is therefore an abundant natural TCR ligand of intraepithelial $CD4^+$ T cells.

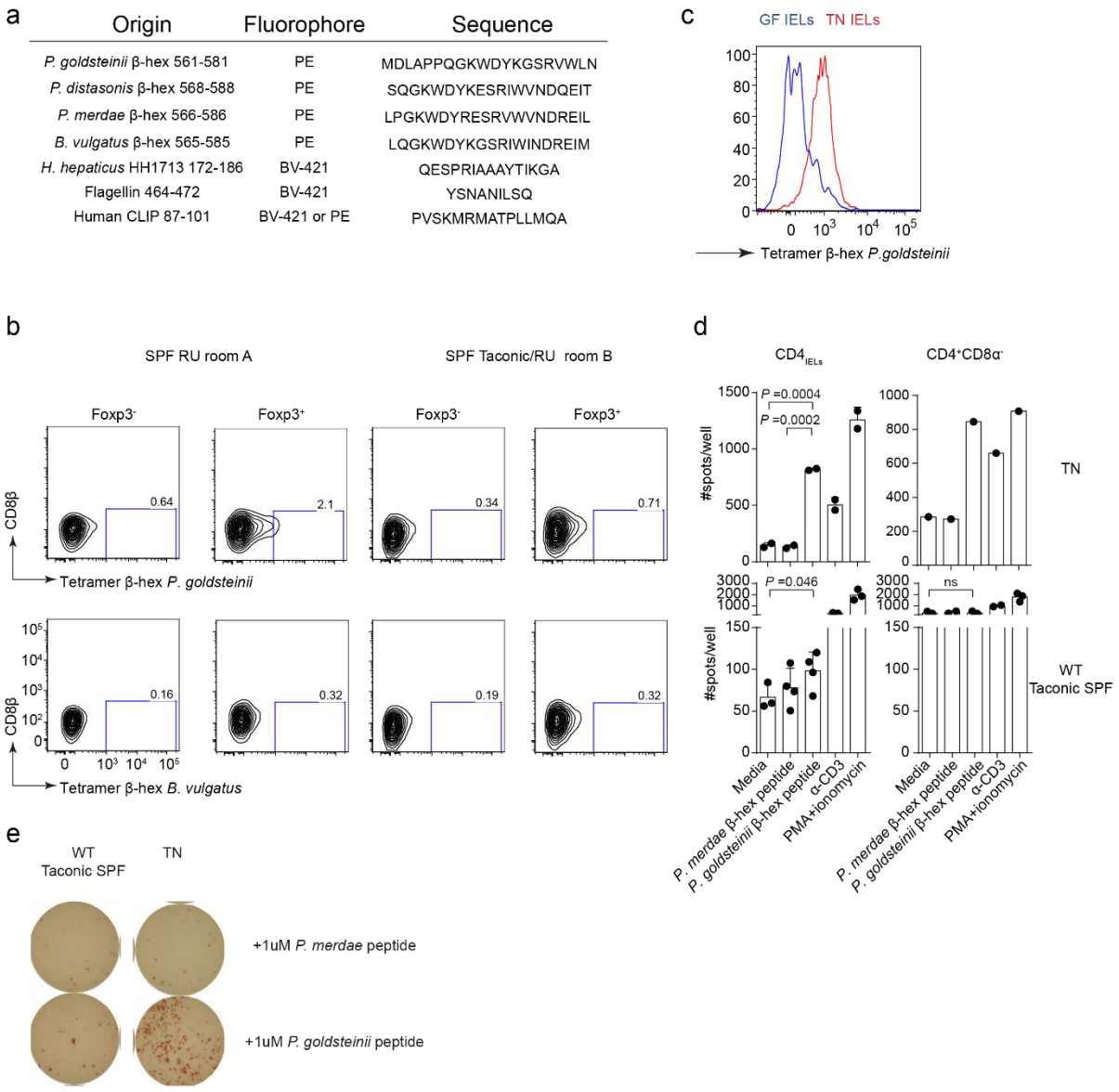

Figure 3.12 β-hexosaminidase MHCII tetramers identify antigen-specific CD4+ T cells in WT SPF mice.

(**a**) List of tetramers used in this study. (**b**) Cells harvested from the IELs of WT germ-free (GF) or TN SPF mice were stained with MHCII *P. goldsteinii* β-hex tetramer. Cells were gated on $CD45^+CD4^+Aqua^-TCR\beta^+TCR\gamma\delta^-$. Histograms show one representative mouse of 3 different mice. (**c**) Cells from the mesenteric lymph nodes (mLN) of SPF mice housed at RU either bred at RU for many generations (SPF RU room A) or bought from Taconic 6 months prior to analysis and housed at RU in a different room (SPF Taconic/RU room B) were stained with the indicated tetramers. Cells were gated on $CD45^+CD4^+Aqua^-TCR\beta^+TCR\gamma\delta^-$ and $Foxp3^{+/-}$ as indicated in the figure. (**d**) $CD4_{IELs}$ from TN or Taconic SPF WT mice were harvested, sorted and co-cultured with splenic DCs isolated from TCRαβKO mice in the presence of 1 M of the indicated peptides (*P. goldsteinii*=KWDYKGSRVWLNDQ, *P. merdae*= KWDYRESRVWVNDQ). After 18h of co-culture, IFN release was measured by ELISpot assay. Dot plots show one representative experiment for TN cells and all analyzed pools of WT mice (3-5 mice/experiment, mean +/- standard deviation). Cells were sorted on $CD45^+CD4^+Aqua^-TCR\beta^+TCR\gamma\delta^-CD8\beta^-$ with $CD8\alpha^+$ or $CD8\alpha^-$ as indicated. (**e**) One representative ELISpot experiment as described in (d).

Next we asked whether TN $CD4_{IELs}$, similarly to Tregs, could protect against intestinal inflammation (*39*). Forced conversion of CD4 cells into $CD4_{IELs}$ protects against colitis (*18*). Transfer of TN cells into immunodeficient recipients do not cause overt intestinal pathology, despite robust proliferation of the transferred cells and IFNγ production(*6*). RNAseq analysis showed that TN $CD4_{IELs}$ express a number of genes associated with regulatory functions (*6*). To test the anti-inflammatory potential of TN $CD4_{IELs}$, we first transferred naïve $CD4^+$ TN T cells into RAG-deficient mice, and after 12 days we transferred congenically-marked WT naïve $CD4^+$ T cells (Fig. 3.13a). WT cells expanded in all organs analyzed, irrespective of the presence of TN cells (Fig. 3.13b). TN cells converted into $CD4_{IELs}$ 4-8 weeks post-transfer but did not differentiate into pTregs (Fig. 3.13c,d), similarly to other commensal-specific T cells that fail to differentiate into pTregs when transferred into Rag-deficient hosts(*40*). Mice that received both TN and WT cells with or without oral β-hex peptide administration were partially protected from colitis, as judged by reduced weight loss and improved histopathological score (Fig. 3.14c-f). The majority of mice that received TN cells were free of ulcers in the colon (Fig. 3.14e). The frequency of WT-derived Tregs was low in all groups, suggesting little or no contribution of pTregs to such protection (Fig. 3.13c,d). When mice received both TN and WT cells, we observed a slight increase in the frequency of WT-Tregs in the LP. Therefore, we cannot formally rule out that those few pTregs contributed to the protective effect observed in mice transferred with TN cells. We conclude that, in the presence of their cognate antigen, TN $CD4^+$ T cells can protect against intestinal inflammation.

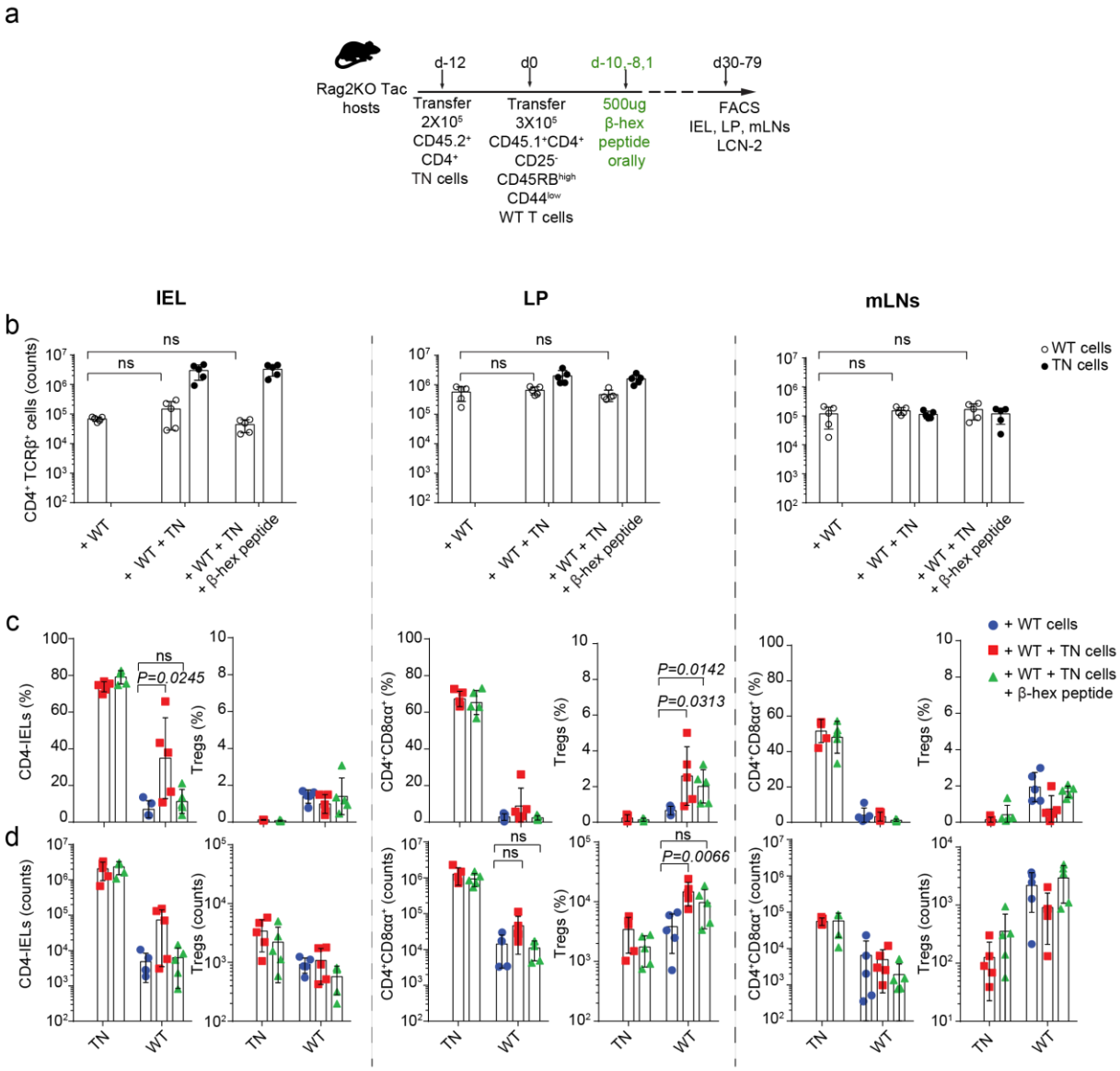

Figure 3.13 Migration and expansion TN and WT CD4+ T cells in lymphocyte-induced colitis.

(**a**) Experimental setup: Taconic Rag2KO received 2X10^5 naïve CD45.2$^+$CD4$^+$ TN cells or not. Twelve days later, the mice received 3X10^5 naïve CD45.1$^+$CD4$^+$ WT cells (day 0). On days -10, -8 and +1 one group of mice received 500µg of *P. goldsteinii* β-hex peptide (KWDYKGSRVWLNDQ) orally by gavage. The mice were weighed every other day throughout the experiment. Mice were euthanized either when they lost 20% of their initial weight or at the end of the experiment. (**b**) Total number of TN (CD45.2$^+$CD4$^+$Aqua$^-$TCRβ$^+$) and WT cells (CD45.1$^+$CD4$^+$Aqua$^-$TCRβ$^+$) in the IEL (left), Lamina Propria (LP, middle) and mesenteric lymph nodes (mLN, right) in all mice analyzed in one experiment (n=5/group). (**c**) Frequency of CD4$_{IELs}$ (CD4$^+$Aqua$^-$TCRβ$^+$TCRγδ$^-$CD8β$^-$CD8α$^+$Foxp3$^-$, CD45.1$^+$CD45.2$^-$=WT, CD45.1$^-$CD45.2$^+$=TN) or Tregs (CD4$^+$Aqua$^-$TCRβ$^+$TCRγδ$^-$CD8β$^-$CD8α$^-$Foxp3$^+$, CD45.1$^+$CD45.2$^-$=WT, CD45.1$^-$CD45.2$^+$=TN) in the IEL (left), LP (middle) and mLN (right). (**d**) Total number of cells in the indicated organs, as described in (c). (b-d) The graphs show mean +/- standard deviation and each symbol one single mouse. P values were calculated using unpaired one-sided Student's t tests. P values <0.05 were considered statistically significant.

Our novel commensal-specific model provides a new tool to study $CD4_{IELs}$ development and can be used to understand how different commensal bacteria shape plasticity, intestinal adaptation and function of $CD4_{IELs}$. The microbiota that resides in different niches of the intestinal mucosal surface can drive functional specialization of $CD4^+$ T cells. We show here, that *P. goldsteinii* and potentially many other *Bacteroidetes* which reside in the lumen and possibly the mucus layer (e.g. *Parabacteroides goldsteinii*)(*41*) are able to induce antigen-specific $CD4_{IELs}$ in a two-step manner. First, by the engagement of the TCR with its cognate antigen, and second by the microbiome-modified intestinal epithelial environment(*42*). Recognition of an antigen such as β-hex, present in a variety of abundant commensals (*Bacteroidetes*) might provide a competitive advantage to $CD4_{IEL}$ precursors to reside in the intestinal epithelium. Deciphering the rules that govern the mutualism between commensals, pathobionts and immune cells shall help us better understand intestinal homeostasis and inflammation, with prospects for controlling inflammation.

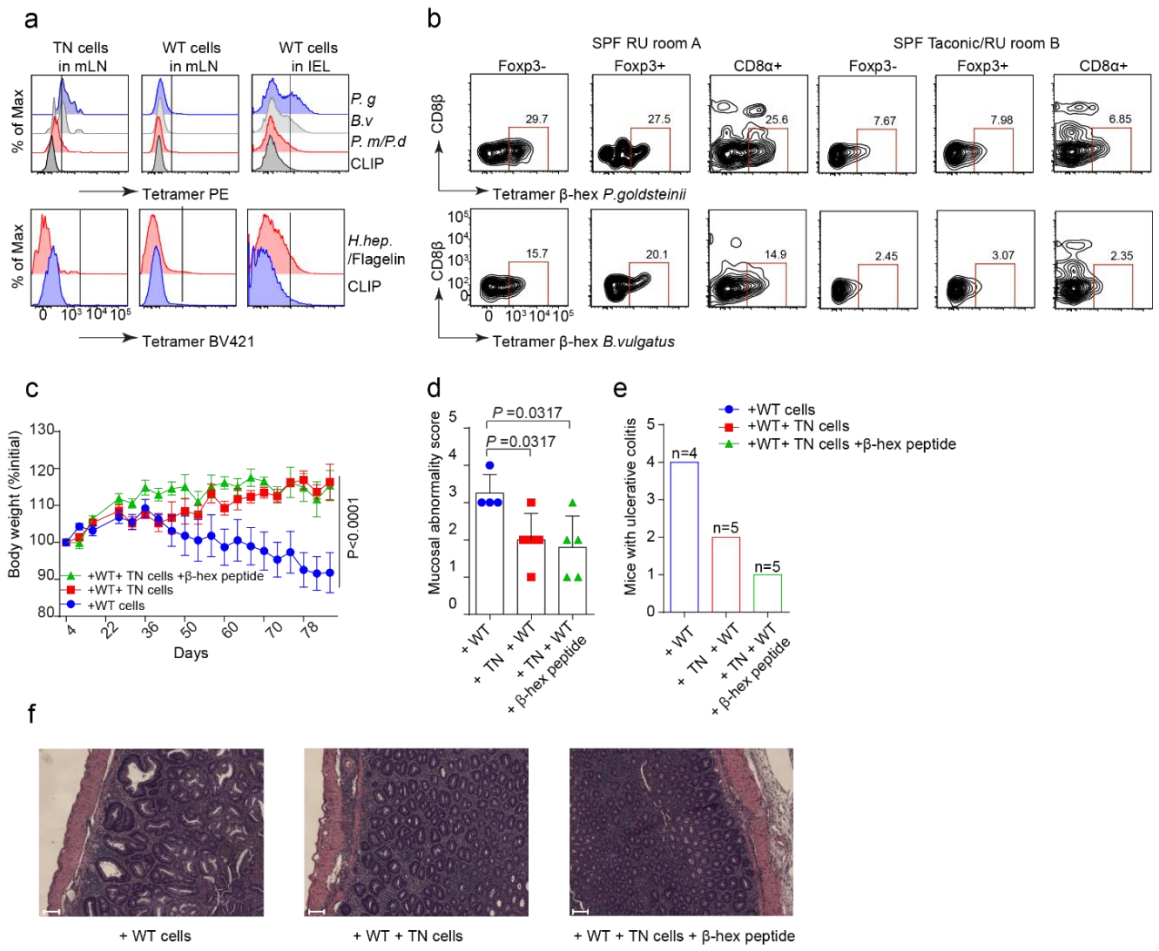

Figure 3.14 The β-hexosaminidase TN epitope is recognized by WT CD4IELs and mediates protection against intestinal inflammation.

(**a**) Naïve TN cells were transferred 24h prior to tetramer staining into congenically-marked WT SPF hosts. Mesenteric lymph nodes (mLNs) and IELs were harvested and stained using the indicated tetramers. Cells were gated on live Aqua^{-}CD45^{+}CD4^{+}TCRβ^{+}TCRγδ^{-}CD8β$^{-/lo}$. (a,b) Each Samples were processed separately for three mice and then pooled for tetramer staining. (**b**) Cells from the IEL of SPF mice housed at Rockefeller University (RU) either bred at RU for many generations (SPF RU room A) or bought from Taconic 6 months prior to analysis and housed at RU in a different room (SPF Taconic/RU room B) were stained with the indicated tetramers (experiment n=4). (**c**) Taconic Rag2KO received 2X10^{5} naïve CD45.2^{+}CD4^{+} TN cells. Twelve days later, mice received 3X10^{5} naïve CD45.1^{+}CD4^{+} WT cells (day 0). One group of mice received 3 doses of 500µg of *P. goldsteinii* β-hexosaminidase (β-hex) peptide (KWDYKGSRVWLNDQ) orally by gavage (at day -10, -8,1). Mice were weighed every other day throughout the experiment. The mice were euthanized either when they lost 20% of their initial weight or at the end of the experiment (day 81). The graph shows weight loss of the mice in the different groups. The graphs show mean/group +/- standard error. P values were calculated using a two-way ANOVA. P values <0.05 were considered statistically significant. (**d**) Mucosal abnormality score of colon H&E stained sections. Mucosal abnormality score is based on histology shown in (f). A Mann-Whitney test was used here (non-parametric data set). P values <0.05 were considered statistically significant. (**e**) Fraction of mice with colonic ulcers at the experimental end point, based on histology analysis shown in (f). (**f**) Photomicrographs of H&E stained large intestine (colon) sections of mice from the indicated colitis groups, representative of 5 mice/group. Scale bar=50µm.

Author contributions

A.B., D.B. and H.P. conceived the study, A.B and D.B designed and performed the experiments. A.B, D.B and H.P wrote the manuscript. D.B performed the biochemical experiments to identify and characterize the TN antigen, with help from A.B and P.B. D.B and A.B. performed the *in vivo* experiments, with help from M.L and P.B. M.L. performed the characterization of WT CD4IELs (Extended Data Fig. 1). M.M supported D.B and A.B with anaerobic cultures, provided mouse isolates and experimental guidance. S.O. analyzed the 16s sequencing data. M.P. provided human bacterial isolates, sequenced and assembled the genomes of the mouse bacterial isolates used in this study. R.C provided support for peptide synthesis and J.L guided D.B with antigen fractionation. J.S. performed MHCII peptide binding assays, under the supervision of A.S. E.A and D.M commented on project design and assisted in data interpretation. H.P and A.B provided guidance and supervised the study. D.B performed the phylogenetic and statistical analyses.

Funding

This work was supported by a grant from the center for Microbiome Informatics and Therapeutics of MIT (D.B, A.B, H.P, P.B). DM, AMB and ML are supported by National Institute of Health grants RO1DK093674-07, R01DK113375 and R01DK093674.

Acknowledgements

We thank S. Kolifrath and J.Jackson for technical support with mouse husbandry, genotyping and colony management at Harvard, and A. Rogoz and S. Gonzalez at Rockefeller University. We thank the hematology flow cytometry facility of BCH, in particular R. Mathieu for assistance with cell sorting, and K. Gordon and K. Chophel at Rockefeller. E. Spooner from the WIBR proteomics core for mass spectrometry analysis, R. Bronson from the rodent histopathology core of Harvard Medical school for histology and scoring. We thank the NIH tetramer core facility for providing all tetramers used in this study, in particular R. Willis for help with staining troubleshooting. We thank T. Lu and P. Silver for allowing us to use their anaerobic chambers and J. Leube for help with the

initial *in vitro* experiments. We are in indebt to C. McClune for assistance with cloning, bioinformatic analyses and project suggestions and D. VanInsberghe for support with phylogenetic analysis. We are grateful to G. Victora for invaluable guidance and support throughout this project. We thank A. Woodham for assistance with ELIspot analysis and all the members of the Ploegh lab for suggestions and fruitful discussions. We thank G. Victora, B. Reis and G. Donaldson for critical discussions and suggestions. This study was initiated at the Whitehead Institute for Biomedical Research.

Materials and methods

Mice

Mice were housed at the Whitehead Institute for Biomedical Research (WIBR), Boston Children's hospital (BCH) and Rockefeller University under specific pathogen–free conditions, in accordance with institutional guidelines and approved by the institutional animal care and use committee of the Massachusetts Institute of Technology, the Boston Children's Hospital (IACUC protocol number 16-12-3328) and Rockefeller University. pTreg TN mice were generated as described(*6*). C57BL/6, C57BL/6 CD45.1, Rag1−/−, Rag2−/−, TCRα−/−, TCRβ−/−, mice were purchased from Taconic Biosciences and Jackson Laboratory and maintained at our facilities. pTreg TN were crossed to C57BL/6 RAG1KO for at least eight generations to generate pTreg TNxRAGKO (TN). TCRαβKO (TCRα$^{-/-}$β$^{-/-}$) were generated by intercrossing TCRα$^{-/-}$ and TCRβ$^{-/-}$. Germ-free (GF) C57BL/6 and Swiss Webster mice were kept in germ-free flexible film isolators (Class Biologically Clean Ltd) at Rockefeller University. For colonization experiments, GF C57BL/6 mice were exported to isocages bioexclusion system (Tecniplast) and housed in isocages for the duration of the experiment (3-5 weeks as indicated in figure legends). Mice housed in tecniplast were given autoclaved food and water.

Antibodies, reagents, and FACS analysis

Fluorescently labeled antibodies were purchased from BD bioscience (anti-Vβ6, RR4-7; anti-CD3, 145-2C11; anti-Vβ5, MR9-4), eBioscience (anti-CD45.1, A20; anti-Foxp3, FJK-16s; anti-CD4, RM4-5; Va2, B20.1; anti-CD11c, N418). BioLegend (anti-CD45.2, 104; anti-CD8α, 53-6.7; anti-CD8β, YTS 156.7.7; anti-CD44, IM7; anti–I-A/I-E, M5/114.15.2, α-CD3, 145-2C11). Proliferation was measured by dilution of cell proliferation dyes CFSE (Sigma-Aldrich) and CellTrace Violet (Life Technologies), according to manufacturer's instructions. The cell viability dye 7-AAD (Via-Probe) and Live/dead fixable Aqua fluorescent reactive dye were purchased from BD Biosciences and ThermoFisher, respectively. Staining with live/dead markers was performed following manufacturer's instructions. Staining for cell surface markers was performed at 4°C for 30min in PBS+1mM EDTA+ 0.5% bovine serum albumin. Intracellular staining was performed according to manufacturer's instructions, using the Foxp3/Transcription Factor Staining Buffer Set (eBioscience). Flow cytometry data were acquired on an LSRFortessa (Becton Dickinson) instrument and analyzed with the FlowJo software package (Tri-Star). Alum (Imject) used for immunizations was obtained from Thermo Fisher Scientific.

Antibiotic treatment

An antibiotic cocktail containing Vancomycin (0.5 g/liter), ampicillin (1.0 g/liter), neomycin (1.0 g/liter) (Amresco), and metronidazole (1.0 g/liter) (Sigma) was given ad libitum in the drinking water(*31*) for the indicated periods as described in the figure legends.

Bacterial growth and culture conditions

Parabacteroides spp. and *Bacteroides spp.* were grown on ASF plates (Becton Dickinson). Single colonies were picked and grown in an anaerobic chamber (Coy Lab Products) using 2.5% H_2, 5% CO_2 and 92.5% N_2 in Brain Heart Infusion (BHI, Becton Dickinson) broth supplemented with 5g/L yeast extract (Becton Dickinson), 10mg/L hemin, 1mg/L Vitamin K3/menadione and 0.5g/L of cysteine-HCl. Under anaerobic growth, both plates and liquid cultures were pre-reduced for 6-10h prior to inoculation. *E.*

faecalis and *L. plantarum* were grown anaerobically in BHI and MRS broth, respectively. *E. coli* was grown aerobically in Luria Broth (LB).

Isolation of bacterial strains

For isolates obtained from mice, 2-3 fecal pellets were homogenized in 1mL of sterile PBS with a stainless-steel bead in a Qiagen Tissue Lyser II. Samples were cleared for 30 sec at 500xg to remove large fecal debris. Supernatants were plated on the indicated media (see supplemental data) and incubated anaerobically for 48h at 37˚C. Isolates were re-streaked twice for isolation of single colonies on the appropriate media before glycerol stocks were made. The supplemental data provide a detailed list of the different strains used in this study. For colonization experiments, *P.goldsteinii* isolates 841 and 33-2-9-2-8 were used in combination. Isolate 33-9-2-8 was used exclusively for antigen purification and as a source of DNA to build the candidate *E. coli* recombinants.

Antigen purification

Overnight cultures of *P. goldsteinii* isolate 33-9-2-8 were diluted 1:100 and grown for another 24h under anaerobic conditions. Cultures were harvested at 2500g for 15min at 4˚C, resuspended in 50mM Tris-HCl, pH 7.4 containing a protease inhibitor cocktail (1 tablet/50ml, Complete, Roche) and 1mg/ml of deoxyribonuclease I (Grade II, Roche) and lysed using a French press (FA-032 Standard CELL, Thermo Fisher). Proteins were precipitated from the lysate, cleared by centrifugation, using increasing concentrations of ammonium sulfate (Molecular biology grade, Sigma Aldrich) at 4˚C for 15min and recovered at 10’000g for 15min. Precipitates were resuspended in 50mM Tris-HCl (pH 7.4) and dialyzed overnight (ThermoFischer, Slide-A-Lyzer™ Dialysis Cassettes, 3.5K MWCO). Activity of each fraction was measured in the TN T cell proliferation assay. Samples containing activity were fractionated by anion exchange chromatography on a Mono Q 5/200 GL column (GE Healthcare, Piscataway NJ) using a gradient from 50mM Tris-HCl (pH 7.4) to 50mM Tris-HCl (pH 7.4) 500mM NaCl. To collect sufficient material, this step was repeated 5 times. Fractions that yielded proliferation of TN T cells were pooled and subjected to cation exchange chromatography on a Mono S 5/200 GL column

(GE Healthcare, Piscataway NJ). The active fractions were again pooled and subjected to buffer exchange (Amicon ultra 3k cutoff, sigma Millipore).

Mass spectrometry analysis

Active fractions from the MonoS chromoatography step were recovered by TCA precipitation, resuspended in a Tris/ Urea buffer, reduced with DTT, alkylated with iodoacetamide and digested with 2µg trypsin/100µl of sample at 37˚C overnight. The resulting peptides were washed, extracted and concentrated by solid phase extraction using Waters Sep-Pak Plus C18 cartridges. Organic solvent was removed and the volumes were reduced to 15 µl using a speed vac for subsequent analyses. The sample was then injected onto a Waters NanoAcquity HPLC equipped with a Aeris 3 µm C18 analytical column (0.075 mm by 20 cm; Phenomenex). Peptides were eluted using standard reverse-phase gradients. The effluent from the column was analyzed using a Thermo Orbitrap Elite mass spectrometer (nanospray configuration) operated in a data-dependent manner for the duration of the 90 minute run. The resulting fragmentation spectra were matched against the Refseq entries for *P.goldsteinii* using Mascot (Matrix Science). Scaffold Q+S (Proteome Software) was used to provide consensus reports for the identified proteins.

Isolation of mononuclear cells from intestine

Small intestines were harvested and mononuclear cells were isolated from the IE compartment and lamina propria as described(*6*)˒(*43*).

Tetramer staining

Cells isolated from the organs indicated in figure 4 and figure S9 were incubated with an Fc blocking agent (BD Pharminogen) for 10min at 4°C. Cells were then stained with tetramers (14 µg/mL in PBS + 0.5% BSA + 1mM EDTA + 0.05% Sodium azide) at 37°C for 1h45min. Cells were counterstained for surface and intracellular markers as described above. For each experiment, 2-3 mice were processed separately and the cells obtained from them pooled for staining with the indicated tetramers.

Elispot

IFNγ ELISpot assays were performed following the manufacturer's recommendations (BD ELISPOT Mouse IFNγ ELISPOT Set, BD Biosciences). Briefly, 96-well ELISpot plates were coated with an IFNγ capture antibody in PBS overnight at 4°C. The plates were blocked in complete RPMI for 2h at RT. $CD4_{IELs}$ ($CD45^+CD4^+Aqua^-TCR\beta^+TCR\gamma\delta^-CD8\beta^-CD8\alpha^+$) and $CD4^+CD8\alpha^-$ ($CD45^+CD4^+Aqua^-TCR\beta^+TCR\gamma\delta^-CD8\beta^-CD8\alpha^-$) isolated from the IEL of 3-5 Taconic SPF mice (4-9 months old) were sorted and co-cultured with DCs purified from the spleens of TCRαβKO mice, as described below (*in vitro* proliferation assay). 20,000-35,000 T cells were combined with DCs in a 1:2 ratio in duplicate in the presence or absence of 1μM of the indicated peptides. Positive control wells contained 1x Cell Stimulation Cocktail (Invitrogen) or 100nM α-CD3 (Biolegend). After plating, cells were incubated for 18h at 37°C. Plates were then washed and incubated with detection biotinylated anti-IFNγ antibody for 2h and followed by incubation with streptavidin–horse radish peroxidase (BD Biosciences) for 1h. Plates were developed with 3-amino-9-ethyl-carbazole substrate (BD ELISPOT AEC Substrate Set) for 10 minutes and air-dried for at least 18 hours. Spots were enumerated using an ImmunoSpot Ultimate Analyzer (Cellular Technology Limited) and normalized to the number of cells seeded to enable comparisons between experiments.

qPCR of fecal DNA

DNA was extracted from fecal pellets using the Qiagen power fecal kit, following the manufacturer's instructions. qPCR was performed using SYBR green master mix (Bio-Rad). Primers used for 16s were 5′-gtgStgcaYggYtgtcgtca-3′ and 5′-

acgtcRtccMcaccttcctc-3 (*44*) 5'-gcagcacgatgtagcaataca-3' and 5'-ttaacaaatatttccatgtggaac-3' for *P.goldsteinii*(*45*) and 5'-atagcctttcgaaagraagat-3' and 5'-ccagtatcaactgcaatttta-3' for *Bacteroides*(*46*). The relative abundance of *P. goldsteinii* and *Bacteroides* were calculated by normalizing bacteria-specific CT to total 16s CT (i.e Relative Abundance of *P. goldsteinii* = $2^{-(CT\ P.\ goldsteinii\ -CT\ 16s)}$).

Fecal bacterial growth

Fecal bacteria from the indicated mice were harvested by resuspending single fecal pellets into 500µl of PBS and spinning briefly to remove fibers. Supernatants were diluted 1:10, 1:100 and 1:1000 and then streaked on Schaedler blood agar, Columbia CNA agar or Bacteroides Bile Esculin Agar (BBE) (Becton Dickinson). Bacteria were grown for 48-72h aerobically or anaerobically as indicated. For the isolation of aerotolerant extracts, ~10 colonies from an anaerobic Schaedler blood agar plate were re-streaked to obtain single colonies, grown for 72h and then exposed to aerobic conditions (stored in the fridge outside anaerobic chamber). The plates were then placed back in the anarerobic chamber and incubated for further 72h before isolation of regrown bacteria.

Bacterial extracts for proliferation assays

Unless specified otherwise, bacterial extracts were prepared from overnight cultures or from bacterial colonies scraped directly off agar plates into PBS. Bacterial pellets obtained by centrifugation at 13,500g for 10 min at 4°C were resuspended in 1 ml of PBS containing protease inhibitors (cOmplete Mini, Roche; 1 tablet per 10 ml of PBS following the manufacturer's instructions) and deoxyribonuclease I (grade II, Roche). Bacteria were lysed by three rounds of sonication (Branson Sonifier 450) for 1 min, 60 pulses, followed by 5 min of cooling on ice between each round (output control, 4; duty cycle, 50%). Cellular debris was removed by centrifugation at 14,000g for 30 min at 4°C. Protein concentrations were assessed using a bicinchoninic acid assay (BCA) assay. For *P. golsteinii* and *P. distasonis* extracts used for the *in vivo* proliferation assays, overnight cultures were spun down at 2,500g for 15min at 4˚C, resuspended in PBS containing protease inhibitor cocktail (1 tablet/50ml, Complete, Roche) and 1mg/ml of deoxyribonuclease I (Grade II, Roche) and lysed using a French press (FA-032 Standard CELL, Thermo Fisher). Supernatants were cleared for 30min at 4,000g in a 100k Amicon column (Sigma-Millipore), followed by two PBS washes. The retentate was used for *in vivo* proliferation assays. Protein concentrations were determined using a BCA assay.

Cloning recombinant *E. coli* and extract preparation

The genes of candidate proteins identified in the LC-MS/MS analysis were cloned into Pet-30b+ (EMD biosciences) using a Gibson cloning strategy. The inserts were designed to contain a C-terminal HA tag to allow confirmation of expression by immunoblot. After introduction into competent BL21 cells candidate antigens were expressed overnight in Terrific Broth at 30°C upon isopropyl β-D-thiogalactopyranoside induction (1 mM) at an OD600 of ~0.6. Overnight cultures were harvested at 13,500g for 10 min at 4°C. The bacterial pellet was resuspended in 1 ml of PBS containing protease inhibitors (cOmplete Mini, Roche; 1 tablet per 10 ml of PBS following the manufacturer's instructions) and deoxyribonuclease I (grade II, Roche). Extracts were then prepared for *in vitro* and *in vivo* proliferation as described above. For each candidate protein, several independent clones were tested in an *in vitro* proliferation assay (see above).

MHC purification and binding assays

Purification of H-2 I-A^b and I-A^d class II MHC molecules by affinity chromatography, and the performance of peptide binding assays based on competition for binding of a high affinity radiolabeled peptide were performed as detailed elsewhere(*47*). Briefly, the mouse B cell lymphoma LB27.4 was used as a source of Class II MHC molecules. A high affinity radiolabeled peptide (0.1-1 nM; peptide ROIV, sequence YAHAAHAAHAAHAAHAA) was co-incubated at room temperature with purified Class II MHC in the presence of a cocktail of protease inhibitors and a candidate inhibitor peptide. Following a two-day incubation, Class II MHC-bound radioactivity was determined by capturing MHC/peptide complexes on mAb (Y3JP, I-Ab; MKD6, I-Ad) coated Lumitrac 600 plates (Greiner Bio-one, Frickenhausen, Germany), and measuring bound radioactivity using the TopCount (Packard Instrument Co., Meriden, CT) microscintillation counter. The concentration of peptide yielding 50% inhibition of the binding of the radiolabeled peptide was calculated. Under the conditions used, where [label]<[MHC] and IC50 ≥ [MHC], the measured IC50 values are reasonable approximations of the true K_D values(*48*),(*49*). Each competitor peptide was tested at six different concentrations covering a 100,000-fold range, and in three or more independent experiments. As a

positive control, the unlabeled version of the radiolabeled probe was included in each experiment.

In vitro proliferation assay

Dendritic cells were purified from spleens and mesenteric lymph nodes of B16-FLT3L-injected mice using the Pan Dendritic Cell Isolation Kit (Miltenyi, Germany). Naïve $CD4^+$ T cells were purified from the spleen and mesenteric lymph nodes of pTreg TN/Rag1KO mice following the manufacturer's instructions (Miltenyi, Germany) and labeled with 2.5 µM CFSE (Sigma) or 3µM CellTrace Violet (ThermoFischer). Purity was always greater than 98% for both DCs and T cells. $1X10^5$ DCs were incubated with bacterial extract (50µg/ml) or peptide (500nM, 50nM, 5nM, 0.5nM, 500pM, 50pM) for 2h before adding $1X10^5$ T cells. Proliferation was assessed by dilution of CFSE or CellTrace Violet after 3.5 days of co-culture.

In vivo proliferation assay

TCRαβKO or CD45.1 mice received the indicated number of CellTrace Violet or CFSE-labeled $CD4^+$ T cells isolated from pTreg TN/Rag1KO mice. Recipients were then immunized with 25µg of bacterial lysate in alum sub-cutaneously or injected intranasally with 2µg of peptide in PBS (no alum) 24h later. Proliferation of cells isolated from the draining lymph node (inguinal lymph node or mediastinal lymph node) was assessed by dilution of the cell proliferation dye.

Colonization

For colonization of GF mice with *P.goldsteinii*, bacteria from frozen glycerol stocks were grown anaerobically for 48h on Schaedler blood agar plates. Single colonies were inoculated in BHIS supplemented with hemin, vitamin K3 and cysteine (see above) and cultures were harvested 18h later. Pelleted bacteria were resuspended in PBS (5ml of culture resuspended in 500µl of PBS) and given orally to GF mice by gavage (200µl/mouse). WT Jax mice were pre-treated with broad spectrum antibiotics for 1-2 weeks prior to colonization. Colonization was performed as described for GF mice above

but mice received bacteria orally for three consecutive days. Colonization status was confirmed by qPCR or 16S sequencing.

Peptide synthesis

Peptides were synthesized on a rink-amide linker resin to produce C-terminal amides (Advanced ChemTech) using a flow-based solid-phase peptide synthesizer at 60˚C, as described(*50*). Deprotection steps were performed by incubating the resin for 45 sec in dimethylformamide (DMF) with piperidine (20% vol/vol) using a constant flow of 20ml/min. The resin was then rinsed at the same flow rate for 1.5 min with DMF. Coupling was performed using standard Fmoc-protected amino acids (4 equivalents), N,N,N,N-Tetramethyl-O-(1H-benzotriazol-1-yl)uronium hexafluorophosphate (HBTU, 4 equivalents), and diisopropylethylamine (DIPEA, 8 equivalents) in DMF at a flow rate of approximately 3 mL per minute. At the end of the synthesis, the resin was rinsed in methanol, followed by dichloromethane and air-dried. Peptides used for *in vivo* experiments were acetylated at the N-terminal amine to increase their stability by inhibiting proteolysis at the N-terminus. N-terminal acetylation was performed on resin by incubation of N-terminally deprotected peptides with a mixture of acetic anhydride, DIPEA and DMF (1:2:8 vol/vol) for 10 minutes, followed by washing with DMF. Peptides were cleaved off the resin and deprotected using 92.5% trifluoroacetic acid, 5% H2O, and 2.5% TIPS, precipitated using cold diethyl ether, collected by centrifugation, air-dried, purified using reversed-phase C18 HPLC (Shimadzu), and lyophilized. Identity of the peptides was confirmed by liquid chromatography-mass spectrometry (Waters Xevo system). Purified peptides were resuspended in deionized water at a concentration of 1mg/ml and stored at -20˚C. Peptides for oral gavage were ordered on Genscript at a purity >= 85%. Minimal epitopes used in *in vitro* proliferation assays were ordered from Genscript (≥ 95% pure).

Isolation of $CD4^+$ T cells

Naïve $CD4^+$ T cells were isolated from spleen and mesenteric lymph nodes using the naïve CD4 T cells isolation kit (Miltenyi, Germany). Purity was always >98%.

Histopathological analysis

Small and large intestines were fixed in 10% (v/v) buffered formalin, paraffin-embedded and stained with hematoxylin and eosin (H&E). Slides were scored blindly by a pathologist at the rodent histopathology core of Harvard Medical School.

Statistical analysis

Mean and standard deviation/error were calculated using GraphPad Prism (GraphPad Software). Unpaired one-sided Student's t tests were used to compare two variables. A Mann-Whitney test was used for non-parametric data sets. Two-way ANOVA was used for analysis change in weight loss in the colitis experiment. P values <0.05 were considered significant and where applicable are indicated in each figure legend.

16S analysis

DNA was extracted from fecal pellets using Quick-DNA Fecal/Soil Microbe Miniprep Kit (Zymo Research), following the manufacturer's instructions. Paired-end 16s Illumina sequencing libraries were constructed using nested PCRs as described (*51*). Libraries were multiplexed and sequenced on an Illumina MiSeq using paired-end 150bp reads at the BioMicro Center of MIT. Primers were trimmed, allowing at most 2 mismatches in the primer sequence. Forward and reverse reads were merged, allowing at most 2 mismatches in the merged sequence and sequences of length 253 ± 5 nucleotides, and quality filtered, discarding sequences with at most 2 expected errors. 99% OTUs were identified with UPARSE(*52*) OTUs were assigned to genera using the Ribosomal Database Project naïve Bayesian classifier(*53*) with 80% bootstrap confidence.

References

1. L. V. Hooper, D. R. Littman, A. J. Macpherson, Interactions between the microbiota and the immune system. *Science* **336**, 1268-1273 (2012).
2. M. G. Rooks, W. S. Garrett, Gut microbiota, metabolites and host immunity. *Nat Rev Immunol* **16**, 341-352 (2016).
3. J. L. Round, S. K. Mazmanian, The gut microbiota shapes intestinal immune responses during health and disease. *Nat Rev Immunol* **9**, 313-323 (2009).
4. K. Atarashi *et al.*, Induction of colonic regulatory T cells by indigenous Clostridium species. *Science* **331**, 337-341 (2011).
5. T. Sujino *et al.*, Tissue adaptation of regulatory and intraepithelial CD4+ T cells controls gut inflammation. *Science* **352**, 1581-1586 (2016).
6. A. M. Bilate *et al.*, Tissue-specific emergence of regulatory and intraepithelial T cells from a clonal T cell precursor. *Sci Immunol* **1**, eaaf7471 (2016).
7. T. Tanoue *et al.*, A defined commensal consortium elicits CD8 T cells and anti-cancer immunity. *Nature* **565**, 600-605 (2019).
8. A. N. Skelly, Y. Sato, S. Kearney, K. Honda, Mining the microbiota for microbial and metabolite-based immunotherapies. *Nat Rev Immunol* **19**, 305-323 (2019).
9. E. Sefik *et al.*, MUCOSAL IMMUNOLOGY. Individual intestinal symbionts induce a distinct population of RORgamma(+) regulatory T cells. *Science* **349**, 993-997 (2015).
10. S. K. Lathrop *et al.*, Peripheral education of the immune system by colonic commensal microbiota. *Nature* **478**, 250-254 (2011).
11. Y. Yang *et al.*, Focused specificity of intestinal TH17 cells towards commensal bacterial antigens. *Nature* **510**, 152-156 (2014).
12. M. Xu *et al.*, c-MAF-dependent regulatory T cells mediate immunological tolerance to a gut pathobiont. *Nature* **554**, 373-377 (2018).
13. J. N. Chai *et al.*, Helicobacter species are potent drivers of colonic T cell responses in homeostasis and inflammation. *Sci Immunol* **2**, (2017).
14. Ivanov, II *et al.*, Induction of intestinal Th17 cells by segmented filamentous bacteria. *Cell* **139**, 485-498 (2009).
15. J. L. Linehan *et al.*, Non-classical Immunity Controls Microbiota Impact on Skin Immunity and Tissue Repair. *Cell* **172**, 784-796 e718 (2018).
16. A. M. Bilate, J. J. Lafaille, Induced CD4+Foxp3+ regulatory T cells in immune tolerance. *Annu Rev Immunol* **30**, 733-758 (2012).
17. M. Shale, C. Schiering, F. Powrie, CD4(+) T-cell subsets in intestinal inflammation. *Immunol Rev* **252**, 164-182 (2013).
18. B. S. Reis, A. Rogoz, F. A. Costa-Pinto, I. Taniuchi, D. Mucida, Mutual expression of the transcription factors Runx3 and ThPOK regulates intestinal CD4(+) T cell immunity. *Nat Immunol* **14**, 271-280 (2013).
19. L. Cervantes-Barragan *et al.*, Lactobacillus reuteri induces gut intraepithelial CD4(+)CD8alphaalpha(+) T cells. *Science* **357**, 806-810 (2017).
20. Y. Umesaki, H. Setoyama, S. Matsumoto, Y. Okada, Expansion of alpha beta T-cell receptor-bearing intestinal intraepithelial lymphocytes after microbial colonization in germ-free mice and its independence from thymus. *Immunology* **79**, 32-37 (1993).
21. M. G. Langille *et al.*, Microbial shifts in the aging mouse gut. *Microbiome* **2**, 50 (2014).
22. D. Mucida *et al.*, Transcriptional reprogramming of mature CD4(+) helper T cells generates distinct MHC class II-restricted cytotoxic T lymphocytes. *Nat Immunol* **14**, 281-289 (2013).

23. L. Helgeland, J. T. Vaage, B. Rolstad, T. Midtvedt, P. Brandtzaeg, Microbial colonization influences composition and T-cell receptor V beta repertoire of intraepithelial lymphocytes in rat intestine. *Immunology* **89**, 494-501 (1996).
24. L. Wojciech *et al.*, Non-canonicaly recruited TCRalphabetaCD8alphaalpha IELs recognize microbial antigens. *Sci Rep* **8**, 10848 (2018).
25. A. Regnault, A. Cumano, P. Vassalli, D. Guy-Grand, P. Kourilsky, Oligoclonal repertoire of the CD8 alpha alpha and the CD8 alpha beta TCR-alpha/beta murine intestinal intraepithelial T lymphocytes: evidence for the random emergence of T cells. *J Exp Med* **180**, 1345-1358 (1994).
26. A. Regnault, P. Kourilsky, A. Cumano, The TCR-beta chain repertoire of gut-derived T lymphocytes. *Semin Immunol* **7**, 307-319 (1995).
27. A. Regnault *et al.*, The expansion and selection of T cell receptor alpha beta intestinal intraepithelial T cell clones. *Eur J Immunol* **26**, 914-921 (1996).
28. B. D. McDonald, J. J. Bunker, I. E. Ishizuka, B. Jabri, A. Bendelac, Elevated T cell receptor signaling identifies a thymic precursor to the TCRalphabeta(+)CD4(-)CD8beta(-) intraepithelial lymphocyte lineage. *Immunity* **41**, 219-229 (2014).
29. C. G. Chapman *et al.*, Characterization of T-cell Receptor Repertoire in Inflamed Tissues of Patients with Crohn's Disease Through Deep Sequencing. *Inflamm Bowel Dis* **22**, 1275-1285 (2016).
30. F. E. Dewhirst *et al.*, Phylogeny of the defined murine microbiota: altered Schaedler flora. *Appl Environ Microbiol* **65**, 3287-3292 (1999).
31. S. Rakoff-Nahoum, J. Paglino, F. Eslami-Varzaneh, S. Edberg, R. Medzhitov, Recognition of commensal microflora by toll-like receptors is required for intestinal homeostasis. *Cell* **118**, 229-241 (2004).
32. I. Lagkouvardos *et al.*, The Mouse Intestinal Bacterial Collection (miBC) provides host-specific insight into cultured diversity and functional potential of the gut microbiota. *Nat Microbiol* **1**, 16131 (2016).
33. J. M. Grondin, K. Tamura, G. Dejean, D. W. Abbott, H. Brumer, Polysaccharide Utilization Loci: Fueling Microbial Communities. *J Bacteriol* **199**, (2017).
34. X. Liu *et al.*, Alternate interactions define the binding of peptides to the MHC molecule IA(b). *Proc Natl Acad Sci U S A* **99**, 8820-8825 (2002).
35. A. G. Wexler, A. L. Goodman, An insider's perspective: Bacteroides as a window into the microbiome. *Nat Microbiol* **2**, 17026 (2017).
36. S. R. Eddy, Accelerated Profile HMM Searches. *PLoS Comput Biol* **7**, e1002195 (2011).
37. M. Poyet, A library of human gut bacterial isolates paired with longitudinal multiomics data enables mechanistic microbiome research. *In revision.* , (2019).
38. D. Esterhazy *et al.*, Compartmentalized gut lymph node drainage dictates adaptive immune responses. *Nature* **569**, 126-130 (2019).
39. F. Powrie, M. W. Leach, S. Mauze, L. B. Caddle, R. L. Coffman, Phenotypically distinct subsets of CD4+ T cells induce or protect from chronic intestinal inflammation in C. B-17 scid mice. *Int Immunol* **5**, 1461-1471 (1993).
40. K. Nutsch *et al.*, Rapid and Efficient Generation of Regulatory T Cells to Commensal Antigens in the Periphery. *Cell Rep* **17**, 206-220 (2016).
41. M. B. Geuking *et al.*, Intestinal bacterial colonization induces mutualistic regulatory T cell responses. *Immunity* **34**, 794-806 (2011).
42. B. S. Reis, D. P. Hoytema van Konijnenburg, S. I. Grivennikov, D. Mucida, Transcription factor T-bet regulates intraepithelial lymphocyte functional maturation. *Immunity* **41**, 244-256 (2014).
43. Y. Valdez *et al.*, Nramp1 drives an accelerated inflammatory response during Salmonella-induced colitis in mice. *Cell Microbiol* **11**, 351-362 (2009).

44. H. Maeda *et al.*, Quantitative real-time PCR using TaqMan and SYBR Green for Actinobacillus actinomycetemcomitans, Porphyromonas gingivalis, Prevotella intermedia, tetQ gene and total bacteria. *FEMS Immunol Med Microbiol* **39**, 81-86 (2003).
45. J. C. Gomes-Neto *et al.*, A real-time PCR assay for accurate quantification of the individual members of the Altered Schaedler Flora microbiota in gnotobiotic mice. *J Microbiol Methods* **135**, 52-62 (2017).
46. T. Matsuki *et al.*, Development of 16S rRNA-gene-targeted group-specific primers for the detection and identification of predominant bacteria in human feces. *Appl Environ Microbiol* **68**, 5445-5451 (2002).
47. J. Sidney *et al.*, Measurement of MHC/peptide interactions by gel filtration or monoclonal antibody capture. *Curr Protoc Immunol* **Chapter 18**, Unit 18 13 (2013).
48. Y. Cheng, W. H. Prusoff, Relationship between the inhibition constant (K1) and the concentration of inhibitor which causes 50 per cent inhibition (I50) of an enzymatic reaction. *Biochem Pharmacol* **22**, 3099-3108 (1973).
49. K. Gulukota, J. Sidney, A. Sette, C. DeLisi, Two complementary methods for predicting peptides binding major histocompatibility complex molecules. *J Mol Biol* **267**, 1258-1267 (1997).
50. M. D. Simon *et al.*, Rapid flow-based peptide synthesis. *Chembiochem* **15**, 713-720 (2014).
51. S. P. Preheim, A. R. Perrotta, A. M. Martin-Platero, A. Gupta, E. J. Alm, Distribution-based clustering: using ecology to refine the operational taxonomic unit. *Appl Environ Microbiol* **79**, 6593-6603 (2013).
52. R. C. Edgar, UPARSE: highly accurate OTU sequences from microbial amplicon reads. *Nat Methods* **10**, 996-998 (2013).
53. Q. Wang, G. M. Garrity, J. M. Tiedje, J. R. Cole, Naive Bayesian classifier for rapid assignment of rRNA sequences into the new bacterial taxonomy. *Appl Environ Microbiol* **73**, 5261-5267 (2007).

Chapter 4 - Induction of commensal-specific IgG1 by pTreg transnuclear T cells

The data presented in this chapter was collected and analyzed by myself, Angelina Bilate, Marianna Agudelo and Laura Fisch. This chapter shows preliminary data and will be prepared for publication after more experiments have been done.

Abstract

The gut epithelium must peacefully co-exist with trillions of microbes, the so-called commensal bacteria or microbiota. The immune response at mucosal surfaces is tightly balanced in order to tolerate the commensals, while eliminating pathogenic bacteria that may invade tissues and cause disease. Even though the intestine harbors a vast diversity of microbial antigens, only a few bacterial species have been shown to induce a cognate adaptive immune response in an otherwise unperturbed setting. Most studies focused on local/mucosal immunity but little is known about systemic commensal-specific responses. Healthy mice and humans harbor commensal-specific IgG1, an isotype strictly dependent on T-cell help, suggesting that commensals can induce systemic responses in the absence of overt signs of infection. In this chapter, I show that members of the microbiota induce an IgG1 response dependent on pTreg transnuclear T (TN) cells. Transfer of TN cells into a T-cell deficient host promotes entry of B cells into germinal centers, class switching and the secretion of commensal-specific IgG1. Because production of antigen-specific IgG1 by B cells requires that B and T cells recognize epitopes that are physically linked, we hypothesized that the TN-induced IgG1 might perhaps recognize a unique antigen, shared with the TN cells. In contrast, TN-induced IgG1s appear to be specific for multiple antigens. What is recognized by TN-induced IgG1 remains unknown.

Introduction

The intestinal mucosa harbors a dense community of microbes that digests polysaccharides indigestible by the host, synthesizes essential vitamins, stimulates maturation of the immune system, and constitutes an ecological niche that interferes with the growth of pathogenic species. In return, the host provides commensals with a habitat rich in energy derived from ingested food. Homeostasis at the gut mucosa is maintained by tightly regulated immune responses, which allow the host to peacefully co-exist with beneficial bacteria, while eliminating pathogenic bacteria that may penetrate tissues. Several mechanisms are in place that promote anatomical confinement of the commensals to the lumen, at some distance from the epithelium. Secretion of immunoglobulin A (IgA) that binds to intestinal commensals precludes microbial adhesion to and invasion of the gut epithelium (*1*). Coating of microbes with IgA can protect the host against toxins and pathogenic bacteria, but at the same time helps maintain a healthy and diverse gut microbiome (*2-4*).

Paradoxically, selective IgA deficiencies are fairly common in humans and are generally not associated with any deleterious phenotypes, intestinal or otherwise (5-7). To explain the absence of obvious pathology, it has been proposed that physical barriers, innate mechanisms, and secretion of IgM antibodies at mucosal surfaces can compensate for this deficiency (*8, 9*). Patients with X-linked hyper-IgM syndrome, deficient in IgG (but also in IgA) production, frequently suffer from severe intestinal damage (10), pointing to a role of IgG in mucosal immune responses. Recent work has suggested that in addition to IgA, anti-commensal IgGs can be induced in a T cell-dependent manner (*11, 12*). It is now clear that IgGs are present at mucosal surfaces and can mediate active humoral responses at this location (*13*). While IgG2b and IgG3 can be induced in a T-cell independent manner, the production of IgG1 is strictly dependent on T cells.

It has been postulated that immune responses to commensals are confined to the intestinal mucosa (*14*). Only those bacteria that penetrate the tissue and reach the mesenteric lymph nodes (MsLN) will promote T cell-dependent responses, including B cell class-switching to the IgG1 isotype in germinal centers (GCs). However, the MsLN of

specific pathogen free (SPF) mice contain abundant GCs, as well as numerous T follicular helper (Tfh) (which mediate B cell class switching) cells, indicating that some commensals can breach the local/systemic barrier. These so-called “spontaneous” GCs are absent from germ-free mice and are thought to contain B cells that recognize commensal bacteria and produce antibodies of the IgG1 isotype. As a result, healthy mice and individuals have low but measurable IgG titers, including IgG1 (9-11) in the absence of deliberate immunization. The presence of commensal-specific IgG1 is strictly dependent on T cell help and is most likely induced primarily in the MsLN, since Peyer’s patches (PP) contain negligible numbers of $IgG1^+$ cells (*12*). Little is known about the identity of the bacteria capable of inducing IgG1, their potential role in immune homeostasis, and their propensity to induce intestinal inflammation.

Although more than half of commensals seem to be coated by IgA in the small intestine, and to a lesser extent in the large intestine, a significant proportion of commensals do not bind IgA. Alternative mechanisms must exist to prevent them to penetrate the mucosa. Perhaps, there is a division of labor between IgA and IgG1 in which commensals not coated with IgA, when getting too close to the epithelium, elicit an IgG1 response. FACS-sorting of commensals coated with serum IgG1 showed that only a limited number of species were able to induce class switching to IgG1, including the mucin-degrading *Akkermansia muciniphila* and *Bacteroides spp.* (*12*). In this chapter we used the commensal-specific transnuclear (TN) model to identify commensals capable of inducing such IgG1 secretion. Transfer of TN cells into T-cell deficient host promotes class switching of B cells in a microbiota-dependent fashion. Because production of antigen-specific IgG1 by B cells requires that B and T cells recognize epitopes that are physically linked, we hypothesized that both the TN and B cell epitopes might be present on the same protein as the simplest explanation for this phenomenon. However, our data suggest, perhaps not unexpectedly, that TN-induced IgG1s recognize multiple proteins.

Results

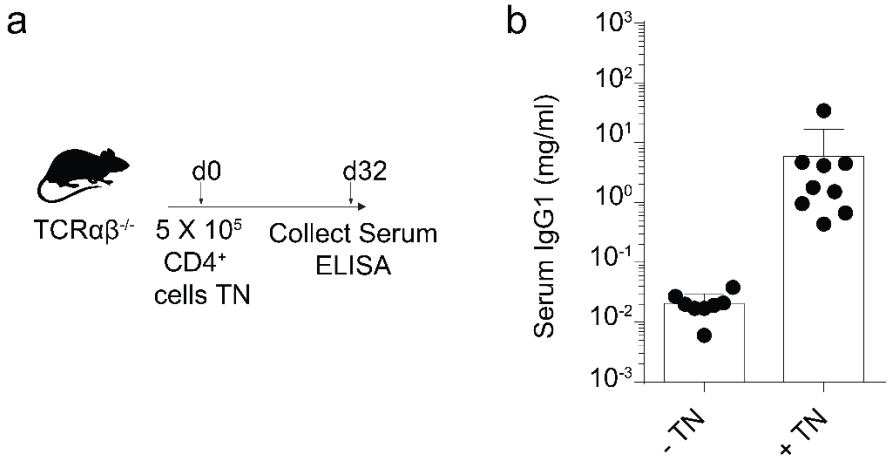

Figure 4.1 Transfer of TN cells into TCRαβ$^{-/-}$ mice promotes IgG1 class switching

(**a**) Experimental setup. TCRαβ$^{-/-}$ received 5*10^5 naïve CD4$^+$CD8α$^-$Foxp3$^-$ TN T cells and after 32 days, the serum was collected and the level of IgG1 was measured by ELISA. (**b**) The graph shows all mice analyzed in the experiment described in (a).

To identify commensals that induce systemic immune responses, we used the TN mouse model in which all CD4$^+$ T cells carry a T cell receptor (TCR) that recognizes commensal bacteria (*15*). CD4$^+$ T cells from the TN mouse line, when transferred into T-cell-deficient (TCRαβ$^{-/-}$) recipients (referred to as TN-recipient mice), can differentiate into peripheral regulatory T cells (pTreg) or CD4CD8αα double-positive intraepithelial cells (CD4$_{IEL}$) in the small intestine (see chapter 2). We reasoned that if the TN cells recognized a commensal capable of inducing systemic responses, they might also differentiate into T follicular helper (Tfh) cells and promote class-switching to IgG1. To test this hypothesis, we transferred 5 x 10^5 naïve TN cells into TCRαβ$^{-/-}$ mice and assessed the serum levels of IgG1 one month later. Elevated concentrations of serum IgG1 showed that TN cells can induce class-switching to IgG1 in B cells (Fig. 4.1). Remarkably, the levels of serum IgG1 in TN-transferred were ~5-20x higher than the typical levels observed for healthy WT C57BL/6 mice (*16*). The higher IgG1 levels in TN-recipient mice could be the result of increased intestinal permeability and bacterial translocation in mice that lack αβT cells, essential for maintaining a robust intestinal barrier. This is in line with the increased commensal-specific IgG1 levels observed in older mice and in patients with Crohn's disease (*12, 17-19*).

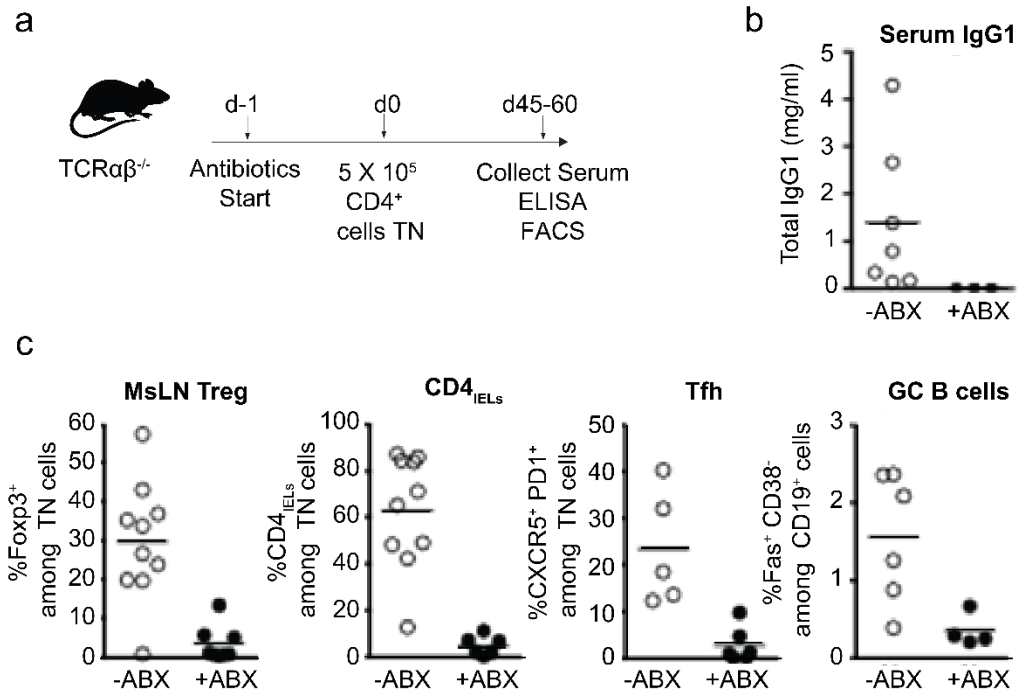

Figure 4.2 Depletion of microbiota abrogates expansion and differentiation of TN cells, and abolishes IgG1 response.

(**a**) Experimental design. TCRαβ$^{-/-}$ mice received 5 * 10^5 naïve CD4$^+$CD8α$^-$Foxp3$^-$ TN T cells with or without antibiotic treatment (Abx) to eliminate the microbiota (ampicillin 1g/l, neomycin 1g/l, metronidazole 1g/l, vancomycin 0.5g/l in the drinking water). (**b**) Serum levels of IgG1 were determined by ELISA. (**c**) The differentiation of the TN T cells into $CD4_{IELs}$, Tregs, T follicular helper cells (Tfh), and induction of germinal centers (GC) B cells was analyzed by FACS. The graphs show all mice analyzed in 3 independent experiments.

To confirm that the microbiota was responsible for activation of TN cells and ensuing IgG1 secretion, we treated the TCRαβ$^{-/-}$ recipients with broad-spectrum antibiotics and assessed whether TN cells still promoted IgG1 secretion. Treatment of TN-recipient mice with a cocktail of antibiotics that eliminates the microbiota prevented class-switching to IgG1 (Fig. 4.2a,b). Upon transfer of the TN cells they expanded and differentiated into Tfh cells in the MsLN and triggered B cells to enter the germinal center (GC) reaction. Both GC and IgG1 require T cell help and are therefore absent from TCRαβ$^{-/-}$ mice that did not receive TN T cells (Fig 4.1) or antibiotic-treated TN-recipient mice (Fig. 4.2).

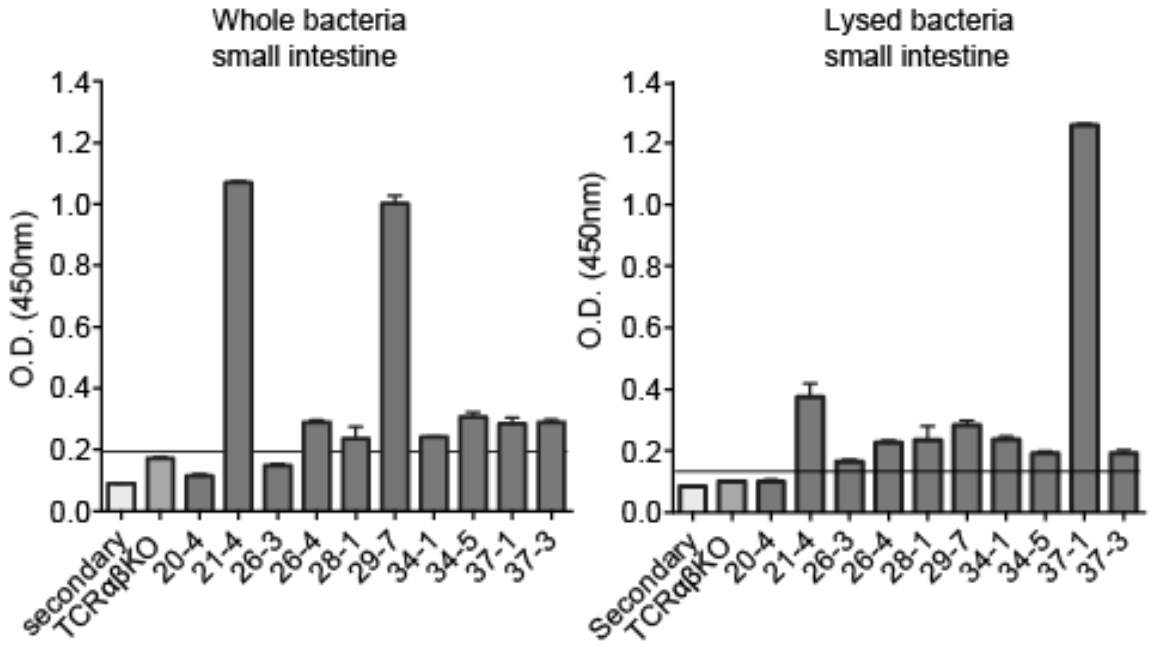

Figure 4.3 The serum of TCRαβ$^{-/-}$ mice that received TN T cells binds to commensal bacteria.

Serum from TCRαβ$^{-/-}$ mice that received TN cells as in Fig.4.2 were tested by commensal-specific ELISA. Plates were coated with whole (Left) or lysed bacteria (Right) isolated from the small intestines of RAGKO mice overnight at 4ºC. Sera were added to the plates at 2.4µg/ml of total IgG1 for 1h. Anti-IgG1 HRP was used to detect binding. Shown is the optical density (O.D.) of each serum. Horizontal line shows the cut-off used based on the O.D. of serum from TCRαβKO mice that did not receive TN T cells.

Because class-switching to IgG1 requires cognate T-cell help, the IgG1s elicited by adoptive transfer (which must have been induced by TN T cells) are likely to bear the same antigen specificity as that of the TN T cells. Accordingly, serum IgG1 from TN-recipient mice binds to commensal bacteria isolated from the small intestine of RAG-deficient mice housed in a SPF facility (Fig. 4.3). We hoped to leverage this information to identify which bacteria are recognized by the TCR of the TN T cells. Of note, not all serum-derived IgG1s bind to the same extent to commensals. While some sera react strongly with intact bacteria, others bind more tightly to bacterial lysates (for example serum derived from mouse 37-1). The reasons for these discrepancies are unclear (see discussion).

To confirm the ELISA data and identify the bacterial species recognized by TN-recipient IgG1, we developed a strategy to sort IgG1-coated bacteria (Fig. 4.4a). We incubated the

serum from a pool of TN-recipient hosts with bacteria extracted from the feces or small intestine (SI) of RagKO mice. Because RagKO mice lack B cells, the use of these mice as a source of commensals ensures the absence of any antibodies in the samples to be tested. To differentiate commensals from small debris and noise, we stained bacteria with the DNA dye, SYTO9, which binds to both live gram-negative and -positive bacteria (*20*). We observed a different pattern of staining with SYTO9 when commensals were derived from the SI or the feces, possibly reflecting differences in bacterial composition (Fig. 4.4b). In the SI, there were two distinct populations of bacteria, referred as Syto9^{high} and Syto9^{low}, while fecal bacteria were stained in more homogeneously. These differences in staining might reflect variations in membrane permeability, for example between gram-positive and negative bacteria, exponentially growing versus stationary phase bacteria or distinct DNA/RNA content (*20*)(22).

Staining with an isotype control antibody yielded little if any staining. In contrast, the IgG1 in TN-recipients stained a small but defined population of SYTO9^{high} bacteria from both the SI and feces. In line with published data, we found that the IgG1 present in the serum of WT mice also recognized commensals. Identification of the bacteria coated with TN-transferred IgG1 remains to be pursued.

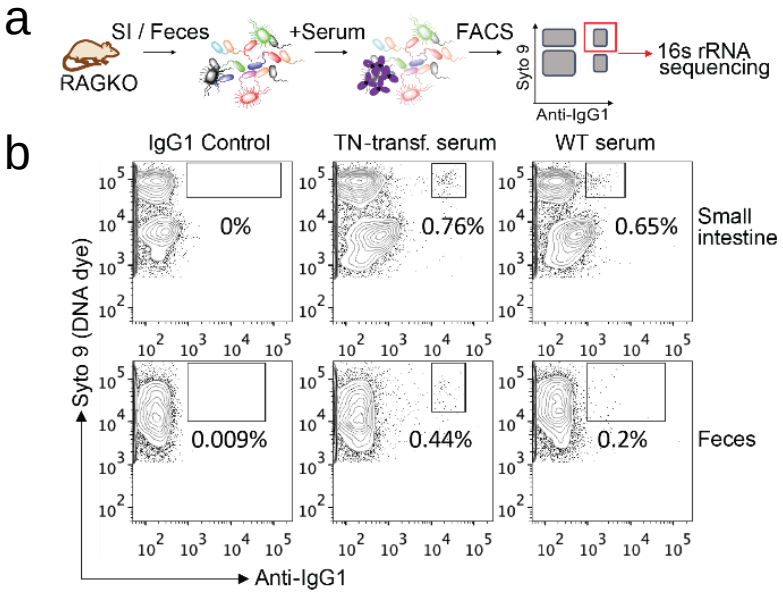

Figure 4.4 Strategy for sorting and sequencing of IgG1-coated bacteria.

(**a**) Scheme used for sorting of IgG1-coated bacteria. (**b**) Small intestine or fecal bacteria were isolated from RAGKO mice and incubated with the indicated serum at 2.4µg/ml of total IgG1. IgG1 control, monoclonal IgG1 against mycotoxin. IgG1-coated bacteria were analyzed by FACS after labeling with anti-IgG1 and DNA-binding dye SYTO9 that stains Gram+ and Gram- bacteria. Dot-plots are representative of 3 independent experiments.

In agreement with the ELISA data, we found that not all TN-recipient mice produced IgG1 equally capable to stain whole bacteria by FACS (Fig. 4.5).

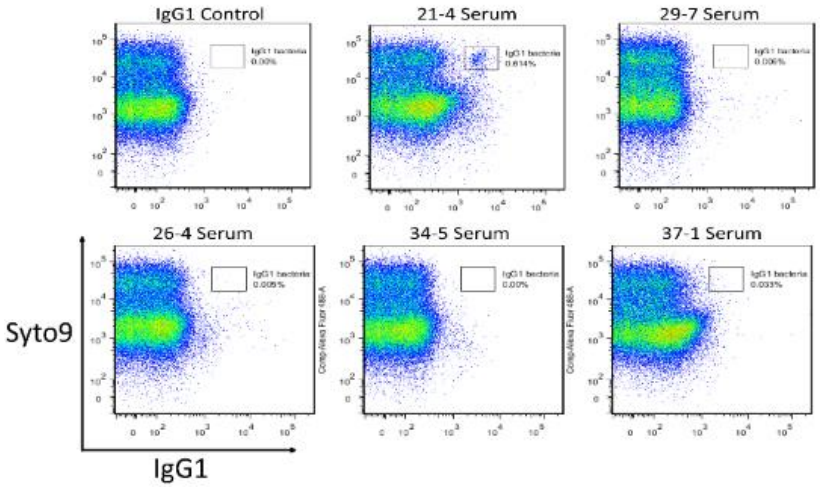

Figure 4.5 Serum IgG1 from TN-recipient mice does not always bind to commensal bacteria.

IgG1 FACS plots of bacteria extracted from RAGKO feces and submitted to staining with the serum of different TCRαβKO mice that received TN T cells as described in Fig. 4.4.

Discussion

In this chapter, I presented the role of commensal-specific TN cells in IgG1 induction. While the data reported here are preliminary, they uncover an interesting phenotype, which deserves more scrutiny. With a few notable examples, there are few studies that combine the reactivity of both T and B cells to commensals in the absence of deliberate immunization (*12, 21*). Much attention has been paid to IgA, the most abundant antibody isotype at mucosal surfaces. However, recent work has suggested that anti-commensal IgGs, including IgG1, IgG2b and IgG3, can be induced in a T cell-dependent manner (*11, 12*). In contrast to IgG2b, IgG3 and IgA, IgG1 is strictly dependent on T cell help. The lack of intestinal pathology associated with selective IgA deficiencies and the frequent

intestinal damage observed in hyper-IgM syndrome both point to a role of IgG in maintenance of intestinal homeostasis (*5-7, 10*).

Here we showed that TN cells transferred into a T-cell deficient host induces MsLN B cells to enter germinal centers and class-switch to IgG1. IgG1 in TN-recipients binds to commensals, as shown by both ELISA and flow cytometry analyses. Not all sera are equally capable of binding commensals, though the only T cells present in recipient mice have a unique TCR. In addition, some sera preferentially bind to intact bacteria, while others bind more strongly to bacterial lysates. These unexpected differences in binding affinities and specificities suggest that the TN cells can provide help to B cells, which recognize distinct antigens (Fig. 4.6). Indeed, production of antigen-specific IgG1 by B cells requires that B and T cells recognize epitopes that are physically linked (*22-24*). The presence of IgG1 of diverse specificities could therefore be explained if β-hex was physically associated with multiple proteins or macromolecular aggregates, some of which recognized by B cells. For example, B cells could recognize surface antigens on whole bacteria or OMVs containing β-hex (Fig. 6a). Alternatively, the TN cells might recognize more than a single antigen and provide help to B cells of different specificities. It will be important to identify the antigens recognized by TN-induced IgG1 and the diversity of IgG1 BCR in TN-transferred mice (Fig. 4.6b).

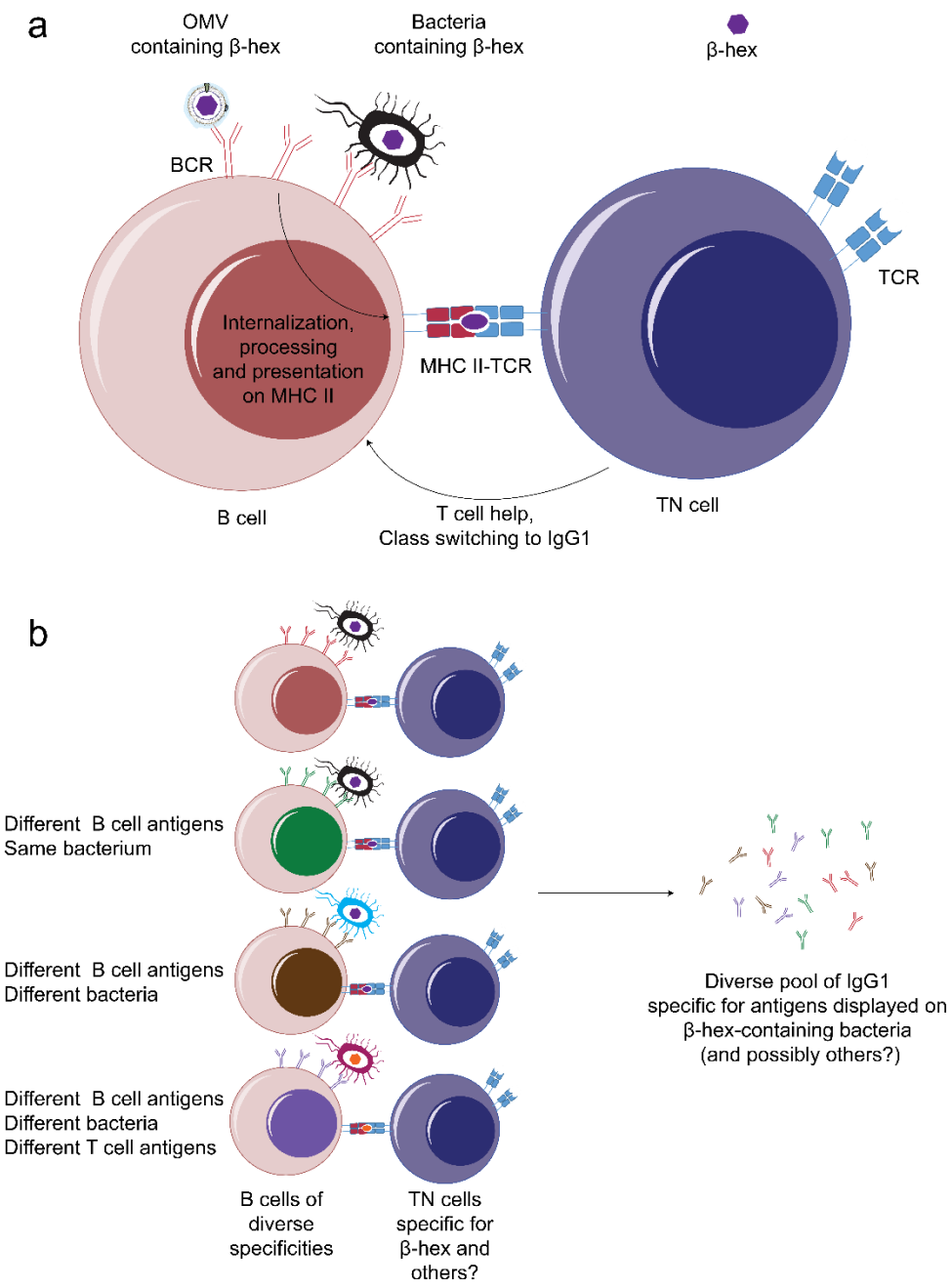

Figure 4.6 Models to explain diverse TN-induced IgG1 responses

(**a**) Class switching of B cells to IgG requires the physical link between the T and B cell epitopes. The supposed multiple specificities displayed by TN-induced IgG1 suggests that TN cells get activated by B cells which recognize distinct protein antigens. This is conceivable if the B cells recognized an antigen on the surface of bacteria or outer membrane vesicles (OMVs) containing β-hex, the TN antigen. Alternatively, TN cells could recognize other commensal-derived antigens in addition to β-hex. Panel (**b**) shows different scenarios which could explain the phenotype described in this chapter.

Materials and methods

Mice

Mice were housed at the Whitehead Institute for Biomedical Research (WIBR) and the Boston Children's hospital (BCH) under specific pathogen–free conditions, in accordance with institutional guidelines and approved by the institutional animal care and use committee of the Massachusetts Institute of Technology and the Boston Children's Hospital (IACUC protocol number 16-12-3328). pTreg TN mice were generated as described (*25*). C57BL/6, Rag1−/−, TCRα−/−, TCRβ−/−, mice were purchased from Taconic Biosciences and Jackson Laboratory and maintained at our facilities. pTreg TN were crossed to C57BL/6 RAG1KO for at least eight generations to generate pTreg TNxRAGKO (TN). TCRαβKO ($TCR\alpha^{-/-}\beta^{-/-}$) were generated by intercrossing $TCR\alpha^{-/-}$ and $TCR\beta^{-/-}$.

Antibodies, reagents, and FACS analysis

Fluorescently labeled antibodies were purchased from BD bioscience (anti-Vβ6, RR4-7; anti-CD3, 145-2C11; CXCR5, 2G8), eBioscience (anti-Foxp3, FJK-16s; anti-CD4, RM4-5; Va2, B20.1; anti-CD11c, N418). BioLegend (anti-CD45.2, 104; anti-CD8α, 53-6.7; anti-CD8β, YTS 156.7.7; anti–I-A/I-E, M5/114.15.2, α-CD3, 145-2C11). The cell viability dye 7-AAD (Via-Probe) and Live/dead fixable Aqua fluorescent reactive dye were purchased from BD Biosciences and ThermoFisher, respectively. Staining with live/dead markers was performed following manufacturer's instructions. Staining for cell surface markers was performed at 4°C for 30min in PBS+1mM EDTA+ 0.5% bovine serum albumin. Intracellular staining was performed according to manufacturer's instructions, using the Foxp3/Transcription Factor Staining Buffer Set (eBioscience). Flow cytometry data were acquired on an LSRFortessa (Becton Dickinson) instrument and analyzed with the FlowJo software package (Tri-Star).

Purification of Naïve CD4$^+$ T cells and adoptive transfer

Naïve CD4$^+$ T cells were isolated from spleen and mesenteric lymph nodes using the naïve CD4 T cells isolation kit (Miltenyi, Germany). Purity was always >98%. For adoptive transfer, six-week-old TCRαβKO mice were injected i.v. with 5 X 10^5 naïve CD4$^+$ T cells in PBS.

Isolation of mononuclear cells from intestine

Small intestines were harvested and mononuclear cells were isolated from the IE compartment and lamina propria as described (*25*),(*26*).

Antibiotic treatment

An antibiotic cocktail containing Vancomycin (0.5 g/liter), ampicillin (1.0 g/liter), neomycin (1.0 g/liter) (Amresco), and metronidazole (1.0 g/liter) (Sigma) was given ad libitum in the drinking water (*27*) for the indicated periods as described in the figure legends.

Labelling of commensals with serum IgG1

The small intestine content of a Rag1KO mouse was harvested by flushing the inside with a total of 3ml of PBS. The content was then spun down at 700g for 5min at 4°C to remove debris. The supernatant was pelleted at 12,000g for 5min at 4°C and resuspended into 2ml of PBS. 50µl of bacteria were then blocked in PBS containing 13% of RagKO serum for 45min at 4°C. The bacteria were then washed with PBS and incubated with serum at a concentration of 2.4µg/ml of IgG1 for 2h at 4°C. As a negative control, the bacteria were stained with an isotype control (Southern biotech, Mouse IgG1 α-T2 mycotoxin, clone 15H6). After 2 washes with PBS, the bacteria were stained with 2µg/ml of α-IgG1-PE for 40min at 4°C. Subsequently, the bacteria were stained with Syto9 for 15min at RT, according to manufacturer protocols (LIVE/DEAD™ BacLight™ Bacterial Viability and Counting Kit, for flow cytometry, ThermoFisher). The bacteria were then washed with PBS and ran on a LSRFortessa (Becton Dickinson) instrument and analyzed with the FlowJo software package (Tri-Star).

ELISA

For serum ELISA, serum was collected from age-matched mice. 96-well high-binding plates (Costar) were coated with 1µg/ml of anti-Ig (Southern Biotech) in PBS overnight at 4°C, rinsed 3x with PBS-T (0.05%Tween-20 in PBS) and blocked in 10% FBS in PBS for 1h at RT. Sera were incubated neat and in 10-fold dilutions for 2h in 10% FBS in PBS. The plates were rinsed 5x and incubated with HRP-coupled secondary antibody recognizing IgG1(1:1,000) for 1h. After rinsing, the plates were developed using OptEIA TMB substrate reagent kit (BD), and the reaction was stopped with 1M hydrochloric acid and the absorbance read at 450-nm. For bacterial ELISA, high-binding plates were pre-coated with poly-L-lysine for 15min, rinsed in PBS and coated overnight with whole bacteria derived from the small intestine or feces (2-5 pellets) as described above or elsewhere (see chapter 3). Plates were coated with either 50µl of 4µg/ml of lysed bacteria or 50µl of bacteria (OD=0.2) in PBS. The plates were then blocked in 2% BSA, 0,5% Tween-20 at RT for 2h. The plates were rinsed and incubated with serum containing 2.4µg/ml of IgG1 for 1h at RT. After washing, the plates were incubated with secondary antibody (α-IgG1, Southern biotech) for 1h at RT. After the final washes, the plates were developed using OptEIA TMB substrate reagent kit (BD), and the reaction was stopped with 1M hydrochloric acid and plate read at 450-nm absorbance.

References

1. O. Pabst, New concepts in the generation and functions of IgA. *Nat Rev Immunol* **12**, 821-832 (2012).
2. N. W. Palm *et al.*, Immunoglobulin A coating identifies colitogenic bacteria in inflammatory bowel disease. *Cell* **158**, 1000-1010 (2014).
3. S. Kawamoto *et al.*, Foxp3(+) T cells regulate immunoglobulin a selection and facilitate diversification of bacterial species responsible for immune homeostasis. *Immunity* **41**, 152-165 (2014).
4. A. J. Macpherson, K. D. McCoy, F. E. Johansen, P. Brandtzaeg, The immune geography of IgA induction and function. *Mucosal Immunol* **1**, 11-22 (2008).
5. J. Fadlallah *et al.*, Microbial ecology perturbation in human IgA deficiency. *Sci Transl Med* **10**, (2018).
6. L. Yel, Selective IgA deficiency. *J Clin Immunol* **30**, 10-16 (2010).
7. N. Wang, L. Hammarstrom, IgA deficiency: what is new? *Curr Opin Allergy Clin Immunol* **12**, 602-608 (2012).
8. L. Mellander, J. Bjorkander, B. Carlsson, L. A. Hanson, Secretory antibodies in IgA-deficient and immunosuppressed individuals. *J Clin Immunol* **6**, 284-291 (1986).
9. P. Brandtzaeg *et al.*, The clinical condition of IgA-deficient patients is related to the proportion of IgD- and IgM-producing cells in their nasal mucosa. *Clin Exp Immunol* **67**, 626-636 (1987).
10. R. S. Geha *et al.*, Primary immunodeficiency diseases: an update from the International Union of Immunological Societies Primary Immunodeficiency Diseases Classification Committee. *J Allergy Clin Immunol* **120**, 776-794 (2007).
11. M. A. Koch *et al.*, Maternal IgG and IgA Antibodies Dampen Mucosal T Helper Cell Responses in Early Life. *Cell* **165**, 827-841 (2016).
12. E. Ansaldo *et al.*, Akkermansia muciniphila induces intestinal adaptive immune responses during homeostasis. *Science* **364**, 1179-1184 (2019).
13. R. E. Horton, G. Vidarsson, Antibodies and their receptors: different potential roles in mucosal defense. *Front Immunol* **4**, 200 (2013).
14. A. J. Macpherson, T. Uhr, Compartmentalization of the mucosal immune responses to commensal intestinal bacteria. *Ann N Y Acad Sci* **1029**, 36-43 (2004).
15. D. B. A. M. Bilate, L. Mesin, M. Agudelo, J. Leube, A. Kratzert, S. K. Dougan, G. D. Victora, H. L. Ploegh, Tissue-specific emergence of regulatory and intraepithelial T cells from a clonal T cell precursor. *Science Immunology*, (2016).
16. A. S. Klein-Schneegans, L. Kuntz, P. Fonteneau, F. Loor, Serum concentrations of IgM, IgG1, IgG2b, IgG3 and IgA in C57BL/6 mice and their congenics at the lpr (lymphoproliferation) locus. *J Autoimmun* **2**, 869-875 (1989).
17. J. Benckert *et al.*, The majority of intestinal IgA+ and IgG+ plasmablasts in the human gut are antigen-specific. *J Clin Invest* **121**, 1946-1955 (2011).
18. H. J. Harmsen, S. D. Pouwels, A. Funke, N. A. Bos, G. Dijkstra, Crohn's disease patients have more IgG-binding fecal bacteria than controls. *Clin Vaccine Immunol* **19**, 515-521 (2012).
19. M. Y. Zeng *et al.*, Gut Microbiota-Induced Immunoglobulin G Controls Systemic Infection by Symbiotic Bacteria and Pathogens. *Immunity* **44**, 647-658 (2016).
20. P. Lebaron, N. Parthuisot, P. Catala, Comparison of blue nucleic acid dyes for flow cytometric enumeration of bacteria in aquatic systems. *Appl Environ Microbiol* **64**, 1725-1730 (1998).
21. E. V. Russler-Germain, S. Rengarajan, C. S. Hsieh, Antigen-specific regulatory T-cell responses to intestinal microbiota. *Mucosal Immunol* **10**, 1375-1386 (2017).

22. S. Britton, N. A. Mitchison, K. Rajewsky, The carrier effect in the secondary response to hapten-protein conjugates. IV. Uptake of antigen in vitro and failure to obtain cooperative induction in vitro. *Eur J Immunol* **1**, 65-68 (1971).
23. N. A. Mitchison, T-cell-B-cell cooperation. *Nat Rev Immunol* **4**, 308-312 (2004).
24. H. L. Ploegh, Bridging B cell and T cell recognition of antigen. *J Immunol* **179**, 7193 (2007).
25. A. M. Bilate *et al.*, Tissue-specific emergence of regulatory and intraepithelial T cells from a clonal T cell precursor. *Sci Immunol* **1**, eaaf7471 (2016).
26. Y. Valdez *et al.*, Nramp1 drives an accelerated inflammatory response during Salmonella-induced colitis in mice. *Cell Microbiol* **11**, 351-362 (2009).
27. S. Rakoff-Nahoum, J. Paglino, F. Eslami-Varzaneh, S. Edberg, R. Medzhitov, Recognition of commensal microflora by toll-like receptors is required for intestinal homeostasis. *Cell* **118**, 229-241 (2004).

Chapter 5 - Engineering *Bacteroides* Outer Membrane Vesicles for immune modulation

The experiments presented here (targeting of antigens to OMVs) are the results of a collaboration between Mark Mimee and myself with support from Logan Jerger, Jasper van der Peet, Juliane Ripka in the labs of Tim Lu and Hidde Ploegh. Mark Mimee developed the OMV targeting tag in collaboration with Logan Jerger and Juliane Ripka. Mark Mimee and I collaborated to study the response of antigen-specific $CD4^+$ T cells to antigens presented on OMVs. For the purpose of this thesis, I focus on my own contributions and summarize the data gathered by my collaborators required to understand this work. I refer the readers to the thesis of Mark Mimee for additional information (*1*).

Abstract

The intestine is colonized by a dense population of microbes collectively known as the microbiota. These microbes have evolved sophisticated strategies to communicate with their host and maintain homeostasis. Outer membrane vesicles (OMVs) are small membranous structures secreted by commensals that can reach immune cells through the intestinal epithelium and modulate immunity. We hypothesized that we could exploit the anti-inflammatory nature of *Bacteroides* OMVs to promote antigen-specific tolerogenic responses in the intestine. Using a combination of proteomics and bioinformatics, we identified proteins targeted to *Bacteroides* OMVs. We used this information to define *Bacteroides* Vesicle Incorporation Tags (BVITs) and create genetic fusions to target passenger proteins to OMVs. Both fusions to full size OMV proteins and smaller truncations efficiently targeted proteins to OMVs of multiple *Bacteroides spp*.. Next, we used BVITs to incorporate model antigens and evaluate how *Bacteroides* OMVs impact antigen presentation as well as $CD4^+$ T cell activation. Antigen-loaded OMVs were processed correctly and presented to antigen-specific $CD4^+$ T cells, both *in vitro* and *in vivo*. We have thus developed a strategy to package heterologous cargo into *Bacteroides* OMVs to manipulate adaptive immune responses.

Introduction

The intestinal immune system faces the daunting task of maintaining homeostasis despite the enormous load and diversity of antigens, microbial as well as food-derived, present at this site. Tolerance to dietary and commensal-derived antigens, while maintaining the ability to eliminate pathogens, requires tight regulation. Failure to maintain this balance has dramatic consequences and can cause food allergies, inflammatory bowel disease or invasive infections (*2*). The dense community of microbes that inhabit the intestine has evolved sophisticated strategies to communicate with both the host and other microbes to maintain homeostasis. Secretion of outer membrane vesicles (OMVs) is one of the means used by commensals to influence the immune system (*3 , 4*).

Outer membrane vesicles (OMVs) are spherical structures of 20-250nM in diameter released by Gram-negative bacteria (*5, 6*). OMVs are liberated under normal growth conditions both *in vitro* and *in vivo*. In the gastrointestinal tract, the intestinal milieu and the mucus layer stimulate release of OMVs by gram-negative bacteria (*7*). OMVs contain material derived from the outer membrane and the periplasm, including DNA, RNA, lipopolysaccharide (LPS), phospholipids, proteins, enzymes and peptidoglycan (Fig 5.1). Their small size, their capacity to reach distant locations (i.e lamina propria) and the ease with which host cells can engulf them, enable OMVs to communicate with the host (*8*). Unlike bacterial pathogens, commensals do not usually interact intimately with host cells (with the exception of segmented filamentous bacteria, SFB, and some *Helicobacter spp.*, (*9, 10*)) and therefore release of OMVs is a mechanism of delivering cargo to locations inaccessible to intact bacterial cells (*8*). In *B. fragilis*, polysaccharide A contained in OMVs promotes the development of Tregs and protects against colitis (*8, 11*). OMVs produced by *B. thetaiotaomicron* can be found in macrophages of the lamina propria. This requires the action of sulfatase to help degrade host mucus (*12*).

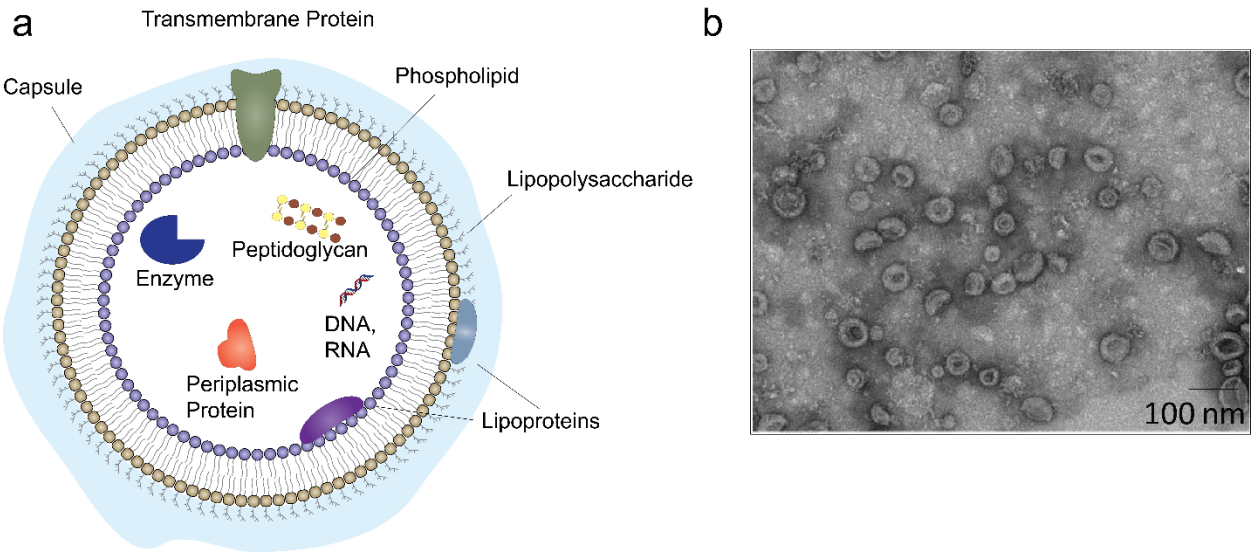

Figure 5.1 Outer membrane vesicles.

(a) Schematic of outer membrane vesicles. (b) Transmission electron micrograph of outer membrane vesicles isolated from *B. thetaiotaomicron*. The figure is adapted from (*1*).

The response of commensal-specific T cells in the intestine is highly context-dependent. Flagellin-specific T cells remain mostly naïve under normal conditions but differentiate into Th1 and Th17 cells when the intestinal barrier loses its integrity (*13, 14*). Expression of SFB antigen on *L. monocytogenes* reprograms the differentiation of antigen-specific T cells from Th17 to Th1 instead. Antigen-specific T cells responses triggered by OMVs are less well defined (*8, 11, 12*). A transgenic T cell line specific for a *B. thetaiotaomicron* OMV antigen provides an interesting model to study these interactions, but suffers from the lack of reagents specific for OMVs (*15*). Despite the presence of the *B. thetaiotaomicron* antigen in OMVs produced *in vitro*, it is unclear whether the antigen is presented to T cells via OMVs *in vivo*. We need new tools to specifically target antigens to OMVs to distinguish responses elicited by OMVs in comparison with intact bacteria.

Here, we describe a strategy to specifically target heterologous protein antigens to OMVs produced by commensals. We chose to focus on *Bacteroides,* as this genus is prominent and highly adapted to the mammalian gut (*16, 17*). In addition, *Bacteroides* species are

important immune modulators in the intestine where they promote anti-inflammatory responses via induction of Tregs (*12, 18-22*). Therefore, targeting antigens to *Bacteroides* OMVs could be a useful means of inducing tolerance and anti-inflammatory responses.

Results

To design a sequence that allows targeting of a heterologous antigen to OMVs, we first identified proteins present in OMVs of *Bacteroides*. Proteomics showed an enrichment of SPII-type lipoproteins in OMVs. A comparison of OMV lipoproteins with intracellular lipoproteins (lipoproteins not identified in OMVs by mass spectrometry) uncovered no immediately identifiable sequence that could be used to target proteins to OMVs (*1*). As an alternative, we used fusions to natural OMV-targeted proteins as anchors. Expression of C-terminal fusions of NanoLuc luciferase to full-length OMV proteins in *B. thetaiotaomicron* led to their enrichment in OMVs, unlike their untagged counterparts (Fig 5.2). Indeed, only fusion proteins were detected by western blot.

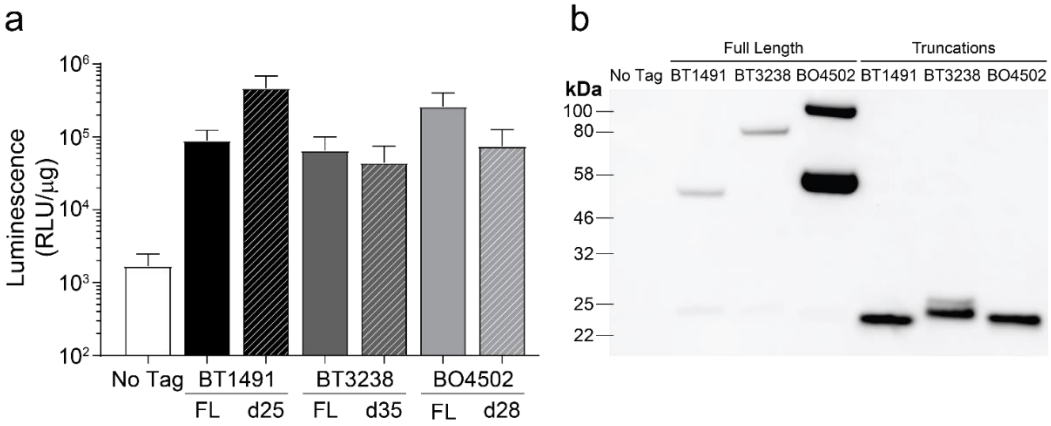

Figure 5.2 Bacteroides Vesicle Incorporation Tag (BVIT) fusion targets proteins to OMVs.

(**a**) Luminescence activity of full length (FL) or truncated lipoprotein OMV anchor fusions to NanoLuc was measured in OMVs purified from *B. thetaiotaomicron*. Luminescence values were normalized to total protein content of OMVs. (**b**) Western blot of *B. thetaiotaomicron* purified OMVs containing full length (FL) or truncated lipoprotein fusions to NanoLuc. 4 µg of purified OMVs were separated by gel electrophoresis and probed with an anti-His serum. Predicted MW: BT1491d25 (21.1kDa); BT3238d35 (22.2 kDa); BO4502d28 (21.5 kDa). Error bars represent standard deviation of three independent biological replicates (n=3). Luminescence activity was normalized to the total protein content of OMVs. The blot shown is representative of three independent experiments. Figure adapted from (*1*).

While fusions to full-length native proteins are sufficient to target heterologous proteins to OMVs, overexpression of a functional protein may negatively affect bacterial fitness and health of the host. We therefore truncated the native proteins to identify a minimal *Bacteroides* Vesicle Incorporation Tag (BVIT) capable of targeting proteins to OMVs. Heterologous expression of luciferase tagged with the minimal sequence yielded equivalent or higher luminescence in OMVs than fusion to full length proteins (Fig 5.2). Fusions to tags derived from BT1491, BT3238 and BO4502 target proteins to the surface of OMVs rather than to the lumen, as shown by proteinase K digestion (*1*). Importantly, BVITs derived from *B. thetaiotaomicron*, *B. fragilis* and *B. ovatus* can target proteins to OMVs not only in *B. thetaiotaomicron* but also in *B. fragilis* and *B. vulgatus* (Fig 5.3). Lipoprotein signal sequences are therefore an efficient means of directing proteins to OMVs across the *Bacteroides* genus, regardless of the species of origin of the tag.

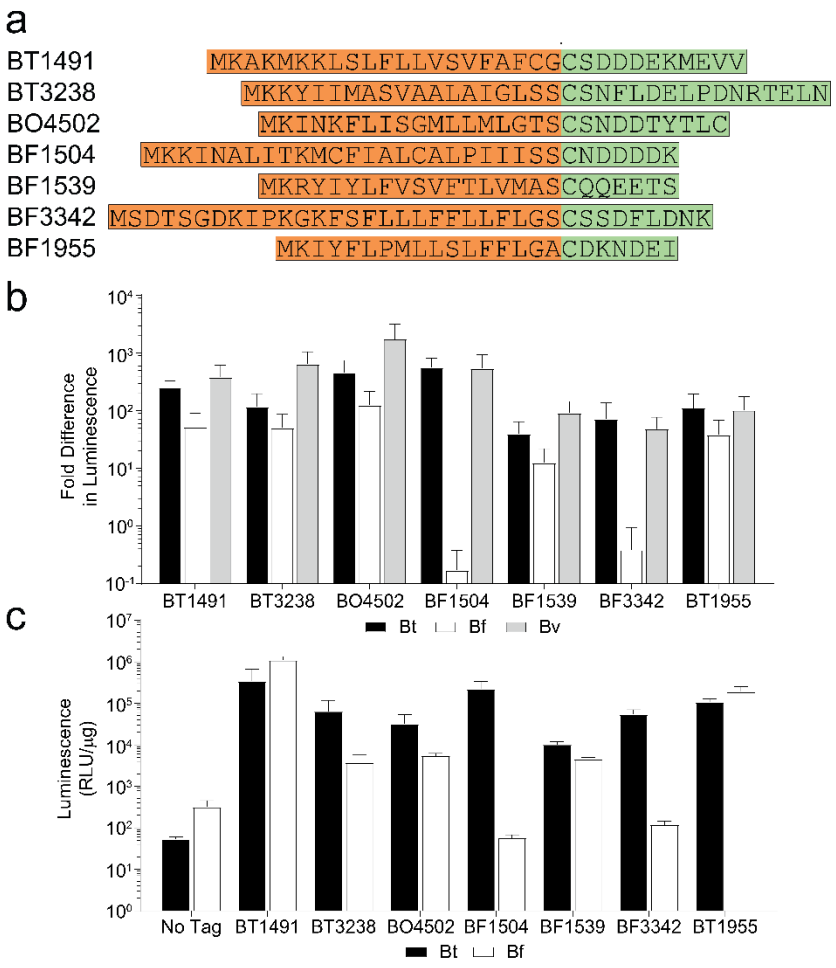

Figure 5.3 BVIT Design Rules Are Applicable to Lipoproteins Across the *Bacteroides* genus.

(**a**) Primary sequences of BVITs derived from *B. thetaiotaomicron*, *B. ovatus* or *B. fragilis* lipoproteins. Arrow indicates SpII cleavage site. (**b**) Fold change in luminescence in BVIT-tagged NanoLuc as compared to a nontagged control in culture supernatants of *B. thetaiotaomicron* (Bt), *B. fragilis* (Bf), and *B. vulgatus* (Bv). (**c**) Luminescence activity in OMVs purified from Bt or Bf expressing NanoLuc fused to various BVITs. Luminescence values were normalized to OMV total protein content. Error bars represent standard deviation of three independent biological replicates (n=3). Figure adapted from (*1*).

To study T cell activation elicited by presentation of OMV-derived antigens, we used two model systems of monoclonal $CD4^+$ T cells, ovalbumin (OVA)-specific OTII cells and β-hex-specific transnuclear (TN) cells. Since the TN cells recognize an antigen expressed by some *Parabacteroides* spp. and *Bacteroides* spp., we first tested whether β-hex is present in OMV. OMVs derived from *P. goldsteinii*, did not induce proliferation of the TN

cells *in vitro* when co-cultured with dendritic cells, suggesting that β-hex is absent from OMVs isolated from this bacterium (Fig 5.4), or -if present- in a form not presentable to T cells.

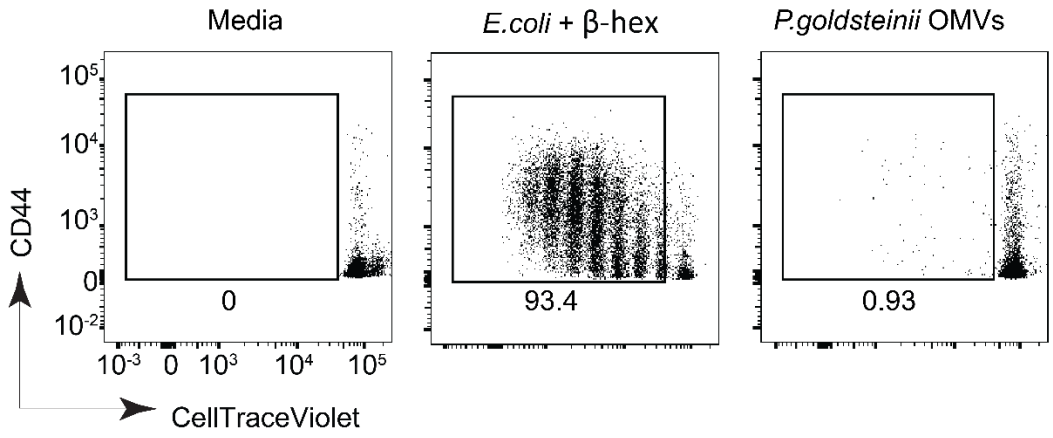

Figure 5.4 *P. goldsteinii* OMVs do not activate TN cells *in vitro*.

Naïve $CD4^+$ TN T cells were labeled with CellTrace Violet and co-cultured with dendritic cells (DCs) purified from B16-Flt3L-injected mice in the presence of 25µg of bacterial extracts derived from *E. coli* overexpressing β-hex or OMVs isolated from *P. goldsteinii* grown *in vitro*. After 3.5 days, CellTrace Violet dilution was assessed by flow cytometry. Dot plots are representative of at least 3 experiments. Cells were gated on $Aqua^-CD4^+V\alpha2^+V\beta6^+$.

Proteins homologous to β-hex from *B. thetaiotaomicron* (BT_0456) and *B. fragilis* (BF1730) were likewise absent from OMVs of these bacteria (*1, 3*). In addition, β-hex is predicted to contain a Sec targeting sequence cleaved by Signal peptidase I (SpI) but no lipoprotein targeting signal (SignalP 5.0, data not shown). Therefore, it is unlikely that β-hex would be found in OMVs. Nevertheless, we generated a knock-out of the β-hex gene to ensure that the responses we observe are derived from OMV-presented antigens only. We used this strain as a control in all subsequent experiment using the TN cells.

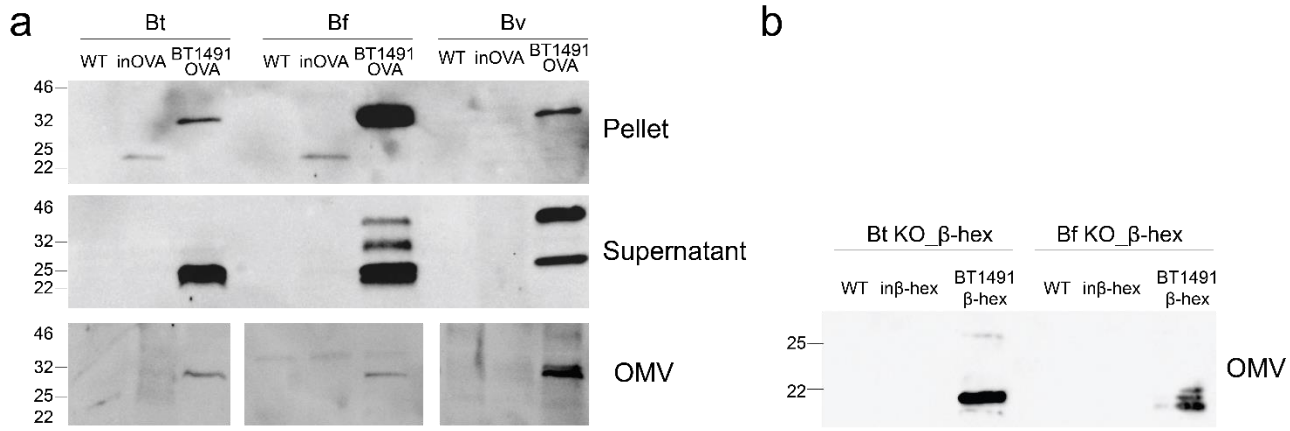

Figure 5.5 Incorporation of Ovalbumin (OVA) and β-hex into *Bacteroides* OMVs.

(**a**) The model antigen ovalbumin (Ova) was expressed intracellularly (inOVA) or fused to the BVIT BT1491d32. Expression in cell pellets, culture supernatants, and purified OMVs derived was analyzed by Western blot against the C-terminal FLAG tag on Ova. 5 µg of *B. thetaiotaomicro*n and 1µg of *B. fragilis* and *B. vulgatus* OMVs were analyzed. Blots are representative of at least three separate experiments. Figure adapted from (*1*). (**b**) Similarly to (a), the model antigen β-hex was expressed intracellularly (inβ-hex) or targeted to OMVs by fusion to BT1491d32. Expression in purified OMVs was analyzed by Western blot against the C-terminal FLAG tag on β-hex. Expected size ~26kDa after processing.

To test whether we could target antigens to OMVs, we fused the BVITs BT1491 to a truncated fragment of the OVA protein or β-hex and assessed their expression in *B. thetaiotaomicron*, *B. fragilis*, and *B. vulgatus* by Western blot. OVA expression was detected in the cellular fraction, in OMVs and in the supernatant. In contrast to OVA found in OMVs, OVA in the supernatant was degraded (Fig 5.5a). To distinguish responses elicited by OMVs and intact bacteria, we also generated control strains that express OVA intracellularly (inOVA). Similar results were observed for the TN antigen (Fig 5.5b).

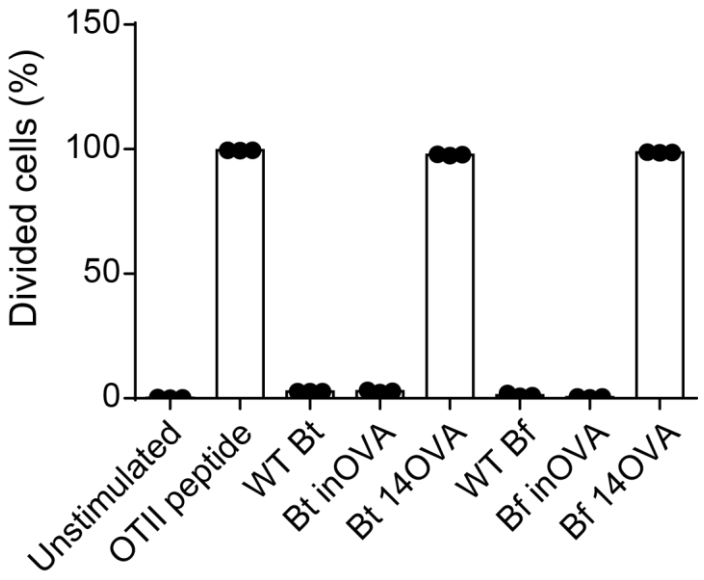

Figure 5.6 Presentation of OVA-Loaded OMVs to Naive OTII $CD4^+$ T Cells.

Naïve $CD4^+$ OTII T cells were labeled with CellTrace Violet and co-cultured with dendritic cells (DCs) purified from B16-Flt3L-injected mice in the presence of 1 µg/mL of OMVs derived from the indicated strains of *B. thetaiotaomicron* (Bt), *B. fragilis* (Bf) or 500nM OTII peptide as a positive control. After 3.5 days, CellTrace Violet dilution was assessed by flow cytometry. Dot plots are representative of at least 3 independent experiments. Cells were gated on $Aqua^-CD4^+V\alpha2^+V\beta5^+$. Each dot is a technical replicate and error bars represent the standard deviation.

Next, we tested whether *Bacteroides* OMVs containing OVA or β-hex were properly processed and presented by dendritic cells (DCs) to OTII and TN cells, respectively. Dendritic cells were cocultured with VioletTrace-labelled OTII cells in the presence of OMVs. While OMVs derived from WT or intracellular targeting (inOVA) strains induced little if any proliferation, OMV containing OVA (1491-OVA) triggered robust proliferation in OTII cells (Fig 5.6). Proliferation of OTII T cells in response to OMVs was associated with release of IFN-γ and IL-10 (Fig 5.7). In line with published data, the presence of *Bacteroides* OMVs was sufficient to promote IL-10 secretion even in the absence of cognate antigen (*8*).

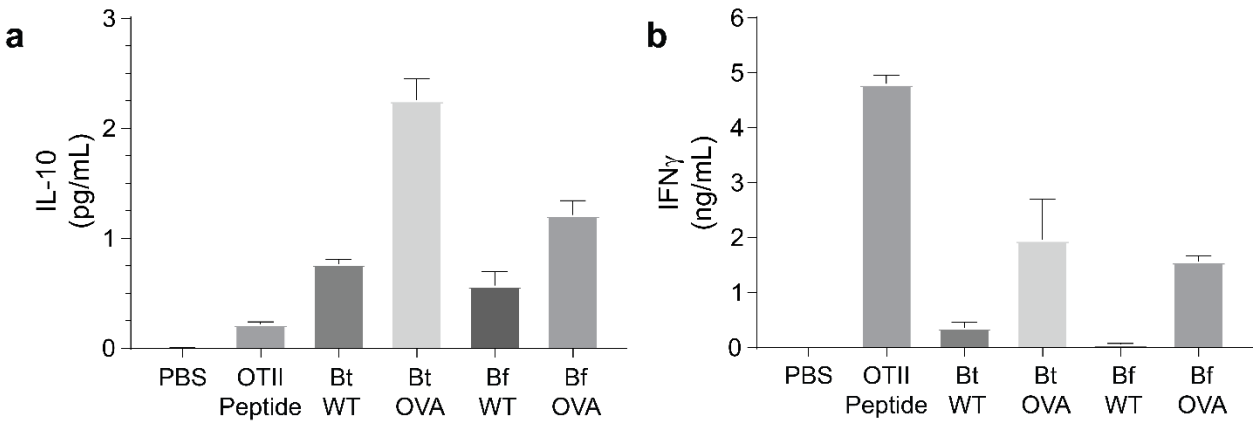

Figure 5.7 Cytokine Profile of OTII *in vitro* proliferation Assay.

Levels of IL-10 (**a**) and IFN-γ (**b**) analyzed by ELISA. Error bars represent standard deviation of three biological replicates (n=3). Figure adapted from (*1*).

In agreement with the responses observed for OTII cells to OVA-OMVs, TN cells were stimulated *in vitro* in the presence of DCs and OMVs which contain the cognate antigen, β-hex (Fig 5.8a). OMVs purified from strains that express β-hex intracellularly fail to activate the TN cells, while β-hex-OMVs induce close to 100% proliferation. Intracellular β-hex is therefore unlikely to be incorporated into OMVs unless when fused to BVIT. Activation of TN cells was associated with release of IFN-γ and to some extent IL-10, more predominantly when stimulated with *B. fragilis* β-hex-OMVs (Fig 5.8b,c). Fusion of BVIT to an antigen is thus an efficient way to specifically target antigens to OMVs, which can then be recognized and presented by DCs.

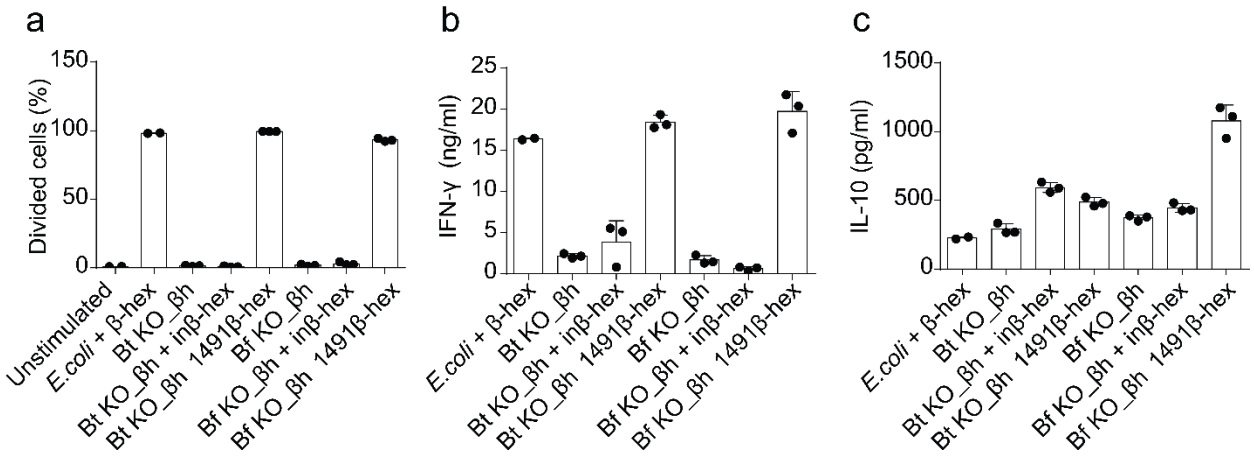

Figure 5.8 TN cells respond to β-hex loaded OMVs *in vitro*.

(**a**) Naïve CD4$^+$ TN T cells were labeled with CellTrace Violet and co-cultured with dendritic cells (DCs) purified from B16-Flt3L-injected mice in the presence of 1µg/mL of OMVs purified from strains of *B. thetaiotaomicron* (Bt) or *B. fragilis* (Bf) knocked-out for the β-hex gene (Bt KO_βh and Bf KO_βh) and expressing a truncated version of β-hex containing the TN epitope either intracellularly (inβ-hex) or in OMVs (1491β-hex). 25µg/mL of *E. coli* overexpressing the full length β-hex serves as a positive control. After 3.5 days, CellTrace Violet dilution was assessed by flow cytometry. Dot plots are representative of at least 3 experiments. Cells were gated on Aqua$^-$CD4$^+$Vα2$^+$Vβ6$^+$. Levels of IFN-γ (**b**) and IL-10 (**c**) analyzed by ELISA. Error bars represent standard deviation of three biological replicates (n=2-4). The graph shows means +/- standard deviation and each symbol represents a technical replicate.

Next, we sought to test whether antigen-loaded OMVs could also stimulate antigen-specific CD4$^+$ T cells *in vivo*. We transferred CD4$^+$ TN T cells into congenically-marked recipients that were then immunized subcutaneously with OMVs derived from the engineered *Bacteroides* strains described above (Fig 5.9a). Robust proliferation of TN T cells occurred in the draining lymph nodes (inguinal lymph nodes; iLNs) of mice that received OMVs purified from *B. thetaiotaomicron* or *B. fragilis* expressing the BVIT 1491(d32) fused to β-hex, but not the non-targeted strains (Bt KO_βh and Bf KO_βh) thus confirming that OMVs can elicit antigen-specific immune responses *in vivo* (Fig 5.9b-d).

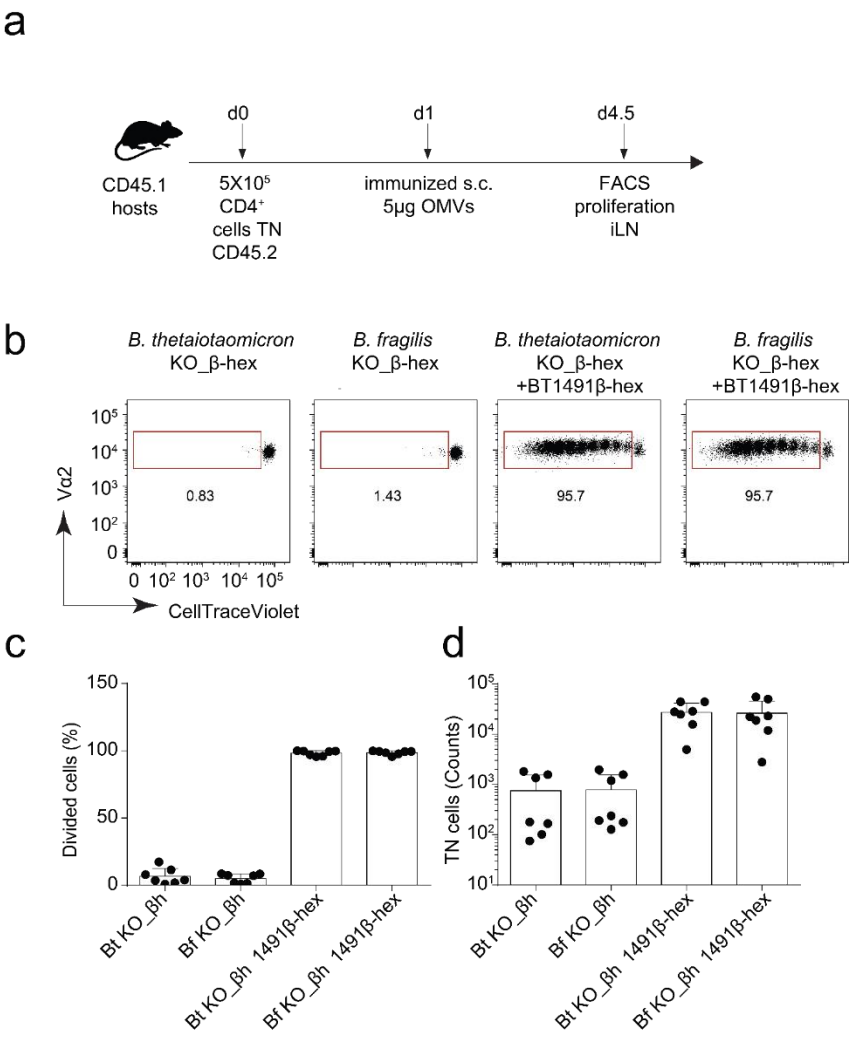

Figure 5.9 β-hex loaded OMVs can activate TN cells *in vivo*.

(**a**) Schematic of the *in vivo* proliferation assay shown in (b-d). Congenically-marked WT CD45.1$^+$ mice received 5x10^5 CellTrace-Violet-labeled naïve CD45.2$^+$ CD4$^+$ TN T cells and were immunized subcutaneously with 5µg of the indicated OMVs adsorbed in alum 1 day later. 3.5 days after immunization, proliferation was assessed in the draining lymph node (inguinal lymph node, iLN) by flow cytometry. (**b**) Dot plot shows dilution of CellTrace-Violet in Aqua$^-$CD45.1$^-$CD45.2$^+$CD4$^+$Vα2$^+$Vβ6$^+$ T cells in one representative mouse per condition. (**c,d**) The graphs show all mice analyzed in two independent experiments. Bt KO_βh= *B. thetaiotaomicron* knocked-out for the β-hex gene, Bf KO_βh= *B. fragilis* knocked-out for the β-hex gene, 1491βhex= fusion of truncation of βhex containing the TN epitope with BT Bt1491 (d32). N=7/group. The graphs show means +/- standard deviation and each symbol represents a single mouse.

Discussion

We developed a strategy to direct heterologous proteins into OMVs of *Bacteroides spp.*. We identified proteins present in OMVs of *B. thetaiotaomicron* by mass spectrometry and used them as fusion partners to specifically target proteins to OMVs. Truncation analysis identified minimal sequences (BVIT) capable of targeting proteins to OMVs. We found that BVIT derived from *B. thetaiotaomicron*, *B. fragilis*, and *B. ovatus* lipoproteins could direct OMV incorporation in several species of the genus *Bacteroides*. Our strategy is versatile and can perhaps be used to promote intestinal health by acting directly on the host immune system or via other resident microbes.

Members of the *Bacteroides* genus use OMVs as shuttles that contain enzymes to allow other microbes to grow on a carbon source for which they lack the genes to metabolize them (*23*). Packaging of 'public good' enzymes and other enzymes, as might be accomplished by the strategy described here, could be used to modify and/or maintain the complex microbial community in the gut and thereby reduce intestinal inflammation (*24*).

We used BVIT to target two model antigens, OVA and β-hex, to OMVs of *B. thetaiotaomicron* and *B. fragilis*. We showed that these engineered OMVs could activate antigen-specific $CD4^+$ T cells both *in vitro* and *in vivo*. In line with published data, stimulation of $CD4^+$ T cells in the presence of antigen presenting cells with *Bacteroides* OMVs promotes the secretion of IL-10, an important anti-inflammatory cytokine produced by regulatory cells (*8*).

With the exception of a handful studies, the role of OMVs on modulating the immune system remains poorly understood (*8, 12, 25*). Oral gavage of *B. fragilis* OMVs can protect mice against colitis, while *B. thetaiotaomicron* OMVs can migrate to the lamina propria and promote intestinal inflammation in susceptible animals (*8 , 12*). OMVs are thus important immune modulators in the intestine, but their exact role remains to be defined especially under homeostatic conditions. Using our BVIT targeting strategy in combination with our newly developed commensal-specific TN model, we are in a unique position to study these complex interactions. Preliminary experiments suggest that our

engineered strains of *B. thetaiotaomicron* and *B. fragilis* can stably colonize the mouse intestine and secrete antigen-loaded OMVs, which are then recognized by antigen-specific $CD4^+$ T cells (Data not shown). It will be important to define the phenotype(s) (surface markers, transcription factors and cytokines) of $CD4^+$ T cells activated in response to antigen-loaded OMVs. If *Bacteroides* OMVs promote antigen-specific tolerance, our strategy could be applied therapeutically for allergic or autoimmune diseases. Engineered OMVs can be used as a versatile platform to modulate host immune responses and to study antigen-specific responses to OMV-derived antigens.

Materials and methods

*adapted from (*1*)

Mice

Mice were housed at the Boston Children's hospital (BCH) under specific pathogen–free conditions, in accordance with institutional guidelines and approved by the institutional animal care and use committee the Boston Children's Hospital (IACUC protocol number 16-12-3328). pTreg TN mice were generated as described (*26*). C57BL/6, C57BL/6 CD45.1. OTII and Rag1−/−, mice were purchased from Taconic Biosciences and Jackson Laboratory and maintained at our facilities. pTreg TN were crossed to C57BL/6 RAG1KO for at least eight generations to generate pTreg TNxRAGKO (TN).

Bacterial Strains and Culture Conditions

B. thetaiotaomicron VPI-5482, *B. fragilis* NCTC9343 and *B. vulgatus* ATCC8482 were routinely cultured in TYG media supplemented with 0.4% glucose in anaerobic conditions at 37°C. (see Chapter 3 Experimental Details: Bacterial Strains and Culture Conditions). All *Bacteroides* media was pre-reduced overnight in the anaerobic chamber overnight before use. For expression studies, TYG was supplemented with 0.2 mM IPTG. E. coli S17-1 λpir was routinely cultured in LB broth (Difco) supplemented with 100 µg carbenicillin where appropriate.

Outer Membrane Vesicle Preparations

Outer membrane vesicles were purified as previously described (*27*). Overnight cultures of *Bacteroides* spp. were subcultured 1:100 in 80mL of pre-reduced TYG in 100mL glass bottles and grown for 16-20h anaerobically at 37°C. Cultures were centrifuged at 10,000 x g for 15 minutes to pellet bacterial cells. Supernatants were filtered through 0.45 µm PVDF membranes (Millipore) to remove residual cells and cellular debris. The filtrate was subsequently ultracentrifuged at 100,000 x g for 2 hours in a 70Ti rotor (Beckman Coulter) to pellet OMVs. The pellets were washed once in equal volumes of cold PBS. The final pellets were resuspended in 0.5mL of sterile PBS. OMV yield was quantified by total protein content as measured by Bradford assay (BioRad).

Genetic Parts and Plasmids

All plasmids were constructed using PCR, DpnI digest, Gibson assembly (*28*), and transformation into E. coli S17 λpir. BVITs and β-hex gene were amplified from purified *B. thetaiotaomicron*, *B. fragilis* or *P. goldsteinii* genomes using Kapa Hifi Polymerase. Gene encoding OVA was synthesized by Integrated DNA Technologies as Geneblocks. Conjugation of constructs in *Bacteroides* spp. were performed as described in (*29*). All protein coding genes were cloned into an IPTG-inducible pNBU1 expression vector.

Luminescence Assays

Overnight cultures of *Bacteroides* strains were subcultured 1:100 in pre-reduced TYG media and grown at 37°C until an OD600 of ~0.6-0.8 (~6h). Samples were centrifuged at 5,000 x g for 5 minutes. Supernatant was removed and saved for later analysis. In some cases, supernatant samples were concentrated using ultrafiltration columns (Amicon, MWCO 10kDa) as per manufacturer's instructions. Pellets were washed twice in PBS and finally resuspended in an equal volume of PBS.

Supernatants, pellets and OMVs were assayed for luminescence activity using the Nano-Glo Luciferase Assay System (Promega) as per manufacturer's instructions. Samples were not lysed before assaying, as the NanoLuc enzyme buffer contains detergents.

Western Blots

Protein samples were analyzed by Western blot using the Bio-Rad Mini-PROTEAN System. *Bacteroides* cell pellets (equivalent of 0.075 OD600 units), *Bacteroides* culture supernatants (equivalent of 0.5mL concentrated using Amicon columns), HT-29 cell lysates (10 µg), or purified OMVs (1-5 µg) were mixed with 4x Laemmli Sample Buffer (Bio-Rad) with 10% β-mecaptoethanol and boiled for 10 minutes. Protein samples were separated on 4-15% Mini-PROTEAN TGX gels in a Tris-SDS-glycine buffer system for 30 minutes at 200V. Proteins were transferred to nitrocellulose membrane using a Tris-glycine-methanol buffer for 60 minutes at 60V. Samples were blocked overnight in 5% milk in PBS with 0.05% Tween 20 (PBST) for anti-His blots, overnight in 2.5 % milk in PBST for anti-FLAG blots, and for 2 hours in 10% BSA Blocking Solution (SeraCare) for anti-P-STAT3 blots. Primary antibody incubations were conducted in appropriate blocking reagent as follows; 1:5000 dilution of Ms anti-His (HIS.H8, Abcam ab18184) for 4 hours at room temperature; 1:2500 dilution of Ms anti-FLAG (M2, Sigma F3165) for 4 hours at room temperature; 1:2000 Rb anti-Phospho-Stat3 (Tyr705) XP (Cell Signaling Technologies, #9145) overnight at 4°C. Secondary antibody incubations were conducted in blocking reagent at room temperature as follows: 1:5000 Rabbit anti-Ms IgG-HRP (Abcam, ab6728) for 1 hour; and, 1:5000 Anti-Rb IgG-HRP (Cell Signaling Technologies, #7074) for 1 hour. Following primary and secondary antibody incubations, blots were washed four times in PBS-T for at least 5 minutes per wash. Blots were developed using SuperSignal West Pico PLUS Chemiluminescent Substrate (Thermo Scientific) for 5 minutes and images were acquired using a Bio-Rad Gel Doc XR+ Gel Documentation System. Image analysis and annotation was performed using ImageLab (Bio-Rad) and Adobe Illustrator for layout.

Antigen Presentation Assays

Dendritic cells were purified with the PanDendritic Cell Isolation Kit (Miltenyi Biotec) from spleens of WT C57BL/6 mice injected with 1×10^6 B16-FLT3L cells. T cells were purified with the Naive $CD4^+$ T Cell Isolation Kit (Miltenyi Biotec) from the spleens and mLNs of

OT-II or TN x Rag1$^{-/-}$ mice and labeled with CellTrace Violet (Thermo Fisher). Purity was always greater than 98% for both dendritic cells and T cells. Dendritic cells (1 x 10^5) were incubated with purified OMVs of bacterial lysate (5 or 1 µg/ml), or 500nM OT-II peptide for 2 hours before the addition of 1×10^5 CD4$^+$ T cells. Bacterial lysates were prepared as described in chapter 3. Cell division was assessed by CellTrace Violet dilution and analyzed by flow cytometry after 3.5 days of co-culture. Cytokine profiles of culture supernatants were determined by ELISA.

In vivo proliferation assay

Six-week-old CD45.1 mice received $5x10^5$ of CellTrace Violet or CFSE-labeled CD4$^+$ T cells isolated from pTreg TN/Rag1KO mice. Recipients were then immunized with 5µg of purified OMVs in PBS/alum sub-cutaneously 24h later. Proliferation of cells isolated from the draining lymph node (inguinal lymph node) was assessed by dilution of the cell proliferation dye.

Antibodies, reagents, and FACS analysis

Fluorescently labeled antibodies were purchased from BD bioscience (anti-Vβ6, RR4-7; anti-Vβ5, MR9-4), eBioscience (anti-CD45.1, A20; anti-Foxp3, FJK-16s; anti-CD4, RM4-5; Va2, B20.1; anti-CD11c, N418). BioLegend (anti-CD45.2, 104; anti-CD44, IM7; anti–I-A/I-E, M5/114.15.2). Proliferation was measured by dilution of cell proliferation dye CellTrace Violet (Life Technologies), according to manufacturer's instructions. The cell viability dye Live/dead fixable Aqua fluorescent reactive dye was purchased from ThermoFisher. Staining with live/dead markers was performed following manufacturer's instructions. Staining for cell surface markers was performed at 4°C for 30min in PBS+1mM EDTA+ 0.5% bovine serum albumin. Intracellular staining was performed according to manufacturer's instructions, using the Foxp3/Transcription Factor Staining Buffer Set (eBioscience). Flow cytometry data were acquired on an LSRFortessa (Becton Dickinson) instrument and analyzed with the FlowJo software package (Tri-Star). Alum (Imject) used for immunizations was obtained from Thermo Fisher Scientific.

ELISA Assays

Concentrations of murine IL-4, IL-10, IL-17, IL-22, IFNγ, and TGFβ were measured as per manufacturer's instructions (R&D Systems, DuoSet ELISA).

References

1. M. Mimee, Thesis, Massachusetts Institute of Technology, (2018).
2. K. Honda, D. R. Littman, The microbiota in adaptive immune homeostasis and disease. *Nature* **535**, 75-84 (2016).
3. W. Elhenawy, M. O. Debelyy, M. F. Feldman, Preferential packing of acidic glycosidases and proteases into Bacteroides outer membrane vesicles. *MBio* **5**, e00909-00914 (2014).
4. S. Rakoff-Nahoum, M. J. Coyne, L. E. Comstock, An ecological network of polysaccharide utilization among human intestinal symbionts. *Curr Biol* **24**, 40-49 (2014).
5. A. Kulp, M. J. Kuehn, Biological functions and biogenesis of secreted bacterial outer membrane vesicles. *Annu Rev Microbiol* **64**, 163-184 (2010).
6. M. Kaparakis-Liaskos, R. L. Ferrero, Immune modulation by bacterial outer membrane vesicles. *Nat Rev Immunol* **15**, 375-387 (2015).
7. A. Bauwens *et al.*, Intrahost milieu modulates production of outer membrane vesicles, vesicle-associated Shiga toxin 2a and cytotoxicity in Escherichia coli O157:H7 and O104:H4. *Environ Microbiol Rep* **9**, 626-634 (2017).
8. Y. Shen *et al.*, Outer membrane vesicles of a human commensal mediate immune regulation and disease protection. *Cell Host Microbe* **12**, 509-520 (2012).
9. M. S. Ladinsky *et al.*, Endocytosis of commensal antigens by intestinal epithelial cells regulates mucosal T cell homeostasis. *Science* **363**, (2019).
10. N. Whibley, A. Tucci, F. Powrie, Regulatory T cell adaptation in the intestine and skin. *Nat Immunol* **20**, 386-396 (2019).
11. J. Ochoa-Reparaz *et al.*, A polysaccharide from the human commensal Bacteroides fragilis protects against CNS demyelinating disease. *Mucosal Immunol* **3**, 487-495 (2010).
12. C. A. Hickey *et al.*, Colitogenic Bacteroides thetaiotaomicron Antigens Access Host Immune Cells in a Sulfatase-Dependent Manner via Outer Membrane Vesicles. *Cell Host Microbe* **17**, 672-680 (2015).
13. Y. Cong, T. Feng, K. Fujihashi, T. R. Schoeb, C. O. Elson, A dominant, coordinated T regulatory cell-IgA response to the intestinal microbiota. *Proc Natl Acad Sci U S A* **106**, 19256-19261 (2009).
14. T. W. Hand *et al.*, Acute gastrointestinal infection induces long-lived microbiota-specific T cell responses. *Science* **337**, 1553-1556 (2012).
15. M. M. Wegorzewska *et al.*, Diet modulates colonic T cell responses by regulating the expression of a Bacteroides thetaiotaomicron antigen. *Sci Immunol* **4**, (2019).
16. R. E. Ley *et al.*, Evolution of mammals and their gut microbes. *Science* **320**, 1647-1651 (2008).

17. J. L. Sonnenburg *et al.*, Glycan foraging in vivo by an intestine-adapted bacterial symbiont. *Science* **307**, 1955-1959 (2005).
18. S. K. Mazmanian, J. L. Round, D. L. Kasper, A microbial symbiosis factor prevents intestinal inflammatory disease. *Nature* **453**, 620-625 (2008).
19. J. L. Round, S. K. Mazmanian, Inducible Foxp3+ regulatory T-cell development by a commensal bacterium of the intestinal microbiota. *Proc Natl Acad Sci U S A* **107**, 12204-12209 (2010).
20. Ivanov, II *et al.*, Specific microbiota direct the differentiation of IL-17-producing T-helper cells in the mucosa of the small intestine. *Cell Host Microbe* **4**, 337-349 (2008).
21. E. B. Troy, D. L. Kasper, Beneficial effects of Bacteroides fragilis polysaccharides on the immune system. *Front Biosci (Landmark Ed)* **15**, 25-34 (2010).
22. C. Ramakrishna *et al.*, Bacteroides fragilis polysaccharide A induces IL-10 secreting B and T cells that prevent viral encephalitis. *Nat Commun* **10**, 2153 (2019).
23. A. G. Wexler, A. L. Goodman, An insider's perspective: Bacteroides as a window into the microbiome. *Nat Microbiol* **2**, 17026 (2017).
24. J. B. Lynch, R. A. Alegado, Spheres of Hope, Packets of Doom: the Good and Bad of Outer Membrane Vesicles in Interspecies and Ecological Dynamics. *J Bacteriol* **199**, (2017).
25. H. Chu *et al.*, Gene-microbiota interactions contribute to the pathogenesis of inflammatory bowel disease. *Science* **352**, 1116-1120 (2016).
26. A. M. Bilate *et al.*, Tissue-specific emergence of regulatory and intraepithelial T cells from a clonal T cell precursor. *Sci Immunol* **1**, eaaf7471 (2016).
27. H. Chutkan, I. Macdonald, A. Manning, M. J. Kuehn, Quantitative and qualitative preparations of bacterial outer membrane vesicles. *Methods Mol Biol* **966**, 259-272 (2013).
28. D. G. Gibson *et al.*, Enzymatic assembly of DNA molecules up to several hundred kilobases. *Nat Methods* **6**, 343-345 (2009).
29. M. Mimee, A. C. Tucker, C. A. Voigt, T. K. Lu, Programming a Human Commensal Bacterium, Bacteroides thetaiotaomicron, to Sense and Respond to Stimuli in the Murine Gut Microbiota. *Cell Syst* **1**, 62-71 (2015).

Chapter 6 - Discussion and perspectives

During my graduate work, I have developed a new model of $CD4^+$ T cells specific for a commensal antigen (TN model). Previous work from the Ploegh lab established the use of transnuclear mouse models to study the development and behavior of antigen-specific T, B and NK T cells. We have expanded these models and showed that a single TCR, derived from a naturally occurring pTreg from the mesenteric lymph nodes, can adopt two different fates in the intestine in response to commensal bacteria (Chapter 2). The TN mice and other commensal-specific mouse models have illuminated the cross-talk between the microbiota and the immune system. In this thesis, I have identified the true ligand of the TN TCR: not only the commensals that can provide the antigen, β-N-acetylhexoseaminidase (β–hex), but also the epitope, thus expanding the tools available to study these complex interactions. In contrast to other commensal-specific T cell models which are thought to each recognize a unique commensal, this TN TCR can recognize a range of *Bacteroidetes*. In addition, TN cells do not induce inflammation in the gut, unlike most other commensal-specific T cells (*1, 2*)(*3*) . In fact, we showed that TN cells were not only non-inflammatory but that they could protect against ulcerative colitis (chapter 3). In chapter 4, I describe the role of TN cells in the induction of commensal-specific IgG1, while in chapter 5, we used the TN model to target antigens to outer membrane vesicles (OMVs). In the present chapter, I present our findings in the context of other published work, address unresolved hypotheses and discuss outstanding questions.

Commensal-specific TCR transgenic models have advanced our understanding of antigen-specific responses in the intestine. While there is a great diversity of microbial species in the intestine, only a minority of commensals induce antigen-specific responses under homeostatic conditions. These few microbes elicit unique and specific responses that are context-dependent. SFB induces quasi-monoclonal Th17 cells in the SiLP, *Helicobacter spp.* induces RORγFoxp3+ Tregs in the colonic lamina propria (cLP), while *A. muciniphila* promotes Tfh differentiation and commensal-specific IgG1 responses. These observations raise several questions: 1) Are we currently limited by the number of available examples or is there indeed only a handful of commensals that elicit antigen-specific T cell responses under homeostatic conditions? 2) If the latter holds true, what is so particular about these microbes? 3) What kind of antigens are recognized and what if

any is their particular significance? I will discuss these questions in the context of the TN and other commensal-specific mouse models.

Microbial niche and immune modulation

One striking feature of the species known to elicit antigen-specific T cell responses under homeostatic conditions is their habitat. Unlike most commensals, these species seem to be present in close proximity of the immune system, either directly attached to the epithelium or in the mucus. For instance, both SFB and *H. hepaticus* associate with the intestinal epithelium, while the mucin-degrading bacterium *A. muciniphila* establishes its niche in the mucus (*4*). In contrast to these examples, flagellin produced by *Clostridia* are only "seen" under inflammatory conditions by the flagellin-specific Cbir1 transgenic T cells, despite the large amount of antigen present in the lumen (*5*). These observations suggest that not all microbial lifestyles are compatible with antigen-specific modulation of the immune system under homeostatic conditions.

Using the TN model, we learnt that *Bacteroidetes* elicit a specific T cell response in the small intestine, but we know little about the niche they occupy. *P. goldsteinii,* like many other *Bacteroidetes,* is found in the ileum and in the large intestine (*6*). Studies in gnotobiotic mice suggest that this bacterium is not tightly attached to the epithelium (*7*-*9*). Interestingly, TN cells proliferate in the small intestine (SI) and in the distal SI draining lymph node but not in the colonic mesenteric lymph node, even though most *P. goldsteinii* is found in the large intestine (LI). It is possible that the more permissive mucus layer present in the SI allows easier access of this antigen to antigen-presenting cells (APCs) and subsequent presentation to T cells. Alternatively, this antigen might not be expressed everywhere in the intestine but only in response to (microbe-derived?) stimuli present in the SI. It remains to be established whether β-hex is present in the LI and if so, why it does not elicit proliferation of TN cells there.

What is the role of β-hex for *P. goldsteinii*?

In this thesis, I have shown how a bacterial enzyme, β-hex, can elicit a specific and protective immune response in the intestine. Despite massive TCR diversity, the immune

system seems to only respond to a limited number of immunodominant epitopes. For instance, SFB-specific TCRs primarily recognize two epitopes (*10*). Similarly, the uncharacterized protein HH_1713 from *H. hepaticus* contains two immunodominant epitopes recognized by most TCRs specific for this pathobiont (*3*). Similar to these results, we found that a fraction of $CD4_{IELs}$ also recognizes the β-hex epitope YKGSRVWLN. Why β-hex is recognized specifically by T cells remains unclear. Deciphering the role of this enzyme might help answer this question.

β-hex is a member of the glycosyl hydrolase family 20 (GH20). The members of this family catalyze the cleavage of terminal β-D-GlcNAc (β-D-N-acetylglucosamine) and β-D-GalNAc (β-D-N-Acetylgalactosamine) residues in N-acetyl-β-D-hexosamine polymers. Due to the remarkable substrate promiscuity exhibited by these enzymes, it is difficult to predict the role of β-hex based solely on catalytic activity. In bacteria, genes encoding proteins in a common pathway are usually clustered together in the genome. β-hex is found on a polysaccharide utilization locus (PUL). These genetic clusters are typical to *Bacteroidetes* and determine which metabolic and anatomic niches these species can occupy (*11, 12*). β-hex is clustered with genes encoding enzymes involved in sialic acid catabolism. Sialic acids are found in all vertebrates and within all tissues but are largely absent from plants, prokaryotes and invertebrates, suggesting that this locus encodes enzymes targeting host-derived glycans (*13*). The intestine is rich in host-derived glycans including mucin, surface glycoproteins on epithelial cells and secreted glycoproteins such as IgA. Any of these glycoproteins could in theory be a substrate of β-hex.

An additional clue comes from the expression pattern of this specific PUL. *Bacteroidetes* are experts at degrading glycans and can use many plant- and host-derived glycoproteins (*11, 14*). PULs are at the center of this process and each species encodes dozens distinct such loci. Instead of expressing all of them constitutively, *Bacteroidetes* tightly regulate the expression of each PUL in response to the presence of the corresponding polysaccharide (*15*). While there is little if any information on PULs derived from *P. goldsteinii*, corresponding PULs in related bacteria are better characterized. The homologous β-hex PUL found in *B. thetaiotaomicron* (PUL #9, BT_0456) is highly expressed when this bacterium is found in the colonic mucus but not the lumen (*16*).

Similarly, expression of the equivalent *B. fragilis* PUL (sgu locus, BF_1730) is upregulated in response to sialoglycoconjugates such as mucins. sgu-deficient *B. fragilis* cannot efficiently use mucin as a carbon source *in vitro*. *In vivo* defects in the sgu locus lead to colonization defects, suggesting that this PUL plays a key role in the establishment of *B. fragilis* in the intestine (*17*).

P. goldsteinii (or other commensals encoding β-hex) could modify its intestinal niche through deglycosylation of dominant environmental proteins such as mucin, extracellular matrix components or IgA. Deglycosylation of immunoglobulins by bacteria as a means to promote invasion has been described (*18*). For example, sialidases and exoglycosidases produced by the pathogen *Streptococcus pneumoniae* deglycosylate glycoproteins such as IgA, which in turn facilitates growth and colonization of the human airways (*19*). In addition, deglycosylation of serum immunoglobulins by *S. pneumoniae* increases its resistance to complement recognition and subsequent neutrophil-mediated killing (*20*). It would therefore be interesting to test whether β-hex can degrade glycans present on immunoglobulins such as IgA.

Is the function of β-hex required for its recognition by the immune system?

Despite the large number of commensal-derived antigens present in the gut mucosa, only a few have been identified as capable of inducing antigen-specific T cell responses. Could the function of β-hex be linked to its recognition by the immune system? As alluded to above, the β-hex locus found in *B. fragilis* is key to its ability to digest mucus and to colonize the intestine. Increased production of β-hex in the mucus might allow APCs within the epithelium to acquire sufficient β-hex antigen and present it to T cells.

Coupling between enzymatic activity of commensal-derived proteins and their capability to be recognized by the immune system has been described. Colonization of colitis-susceptible mice (dnKO) with *B. thetaiotaomicron* triggers the development of fulminant colitis (*21*). In these mice, development of pathology depends on stimulation of the immune system in the lamina propria by antigens derived from outer membrane vesicles (OMVs) produced by *B. thetaiotaomicron*. Penetration of the LP by OMVs requires the activity of sulfatases present on OMVs, as sulfatase-deficient *B. thetaiotaomicron* OMVs

cannot access the LP and do not trigger colitis in these susceptible mice. A catalytically inactive mutant of β-hex would allow an assessment of whether these mutant commensals can be recognized by the TN T cells *in vivo*.

How is β-hex acquired by antigen-presenting cells?

Since not all commensal-derived antigens are equally capable of eliciting a T cell response in the intestine, I hypothesize that the ability of these antigens to reach the epithelium is critical for their recognition by the immune system. As described above, Cbir1 T cells remain mostly naïve in healthy mice, despite the large amount of flagellin present in the intestine (*5*). In contrast, secreted antigens and OMV-derived antigens might be more readily accessible to APCs than bacteria-associated antigens such as flagellin (*21, 22*). Coupling the ability of degrading glycans to acquisition of antigen might be yet another strategy to ensure uptake by APCs (see above). Alternatively, whole bacteria could be engulfed via extension into the lumen of $CX3CR1^{+}$ macrophages present in the LP. However, this does not seem to be the primary mode of antigen presentation for TN cells, since $CXCR3^{GFP/GFP}$ mice, which lack transepithelial dendrites, still support activation and development of TN cells into $CD4_{IELs}$ and pTregs (data not shown).

Is β-hex secreted or present in OMVs? β-hex is predicted to possess an N-terminal signal sequence (using SignalP, data not shown), but no other transmembrane domains. This suggests a possible periplasmic location, secretion in extracellular space or the presence of β-hex in OMVs. *P. goldsteinii* OMVs derived from *in vitro* cultures do not activate the TN T cells, suggesting that β-hex is not targeted to OMVs (see chapter 5). Raising a polyclonal serum against β-hex would be useful to identify its subcellular localization.

Do $CD4_{IELs}$ recognize abundant antigens?

The immune system at the gut mucosal surface is continuously stimulated and educated by the dense community of microbes at that location. The diversity of microbial and dietary antigens present at the gut mucosal surface and the critically exposed position of IELs,

would predict that this population of lymphocytes might recognize a large, diverse set of antigens. However, TCR repertoire analyses showed that IELs, including $CD4_{IELs,}$ in fact exhibit low TCRs diversity (*23-31*). A limited number of antigens might therefore suffice to shape this compartment.

If $CD4_{IELs}$ recognize only a few antigens, what might be so special about them? Here, we identified the first antigen recognized by TN $CD4_{IELs}$, the antigen β-hex. We found that this antigen is also recognized by WT $CD4_{IELs}$. In contrast to most other commensal-specific TCR models, we found that the TN TCR can recognize conserved epitopes encoded by a large population of *Bacteroidetes*. Bacteria belonging to this phylum are highly abundant across mammals and are important modulators of the immune system (*11*) . Based on this information, β-hex and other $CD4_{IELs}$-recognized antigens might be abundant in the intestine. A T cell bearing a TCR capable of recognizing abundant antigens should have a competitive advantage in establishing itself in a niche of limited size, such as within the epithelium. This hypothesis is supported by experiments showing that ovalbumin (OVA)-specific $CD4^+$ T cells (OTII) convert into $CD4_{IELs}$ when their hosts are provided with large amounts of OVA in their drinking water (*32*).

In addition to their abundance, $CD4_{IELs}$ antigens might interact with their cognate TCRs with high affinity. $CD4_{IELs}$ express the homodimer coreceptor CD8αα which can bind to the non-classical MHC-I molecule, TL antigen on, epithelial cells (*33, 34*). Interaction of CD8αα with the TL antigen attenuates TCR activation and represses proliferation of CD8αα-expressing IELs (*35*). Clonal expansion within the epithelium would therefore require the presence of an abundant and/or high affinity TCR antigen to compensate for the negative effect exerted by the TL antigen. If this hypothesis is correct, one would expect to observe a higher diversity of TCRs among $CD4_{IELs}$ harvested from $TL^{-/-}$ mice.

Does *P. goldsteinii*, *B. vulgatus* or *B. fragilis* also activate the aryl hydrocarbon receptor?

Development of IELs, including that of $CD4_{IELs}$ depends on aryl hydrocarbon receptor (AHR) signaling (*25*). The absence of AHR signaling arrests development of $CD4_{IELs}$ prior to the characteristic down-regulation of Thpok (*25*). Colonization of mice with *L. reuteri*

promotes development of $CD4_{IELs}$ via secretion of tryptophan metabolites, which signal through the AHR. Besides their ability to produce metabolites that engage the AHR, microbes use indole derivatives for a range of purposes, including cell-to-cell communication, drug resistance, plasmid stability and biofilm formation (*36*). As a matter of fact, many commensals of diverse phylogenetic backgrounds produce indole-derivates that can signal through the AHR (*36, 37*). While *L. reuteri* is the first commensal identified to promote the development of $CD4_{IELs}$ via AHR activation, it is likely that other commensals have the same ability.

Activating epitopes for the TN TCR have been found in a range of *Bacteroidetes* species. Since both TCR activation and AHR induction are essential for $CD4_{IELs}$ development, it would be interesting to test whether these *Bacteroidetes spp.* also produce tryptophan metabolites capable of activating the AHR. For instance, *B. fragilis* produces indoleacetic acid (IAA) and indolelactic acid (ILA), both of which are AHR ligands (*37*). However, *P. goldsteinii* and *B. vulgatus* are usually considered indole-negative bacteria (*38, 39*). This would explain why monocolonization of germ-free mice with *P. goldsteinii* is not sufficient to promote differentiation of $CD4_{IELs}$. Of note, monocolonization with *L. reuteri* is also not sufficient to allow $CD4_{IELs}$ development (*25*). It remains to be established whether other commensals which are theoretically capable to both activate the TN cells and produce AHR ligands, such as *B. fragilis*, are sufficient to promote the development of $CD4_{IELs}$. Additional pathways such as IFNγ are also important for $CD4_{IELs}$ differentiation and it is unclear whether any commensal could provide all of the required signals on its own (*40*). Monocolonization might never be sufficient as other commensals might be required to promote the expression of the required molecules by for example *B. fragilis*.

A comparison of the bacterial composition in animals high in $CD4_{IELs}$ (Charles River (CR) Kingston NY and neomycin-treated CR) and low in $CD4_{IELs}$ (Jackson) shows that not only is *L. reuteri* enriched in animals with more $CD4_{IELs}$ but they also contain a few species from the S24-7 *Bacteroidales* family, related to *Bacteroides* and *Parabacteroides*. Based on this information, I propose that there is a division of labor between the many species that inhabit the different micro-niches of our intestines. Abundant antigens, such as β-hex produced by *Bacteroidetes,* might provide the TCR activation signal required for the

development of $CD4_{IELs}$, while other species such as *L. reuteri* provide additional essential factors such as indoles or other metabolites.

How do $CD4_{IELs}$ protect mice against colitis?

Using the TN model, we showed that β-hex-specific $CD4_{IELs}$ could protect against intestinal inflammation in the lymphocyte-induced colitis model. However, the mechanism responsible for this reduction in inflammation remains to be established. $CD4_{IELs}$ display a regulatory cytokine signature similar to that of Tregs or Tr1 cells, including the expression of IL-10, TGF-β and IFN-γ (*41, 42*). However, unlike these other regulatory cells, differentiation of $CD4_{IELs}$ seems to be enhanced under inflammatory conditions as seen in $IL10^{-/-}$ and $Rag2^{-/-}$ mice (*41, 43-47*).

It is remarkable that a population of cells present in the small intestine can reduce inflammation at a distance in the large intestine. Secretion of IL-10 by $CD4_{IELs}$ in the small intestine could be an important mechanism to reduce inflammation in the large intestine (*41, 42, 48, 49*). Since IL-10 is a potent immunosuppressive cytokine, it is possible that even low levels of SI-derived IL-10 reaching the LI would suffice to prevent inflammation.

P. goldsteinii could have a much broader role in host physiology (*50*). Colonization with *P. goldsteinii* prevents body weight increase and reduces the levels of inflammation in obese mice. Altered intestinal barrier function contributes to the development of obesity and type-2 diabetes, a process prevented by colonization with *P. goldsteinii*. Could this process be mediated by $CD4_{IELs}$ induced in response to *P. goldsteinii*? In this model, *P. goldsteinii* promoted intestinal integrity, improved barrier function and increased IL-10 production in the intestine, all of which are functions typically mediated by IELs (*51*) .

References

1. S. K. Lathrop *et al.*, Peripheral education of the immune system by colonic commensal microbiota. *Nature* **478**, 250-254 (2011).
2. J. N. Chai *et al.*, Helicobacter species are potent drivers of colonic T cell responses in homeostasis and inflammation. *Sci Immunol* **2**, (2017).
3. M. Xu *et al.*, c-MAF-dependent regulatory T cells mediate immunological tolerance to a gut pathobiont. *Nature* **554**, 373-377 (2018).
4. N. Whibley, A. Tucci, F. Powrie, Regulatory T cell adaptation in the intestine and skin. *Nat Immunol* **20**, 386-396 (2019).
5. Y. Cong, T. Feng, K. Fujihashi, T. R. Schoeb, C. O. Elson, A dominant, coordinated T regulatory cell-IgA response to the intestinal microbiota. *Proc Natl Acad Sci U S A* **106**, 19256-19261 (2009).
6. R. B. Sarma-Rupavtarm, Z. Ge, D. B. Schauer, J. G. Fox, M. F. Polz, Spatial distribution and stability of the eight microbial species of the altered schaedler flora in the mouse gastrointestinal tract. *Appl Environ Microbiol* **70**, 2791-2800 (2004).
7. M. Sakamoto, Y. Benno, Reclassification of Bacteroides distasonis, Bacteroides goldsteinii and Bacteroides merdae as Parabacteroides distasonis gen. nov., comb. nov., Parabacteroides goldsteinii comb. nov. and Parabacteroides merdae comb. nov. *Int J Syst Evol Microbiol* **56**, 1599-1605 (2006).
8. Y. Momose, S. H. Park, Y. Miyamoto, K. Itoh, Design of species-specific oligonucleotide probes for the detection of Bacteroides and Parabacteroides by fluorescence in situ hybridization and their application to the analysis of mouse caecal Bacteroides-Parabacteroides microbiota. *J Appl Microbiol* **111**, 176-184 (2011).
9. M. B. Geuking *et al.*, Intestinal bacterial colonization induces mutualistic regulatory T cell responses. *Immunity* **34**, 794-806 (2011).
10. Y. Yang *et al.*, Focused specificity of intestinal TH17 cells towards commensal bacterial antigens. *Nature* **510**, 152-156 (2014).
11. A. G. Wexler, A. L. Goodman, An insider's perspective: Bacteroides as a window into the microbiome. *Nat Microbiol* **2**, 17026 (2017).
12. S. M. Lee *et al.*, Bacterial colonization factors control specificity and stability of the gut microbiota. *Nature* **501**, 426-429 (2013).
13. A. Varki, *Essentials of glycobiology*. (Cold Spring Harbor Laboratory Press, Cold Spring Harbor, NY, 1999), pp. xvii, 653 p.
14. E. C. Martens, N. M. Koropatkin, T. J. Smith, J. I. Gordon, Complex glycan catabolism by the human gut microbiota: the Bacteroidetes Sus-like paradigm. *J Biol Chem* **284**, 24673-24677 (2009).
15. V. Raghavan, E. C. Lowe, G. E. Townsend, 2nd, D. N. Bolam, E. A. Groisman, Tuning transcription of nutrient utilization genes to catabolic rate promotes growth in a gut bacterium. *Mol Microbiol* **93**, 1010-1025 (2014).
16. H. Li *et al.*, The outer mucus layer hosts a distinct intestinal microbial niche. *Nat Commun* **6**, 8292 (2015).
17. H. Nakayama-Imaohji *et al.*, Characterization of a gene cluster for sialoglycoconjugate utilization in Bacteroides fragilis. *J Med Invest* **59**, 79-94 (2012).
18. M. Collin, A. Olsen, EndoS, a novel secreted protein from Streptococcus pyogenes with endoglycosidase activity on human IgG. *EMBO J* **20**, 3046-3055 (2001).
19. S. J. King, K. R. Hippe, J. N. Weiser, Deglycosylation of human glycoconjugates by the sequential activities of exoglycosidases expressed by Streptococcus pneumoniae. *Mol Microbiol* **59**, 961-974 (2006).

20. A. B. Dalia, A. J. Standish, J. N. Weiser, Three surface exoglycosidases from Streptococcus pneumoniae, NanA, BgaA, and StrH, promote resistance to opsonophagocytic killing by human neutrophils. *Infect Immun* **78**, 2108-2116 (2010).
21. C. A. Hickey *et al.*, Colitogenic Bacteroides thetaiotaomicron Antigens Access Host Immune Cells in a Sulfatase-Dependent Manner via Outer Membrane Vesicles. *Cell Host Microbe* **17**, 672-680 (2015).
22. S. Veenbergen *et al.*, Colonic tolerance develops in the iliac lymph nodes and can be established independent of CD103(+) dendritic cells. *Mucosal Immunol* **9**, 894-906 (2016).
23. L. Helgeland, F. E. Johansen, J. O. Utgaard, J. T. Vaage, P. Brandtzaeg, Oligoclonality of rat intestinal intraepithelial T lymphocytes: overlapping TCR beta-chain repertoires in the CD4 single-positive and CD4/CD8 double-positive subsets. *J Immunol* **162**, 2683-2692 (1999).
24. L. Helgeland, J. T. Vaage, B. Rolstad, T. Midtvedt, P. Brandtzaeg, Microbial colonization influences composition and T-cell receptor V beta repertoire of intraepithelial lymphocytes in rat intestine. *Immunology* **89**, 494-501 (1996).
25. L. Cervantes-Barragan *et al.*, Lactobacillus reuteri induces gut intraepithelial CD4(+)CD8alphaalpha(+) T cells. *Science* **357**, 806-810 (2017).
26. L. Wojciech *et al.*, Non-canonicaly recruited TCRalphabetaCD8alphaalpha IELs recognize microbial antigens. *Sci Rep* **8**, 10848 (2018).
27. A. Regnault, A. Cumano, P. Vassalli, D. Guy-Grand, P. Kourilsky, Oligoclonal repertoire of the CD8 alpha alpha and the CD8 alpha beta TCR-alpha/beta murine intestinal intraepithelial T lymphocytes: evidence for the random emergence of T cells. *J Exp Med* **180**, 1345-1358 (1994).
28. A. Regnault *et al.*, The expansion and selection of T cell receptor alpha beta intestinal intraepithelial T cell clones. *Eur J Immunol* **26**, 914-921 (1996).
29. A. Regnault, P. Kourilsky, A. Cumano, The TCR-beta chain repertoire of gut-derived T lymphocytes. *Semin Immunol* **7**, 307-319 (1995).
30. B. D. McDonald, J. J. Bunker, I. E. Ishizuka, B. Jabri, A. Bendelac, Elevated T cell receptor signaling identifies a thymic precursor to the TCRalphabeta(+)CD4(-)CD8beta(-) intraepithelial lymphocyte lineage. *Immunity* **41**, 219-229 (2014).
31. C. G. Chapman *et al.*, Characterization of T-cell Receptor Repertoire in Inflamed Tissues of Patients with Crohn's Disease Through Deep Sequencing. *Inflamm Bowel Dis* **22**, 1275-1285 (2016).
32. T. Sujino *et al.*, Tissue adaptation of regulatory and intraepithelial CD4+ T cells controls gut inflammation. *Science* **352**, 1581-1586 (2016).
33. H. Cheroutre, L. Madakamutil, Acquired and natural memory T cells join forces at the mucosal front line. *Nat Rev Immunol* **4**, 290-300 (2004).
34. M. Wu, L. van Kaer, S. Itohara, S. Tonegawa, Highly restricted expression of the thymus leukemia antigens on intestinal epithelial cells. *J Exp Med* **174**, 213-218 (1991).
35. D. Olivares-Villagomez *et al.*, Thymus leukemia antigen controls intraepithelial lymphocyte function and inflammatory bowel disease. *Proc Natl Acad Sci U S A* **105**, 17931-17936 (2008).
36. J. H. Lee, J. Lee, Indole as an intercellular signal in microbial communities. *FEMS Microbiol Rev* **34**, 426-444 (2010).
37. H. M. Roager, T. R. Licht, Microbial tryptophan catabolites in health and disease. *Nat Commun* **9**, 3294 (2018).
38. Y. Song *et al.*, "Bacteroides goldsteinii sp. nov." isolated from clinical specimens of human intestinal origin. *J Clin Microbiol* **43**, 4522-4527 (2005).

39. S. G. Jenkins, R. J. Birk, R. J. Zabransky, Differences in susceptibilities of species of the Bacteroides fragilis group to several beta-lactam antibiotics: indole production as an indicator of resistance. *Antimicrob Agents Chemother* **22**, 628-634 (1982).
40. B. S. Reis, D. P. Hoytema van Konijnenburg, S. I. Grivennikov, D. Mucida, Transcription factor T-bet regulates intraepithelial lymphocyte functional maturation. *Immunity* **41**, 244-256 (2014).
41. G. Das *et al.*, An important regulatory role for CD4+CD8 alpha alpha T cells in the intestinal epithelial layer in the prevention of inflammatory bowel disease. *Proc Natl Acad Sci U S A* **100**, 5324-5329 (2003).
42. M. L. Hanson *et al.*, Oral delivery of IL-27 recombinant bacteria attenuates immune colitis in mice. *Gastroenterology* **146**, 210-221 e213 (2014).
43. A. M. Bilate *et al.*, Tissue-specific emergence of regulatory and intraepithelial T cells from a clonal T cell precursor. *Sci Immunol* **1**, eaaf7471 (2016).
44. J. Wei *et al.*, Antagonistic nature of T helper 1/2 developmental programs in opposing peripheral induction of Foxp3+ regulatory T cells. *Proc Natl Acad Sci U S A* **104**, 18169-18174 (2007).
45. S. Hadjur *et al.*, IL4 blockade of inducible regulatory T cell differentiation: the role of Th2 cells, Gata3 and PU.1. *Immunol Lett* **122**, 37-43 (2009).
46. L. Ulloa, J. Doody, J. Massague, Inhibition of transforming growth factor-beta/SMAD signalling by the interferon-gamma/STAT pathway. *Nature* **397**, 710-713 (1999).
47. D. Caretto, S. D. Katzman, A. V. Villarino, E. Gallo, A. K. Abbas, Cutting edge: the Th1 response inhibits the generation of peripheral regulatory T cells. *J Immunol* **184**, 30-34 (2010).
48. P. Poussier, T. Ning, D. Banerjee, M. Julius, A unique subset of self-specific intraintestinal T cells maintains gut integrity. *J Exp Med* **195**, 1491-1497 (2002).
49. H. De Winter *et al.*, Regulation of mucosal immune responses by recombinant interleukin 10 produced by intestinal epithelial cells in mice. *Gastroenterology* **122**, 1829-1841 (2002).
50. T. R. Wu *et al.*, Gut commensal Parabacteroides goldsteinii plays a predominant role in the anti-obesity effects of polysaccharides isolated from Hirsutella sinensis. *Gut* **68**, 248-262 (2019).
51. H. Cheroutre, F. Lambolez, D. Mucida, The light and dark sides of intestinal intraepithelial lymphocytes. *Nat Rev Immunol* **11**, 445-456 (2011).

Chapter 7 - Appendix: Site-specific labeling of Ovalbumin-specific B cell receptor

D. Bousbaine, Z. Li, T. Fang and H. Ploegh

This chapter is currently in preparation for publication.

Abstract

Expression of the B cell receptor (BCR) is essential for survival, development and effector functions of B cells. Naive B cells express surface IgM and IgD, while surface IgG1 is expressed by memory B cells. Despite similar overall structures, the different BCR isotypes show differences in distribution and expression levels, thus impacting B cell fate. The dynamics of BCR behavior have been difficult to explore due to a lack of appropriate tools that can track the BCR without causing concomitant activation. Using CRISPR-Cas9, we inserted a sortase recognition motif (LPETG) at the C-terminus of the OB1 transnuclear ovalbumin-specific Cκ chain (κ-LPETG mice). The surface BCR from κ-LPETG mice is fully functional and can be labelled site-specifically with biotin or with fluorophores. We found that κ-LPETG mice have a near-normal B cell development, with an increase in Igλ-producing cells, presumably due to massive contraction of the κ locus V-region cluster. Using the κ-LPETG mice, we quantified the number of BCRs on the surface of IgM/IgD and IgG1 B cells. IgG1 BCRs are present at much reduced density yet with increased oligomerization, compared to naïve mature B cells carrying IgM and IgD BCRs. The isotype of the Ig heavy chain thus dictates surface expression and nano-scale organization of the BCR.

Introduction

The immune system can recognize and respond to an impressive number of antigens. The B cell receptor (BCR) recognizes antigens and so contributes to specific and long-lasting defenses against a wide range of pathogens (*1*). The BCR is a complex of proteins that consists of membrane immunoglobulin (mIg), composed of two identical heavy and light chains, each with a variable (V) and a constant (C) region, together with the Igα and Igβ accessory proteins (*2*). The latter contain immunoreceptor tyrosine-based activation motifs (ITAMs) required for signal transduction (*3, 4*). The variable portion of mIg is responsible for antigen (Ag) binding while the C regions determine the BCR isotype and effector functions (*3*). Naïve mature B cells express two Ig isotypes on their surface: IgM and IgD. In response to antigen and costimulatory signals, B cells may switch to other isotypes (IgG, IgA or IgE) with retention of the heavy chain's V region sequence. It has been proposed that the BCR isotype could affect specificity and affinity of the BCR for its antigen (*3, 5, 6*).

Upon binding of Ag to the variable portion of the BCR, B cells launch a cascade of intracellular signals (*7*) essential for their proliferation. BCR engagement also leads to internalization, processing and presentation of Ag on Class II MHC molecules (*7*). The display of peptide- Class II MHC molecules is essential for activation of T cells that provide help in the differentiation of B cells into antibody-secreting cells (*7*). BCR-triggered events control a series of cell-fate decisions at several checkpoints during B cell development (*1*). Therefore, BCR engagement must be tuned to respond appropriately to execute each of these critical functions: [1] survival upon receipt of "tonic" signals, [2] production of antibodies/present Ag to T cells upon activation and [3] differentiation into a specific cell type. The molecular basis that governs fate decisions in the periphery is not well understood. Likewise, the detailed molecular features that allow signal transduction upon BCR engagement remain to be clarified. A growing body of evidence points to changes in nano-scale organization of the BCR as critical for activation, survival and fate decisions (*5, 7-9*).

Visualization of surface receptors can provide new insights into their function. Direct labeling of the BCR without concomitant activation in the course of live cell imaging remains a challenge. Visualization of the BCR either relies on the use of antibody reagents directed to the BCR or involves the use of labeled antigens. Either approach can lead to activation of B cells and thus precludes an accurate assessment of BCR organization prior to and upon Ag binding (*10-12*). Other approaches rely on labeling of the peripherally associated accessory BCR subunits Igα and

Igβ with fluorescent proteins (~25 kDa for GFP) as genetic fusions, providing at best an indirect readout (*13*). Therefore, there is a clear need to develop a strategy to directly label BCRs on live primary B cells with minimal perturbation.

Here we introduced a new, generalizable method to introduce a label into the BCR in a minimally perturbing manner. We exploited Cas9/CRISPR to engineer a sortase (SrtA) recognition motif (LPETG) into the κ locus of mice that bear an IgG1 BCR specific for ovalbumin. These mice were generated by somatic cell nuclear transfer and contain rearranged IgH and κ loci at their endogenous locations. The OB1 mice thus retain the capacity for secondary κ chain rearrangements, as well as class switch recombination for the IgH locus and somatic hypermutation of the rearranged IgH and κ loci. The modified locus encodes a κ light chain that can be modified enzymatically and site-specifically with any small molecule substituent of choice, including biotin and fluorophores. BCRs on B cells derived from κ -LPETG mice are fully functional after labeling with SrtA. Using this strategy, we compared the organization and density of BCRs on the surface of B cells of different isotypes. The membrane-bound IgG1 chain differs from the IgM heavy chain in the presence of a cytoplasmic tail of 28 residues. This tail contains residues that could be substrates for post-translational modifications such as phosphorylation or ubiquitylation, which might endow IgG1 BCRs with properties fundamentally different from IgM/IgD BCRs, for example their interaction with elements of the cytoskeleton. Unlike IgM/IgD, we find that IgG1 BCRs organized in nanoclusters at rest. Furthermore, we estimate the total number of IgG1 BCRs on the surface of naïve B cells to be 400,000, three times lower than that of IgM/IgD BCRs, notwithstanding the fact that transcriptional control elements do not obviously differ for these isotypes.

Results

Site-specific labelling of the B cell receptor using Sortase A

Using somatic cell nuclear transfer, we generated a line of transnuclear mice that have B cells of defined specificity. The OB1 line makes an IgG1 that recognizes ovalbumin, the precise epitope of which has been identified (*14, 15*). To create a model that allows labeling and engagement of the BCR in a manner that would avoid its crosslinking, we used Cas9/CRISPR gene editing to generate germline-modified OB1 mice bearing a LPETG motif, preceded by a 6-residue linker, at the C-terminus of the Cκ domain (Fig. 7.1A), similarly to (*16*). The configuration of the modified κ locus deserves comment, as it has implications for interpretation of the labeling patterns that will be described below. The OB 1 κ chain uses Vκ1-135, which is located at the 5' end of the Vκ cluster, with only one functional upstream Vκ 2-137 gene remaining. The use of the Jκ1 segment leaves three functional J segments available for secondary rearrangements. In the presence of the OB1 rearranged IgG1 heavy chain, Vκ 1-135 is used preferentially. When the modified κ locus is placed on a WT IgH background, both Vκ 1-135 and the upstream Vκ 2-137 participate in rearrangement, the latter requiring what would be considered a secondary rearrangement. In any case, it is the Cκ exon that carries the LPETG modification, so that -regardless of the Vκ segment used- the resulting κ chain and the BCRs of which it is part of should be suitable SrtA substrates.

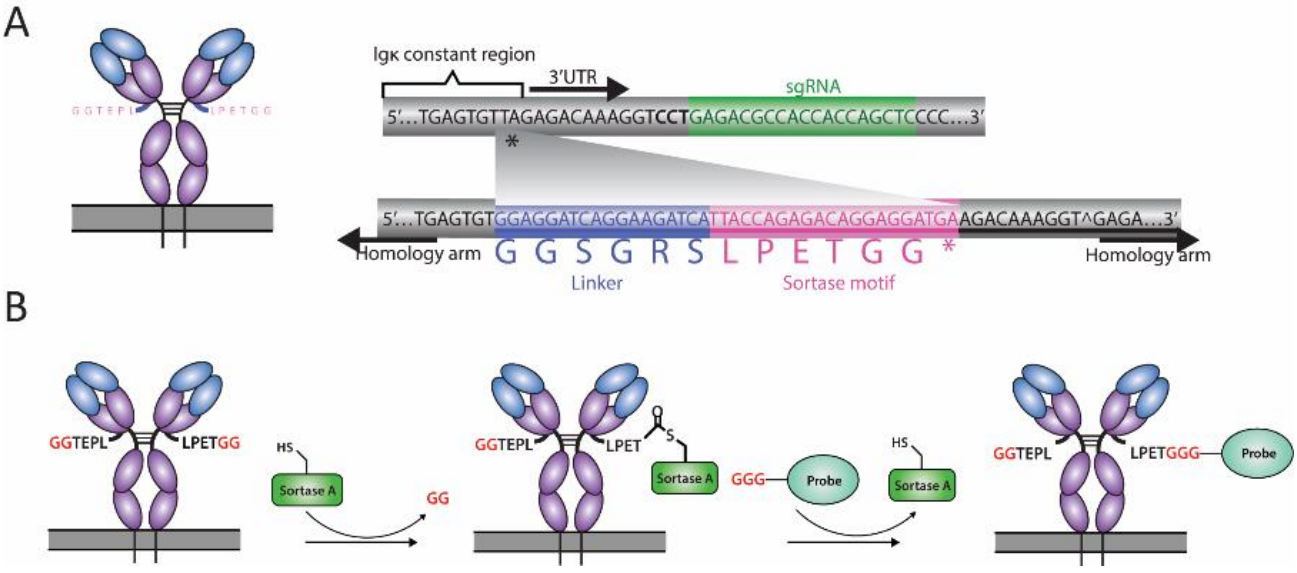

Figure 7.1 The κ -LPETG mouse model

(**A**) The κ -LC constant region was targeted using CRISPR/Cas9 to intoduce a SrtA motif at the κ C-terminus. The gRNA is indicated in green, the linker in blue and the SrtA motif in pink. (**B**) The κ -LPETG

motif on the BCR can be targeted by any substituent of choice (biotin, oganic dyes, proteins, peptides, radioactive isotopes, DNA) using SrtA. SrtA cleaves between the T and G in the LPETG motif to produce an acyl-enzyme intermediate. The glycine N-terminus of the GGG motif on the probe can then initiate a nucleophilic attack resulting in a covalent (peptide) linkage of the probe to the BCR.

Sortase A (SrtA) is a transpeptidase that allows the attachment of any substituent of choice containing a GGG at its N-terminus to the LPXTG SrtA recognition motif (Fig. 7.1B). A molecular model of a full-sized IgG1 molecule shows that the C-terminus of the κ-light chain is exposed (*17*). By extending the κ C-terminus with an LPETG motif, we hypothesized that the SrtA recognition site would be accessible to exogenously added SrtA. We incubated serum antibodies isolated from Igκ-LPETG mice with recombinant SrtA in the presence or absence of a (Gly)3-biotin nucleophile. Successful labeling results in the appendage of the (Gly)3-biotin moiety to the C-terminus of the modified κ light chain. When using serum isolated from wild-type (WT) mice we observed no labeling of κ chains under any condition. Immunoglobulins from animals that carry the modified OB1 κ light chains showed labeling only when both SrtA and the (Gly)3-biotin nucleophile were included. Detection of the biotinylated κ light chain with streptavidin-horse radish peroxidase (HRP) conjugate on immunoblots yielded a single labeled polypeptide of the appropriate molecular weight (Fig. 7.2A). Because mammalian cells do not possess naturally occurring surface proteins with an exposed LPXTG motif, we expect B cells from WT mice to be refractory to SrtA labeling unless they carry the κ-LPETG motif. Accordingly, labeling of the Igκ -LPETG BCR on naive B cells is rapid (minutes) and specific (Fig. 7.2B,C). A plateau is reached after ~ 30 minutes of incubation (fig. 7.2C). In addition to GGG-biotin, κ-LPETG BCRs were readily labelled with other substituents, including GGG-Alexa-647 and GGG-Cy5 (Fig. 7.2D).

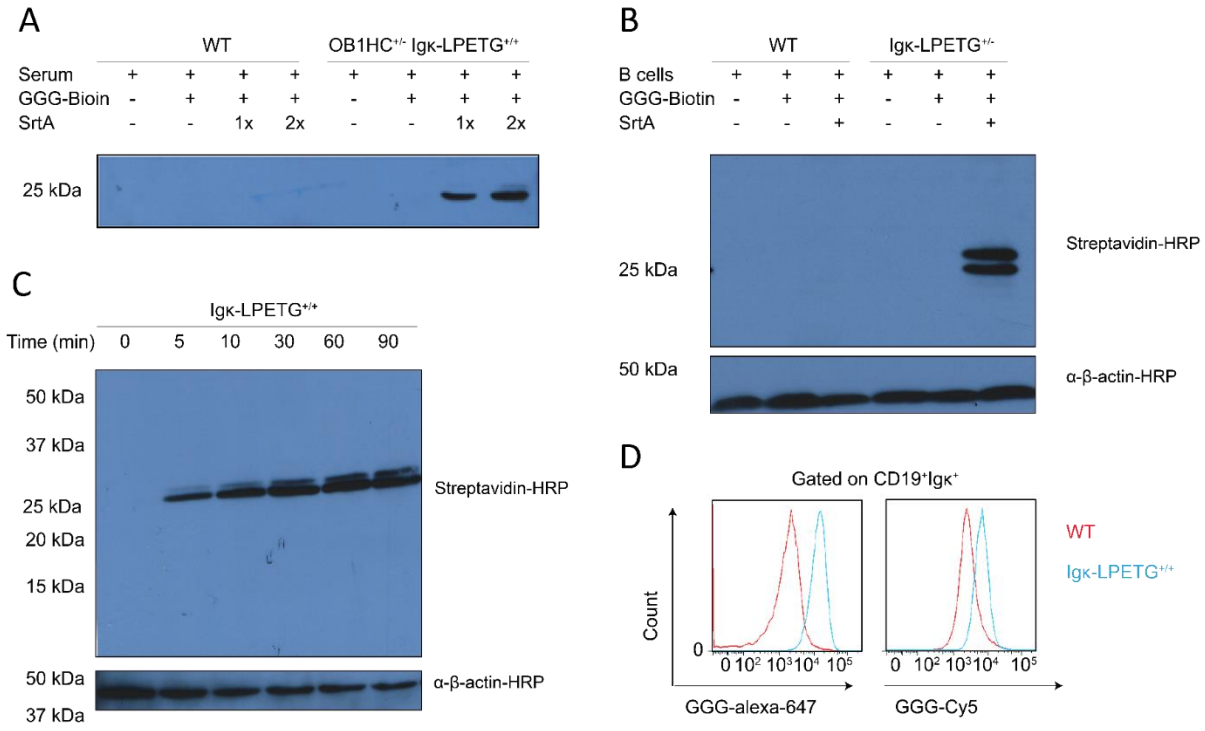

Figure 7.2 Specific labeling of Igκ LPETG-derived serum immunoglobulins and purified B cells using SrtA

(**A**) Serum from OB1HC$^{+/-}$ Igκ -LPETG$^{+/+}$ mice was labeled using GGG-biotin and StrA. Immunoglobulins were then immunoprecipitated with protein G and analyzed by immunoblot using streptavidin-HRP. (**B**) Purified primary B cells from Igκ -LPETG mice were labelled using GGG-biotin and StrA. The B cells were then lysed and analyzed by immunoblot using streptavidin-HRP. The doublet is attributable to the use of the Vκ1-135 and the Vκ 2-137 segments (see text) (**C**) Purified primary B cells isolated from Igκ -LPETG$^{+/+}$ mice were labeled as described in (B) for different durations. (**D**) Primary B cells from Igκ -LPETG$^{+/+}$ mice were labeled as described in (B) using GGG-Alexa-647 or GGG-Cy5 as nucleophiles. The cells were then surface stained and analyzed by flow cytometry. The cells were gated on AAD^{-}CD19^{+}Igκ^{+} cells. All blots and FACS plots shown are representative of at least 3 independent experiments.

Preferential association of the OB1 κ-chain with the OB1 IgG1 heavy chain.

The VJ rearrangement in the OB1 mice involves Vκ1-135, a Vκ gene near the 5' end of the locus, with only a single functional Vκ segment, Vκ2-137, remaining at the 5' end of the Vκ cluster, all of the intervening Vκ gene segments having been deleted in the course of rearrangement (Fig 7.3 A,B). The Jκ segment used is Jκ1, with three additional 3' J segments remaining, which therefore allow secondary rearrangements (*15*). Breeding experiments in which we placed the

modified κ locus on WT IgH background showed that the 5'-most Vκ segment is indeed functional and can be accessed by a secondary Vκ rearrangement. With the modified κ locus on a wildtype IgH background, B cells for the most part produce the OB1 κ light chain, with a minor fraction producing a distinct κ chain that derives from a secondary rearrangement, as shown by blotting for SrtA-labelled κ light chains, by deep sequencing of the Vκ repertoire and by metabolic labeling of plasmablasts derived from κ-LPETG mice (Fig. 7.3 C-F). Such secondary rearrangement would place the Vκ2-137 segment in a functionally correct arrangement with the modified Cκ exon and thus yield a light chain that is also a SrtA substrate. In contrast, if the modified κ locus is placed on the OB1 HC background, virtually all such secondary rearrangements are suppressed (Fig 7.3 C), indicative of preferential association of the OB1 IgG1 HC with the OB1 κ chain. A single copy of the OB1 HC locus suffices, as allelic exclusion at the HC locus ensures its preferential expression. Once a complete OB1 BCR has been formed, no further rearrangements occur.

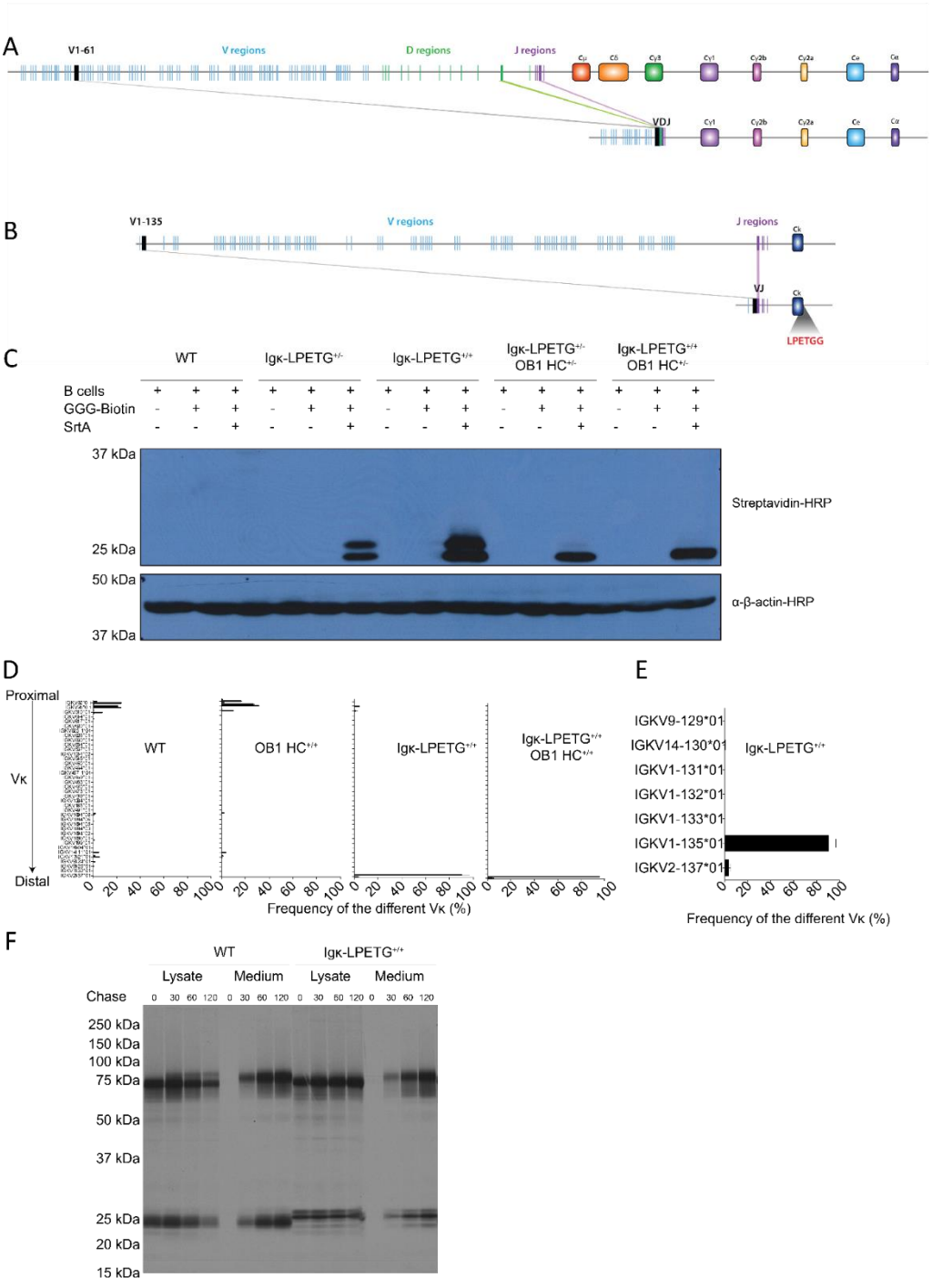

Figure 7.3 Organization of the heavy and light chain of the OB1-LPETG mouse model

(**A**) Schematic of the OB1 heavy chain locus. The OB1 heavy chain locus is pre-rearranged and encodes an IgG1 BCR. (**B**) The κ-light chain of OB1 is composed of the Vκ1-135 segment, which is positioned near the 5' end of the locus. Secondary rearrangements in OB1 are rare because only one additional Vκ fragment (Vκ2-137) remains in OB1 pre-rearranged Vκ allele. (**C**) Purified primary B cells from the indicated mice were labelled using GGG-biotin and SrtA for 1.5h on ice. The B cells were then lysed and analyzed by immunoblot using streptavidin-HRP. The blot is representative of at least 3 independent such experiments. (**D**) RNAseq analysis of the Vκ usage in the indicated mice. 1000 $AAD^{-}CD19^{+}Ig\kappa^{+}Ig\lambda^{-}$ cells were sorted, lysed and their RNA reverse-transcribed and amplified using κ-specific primers. Reads were mapped to the different Vκ segments using IMGT (*18*). Two different mice were analyzed per genotype. (**E**) Vκ usage of Igκ-LPETG$^{+/+}$ mice as described in (D), zoomed in on the distal part of the Vκ cluster. (**F**) Purified B cells from the indicated mice were cultured for 4 days in complete RPMI containing LPS (20μg/ml). The cells were harvested and radiolabeled with [^{35}S] methionine/cysteine for 10min at 37°C and chased for the indicated times. Supernatants and cell lysates were collected and immunoprecipitated using sepharose beads and α-Ig antibody for 2h at 4°C. Bound proteins were released by boiling the beads in SDS buffer.

B cell development in OB1-κ LPETG mice shows an aberrant κ to λ ratio.

We performed flow cytometry analysis to characterize B cell development in κ-LPETG mice. Compared to WT mice, we found an increase in the number of λ-producing cells in the spleen in addition to a decreased κ to λ ratio for serum immunoglobulins (Fig. 7.4A-C). In WT mice, fewer than 5% of mature B cells are Igλ. However, OB1-κ LPETG$^{+/+}$ mice have 20-40% of $Ig\lambda^{+}$ B cells in the spleen. The B cell compartment appears otherwise normal. In the bone marrow, the B cell compartment derived from κ-LPETG mice shows a slight increase in pre-B cells compared to WT cells, although not statistically different from OB1 LC$^{+/+}$ (Fig. 7.4 D). There is a slight decrease in spleen follicular B cells when compared to WT cells but not in comparison with OB1 LC$^{+/+}$. We conclude that apart from the decreased κ to λ ratio, the B cell compartment shows no major aberrations. Presumably not all newly generated VDJ combinations pair equally well with Vκ1-135 or Vκ2-137, thus favoring outgrowth of B cells with λ light chains.

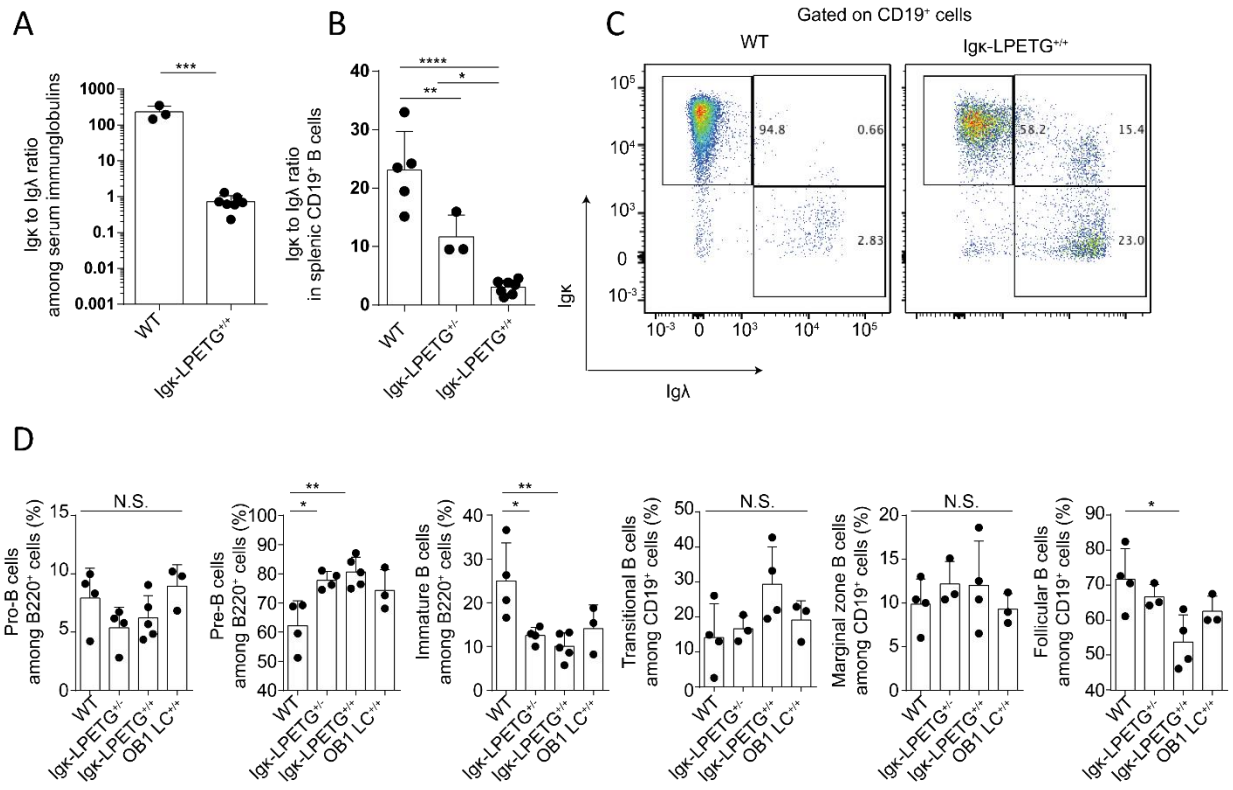

Figure 7.4 Igκ-LPETG mice have near normal B cell development

(**A**) Serum immunoglobulins from the indicated mice were analyzed by ELISA. All mice analyzed are shown. Unpaired Student's t test was performed to compare the ratio of serum Igκ to Igλ antibodies. ***, P=0.002. (**B**) Splenic B cells were labelled for surface markers and gated on AAD$^-$CD19$^+$Igκ$^+$Igλ$^-$ or AAD$^-$CD19$^+$Igκ$^-$Igλ$^+$ and their ratio plotted. The graph shows all mice analyzed. One-way ANOVA was performed to compare the ratio of Igκ and Igλ splenic B cells in the indicated mice. (**C**) Representative plots of experiment shown in (B). (**D**) Populations within the B cell compartment were identified as described by flow cytometry (*15*). Bone marrow: Pro-B cells (AAD$^-$B220$^+$CD43^{high}CD19^{low}), Pre-B cells (AAD$^-$B220$^+$CD43$^{int.}$CD19$^{int.}$) and Immature B cells (AAD$^-$B220$^+$CD43^{low}CD19^{high}). Spleen: Transitional B cells (AAD$^-$CD19$^+$CD21$^{low/-}$CD23$^-$), Marginal zone B cells (AAD$^-$CD19$^+$CD21$^+$CD23$^{low/-}$) and Follicular B cells (AAD$^-$CD19$^+$CD21^{int}CD23^{int}). The graphs shown here include all mice analyzed. (A-D) N.S.: P > 0.05, *:P ≤ 0.05, **:P ≤ 0.01, ***:P ≤ 0.001, ****: P ≤ 0.0001. All graphs show the mean + SD.

Labeling of the OB1 κ-LPETG chain does not activate B cells.

We examined whether enzymatically affixing a biotin label to the C-terminus of the κ light chain would suffice to trigger signaling via the BCR. We took advantage of the fact that the SrtA variant used for labeling retains enzymatic activity at 0°C. We could thus perform labeling experiments at 0°C, remove the enzyme together with the added excess nucleophile and return cells to 37°C, followed by interrogation of ERK phosphorylation as an indicator of B cell activation. For reference purposes, we included an incubation with a polyclonal α-IgM to achieve crosslinking of the BCR

and subsequent ERK phosphorylation. We observed biotinylation only for B cells from mice that carry the modified κ-LPETG chain and only when both enzyme and (Gly)3 nucleophile were present (Fig. 7.5A). The levels of phospho-ERK were comparable for B cells that received no treatment compared to B cells that had been labeled using SrtA and the (Gly)3-biotin nucleophile. The increase in phospho-ERK required the inclusion of a crosslinking α-IgM and was similar for WT and κ-LPETG$^{+/+}$ B cells, regardless of whether the κ chains had been enzymatically biotinylated or not. An examination of Ca^{2+} flux yielded similar results (Fig. 7.5B). Crosslinking of the BCR with α-IgM produced a robust Ca^{2+} flux, regardless of labeling status, whereas the act of labeling itself produced no Ca^{2+} flux. B cells of κ-LPETG mice are therefore functional. The SrtA motif present on the κ-light chain does not obviously affect activation of B cells nor does SrtA labeling lead to or inhibit B cell activation.

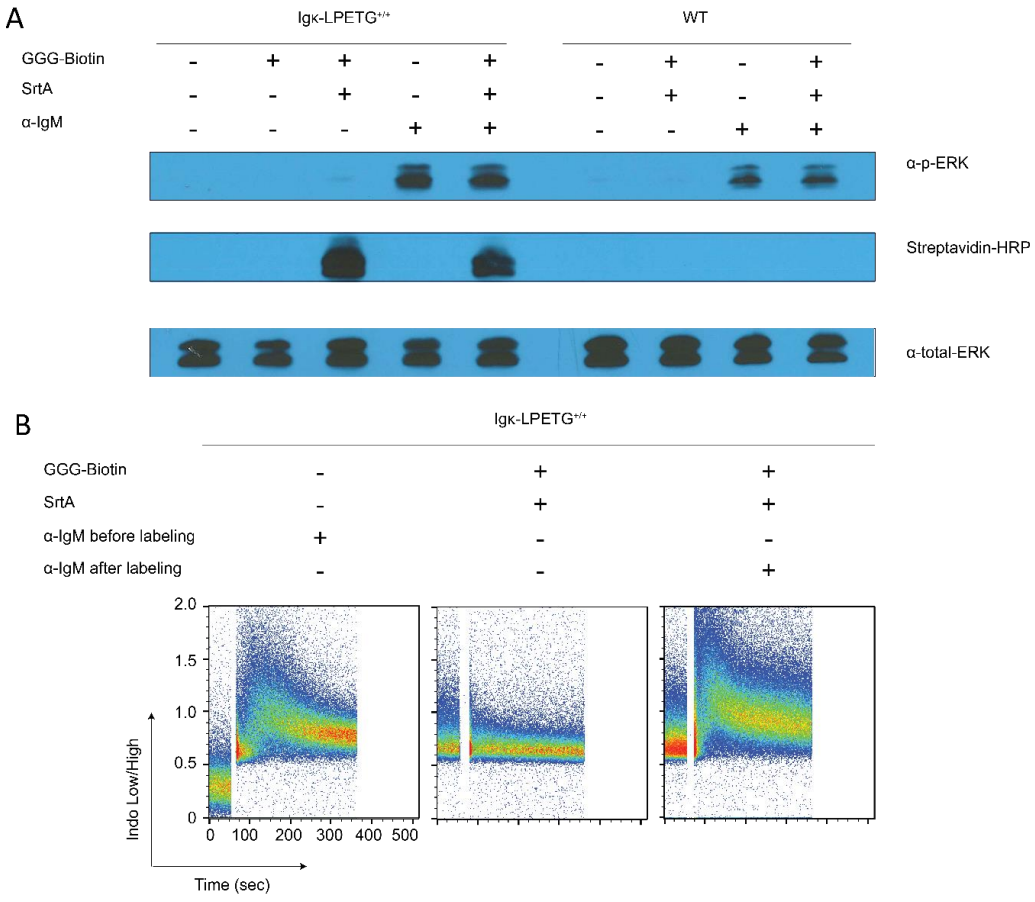

Figure 7.5 SrtA labeling does not activate B cells

(**A**) Purified primary B cells from the indicated mice were labelled or not using GGG-biotin and SrtA for 1.5h on ice. The B cells were then equilibrated at 37°C for 5min and stimulated with 5 µg/ml anti-IgM for 3min. The B cells were then lysed in SDS sample buffer and analyzed by immunoblot using streptavidin-HRP, α-P-ERK and α-total-ERK. The blot shows one representative of at least 3 independent experiments. (**B**) Igκ-LPETG$^{+/+}$ B cells were labelled or not with SrtA and GGG-Biotin, loaded with Ca^{2+}-sensitive Indo-1 AM dye, equilibrated at 37°C for 1-2min and collected for 1min (baseline). Next, 5 µg/ml α-IgM was added or not and collected for 5 additional minutes. Both panels show representative of at least three independent experiments.

IgM/IgD and IgG1 BCRs are organized differently on the surface of B cells

BCR density and nano-scale organization influence B cell fate (*5, 7-9*). While expression of IgG1 BCR supports development of B cells in most models, some subsets can be reduced, suggesting that the presence of an IgG1 instead of an IgM/IgD BCR could affect B cell fate (*15, 19*). We hypothesized that IgG1-carrying B cells displayed a BCR density and organization that differs from IgM/IgD B cells. To test this hypothesis, we isolated naïve IgM/IgD-carrying B cells from κ-LPETG$^{+/+}$ and IgG1 B cells from OB1 κ-LPETG$^{+/+}$ mice and labelled them with GGG-Alexa-647 and SrtA. The BCR was distributed very differently for IgM/IgD and OB1 IgG1 B cells (Fig. 7.6A). While IgM/IgD B cells display a smooth distribution of BCRs, IgG1-expressing OB1 cells showed more concentrated punctate structures of BCRs. Next, we tested whether the BCR density was also altered in B cells of different isotypes. We isolated splenic B cells from WT and OB1 κ-LPETG$^{+/+}$ stained surface markers for flow cytometry analysis. Confirming previously published results in WT mice (*20*), IgG1 carrying splenic B cells derived from the monoclonal OB1 κ-LPETG$^{+/+}$ mice showed significantly lower Igκ median fluorescence intensity (MFI) as compared to IgM/IgD-expressing naïve WT splenic B cells. BCRs of different isotypes thus display distinct density and organization on the surface of B cells.

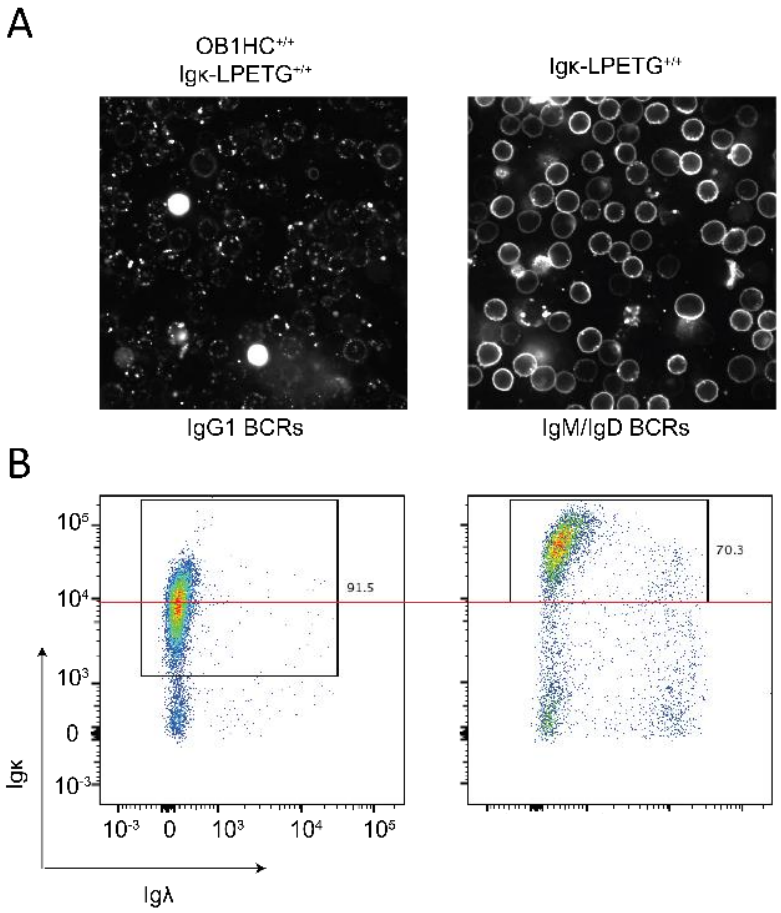

Figure 7.6 Altered BCR organization in IgG1 B cells

(**A**) Purified primary B cells from the indicated mice were labelled using GGG-biotin and SrtA for 1.5h on ice. The B cells were then rinsed, loaded on poly-L-lysine-coated chambers and visualized on a fluorescence microscope. The image on the left shows labeling of IgG1 BCRs (OB1 κ-LPETG$^{+/+}$), while the image on the right shows IgM/IgD BCRs (κ-LPETG$^{+/+}$). Panel A shows one representative image/group of at least two independent experiments. (**B**) Splenic B cells from the indicated mice were labelled for surface markers for 30min at 4°C, rinsed and analyzed by flow cytometry. Cells are gated on 7-AAD^{-}CD19^{+} cells. Plots show one representative of at least 3 independent experiments.

Using the κ-LPETG model to quantify the total number of BCRs in B cells

The changes in BCR density and organization in B cells of different isotypes prompted us to enumerate the number of BCRs on primary B cells. While the numbers of IgM and IgD on the surface have been estimated by flow cytometry, the number of BCRs on primary B cells of isotypes other than IgM is not known (*21*). We made use of the LPETG motif to site-specifically install a single biotin moiety at the C-terminus of each Cκ chain. In similar fashion, we modified a SrtA ready version of eGFP with biotin. The modified version of GFP carries a C-terminal His tag,

preceded by a SrtA motif. Upon cleavage of the SrtA motif, the His tag is lost, thus enabling purification of the desired product through application to a Ni-NTA matrix. SrtA itself is likewise equipped with a His tag, so that in a single step both unreacted GFP and SrtA can be removed. The biotinylated GFP product was further purified by FPLC and characterized by mass spectrometry and determined to carry one biotin molecule per molecule of GFP. We chose GFP to ensure that the size of the proteins to be compared would be sufficiently similar not to lead to discrepancies in transfer efficiency in the course of immunoblotting. We examined the level of biotinylated κ-chain for a mouse that carried a wild type IgH locus, and whose primary B cells thus mostly display IgM/IgD at their surface and compared it with B cells from an OB-1 κ-LPETG$^{+/+}$ mouse, which displays exclusively IgG1 at the B cell surface (Fig. 7.7) (*15*). To estimate the number of BCRs, we considered the frequency of Igκ^{+} B cells as measured by flow cytometry and the fact that each BCR carries two identical light chains. We also assumed that the transfer efficiency of GFP and κ chains was identical, with an assumed enzymatic labeling efficiency for both surface IgG1 and IgM/IgD BCRs of 100%. This will obviously yield an underestimate of the actual numbers of surface-disposed BCRs. With these reservations, we estimated the total number of BCRs of IgM/IgD-expressing B cells to be ~1.1 million per cell, whereas the number of IgG1 BCRs is approximately 400,000 per cell (Fig. 7.7). These results are in line with the reduced levels of BCRs observed by flow cytometry (Fig. 7.6). Ig light chains are produced in molar excess over heavy chains. This suggests that it is the level of the Ig heavy chain that is the limiting factor.

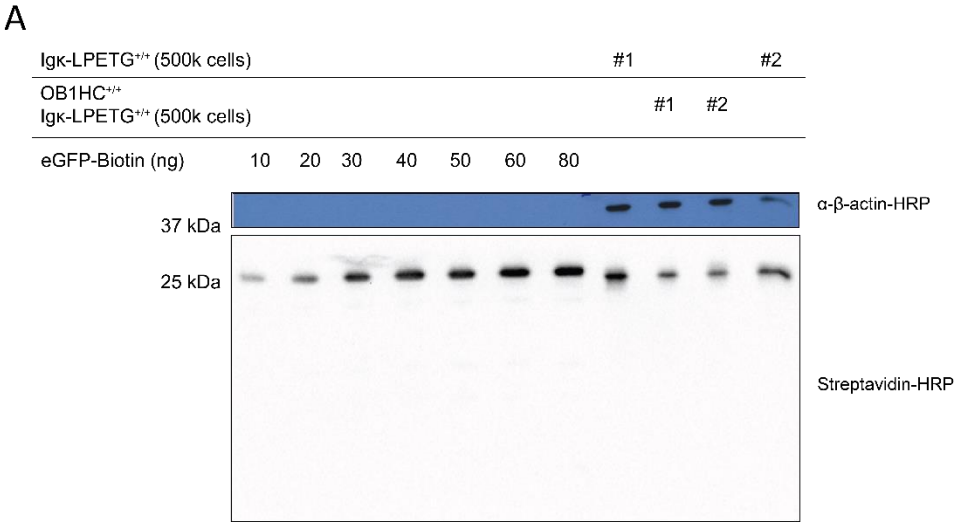

Figure 7.7 Quantification of the number of BCRs on the surface of naive B cells

(**A**) Purified primary B cells from the indicated mice were labelled using GGG-biotin and SrtA for 1.5h on ice. The B cells were then rinsed, lysed and analyzed by immunoblot using streptavidin-HRP. 500k cells were loaded per well. To quantify the amount of labeling, we included a ladder of eGFP-biotin, which carries a single molecule of biotin per GFP. The blot shows one representative of 2 independent experiments.

Discussion

We have developed a method to site-specifically track the BCR on naive B cells in a minimally perturbing manner. We found that the presence of the SrtA motif installed on Cκ did not affect the ability of B cells to be activated, nor did labeling with biotin or a fluorophore lead to activation. Using this method, we found that IgG1 BCRs were organized in clusters on the surface of B cells unlike IgM/IgD BCRs, which displayed a more diffuse distribution.

The levels of BCRs on the surface of B cells likely affect BCR function, due to differences in cytoplasmic tails and/or receptor organization. We measured the total number of SrtA accessible IgG1 BCRs on naïve B cells and show that there are fewer of them than IgM/IgD BCRs. Lower surface expression of IgG1 BCRs has been seen in mice carrying polyclonal IgG1 B cells (*20*). Interestingly, these polyclonal IgG1 mice present a more than 10-fold reduction in peripheral B cells. Conversely, another IgG1 polyclonal model that enhances surface IgG1 expression (by deletion of the intronic polyA site to enhance membrane IgG1 over secreted IgG1) has little B cell development phenotypes (*19*). Monoclonal IgG1-bearing OB1 B cells show near-normal B cell development (*15*). Together, these findings highlight how to both BCR density and specificity are critical for B cell fate decisions. The mechanistic relationship between antigen specificity and BCR organization remains poorly understood. However, the κ-LPETG mice presented here offer a flexible strategy to investigate this. By crossing our κ-LPETG model with polyclonal mouse models, such as the IgG1 expressing Ighγ1/γ1 strain developed by Wesemann and colleagues, the dynamics of receptor organization in B cells of a unique isotype but diverse specificity can be monitored.

With a few notable exceptions (*22*)(*23*)(*5*), most of our knowledge concerning Ag-specific BCR in primary B cells pertains to IgM/IgD BCRs, one of the two isotypes present in resting B cells(*24*). However, IgM and IgD lack a substantive cytoplasmic tail and therefore rely entirely on Igα/Igβ for signal transduction (*24*). In contrast, all other isotypes (IgG1, IgG2a, IgG2b, IgG3, IgE and IgA) possess longer, highly conserved, cytoplasmic tails(*24*) been implicated in downstream signaling(*22, 25-28*). Experiments exploring surface BCRs of isotypes different than IgM and of known specificity have mostly relied on *in vitro* class-switch recombination, which have failed to provide homogenous B cell populations (*29*). Notably, the extracellular portion of the constant region is also considerably diverse structurally. While the different extracellular regions of the different BCR isotypes possess a similar overall structure, the length and flexibility of their hinge region are very different. The OB1 model is a unique system to study IgG1 BCR activation since

the OVA epitope has been mapped and can be mimicked by synthetic peptides providing unprecedented control of Ag valency (*14*). While the findings presented in this project focus on B cells at rest, we predict that the model and tools developed here will constitute a valuable system to study monovalent engagement of the BCR.

Materials and methods

Mice

Transnuclear OB1 RAG-proficient (C57BL/6 background) (*15*). κ-LPETG mice (mixed OB1 LC C57BL/6 and 129 background) were generated as described (*16*) and OB1 HC- κ-LPETG were obtained by crossing κ-LPETG mice with OB1 RAG-proficient mice. All animals were maintained under specific pathogen–free conditions, and experiments were performed with approval of the Committee for Animal Care and the Association for the Assessment and Accreditation of Laboratory Animal Care. C57BL/6 were purchased from Jackson Laboratory and maintained at our facilities (Whitehead Institute and Boston Children's hospital). All experiments were performed on 6-12 weeks old mice.

Reagents, antibodies and flow cytometry

Reagents and antibodies were obtained from ThermoFisher (β-actin, clone BA3R; Streptavidin-HRP, ref. 21130), Southern Biotech (αIg, ref. 1010-01; αIgκ, ref. 1050-05; αIgλ, ref. 1060-05; αIgM, ref. 1021-01; αIgκ, ref. 1050-05 and ref. 1170-09L; αIgλ, ref. 1175-02), Biolegend (CD23, B3B4; CD21, 7E9; CD43, S11), BD (CD19, 1D3; B220, RA3-6B2; CD16/CD32, 2.4G2). Cell viability dye 7-AAD (Via-Probe) was purchased from BD Biosciences and used following manufacturer's instructions. Flow cytometry data were acquired on an LSRFortessa (Becton Dickinson) or LSR II instrument and analyzed with the FlowJo soft-ware package (Tri-Star). Surface markers were stained at 4°C for 25 min in the presence of Fc block (BD) in PBS+1mM EDTA+ 0.5% bovine serum albumin. Indo-1 AM was purchased from Invitrogen. Anti-IgG1 (unlabeled and conjugated to HRP) was obtained from Southern Biotech.

Sortase labeling

Sortagging reactions were performed using the hepta-mutant version of Sortase A (SrtA) from *Staphylococcus aureus*, which is calcium-independent and exhibit an enhanced activity (*30, 31*). The enzyme was produced as described elsewhere (*32*). SrtA probes (GGG-Biotin, GGG-alexa-647 and GGG-Cy5) were produced in house as described (*33*). 3-5*10^6 B cells were labelled with 60µM of SrtA and 600µM of probe in complete RPMI on ice for 1.5h or the indicated time. Labelled cells were washed 3 times with cold PBS. For immunoglobulin labeling, serums from the indicated mice were collected and used in a SrtA reaction as described (*16*). Immunoglobulins were then isolated using protein-G beads and the beads-containing the labelled immunoglobulins boiled in

SDS sample buffer to release the bound material. The sample was then submitted to SDS-PAGE, blotted using Streptavidin-HRP.

B cell purification

Untouched B cells were purified by negative selection using CD43 Dynabeads (Life Technologies) according to the manufacturer's recommendations. Purity was always >90%.

RNA-seq library preparation and sequencing

One thousand $CD19^{+}Ig\kappa^{+}Ig\lambda^{-}$ cells were sorted using a FACS Aria II cell sorter and lysed in a guanidine thiocyanate buffer (Qiagen) supplemented with 1% β-mercaptoethanol. RNA was isolated using solid-phase reversible immobilization bead cleanup, reverse-transcribed into complementary DNA and pre-amplified as previously described (*34-36*). Sequencing was performed on an IlluminaHiSeq2000. Vκ gene segments were assigned using IMGT (*18*).

Microscopy

Naïve B cells were purified labelled with Sortase and GGG-Alexa-647, attached to poly-l-lysine–coated chamber slides in phenol red–free RPMI medium supplemented with 10% heat-inactivated FBS. Images were acquired at room temperate on a Nikon Eclipse Ti wide field microscope.

Ca^{2+} flux

Naïve B cells were resuspended in serum-free RPMI and labelled with INDO-1 AM for 30min at 37°C. The cells were then washed and left at RT for 20min to enable desterification of the dye. Cells were equilibrated at 37°C for 1-2min before flow cytometry analysis. Signals at 485 nm (HI) and 410 nm (LO) were collected for 1 min to record baseline Ca^{2+} levels as the ratio of Indo LO/HI. The cells were then stimulated with the indicated reagents and Ca^{2+} levels recorded for additional 5 min. Data were collected in a FACS LSR instrument (BD) and analyzed using FlowJo software (Tree Star).

Serum ELISA

Serum was collected from age-matched mice. 96-well high-binding plates (Costar) were coated with 1µg/ml of anti-Ig (Southern Biotech) in PBS overnight at 4°C, rinsed 3x with PBST (0.05%Tween-20 in PBS) and blocked in 10% FBS in PBS for 1h at RT. Serum were incubated neat and in 10-fold dilutions for 2h in 10% FBS in PBS. The plates were rinsed 5x and HRP-

coupled secondary antibodies recognizing Igκ and Igλ (1:1,000) for 1h. After rinsing, the plates were developed using OptEIA TMB substrate reagent kit (BD), and the reaction was stopped with 1M hydrochloric acid and plate read at 450-nm absorbance.

Metabolic Labeling and Immunoprecipitation

B cells were cultured in complete RPMI with 10% FBS containing LPS (20 μg/mL) were added to the culture medium. Plasmablasts were starved for 1h in methionine- and cysteine-free medium and pulsed for 10min with [35S] methionine/cysteine (PerkinElmer). Supernatant were harvested and the cells lysed in Nonidet P-40 buffer (1%NP-40 in HEPES buffer pH 6.8 containing protease inhibitors (Roche)). B cell receptors and immunoglobulins were immunoprecipitated as described (*37*).

Immunoblotting

For p-ERK, B cells were rested overnight at 37°C in complete RPMI. The next day, the cells were equilibrated at 37°C before adding the stimuli. Cells were lysed using RIPA buffer (20 mM Tris pH 7.5, 1 mM EDTA, 100mM NaCl, 1% Triton X-100, 0.5% Sodium deoxucholate and 0.1% SDS), and lysates analyzed by SDS-PAGE and immunbloting using α-P-ERK, α-total ERK (CST), α-β-actin and streptavidin-HRP (ThermoFisher).

Statistical analysis

Mean and SD values were calculated with GraphPad Prism (GraphPadSoftware). Unpaired Student's t test was used to compare two variables, while one-way ANOVA was used for multiple comparisons. P values of <0.05 were considered significant and are indicated in the figure or figure legends.

Authors contributions

D.B and H.P designed the research and wrote the paper. D.B performed the research and analyzed the data. D.B, Z. L. and T.F. contributed new reagents.

Acknowledgements

We thank the WIBR Flow Cytometry and genome core facilities for sorting cells, analyzer use and for the sequencing, I. Barrassa (Department of Bioinformatics and Research Computing, WIBR)

for assistance with RNA-seq analysis and Tom DiCesare with illustrations, J. Jackson and S. Kolifrath for assistance with mouse husbandry genotyping and colony management. We are thankful to M. Hagiwara and J. Ling for help with pulse chases and labeling quantification, respectively. We are in debt to R. Cheloha, N. McCaul and G. Victora for invaluable discussions and suggestions on this project and A. Avalos for initial guidance. We thank the Ploegh lab for suggestions and fruitful discussions. This work was supported by a grant from the National Institutes of Health and D.B received support from the Boehringer Ingelheim.

References

1. T. Kurosaki, H. Shinohara, Y. Baba, B cell signaling and fate decision. *Annual review of immunology* **28**, 21-55 (2010).
2. J. Hombach, T. Tsubata, L. Leclercq, H. Stappert, M. Reth, Molecular components of the B-cell antigen receptor complex of the IgM class. *Nature* **343**, 760-762 (1990).
3. E. Surova, H. Jumaa, The role of BCR isotype in B-cell development and activation. *Advances in immunology* **123**, 101-139 (2014).
4. M. Reth, Antigen receptor tail clue. *Nature* **338**, 383-384 (1989).
5. R. Ubelhart *et al.*, Responsiveness of B cells is regulated by the hinge region of IgD. *Nature immunology* **16**, 534-543 (2015).
6. A. Casadevall, A. Janda, Immunoglobulin isotype influences affinity and specificity. *Proceedings of the National Academy of Sciences of the United States of America* **109**, 12272-12273 (2012).
7. S. K. Pierce, W. Liu, The tipping points in the initiation of B cell signalling: how small changes make big differences. *Nature reviews. Immunology* **10**, 767-777 (2010).
8. K. Klasener, P. C. Maity, E. Hobeika, J. Yang, M. Reth, B cell activation involves nanoscale receptor reorganizations and inside-out signaling by Syk. *eLife* **3**, e02069 (2014).
9. J. Yang, M. Reth, Oligomeric organization of the B-cell antigen receptor on resting cells. *Nature* **467**, 465-469 (2010).
10. P. Tolar, J. Hanna, P. D. Krueger, S. K. Pierce, The constant region of the membrane immunoglobulin mediates B cell-receptor clustering and signaling in response to membrane antigens. *Immunity* **30**, 44-55 (2009).
11. R. J. Petrie, J. P. Deans, Colocalization of the B cell receptor and CD20 followed by activation-dependent dissociation in distinct lipid rafts. *Journal of immunology* **169**, 2886-2891 (2002).
12. P. C. Maity *et al.*, B cell antigen receptors of the IgM and IgD classes are clustered in different protein islands that are altered during B cell activation. *Science signaling* **8**, ra93 (2015).
13. P. Tolar, H. W. Sohn, S. K. Pierce, The initiation of antigen-induced B cell antigen receptor signaling viewed in living cells by fluorescence resonance energy transfer. *Nature immunology* **6**, 1168-1176 (2005).
14. A. M. Avalos *et al.*, Monovalent engagement of the BCR activates ovalbumin-specific transnuclear B cells. *J Exp Med* **211**, 365-379 (2014).
15. S. K. Dougan *et al.*, IgG1+ ovalbumin-specific B-cell transnuclear mice show class switch recombination in rare allelically included B cells. *Proc Natl Acad Sci U S A* **109**, 13739-13744 (2012).
16. T. Maruyama *et al.*, Increasing the efficiency of precise genome editing with CRISPR-Cas9 by inhibition of nonhomologous end joining. *Nat Biotechnol* **33**, 538-542 (2015).
17. E. O. Saphire *et al.*, Crystal structure of a neutralizing human IGG against HIV-1: a template for vaccine design. *Science* **293**, 1155-1159 (2001).
18. M. P. Lefranc *et al.*, IMGT, the international ImMunoGeneTics information system. *Nucleic Acids Res* **37**, D1006-1012 (2009).
19. A. Waisman *et al.*, IgG1 B cell receptor signaling is inhibited by CD22 and promotes the development of B cells whose survival is less dependent on Ig alpha/beta. *J Exp Med* **204**, 747-758 (2007).
20. P. Tong *et al.*, IgH isotype-specific B cell receptor expression influences B cell fate. *Proc Natl Acad Sci U S A* **114**, E8411-E8420 (2017).
21. F. Gasparrini *et al.*, Nanoscale organization and dynamics of the siglec CD22 cooperate with the cytoskeleton in restraining BCR signalling. *EMBO J* **35**, 258-280 (2016).

22. T. Kaisho, F. Schwenk, K. Rajewsky, The roles of gamma 1 heavy chain membrane expression and cytoplasmic tail in IgG1 responses. *Science* **276**, 412-415 (1997).
23. M. Reth, Antigen receptors on B lymphocytes. *Annual review of immunology* **10**, 97-121 (1992).
24. Y. Xu *et al.*, No receptor stands alone: IgG B-cell receptor intrinsic and extrinsic mechanisms contribute to antibody memory. *Cell research* **24**, 651-664 (2014).
25. A. Waisman *et al.*, IgG1 B cell receptor signaling is inhibited by CD22 and promotes the development of B cells whose survival is less dependent on Ig alpha/beta. *Journal of Experimental Medicine* **204**, 747-758 (2007).
26. S. W. Martin, C. C. Goodnow, Burst-enhancing role of the IgG membrane tail as a molecular determinant of memory. *Nature immunology* **3**, 182-188 (2002).
27. G. Achatz, L. Nitschke, M. C. Lamers, Effect of transmembrane and cytoplasmic domains of IgE on the IgE response. *Science* **276**, 409-411 (1997).
28. M. Bracke, J. W. Lammers, P. J. Coffer, L. Koenderman, Cytokine-induced inside-out activation of FcalphaR (CD89) is mediated by a single serine residue (S263) in the intracellular domain of the receptor. *Blood* **97**, 3478-3483 (2001).
29. W. Liu, T. Meckel, P. Tolar, H. W. Sohn, S. K. Pierce, Intrinsic properties of immunoglobulin IgG1 isotype-switched B cell receptors promote microclustering and the initiation of signaling. *Immunity* **32**, 778-789 (2010).
30. I. Chen, B. M. Dorr, D. R. Liu, A general strategy for the evolution of bond-forming enzymes using yeast display. *Proc Natl Acad Sci U S A* **108**, 11399-11404 (2011).
31. H. Hirakawa, S. Ishikawa, T. Nagamune, Design of Ca2+-independent Staphylococcus aureus sortase A mutants. *Biotechnol Bioeng* **109**, 2955-2961 (2012).
32. M. W. Popp, J. M. Antos, G. M. Grotenbreg, E. Spooner, H. L. Ploegh, Sortagging: a versatile method for protein labeling. *Nat Chem Biol* **3**, 707-708 (2007).
33. C. P. Guimaraes *et al.*, Site-specific C-terminal and internal loop labeling of proteins using sortase-mediated reactions. *Nat Protoc* **8**, 1787-1799 (2013).
34. J. J. Trombetta *et al.*, Preparation of Single-Cell RNA-Seq Libraries for Next Generation Sequencing. *Curr Protoc Mol Biol* **107**, 4 22 21-24 22 17 (2014).
35. J. M. Tas *et al.*, Visualizing antibody affinity maturation in germinal centers. *Science* **351**, 1048-1054 (2016).
36. T. Tiller, C. E. Busse, H. Wardemann, Cloning and expression of murine Ig genes from single B cells. *J Immunol Methods* **350**, 183-193 (2009).
37. A. M. McGehee *et al.*, XBP-1-deficient plasmablasts show normal protein folding but altered glycosylation and lipid synthesis. *J Immunol* **183**, 3690-3699 (2009).